THE UNIVERSITY OF QUEENSLAND

AUSTRALIA

Surface Hydrological Modelling for Rehabilitated Landforms

Qi Shao

Bachelor of Agriculture (Forestry), Master of Science (Natural Resources)

A thesis submitted for the degree of Doctor of Philosophy at

The University of Queensland in 2014

Sustainable Minerals Institute

Abstract

Rehabilitated landforms are often characterised by topographies, material properties and vegetation features untypical for the environment they are constructed in. Changed topography, decreased infiltration capacity and reduced vegetation cover often result in altered surface hydrological behaviours, typically resulting in increased surface runoff, which may be the cause for serious soil erosion, downstream contamination, revegetation failure and potential destruction of waste containment facilities.

Proper rehabilitation planning, including the landform designs and revegetation strategies, together with the suitable water management, could help minimize these potential harmful environmental consequences and improve landform stability. This requires a good understanding and estimation of the surface hydrological processes in the rehabilitated landforms. A critical literature review in this thesis, however, has identified that there are still some uncertainties remaining in many areas of the surface hydrology research, including the major influencing factors and their combined and quantified effects on the surface hydrological process, the efficient determination of the unmeasurable parameters for the infiltration modelling, the evaluation and application of modified infiltration models for the simulation of complex rainfall conditions, and the accurate and effective methods for runoff modelling at different spatial or temporal scales.

Furthermore, most of previous studies have focused on the surface hydrology in the agricultural, forestry and other natural systems, while limited effort has been made towards the disturbed environment such as the mining areas. The hydrologic theories, principles and models established in the natural environment thus may not be applicable to the rehabilitated environment because of the differences in their geomorphic features, surface hydraulic properties, spatial scales and landform complexities.

The two major objectives of this research therefore were: (1) to evaluate the classical and modified infiltration models and estimate their parameters from major controlling factors by conducting small scale plot studies; and (2) to develop a more effective and universal surface runoff model by incorporating the evaluated infiltration models and Cellular Automata theories, and apply it for the simulation of runoff behaviours on the rehabilitated landforms.

The infiltration experiments were firstly carried out at an experimental farm of the University of Queensland, located at Pinjarra Hills, Queensland, eastern Australia. Field plots of a size

of 1 m × 1 m were set up to evaluate the performance of four classical infiltration models (i.e., Philip, Green-Ampt, Holtan and Horton models) and three modified infiltration models (i.e., modified Holtan, Green-Ampt and Horton models) under different site conditions, using the continuous rainfall or sequences of rainfall events generated by a field rainfall simulator. All these models demonstrated satisfactory and comparative performance, except for the modified Horton model, which however, showed greatly increased accuracies after the improvement made in this study. In addition, predictive regression equations were successfully developed for the unmeasurable parameters in the four classical infiltration models, on the basis of their identified major controlling factors. A simplified set of equations were also developed from five readily obtainable factors, thus improving the outcomes in regard to the effort, time and cost in determining these parameters.

The well evaluated infiltration models laid a solid foundation for the prediction of runoff production as infiltration is recognised as an important regulator in surface hydrology that determines the quantity of incoming precipitation, which becomes surface runoff or contributes to soil moisture. On this basis, a novel surface runoff model (RunCA) was further proposed in this research by taking the advantages of Cellular Automata (CA), based on the cardinal-direction-priority principle, the minimization-of-difference algorithm and the calculated spatially varied flow velocities. The systematic validation of RunCA by the analytical solution under simplified conditions, the laboratory experiments on small plots and the field measurements (data taken from literature) at Pine Glen Basin, USA demonstrated its ability in simulating the spatial and temporal variations in the unsteady state runoff behaviours at different scales. RunCA also showed potential advantages over some other hydrologic models in terms of simulation accuracy, computational efficiency and scale flexibility.

The validated RunCA model was then applied to a case study to assess the runoff performance on a rehabilitated mining landform at Ranger Uranium Mine, located at Northern Territory, Australia. Good agreement was achieved between the simulated and observed discharge volumes, runoff curves and flow distributions for the rainfall events monitored during four water years from 2009 to 2013. Simulation results also indicated the role of designed surface rip lines in reducing runoff and their insufficiency during several extreme rainfall events. New virtual landforms were therefore created by increasing the heights of rip lines and an optimum design was suggested by comparing the simulated runoff results of RunCA. The application of RunCA was further discussed by scenario analysis performed on

virtual objects to broaden the aspects in mined land rehabilitation designs, including landform designs of batter slopes and tailings dams, revegetation strategies and cover constructions. These results have proven the efficacy of RunCA as a simulation tool to optimise rehabilitation designs.

In conclusion, this thesis has improved our understanding on the effects of various factors on the soil infiltration behaviours and facilitated the determination of infiltration parameters by developing predictive equations. It also contributes the surface hydrologic modelling through the evaluation of different infiltration models and the development of a novel CA-based surface runoff model. The developed runoff model provides a powerful simulation tool for the sustainable landform design and effective water management, which would minimise the potential harmful environmental consequences and increase the success of the long-term stability of rehabilitated landforms.

Declaration by author

This thesis is composed of my original work, and contains no material previously published or written by another person except where due reference has been made in the text. I have clearly stated the contribution by others to jointly-authored works that I have included in my thesis.

I have clearly stated the contribution of others to my thesis as a whole, including statistical assistance, survey design, data analysis, significant technical procedures, professional editorial advice, and any other original research work used or reported in my thesis. The content of my thesis is the result of work I have carried out since the commencement of my research higher degree candidature and does not include a substantial part of work that has been submitted to qualify for the award of any other degree or diploma in any university or other tertiary institution. I have clearly stated which parts of my thesis, if any, have been submitted to qualify for another award.

I acknowledge that an electronic copy of my thesis must be lodged with the University Library and, subject to the General Award Rules of The University of Queensland, immediately made available for research and study in accordance with the *Copyright Act 1968*.

I acknowledge that copyright of all material contained in my thesis resides with the copyright holder(s) of that material. Where appropriate I have obtained copyright permission from the copyright holder to reproduce material in this thesis.

Publications during candidature

Peer-reviewed journal paper

Shao, Q. and Baumgartl, T., 2014. Estimating Input Parameters for Four Infiltration Models from Basic Soil, Vegetation, and Rainfall Properties. Soil Science Society of America Journal, 78(5), 1507-1521, doi: 10.2136/sssaj2014.04.0122.

Shao, Q. and Baumgartl, T., 2015. Field Evaluation of Three Modified Infiltration Models for the Simulation of Rainfall Sequences. Soil Science (submitted and under review).

Shao, Q., Weatherley, D., Huang, L. and Baumgartl, T., 2014. RunCA: A Cellular Automata Model for Simulating Surface Runoff at Different Scales. Journal of Hydrology (submitted and under review).

Shao, Q., Saynor, M., Lowry, J., Lu, P. and Baumgartl, T., 2015. Simulating Surface Runoff Using a Cellular Automata Approach: a Case Study from the Ranger Uranium Mine. Earth Surface Processes and Landforms (submitted and under review).

Peer-reviewed conference paper

Shao, Q., Baumgartl, T., Huang, L. and Weatherley, D., 2014. A Cellular Automata-based Run-off Model and its Application in Mined Land Rehabilitation Designs. Proceedings of Life-of-Mine 2014 Conference, Brisbane, Australia: 81-96.

Conference abstracts

Shao, Q., Baumgartl, T., Huang, L. and Weatherley, D., 2014. A Cellular Automata Based Model for Simulating Surface Hydrological Processes in Catchments. European Geosciences Union General Assembly 2014. Vienna, Austria, 27 April – 02 May 2014.

Shao, Q., Baumgartl, T. and Weatherley, D., 2013. RunCA: A Cellular Automata Model for Simulating Surface Runoff. AOGS 10th Annual Meeting. Brisbane, Australia, 24 – 28 June 2013.

Shao, Q., Baumgartl, T. and Weatherley, D., 2012. Development and initial testing of a surface runoff simulation model based on Cellular Automata. Joint Australian and New Zealand Soil Science Conference. Hobart, Australia, 2 – 7 December 2012.

Shao, Q., 2011. Understanding, Measurement and Prediction of Infiltration-runoff Processes on Rehabilitated Mined Land. 3rd annual SMI RHD Conference. Sustainable Minerals Institute, University of Queensland, Brisbane, Australia, 22 – 23 November 2011.

Publications included in this thesis

Shao, Q. and Baumgartl, T., 2014. Estimating Input Parameters for Four Infiltration Models from Basic Soil, Vegetation, and Rainfall Properties. Soil Science Society of America Journal, 78(5), 1507-1521, doi: 10.2136/sssaj2014.04.0122. ***– Incorporated as Chapter 3****.*

Contributor	Statement of contribution
Qi Shao	Designed experiments (80%) Analysis and interpretation of data (90%) Wrote and edited paper (90%)
Thomas Baumgartl	Designed experiments (20%) Analysis and interpretation of data (10%) Wrote and edited paper (10%)

Shao, Q. and Baumgartl, T., 2015. Field Evaluation of Three Modified Infiltration Models for the Simulation of Rainfall Sequences. Soil Science (submitted and under review). ***– Incorporate as Chapter 4****.*

Contributor	Statement of contribution
Qi Shao	Designed experiments (80%) Analysis and interpretation of data (90%) Wrote and edited paper (90%)
Thomas Baumgartl	Designed experiments (20%) Analysis and interpretation of data (10%) Wrote and edited paper (10%)

Shao, Q., Weatherley, D., Huang, L. and Baumgartl, T., 2014. RunCA: A Cellular Automata Model for Simulating Surface Runoff at Different Scales. Journal of Hydrology (submitted and under review). ***– incorporated as Chapter 5 and Chapter 6****.*

Contributor	Statement of contribution
Qi Shao	Model development (80%)

	Analysis and interpretation of data (90%) Wrote and edited paper (85%)
Dion Weatherley	Model development (10%) Wrote and edited paper (5%)
Longbin Huang	Wrote and edited paper (5%)
Thomas Baumgartl	Model development (10%) Analysis and interpretation of data (10%) Wrote and edited paper (5%)

Shao, Q., Saynor, M., Lowry, J., Lu, P. and Baumgartl, T., 2015. Simulating Surface Runoff Using a Cellular Automata Approach: a Case Study from the Ranger Uranium Mine. Earth Surface Processes and Landforms (submitted and under review). ***– Incorporated as Chapter 7****.*

Contributor	Statement of contribution
Qi Shao	Field measurement (70%) Analysis and interpretation of data (70%) Wrote and edited paper (80%)
Mike Saynor	Field measurement (20%) Analysis and interpretation of data (15%)
John Lowry	Analysis and interpretation of data (10%)
Ping Lu	Field measurement (10%) Analysis and interpretation of data (5%) Wrote and edited paper (5%)
Thomas Baumgartl	Wrote and edited paper (10%)

Shao, Q., Baumgartl, T., Huang, L. and Weatherley, D., 2014. A Cellular Automata-based Run-off Model and its Application in Mined Land Rehabilitation Designs. Proceedings of Life-of-Mine 2014 Conference, Brisbane, Australia: 81-96. – ***Incorporated as Chapter 8****.*

Contributor	Statement of contribution
Qi Shao	Model development (80%) Analysis and interpretation of data (90%) Wrote and edited paper (90%)
Thomas Baumgartl	Model development (10%)

	Analysis and interpretation of data (10%) Wrote and edited paper (10%)
Longbin Huang	Model development (5%)
Dion Weatherley	Model development (5%)

Contributions by others to the thesis

Energy Resources of Australia Ltd (ERA) constructed the trial landform at Ranger Uranium Mine, installed soil moisture probes on this landform and collected the soil moisture data. The Supervising Scientist Division set up the runoff plots on this trial landform, produced the Digital Elevation Maps of these plots, installed the instruments for rainfall and runoff monitoring, and collected, processed and supplied the rainfall and runoff data. Infiltration measurements on this landform were the joint effort of University of Queensland, Charles Darwin University and ERA.

Dr Thomas Baumgartl made great contributions to the interpretation of experimental data and critically revised the draft of the thesis.

Statement of parts of the thesis submitted to qualify for the award of another degree

None

Acknowledgements

Throughout my PhD ‘adventure’, there is a long list of people I wish to thank and acknowledge. Without them, this journey would not have been so enjoyable, rewarding and worthwhile.

On the top of the list, I would like to express my sincere gratitude to my supervisors for your guidance and constant support, in particular, Dr Thomas Baumgartl for the trust, freedom and the abundant opportunities you have given me in exploring and pursuing my own research interest. You have never failed to provide time, advices and necessary resources when I needed them. It is a great honour to work with you. My thanks also go to Dr Dion Weatheley, who trained me C++ from the beginning with great patience and enthusiasm and gave me valuable guidance on the modelling work. I am also grateful to Dr Longbin Huang for your kindness, encouragement and invaluable academic comments and suggestions to improve my work.

I gratefully acknowledge the assistance of many people in the field experiments. The rainfall simulation trials could not have been conducted without the technical support of Dr Rob Loch and Tim Loch from Landloch Pty Ltd. or the aid of Vinod Nath from Centre for Mined Land Rehabilitation (CMLR). I would also like to thank Dr Mike Saynor and John Lowry from Supervising Scientist Division, Dr Ping Lu and Graeme Passmore from ERA and Jillianne Segura from Charles Darwin University for the collection and processing of the field data at Ranger Uranium Mine.

I would like to thank Prof David Mulligan for supporting my PhD application and allowing me to have such a great opportunity to study at CMLR. My research would not have been possible without the financial assistance from the China Scholarship Council, University of Queensland International Scholarship (UQI), Sustainable Minerals Institute (SMI) and CMLR.

I would like to extend my acknowledgements to all my friends and colleagues in SMI. Yumei, Chris, Nisha, Jiajia, Shirley, Vinod, Sven, Mingrui, Fang, Allen, Shasha and Zhengyu, thank you all for your friendship, encouragement and endless support in both my study and life.

Last but not least, I am so grateful to Mum and Dad for your unconditional love and support through my entire life. You have inspired me to achieve my goals. I hope I have made both of you proud. I wish to express my heartfelt appreciation to my dear wife, Jingjing, who has left everything behind to marry me and come to Australia, for your love, understanding, sacrifices and company.

Keywords

surface hydrology, rehabilitated landforms, infiltration, rainfall simulation, hydrological modelling, surface runoff, cellular automata, model validation

Australian and New Zealand Standard Research Classifications (ANZSRC)

ANZSRC code: 040608, Surfacewater Hydrology, 60%
ANZSRC code: 050305, Soil Physics, 30%
ANZSRC code: 050207, Environmental Rehabilitation (excl. Bioremediation), 10%

Fields of Research (FoR) Classification

FoR code: 0502 Environmental Science and Management, 70%
FoR code: 0406 Physical Geography and Environmental Geoscience, 30%

Table of Contents

List of Figures

List of Tables

List of Abbreviations

CA	Cellular Automata
CMLR	Centre for Mined Land Rehabilitation
DEM	digital elevation map
ERA	Energy Resources of Australia Ltd
eriss	Environmental Research Institute of the Supervising Scientist
GIS	Geographic Information System
IMHR	improved modified Horton infiltration model
Max.	maximum value
MGA	modified Green-Ampt infiltration model
MHL	modified Holtan infiltration model
MHR	modified Horton infiltration model
Min.	minimum value
PC	principle component
PCA	principle components analysis
PTF	pedotransfer functions
RS	remote sensing
RunCA	Runoff Model Based on Cellular Automata
SCS	the U.S. Soil Conservation Service
SD	standard deviation
SMI	Sustainable Minerals Institute
TDR	time-domain reflectometer
UQ	the University of Queensland

List of Symbols

A	soil water transmissivity (mm h^{-1})
a	a constant in Holtan infiltration model ($mm^{-0.4}$ h^{-1})
Clay	clay content (<0.002 mm) (g g^{-1})
Cover	vegetation cover (m^2 m^{-2})
D	control zone depth (mm)
Depth	top soil depth (m)
DR	total soil drainage volume (mm)
d_t	soil drainage rate (mm h^{-1})

EF	Nash-Sutcliffe efficiency
F	total flow for each cell (mm)
f	actual flow amount from central cell to neighbour cell (mm)
f_0	total outflow from central cell (mm)
f_p	potential flow amount from central cell to neighbour cell (mm)
Gravel	gravel content (2.0-5.3 mm) (g g^{-1})
h	water depth in the central cell (mm)
Height	vegetation height (m)
i_0	initial infiltration rate (mm h^{-1})
i_f	final steady infiltration rate (mm h^{-1})
INF	total infiltration volume (mm)
i_p	infiltration capacity (mm h^{-1}) at time t
I_t	cumulative infiltration (mm) at time t
i_t	infiltration rate (mm h^{-1}) at time t (h)
k	infiltration decay coefficient in Horton infiltration model (h^{-1})
K_s	saturated hydraulic conductivity (mm h^{-1})
L	cell side length (m)
LAI	leaf area index
N	number of observations during the prediction period
n	Manning's roughness coefficient
O_i	observed value at comparison point i
$\bar{O}$	arithmetic mean of observed values
P	a constant in Holtan equation
P_{cum}	cumulative interception (mm)
PE	percentage of error (%)
PE-I	percentage error in total infiltration volume
PE-TR	percentage error in total runoff volume (%)
PE-θ_0	percentage error in initial soil moisture
P_{max}	maximum interception storage capacity (mm)
P_i	predicted value at comparison point i
$\bar{P}$	arithmetic mean of predicted values
Q_p	peak discharge rate (mm h^{-1})
Q_t	total discharge (mm)

r	Pearson correlation coefficient
R_1	initial rainfall intensity (mm h^{-1})
R^2	coefficient of determination
Rain	rainfall intensity (mm h^{-1})
RC	runoff coefficient (%)
R_{cum}	cumulative rainfall (mm)
R_e	effective rainfall (mm)
R_i	input rainfall (mm)
RMSE	root mean square error
Root	root content (g/100cm^3)
R_t	rainfall intensity (mm h^{-1}) at time *t*
S	soil water storage potential in Holtan infiltration model (mm)
s	water surface slope
S_0	sorptivity (mm $h^{-0.5}$)
Sand	sand content (0.02-2.0 mm) (g g^{-1})
SAT%	initial saturation degree (%)
Silt	silt content (0.002-0.02 mm) (g g^{-1})
Slope	slope gradient (%)
Stone	stone content (>5.3 mm) (g g^{-1})
S_t	soil storage potential at time *t* (mm)
S_t'	cumulative soil water amount at time *t* (mm)
T	time for water to travel from central cell to neighbour cell (s)
T_p	time to peak (min)
θ_0	initial water content (cm^3 cm^{-3})
θ_{FC}	field capacity (m^3 m^{-3})
θ_s	saturated water content (cm^3 cm^{-3})
λ	a constant in modified Green-Ampt infiltration model (mm)
ρ_b	bulk density (g cm^{-3})
ϕ	porosity (m^3 m^{-3})
ψ_f	suction at the wetting front (mm)
Δt	time step for calculation (min)

Chapter 1 Introduction

1.1 Problem statement

An increasing area of land is disturbed by human activities, such as mining. In order to minimise the serious and long-lasting environmental and social impacts brought by these disturbed landforms, there is a requirement to implement rehabilitation practices following the disturbance. For example, the Australian and New Zealand Minerals and Energy Council (ANZMEC) and the Minerals Council of Australia (MCA) jointly published the Strategic Framework for Mine Closure (ANZMEC 2000), which states that the mining industry is responsible for rehabilitation of mine disturbance in an environmentally and socially acceptable way. Each State and Territory government in Australia also regulates mining impacts through the authorisations for mine leases, such as the Environmental Authority (EA) issued by the Queensland Department of Environment and Resource Management (DERM) under the *Environment Protection Act 1994*.

Rehabilitation is defined as "the process of reshaping and revegetating land to restore it to a stable landform" (EPA, 2006), and the four general goals for rehabilitation are (1) safe to humans and wildlife; (2) non-polluting; (3) stable and (4) able to sustain an agreed post-mining land use (Protection, 2014). To reach these objectives, over the past decades considerable effort has been made toward the rehabilitation of the disturbed landforms, and major advances have been achieved in the rehabilitation technologies. However, there are still major challenges ahead, with an important one being the long-term stability of the rehabilitated landforms.

Since most geographic, topographic, pedologic and vegetative parameters contributing to the surface hydrology of the natural landforms are altered during the reconstruction and rehabilitation phases, the hydrological processes in the rehabilitated landforms are greatly changed from their original conditions (Darmer and Dietrich, 1992; Guebert and Gardner, 2001). Typically, large amount of destruction and reconfiguration of the landscape may result in many elevated man-made structures (e.g., waste rock dumps) with steep and straight outer slopes are created, the surface infiltration capacities are decreased due to the disruption of the soil profile (Jorgensen and Gardner, 1987; Lemieux, 1987), and the vegetation cover is reduced especially at the early phases of rehabilitation (Majer, 1989). All these would contribute to the significant increase in the quantity of the surface runoff (Ritter and Gardner, 1993; Sabey and Kitt, 1982). These altered surface hydrological behaviours may cause serious environmental consequences (Figure 1.1), including:

Soil erosion

Erosion by water is one of the major consequences of increased surface runoff. Erosion features would have a great impact on the land use planning and management. An intense soil erosion may also result in the exposure of encapsulated contaminants in the rehabilitated landforms, and the channels created by erosion may in turn increase the runoff volume.

Downstream degradation

The adverse impact of elevated levels of runoff and erosion can even extend to offsite areas by transmitting pollutant rapidly in both soluble and particulate forms. For instance, spoil substrate, waste rocks or tailings containing harmful minerals or ions, which are exposed to the environment through the mining process, can be transported by overland flow to the surrounding area and pollute waterways. The subsequent degradation of downstream water quality would have negative impacts on surrounding environment and communities (Evans, 2000).

Landform instability

Excessive runoff can cause the land to be unstable and prone to environmental disasters such as landslide and debris flows. More seriously, elevated runoff could render the catastrophic destruction of waste containment facilities, such as the collapse of waste rock dumps and breakage of tailings dams, and hence release of large amount of waste materials to the environment and pose profound threats to the environment and the safety of local residents.

Revegetation failure

Accelerated runoff would also lead to the increased loss of top soil, nutrients and fertilizer, as well as the water deficit which may both cause the revegetation failure and biodiversity loss in these rehabilitated landforms (Haigh, 1992; Kapolka and Dollhopf, 2001; Nicolau and Asensio, 2000).

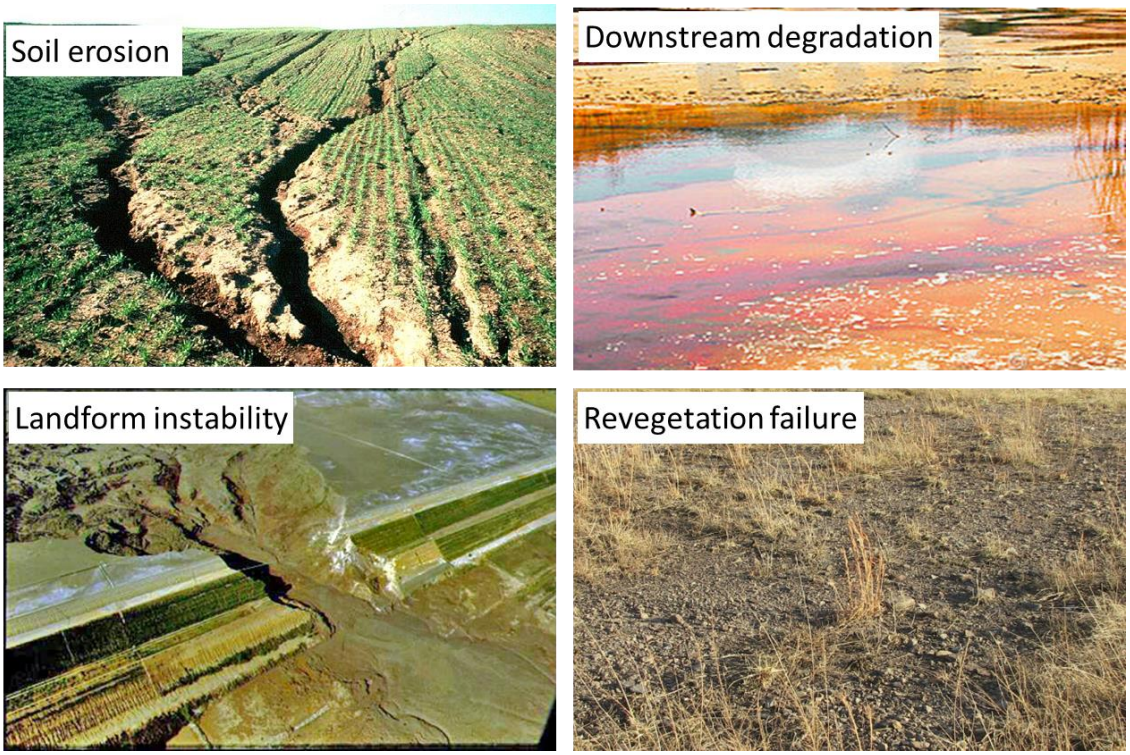

Figure 1.1 Environmental consequences caused by increased surface runoff in the rehabilitated landforms (source: Google images).

These consequences would be more serious in the regions of high rainfall intensity and amount, where the detrimental runoff events are more likely to occur. Recent studies have also identified the increased frequency of extreme precipitation events and the increased rainfall intensity in many regions around the world due to the climate change and human activities (Berg et al., 2013; Gordon et al., 1992; Jones et al., 2013; Min et al., 2011; Suppiah and Hennessy, 1998), which leads to an increasing risk of surface runoff. Therefore, appropriate rehabilitation planning, including landform design and revegetation strategies, together with the suitable water management, are required to minimize these potential harmful consequences caused by runoff. This requires the knowledge of major influencing factors and their effects on the surface hydrology. Many uncertainties, however, still remain in this area. It is also essential to determine the infiltration characteristics and to identify the sources and the magnitude of surface runoff in the rehabilitated landforms. While numerous relevant studies have been carried out in the agricultural, forestry and other natural systems, limited effort has been made towards the disturbed environment such as the mining areas. It is therefore unclear that whether the hydrologic theories, principles and relationships established in the natural environment would be applicable to the rehabilitated environment. Besides, most of existing hydrologic models were primarily developed for the simulation of natural hill-slopes or catchments, and they tend to produce unexpected errors when

applied to the rehabilitated landforms because of the changed spatial or temporal scales and complexities. These research gaps therefore motivated the research presented in this work to improve the understanding of surface hydrological processes in rehabilitated landforms and to develop an effective model for runoff prediction, on the basis of a critical review of research findings in literatures, utilization of Cellular Automata (CA) theory and principles, and data acquired from field experiments conducted at different scales.

1.2 Research Aim and Objectives

The key aim of this study is to provide supportive information to achieve long-term stability of rehabilitated landforms by improving rehabilitation design and water management on the basis of well understood and predicted surface hydrological processes and properties.

To achieve this aim, there are four key research objectives:

1) To identify major controlling factors of infiltration process and quantifying their relationships with infiltration parameters in small scale trials.
2) To evaluate the performance of modified infiltration models for the simulation of complex rainfall situations.
3) To develop a more effective and universal surface runoff model by incorporating the evaluated infiltration models and linking them to Cellular Automata theories.
4) To simulate the surface hydrological processes in rehabilitated landforms using the developed runoff model.

The hypothesis and assumptions of this research:

- Performance of infiltration models can be evaluated by the infiltration experiments conducted on small scale plots using the rainfall produced by the field rainfall simulator, and their input parameters can be quantitatively predicted from relevant soil, vegetation, and rainfall properties.
- The production and distribution of the infiltration-excess runoff in the rehabilitated landforms can be simulated by linking the surface hydrologic properties (e.g., infiltration) with the Cellular Automata (CA) method.

1.3 Thesis outline

This thesis is structured into nine chapters. It shows the development of a novel Cellular Automata runoff model on the basis of evaluated infiltration models, and demonstrates its validation at different scales and application to the rehabilitated landforms. Figure 1.2 is a flow chart outlining the structure of the thesis and links the thesis chapters to the research objectives.

Chapter 1 introduces the problems associated with the surface hydrology in the rehabilitated landforms, based on which the research aim and objectives are proposed.

Chapter 2 reviews literature on general principles and affecting factors of surface hydrology, current methods for modelling infiltration and surface runoff, and the basic theories of Cellular Automata. Several research gaps are then identified.

Chapter 3 and **Chapter 4** are both based on the rainfall simulation experiments conducted on small scale field plots, with the purpose to investigate the infiltration behaviours and models. Specifically, Chapter 3 focus on the evaluation of four classical infiltration models and the estimation of their input parameters from basic affecting factors, while Chapter 4 is related to three modified infiltration models and the evaluation of their performance under complex rainfall conditions.

On the basis of the evaluated infiltration models in the previous two chapters, in **Chapter 5** a Cellular Automata based surface runoff model is developed by incorporating these infiltration models. Its performance is then validated at different spatial scales in **Chapter 6**.

After the initial validation, in **Chapter 7** the developed runoff model is further applied in a case study to assess the runoff performance on a rehabilitated landform of a mine site. In **Chapter 8** some hypothetical scenario analysis is conducted to discuss the application of this runoff model in different aspects of mined land rehabilitation designs.

Chapter 9 summarises the major findings and contributions and analyses the limitations of this study, based on which further research is recommended.

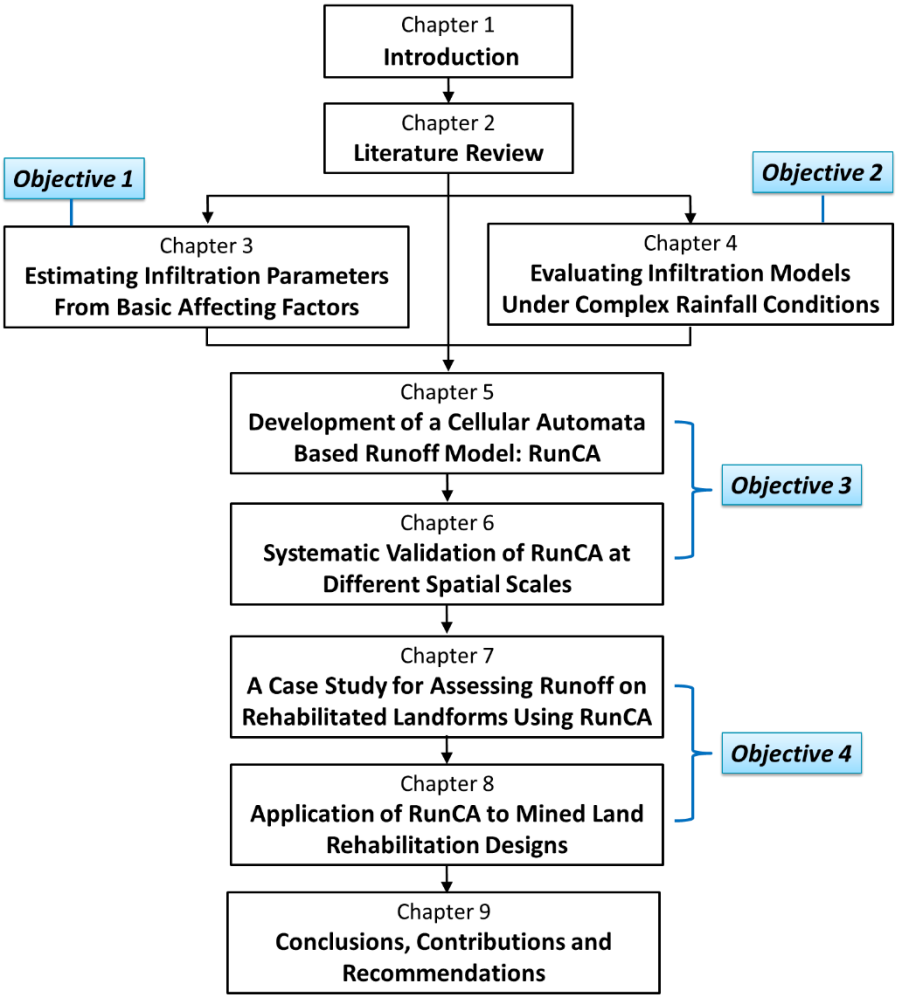

Figure 1.2 Flow chart of the thesis structure, linking the thesis chapters to the research objectives.

Chapter 2 Literature Review

The following literature review explains the basic principles in surface hydrology, analyses the hydrological behaviours in rehabilitated landforms, summarises the factors that control surface hydrological processes, discusses existing prediction models for both infiltration and surface runoff, and introduces the basic theory and application of Cellular Automata.

2.1 Surface Hydrological Processes

Figure 2.1 demonstrates the typical surface hydrological processes on the natural landforms. When precipitation occurs, a portion of rainfall may be intercepted by vegetation, while the remaining amount may fall onto the ground surface and entre the vadose zone of the soil through an infiltration process. Similarly, water stored in the soil may return to atmosphere by the evapotranspiration process. When the rainfall rate exceeds the infiltration capacity of surface soil, excess water will run off on the ground surface and thus the infiltration-excess runoff occurs. The infiltrated water will contribute to the increase of soil moisture, and when the soil is saturated, the saturation-excess runoff may take place. Subsurface flow may also occur dependent on soil properties and topographic conditions, and in some occasions subsurface water would return to the ground surface and contribute to the surface runoff.

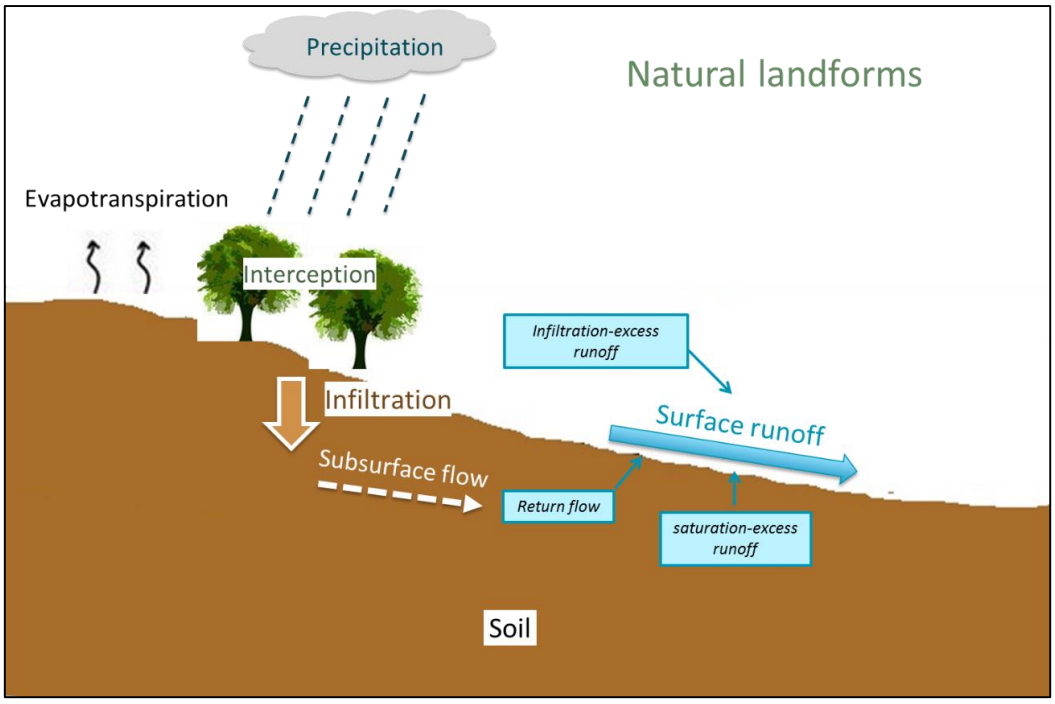

Figure 2.1 Typical surface hydrological processes on natural landforms.

It can be seen that while precipitation is the major driving factor for the surface hydrology, infiltration is the major regulator in this process as it determines how much water will enter the soil layer and how much would flow over the ground surface. Surface runoff is the major consequence which may cause some environmental issues, such as soil erosion, pollutant transport and others. Therefore, these two important components, surface runoff and infiltration, are discussed in more detail in the following sections.

2.1.1 Mechanisms of surface runoff generation

In order to well understand and predict the surface runoff in a study area, it is essential to identify how and when runoff is produced. In fact, runoff can be generated along several distinctively different paths, depending on climatic factors, topography, soil characteristics, vegetation and geology. There are basically three major runoff generation mechanisms as shown in Figure 2.1.

2.1.1.1 Infiltration-excess runoff

The infiltration-excess runoff, also known as the Hortonian runoff, was first described by Horton (1933) and further investigated by Chorley (1978). It occurs when the rate of the incoming precipitation exceeds the infiltration capacity of the soil (Dunne, 1978). More specifically, during a rainfall event and especially at the beginning phase, when the infiltration capacity of the soil is greater than the rainfall rate, all the rainfall will infiltrate into soil and no runoff occurs. The infiltrated water increases the water content at the surface, leading to a reduced infiltration capacity. When the infiltration capacity becomes less than the rainfall rate, ponding at the surface occurs and will become surface runoff once the depressions on the soil surface are filled. Then the surface runoff can be estimated as the difference between the infiltration rate and rain rate. According to the criteria reported by Freeze (1980), the necessary conditions for the generation of infiltration-excess runoff are: (1) Rainfall rate is greater than the saturated hydraulic conductivity of the soil, and (2) Rainfall duration is longer than the required time to ponding for a given initial soil water profile. Therefore, this type of runoff usually occurs in areas where infiltration is restricted or the water table is deep. It is the dominant flow path in many arid and semi-arid regions where surface vegetation is absent or sparse, and in association with thin soil profiles and high exposure to rainfall impact resulting in low infiltration capacity. In humid regions, occurrence of this mechanism is also quite common, when rainfall intensities are high enough.

2.1.1.2 Saturation-excess runoff

Runoff also occurs when the soil becomes saturated, and any additional incoming precipitation cannot infiltrate the saturated areas and hence becomes overland flow. Surface runoff occurring as a result of these saturated areas is referred to as saturation-excess runoff, also known as the Dunne mechanism (Dunne and Black, 1970). The areas prone to saturation usually have shallow water table levels or interflow levels, or shallow soil layers underlain by a low-permeable and restrictive zone (e.g., bedrock for natural landforms and tailings for rehabilitated mining landforms). All these conditions result in small soil storage capacities. Therefore, precipitation infiltrating into the soil raises the water table or interflow levels, fills the soil pores and leads to surface saturation. At any time less than the time to saturation, the infiltration rate is equal to the rainfall rate and there is no runoff. At a time equal or greater than the time to surface saturation, the storage capacity of the soil is filled resulting in no infiltration, and for such situations, all rainfall generates runoff.

Saturation-excess runoff has been identified as the most important flow process in humid forested catchments (Dunne and Black, 1970). It has also been described as the dominant flow process for areas of convergent flow (hollows) within a catchment area (Anderson and Kneale, 1982), as well as in groundwater discharge areas within a forested wetland site (Waddington et al., 1993).

2.1.1.3 Subsurface runoff and return flow

In some cases, the infiltrated water may also run laterally below the ground surface. This flow is called subsurface runoff which would most likely occur in areas with relatively steep hill-slopes that had permeable soil overlying an impermeable layer (e.g. bedrock) (Whipkey, 1965). Subsurface runoff could become surface runoff not only by intersecting a stream channel, but also by returning to the surface as return flow if the within-mantle downslope route is restricted by the subsurface outcropping or a saturated area. The contributions to catchment discharge via this mechanism can be the direct subsurface flow discharge via a seepage face into a channel or stream, or more importantly, subsurface runoff can create expanded saturated areas where saturation overland flow and return flow occur (Anderson and Burt, 1990).

Different runoff generation mechanisms result in quite distinct hydrographs. The infiltration-excess hydrograph displays short lag times and times to peak, steep rising and recession limbs and high instantaneous peak discharge. Hydrographs for catchments where saturation-excess runoff predominates are similar to infiltration-excess hydrographs when antecedent soil moisture conditions are high, otherwise, there is a longer lag time and time to peak due to the delay as the soil saturate. Subsurface runoff hydrographs are generally of lower instantaneous peak intensity, the peak is delayed with longer lag times and the rising and recession limbs are gradual (Dunne, 1978). However, different

runoff mechanisms can exist in a heterogeneous landscape at the same time and the timing and shape of the hydrograph is a composite of the dominance of the different flow pathways.

2.1.2 Roles of infiltration in regulating surface hydrology

Infiltration process determines the quantity of incoming precipitation which becomes surface runoff or contributes to soil moisture or groundwater (Dunne, 1978). Previous studies have found that for a given hill-slope or catchment, the dominant runoff process is regulated by soil infiltration capacity (also known as infiltrability), which is the rate at which water enters at the soils surface, and is expressed in units of cm min^{-1} or mm h^{-1} (Shukla et al., 2004). For example, Martinez-Mena (1998) observed that infiltration-excess runoff mechanism occurs in the more degraded areas with low organic carbon content (< 0.5%) and low infiltrability (< 5 mm h^{-1}), while a saturation-excess runoff mechanism occurs in the less degraded areas with a high organic carbon content (> 2%), high infiltrability (> 8 mm h^{-1}) and covered by a dense plant cover (> 50%). The field studies conducted by Zhu et al. (1997) concluded that the observed spatial non-uniformity of runoff generation is a result of the spatial variability in soil infiltration capacities. In humid areas, this variability is mainly attributed to spatial differences in soil moisture while in semi-arid and arid areas, it is mainly controlled by rainfall characteristics and the surface soil physical properties (Lavee and Yair, 1987). Because of its important role in regulating the surface hydrological processes, it is essential to investigate the infiltration characteristics in a study area.

2.1.3 Surface hydrological processes in rehabilitated landforms

The surface hydrological processes in rehabilitated landforms may be dramatically altered from those in the natural landforms due to the extensive disturbance during the rehabilitation process. Typically, in order to minimise the 'footprint' of waste materials generated from, for example, the mining process, many man-made structures, such as waste rock dumps, are often built as elevated structures with steep and straight outer slopes (Figure 2.2) which may result in high surface runoff rates. The vegetation cover is often small especially in the early stage of rehabilitation, leading to reduced interception. In addition, the physical properties of the rehabilitated soils are dramatically altered from their natural condition, and exhibit increase in bulk density, decrease in soil depth, loss of soil structure, altered texture and reduction in porosity. Consequently, new rehabilitated soils have the infiltration capacities that can be an order of magnitude lower than those of surrounding undisturbed soils (Jorgensen and Gardner, 1987; Lemieux, 1987), and are considered to have relatively high runoff potential. It has been

found that there is a greater volume of surface storm runoff, up to 55% of rainfall per event, on rehabilitated mined land compared to less than 10% on non-mined pasture in central Pennsylvania (Ritter and Gardner, 1993). Since infiltration into newly rehabilitated soils is characteristically low, surface runoff is likely to be dominated by the infiltration-excess overland flow (Jorgensen and Gardner, 1987; Lemieux, 1987; Ritter and Gardner, 1993). Figure 2.2 shows the typical surface hydrological processes in the disturbed and rehabilitated landforms, where the infiltration-excess runoff generation mechanism contributes to the majority of surface runoff, while the other runoff generation paths, such as the saturation-excess runoff and subsurface runoff, are negligible.

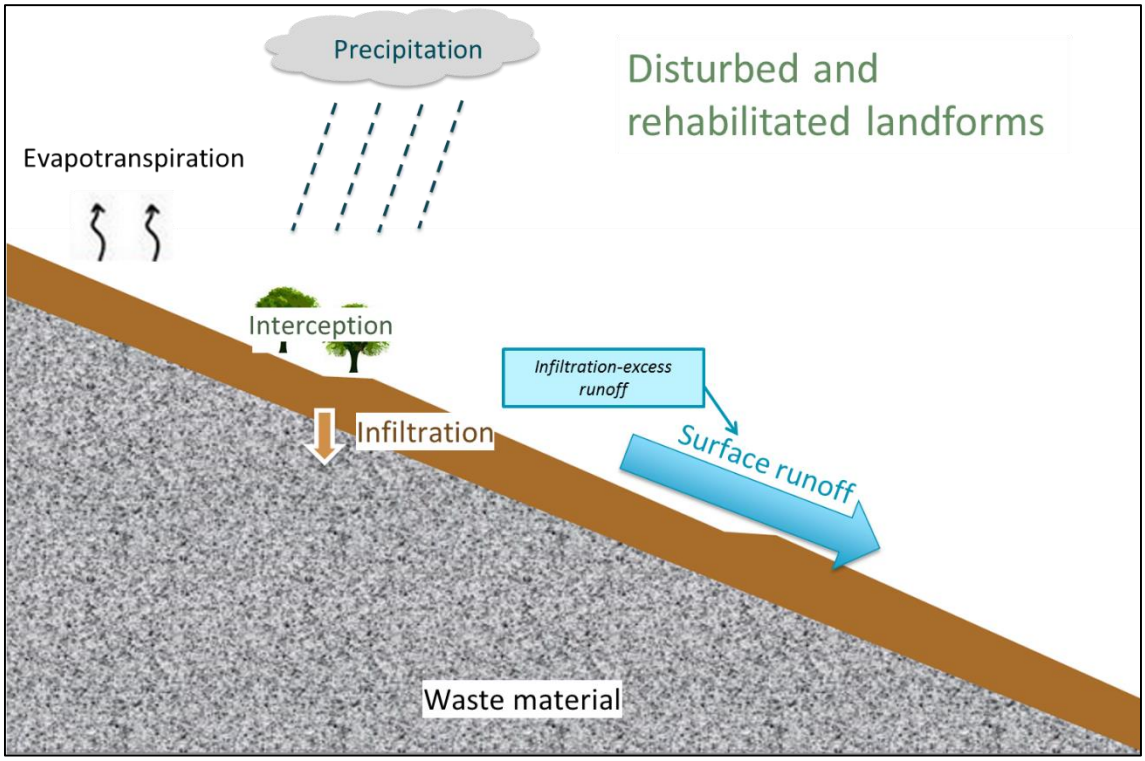

Figure 2.2 Typical surface hydrological processes on rehabilitated landforms.

Nevertheless, Schroeder (1987) identified time since rehabilitation as a factor in the reduced surface runoff from rehabilitated areas in North Dakota, where surface runoff from a 7-year-old rehabilitated field was lower than that from an adjacent 4-year-old site, and was comparable to the natural grassland site when the soil profile was dry. Also, as vegetation establishes and pedogenic processes begin, alterations in soil characteristics may increase infiltration rates in rehabilitated areas (Jorgensen and Gardner, 1987), and the dominant runoff path would likely change in response to increased infiltration. For example, in a rehabilitated catchment in Pennsylvania (Guebert and Gardner, 1992), infiltration rates increased steadily over four years to near pre-mining levels. The tracer dye research and the

hydrographs analysis in this area both indicated that the dominant runoff path changed from infiltration-excess runoff to subsurface runoff through large macropores, and more of the discharge volume was attributed to saturation-excess runoff than infiltration-excess runoff.

While a relatively complete theoretical system is available for the surface hydrological processes on the natural landforms, there is a lack of relevant studies for the disturbed and rehabilitated landforms where the hydrological behaviours can be significantly different. Some well-established methods and models in the natural environment may not suit this altered environment. Therefore, more specific in-depth investigations are required to understand and predict the surface hydrology in these rehabilitated landforms. The characterisation of the infiltration process and the identification of the dominant runoff generation mechanisms are the foundation for this purpose, which would, however, also demand the knowledge of the factors and their effects on these processes that are discussed in the following section.

2.2 Factors Influencing Surface Hydrology

From above discussion we can see that the hydrological processes are rather complex, especially, the infiltration characteristics and runoff behaviours are highly variable in space and time. This complexity and variability is largely associated with the heterogeneous distribution of various affecting factors, and the knowledge of the sources and patterns of variation in these processes and their affecting factors is crucial for understanding and modelling the hydrological functioning (Mayor et al., 2009), and guiding the water and soil management in these environments.

A lot of studies have been performed to identify the affecting factors and determine their relationships with infiltration and runoff processes, and important advances have taken place in recent decades. Some experiments were carried out in the laboratory under simulated rainfall for the identification of singular parameters influencing the runoff processes, including slope length (Bryan and Poesen, 1989), surface roughness (Gómez and Nearing, 2005) and rainfall intensity (Römkens et al., 2002). Small plot studies ($\leq 1m^2$) with rainfall simulations have been widely used, especially in semi-arid Spain, where the investigations include the vegetation patches, landscape types, antecedent soil moisture conditions and their interacted effects on infiltration and runoff (Mayor et al., 2009), soil and topographic controls on runoff generation (Wilcox et al., 2007), and the role of soil surface components (vegetation, rock outcrop, fracture, and soil crust) in regulating infiltration-runoff processes (Li et al., 2011). At the same time, large plot ($\geq 10m^2$) simulations have also been used. For example, four large-scale rainfall simulation experiments were conducted on different shrub lands and an abandoned site to determine hydrological characteristics in relation to spatial patterns in soil, vegetation and morphology

(Bergkamp et al., 1996). A study using simulated rain and overland flows was carried out on a 6-km-long bund constructed in Australia for assessing the rehabilitation of mining areas with special regard to infiltration and erosion susceptibility and to parameterise simulation models (Loch, 2000b; Loch et al., 2000). In addition, the hydrological processes at hill-slope and catchment scales have also been monitored and studied: Cammeraat (2004) found that runoff depth and runoff coefficient of hill-slopes were significantly correlated with rainfall intensity and depth and antecedent 20-day precipitation; Kirkby et al. (2002) identified the influence of land use, soils and topography on the delivery of hill-slope runoff to channels.

From the studies carried out at different scales, the hydrological processes can be concluded to be affected by various factors and parameters. Generally, these controlling factors can be summarised into five categories, including climate, soil properties, surface condition, topography and vegetation, which will be discussed in details as follows.

2.2.1 Climate

In different climate zones or under various weather conditions, the hydrological behaviours within a catchment may be quite different, due to the impacts of climate characteristics, like precipitation, temperature, wind, solar radiation and seasonal variation. Rainfall and seasonal variation would have the greatest influences on catchment hydrology since they are directly related to infiltration and runoff processes.

2.2.1.1 Rainfall characteristics

Rainfall, as the most important component of precipitation and a major source of water flow, has a large influence on the hydrological behaviour. There are several characteristics that can describe rainfall events.

Rainfall intensity

Rainfall intensity is one of the most common rainfall properties. Cook (1946) noted a dependence of infiltration rate on rainfall intensity and attributed it to more complete ponding of the surface. On some soils, infiltration rate is negatively correlated with rainfall intensity because of the development of surface seals (Mclntyre, 1958). However, on soils which do not form seals, infiltration rate increases with rainfall intensity because of the tendency for higher rainfall intensities to exceed the saturated hydraulic conductivity of larger proportions of the soil surface and thereby to raise the spatially averaged hydraulic conductivity (Dunne et al., 1991). Moldenhauer et al. (1960) examined rainfall and

runoff records from plots during natural rainstorms, and found the φ index ((total storm rainfall - total storm runoff)/duration of excess precipitation) to be strongly dependent on rainfall intensity. Hawkins (1982) reviewed other published interpretations of rainfall and runoff records and concluded that the proportion of a drainage basin generating overland flow would increase as rainfall intensity increased.

Kinetic energy

Usually, a certain amount of rainfall could occur in two different forms: rainfall over a long period of time with low intensity and short time intervals of rainfall with high intensity, with the kinetic energy per unit mass varying considerably during a single rainfall event. Foley (1991) simulated both high energy and low energy rainfall events by placing a mesh screen 10 cm above the soil surface to absorb raindrop energy. Kinetic energy of high energy rain was of the order of 33 J m^{-2} mm^{-1} (Marston, 1980), while under the mesh, kinetic energy was greatly reduced. In this test, significantly greater infiltration rate occurred under low energy rain than under high energy rain, and this marked reduction in infiltration associated with high energy rain was typically described as surface sealing. Aggregate breakdown and soil surface compaction by raindrops has been strongly correlated with increasing rainfall energy over a range of soils (Bradford et al., 1987).

Additionally, some other rainfall properties, such as cumulative rainfall, rainfall amount, raindrop size, rainfall depth and duration have also been used to describe rainfalls. Based upon these characteristics, rainfall events could be classified into different types to identify their impacts on runoff and erosion. For instance, 130 erosive rainfall events were grouped into four rainfall types based on precipitation depth, duration and maximum 30-min intensity in red soil region of southern China, with erosive rainfall type I being the group of rainfall events with low intensity, high frequent occurrence and very short duration, while type IV consisting of rainfall events with the highest intensity, the longest duration and infrequent occurrence. Erosive rainfall type II and III, however, were composed of rainfall events which have moderate rainfall characteristics (Huang et al., 2010).

2.2.1.2 Seasonal variations

Seasonal variation is another important climate factor that would affect the hydrological functions. For example, seasonal variations in soil surface state and soil moisture can lead to large shifts in soil hydrological responses as investigated for Mediterranean climate conditions, where in general the soil hydrological responses were slower during the transition between winter and spring and were characterised by higher infiltration, which could be explained by the occurrence of freeze–thaw cycles that disrupt the soil surface and increased soil porosity (Cerdà, 1997; Regüés and Gallart, 2004). In contrast, faster responses and subsequent decreases in infiltration rates took place throughout the year

until autumn, which can be explained by soil surface consolidation (associated to crusting), due to the occurrence of subsequent storms until summer, and a later increase in soil moisture at the beginning of autumn (Torri et al., 1999).

2.2.2 Soil properties

Previous studies have verified that soil properties play an important role on hydrological processes. For instance, the mechanisms of runoff generation have been found to depend on soil properties such as organic carbon, soil substrate (Martinez-Mena et al., 1998), soil depth (Mayor et al., 2009) and initial soil moisture (Calvo-Cases et al., 2003). Generally, the soil properties include both physical and hydraulic properties. The soil physical properties also have various sub-factors such as soil texture, bulk density, total porosity, macropore density and soil depth, while the soil hydraulic properties include sub-factors like hydraulic conductivity, water retention characteristics and initial water content. Some of these properties have been widely investigated for many years, as discussed below.

2.2.2.1 Soil texture

Soil texture is determined by particle size distribution, and is an important factor in determining infiltration rate and infiltrated volume from rehabilitated surface-mined catchment (Jorgensen and Gardner, 1987). Ekwue (2009) observed that infiltration was highest in sandy loam, followed by clay loam and the lowest in clay soil. The reverse was obtained for surface runoff, with the clay soil maintaining a far greater surface runoff than the clay loam and the sandy soil. But Willard (2010) did not achieve similar results, with no relationship found between fine particles and runoff/infiltration production, however, the role of rock sized particles (> 2mm) was emphasised in his study. It was suggested that as the percentage of rocks increased, runoff decreased and infiltration increased, because the larger diameter of rock particles compared to fine soil particles created a larger proportion of coarse pores which favoured infiltration.

2.2.2.2 Bulk density

Meek et al. (1992) found that an increase in bulk density from 1.6 Mg m^{-3} to 1.8 Mg m^{-3} decreased average infiltration rates by 54% in a sandy loam soil. It is concluded that compacted areas with high bulk density start contributing to runoff first during the rainfall event at the field scale, and as the duration of storm increases, areas with less compaction and low to medium bulk density become saturated depending upon the storm duration and intensity (Gupta, 2003). Soil compaction, a process by which soil particles are rearranged into a denser state, was found to be the most important factor

affecting bulk density of a certain soil. This is commonly caused by natural forces or human-induced mechanical loads such as wheel traffic and tillage (Ekwue and Harrilal, 2010). It leads to the increase in bulk density and thus reduction in soil porosity, aeration, macro-porosity and hydraulic conductivity (Tekeste et al., 2006). As a result, infiltration decreases while surface runoff increases.

2.2.2.3 Macropores

Macropores in natural soils, whether created from root channels, burrowing animals and insects, freeze-thaw cycles and/or the dissolution of minerals, are continuous openings with diameters ranging from 0.001 to >0.5 cm that permit channelized, preferential flow (Beven and Germann, 1982). Macropores may represent only a small percentage of the surface area of a soil (< 1%) and are generally undetected by bulk density measurements. Yet, they greatly increase the rate of infiltration by increasing the volume of storage that must be filled before surface runoff is initiated and by providing an important pathway for the quick preferential flow (Beven and Germann, 1981). Aubertin (1971) found that the infiltration rate of forest soils was significantly influenced by macropores, which served as the primary mechanism influencing the progression of runoff towards streams. Guebert (2001) also concluded that macropores have a profound effect on the increase of infiltration and shallow subsurface flow of water on a rehabilitated surface mine.

2.2.2.4 Soil depth

Soil depth is a crucial factor particularly in the case of very shallow soils or shallow water tables. Since the storage capacity of these soils is small, vertical percolation and subsurface flow may cause soil to become saturated throughout its depth, and ponding and saturation-excess runoff will occur at the time when no further soil water storage is available. The relatively rapid saturation of the entire soil profile could mask the influence of other factors on the infiltration rates, especially the final steady infiltration rates. Some studies have found that the increasing soil depth increases infiltration, and that small changes in soil depth can have a large impact on infiltration rates (Mayor et al., 2009; Wilcox et al., 1988).

2.2.2.5 Initial soil water content

Several studies have reported lower infiltration rates and higher runoff coefficients under wet versus dry soil conditions (Cerdà, 1997; Simanton and Renard, 1982). Gupta (2003) observed that runoff generation areas increased with an increase in the initial soil water content on a field scale. Soil moisture may also indirectly impact the hydrological processes by affecting other controlling factors such as the stability of soil aggregates (Boix-Fayos et al., 1998) due to its relevance to the capillary

head distribution, hydraulic gradient, soil hydraulic conductivity and mobility of fine particles (Mualem et al., 1990).

Besides of those factors discussed above, some other soil properties are also related to infiltration and runoff processes. For example, Descroix et al. (2001) and Huang (2010) found that soil organic matter content was negatively correlated with runoff. In addition, some soil amendments have been used to improve the soil hydrologic properties. Peat was found to be able to increase saturated hydraulic conductivity and reduce bulk density, consequently increasing the infiltration capacity of the soils and reducing runoff (Ekwue and Harrilal, 2010). Sawdust was added to a bentonite mine spoil and was proven to have effects on increasing soil structural stability and permeability, leading to a higher infiltration rate on the spoil amended with sawdust (Voorhees, 1986).

2.2.3 Surface conditions

The ground surface conditions, including stone cover, crust cover, roughness and fractures, are key explanatory variables for the hydrological behaviour, especially on bare soils. Mayor et al. (2009) found that these surface properties explained part of the variation in runoff rates and time to runoff, especially in the case of dry soils. Results of rainfall simulation studies carried out by Li (2011) confirmed that soil surface characteristics played a dominant role in controlling runoff and infiltration at plot scale in karst landscapes.

2.2.3.1 Rock fragments

Recently there has been a growing interest in soils containing abundant rock fragments. Rock fragments are stones and soil particles 2 mm or larger in diameter and include all material that has horizontal dimensions smaller than a pedon (Miller and Guthrie, 1984). Some researchers noted an increase in infiltration and a reduction of runoff and erosion with the effect of rock fragments under both laboratory and field conditions (Adams, 1966; Lavee and Poesen, 1991; Sanchez and Wood, 1987). This can be explained by several reasons. Firstly, the cover of rock fragments influences the underlying soil by increasing organic matter content and porosity, improving aggregation, reducing bulk density and preventing the formation of crusts, consequently enhances infiltration. Then, a stony surface favours more rapid infiltration and deeper penetration also because the contact between the rock fragments and the soil matrix favours a faster and deeper flow (Poesen et al., 1990). Besides, the rock fragments can intercept large quantities of rain and absorb part of it, especially where the rock fragments are weathered (El Boushi and Davis, 1969). Another reason is the greater roughness caused by rock fragments, which slows runoff and enhances infiltration. For example, Cerdà (2001) found

that the times necessary to transform the ponding into runoff and the surface runoff into runoff outlet increase with greater rock fragment cover due to the greater soil roughness, and Meyer et al. (1972) observed that on cultivated land, surface runoff is reduced from 40.6 cm s^{-1} on bare soils to 2.54 cm s^{-1} on soils covered with fragments.

Nevertheless, other authors found a negative relation between the rock fragment cover and the soil hydrological response (Abrahams and Parsons, 1991; Wilcox et al., 1988). Li et al. (2011) observed no runoff at plots where rock fragments rested on the soil surface, but relatively large runoff at plots where rock fragments are usually embedded in the surface, and concluded that when rock fragments were embedded in the surface, they contributed to the establishment of a continuous crust which inhibited infiltration and promoted runoff. Therefore, the effects of rock fragment position and size in the profile, as well as the structure of the fine earth on runoff production could be the reasons for the contrasting effects of rock fragment on infiltration and runoff found by different researchers (Poesen et al., 1990).

2.2.3.2 Surface sealing/crust

Surface runoff can be mainly the result of crust formation on some soil surfaces during rainstorms. Basically two different types of crusts can be formed on a soil surface, pioneer biological crusts of cyanobacteria and lichens and the mechanical crust caused by rain. The latter rainfall induced soil surface sealing is more common, and its effects on infiltration has been studied under laboratory conditions and in some field experiments (Al-Qinna and Abu-Awwad, 1998; Fattah and Upadhyaya, 1996). Crust formation is a result of raindrop impact over the soil surface and of aggregate dispersion (McIntyre, 1958). McIntyre found the crust to consist of two distinct parts: an upper skin seal attributed to compaction due to raindrop impact and a "washed-in" zone of reduced porosity attributed to fine particle movement and accumulation. The permeability of deeper layers was about 800 times that of the "washed-in" layer and about 2000 times that of the skin seal. Sealing would therefore cause problems such as low infiltration rate, large amount of runoff and erosion. Experimental work has revealed that a large number of soil properties, including aggregate size distribution, initial bulk density, texture (Tarchitzky et al., 1984) and chemical conditions (Shainberg, 1992) would affect seal formation. The rainfall characteristics, i.e., intensity, kinetic energy, and electrical conductivity (Baumhardt, 1985), as well as the initial water content distribution in the sealing soil profile (Le Bissonnais and Singer, 1992), were also found to play a role in shaping the seal properties and the corresponding infiltration curve.

2.2.4 Topography

Topography controls the generation of runoff on hill-slopes and the delivery of hill-slope runoff to the stream valley. Researchers have observed that surface topography influenced both the location of runoff generation areas and the transport of subsurface and surface runoff (Anderson and Burt, 1978; Dunne et al., 1975). The final landscape features of a rehabilitated landform determine the stability of the re-contoured hill-slope, the stability of the catchment channel and the shape of the storm hydrograph. Since the cost of re-contouring represents a major cost in rehabilitation of mined land, and a small change in the degree and length of slope can have a major impact on the cost of re-contouring the landscape (Bonta, 1991), it is essential to have a precise understanding of the consequence of topography on hydrological behaviour.

2.2.4.1 Slope gradient and length

From observations on an experimental field, Gupta (2003) concluded that areas with moderate to high slopes (> 3%) firstly became runoff contributing areas as compared with areas having a flatter slope (< 3%). This was explained by the fact that a flatter slope has longer contact time for runoff to infiltrate into soil. Fox et al. (1997) also found that infiltration was lower and runoff was higher with increasing slope gradients due to more rapid runoff velocities. However, increased slope gradient does not consistently translate into increased surface runoff. Warrington et al. (1989) investigated the effect of slope angle and addition of phosphogypsum on infiltration and runoff, and they reported no obvious relationships between slope angle and percentage of runoff for the untreated plots, but when phosphogypsum was added, runoff decreased with increasing slope angle. Also, surface runoff from a rehabilitated hill-slope with a 0.8% gradient was higher than that from a rehabilitated hill-slope with a 6.8% gradient (Schroeder, 1987). The uncertainties in relationships between slope gradient and surface runoff may be due to the effects of some other factors, such as soil compaction and vegetation, which may override the effects of topography. Another reason is explained by Dunne et al. (1991) that the runoff depth increases when the slope gradient or length is increased. As a result, more of the microtopographical high areas along the hill-slopes are inundated with surface runoff. These areas, which can be mounds of vegetation, have greater infiltration rates than the depressional areas between the vegetation mounds. As a result, the apparent infiltration rate increases with the greater runoff depth downslope.

2.2.4.2 Slope shape and aspect

Form or shape of a landscape also influences water flow. Some previous studies have shown that convex or linear slopes tended to have higher rates of runoff than concave or S-shape slopes (Hancock,

2004; Toy and Chuse, 2005; Willard, 2010). This can be explained by the fact that the runoff velocity may decrease downslope as the gradient decreases on a concave or S-shape hill-slope (Willard, 2010). The decreased flow velocity allows longer time for runoff to infiltrate into the soil and thus reduces the runoff rate. In addition, convergent zones generally produced greater stream discharge per unit catchment area than divergent or straight zones because they increased the potential to transfer greater volumes of water as saturation-excess runoff at the base of the hill-slope to the stream valley (Eerkes, 2003).

Hydrologic processes also vary depending on slope aspect. Since soil temperature, transpiration rates, and evaporation rates vary across the landscape in association with changes in topographic position (Pierson et al., 2002), slope aspect affects soil moisture of the hill-slopes and therefore surface runoff.

2.2.4.3 Micro-topography

In addition to the topographic characteristics of large scales such as hill-slope or landscape, the local micro-topography also has significant impact on infiltration and runoff generation. For instance, micro-topography can attenuate and delay surface flows, because surface depressions first need to be filled until a specific surface water storage threshold is exceeded and surface flow towards the stream channel can be initiated (Antoine et al., 2009). Micro-topography was found to strongly affect runoff directions, velocities and depths and result in surface runoff along well defined micro-channels in the overland flow simulation studies conducted on small plots with micro-topography (Esteves et al., 2000).

2.2.5 Vegetation

Vegetation has been found to have great influence on surface hydrology. Higher infiltration and lower runoff was measured on vegetation patches compared to bare soils by small plot studies (Dunne et al., 1991; Wilcox et al., 1988). Some studies have also concluded that runoff rates and peak flows are reduced by vegetation in agricultural, pastoral (McIvor et al., 1995) and reforested areas (Ranjith B, 1995), as well as on rehabilitated mined soils (Loch, 2000a).

2.2.5.1 Effects of vegetation

Vegetation can influence hydrological processes by affecting rainfall interception, infiltration, evaporation and soil water storage. The impact of vegetation in explaining high infiltration rates and low runoff rates observed by various studies can be attributed to a number of direct and indirect effects.

Rainfall interception

Plant canopies split rainfall into different components (interception, throughfall and stemflow), modifying the volume and intensity of the effective rainfall reaching the soil surface. Surface runoff can be reduced because well grown vegetation can intercept large amounts of rainfall. For example, Owens et al. (2006) found that Ashe juniper canopy cover intercepts approximately 40% of total precipitation during a moderate precipitation event, and can increase to 96% with a decrease in rainfall intensity and duration. Vegetation canopy and litter-fall can also protect the soil surface against the impact of raindrops, reduce their kinetic energy (Deuchars et al., 1999), stimulate the formation and stabilization of soil aggregates (Zuazo and Pleguezuelo, 2009), prevent surface sealing (Foley et al., 1991), and consequently enhance infiltration.

Soil improvement

The differences in the hydrological behaviour between bare and vegetated areas are also attributed to the general improvement of the soil structure made by plants, which typically increase soil organic matter and aggregate stability (Blackburn, 1975), improve macropores (Bergkamp et al., 1996), and decrease bulk density and penetration resistance (Greene, 1992). These improved soil physical properties under vegetated patches are generally translated into higher infiltration rates and lower runoff compared with adjacent bare soils (Puigdefábregas, 2005).

Surface roughness

The increase of infiltration and decrease of runoff can also be explained by the greater surface roughness caused by vegetation. On hill-slopes, vegetation plays an important role in decreasing the average velocity of flow, increasing its residence time and allowing significant post-storm infiltration to decrease runoff volumes (Dunne and Dietrich, 1980). Similarly, a well vegetated channel also provides resistance to overland flow and allows more time for surface runoff to infiltrate (Harms, 1996).

2.2.5.2 Vegetation coverage

Although vegetation has been realised to have great impacts on the hydrological function, the specific relationships between vegetation coverage and infiltration or runoff are not very clear yet. For example, Marston (1952) and Kincaid et al. (1964) failed to discover any simple relationship between vegetation cover density and infiltration capacity measured with infiltrometers, whereas Smith and Leopold (1942) documented large changes in infiltration with only modest changes in vegetation density. Littleboy et al. (1996) found a linear relationship between straw cover and runoff curve number, while the data from the study of Loch (2000a) showed a curvilinear response at the lower levels of vegetation coverage. However, the determination of optimum vegetative cover thresholds which ensure the

biological control of hydrological processes has been stressed for the rehabilitation of both natural and man-made landscapes, with several studies in natural Mediterranean environments showing that runoff increases drastically when vegetation cover drops below 30% (Francis and Thornes, 1990), and the restoration of 50% cover with herbaceous vegetation being decisive by some researchers for site stabilization in human-made systems (Andrés and Jorba, 2000; Loch, 2000b).

2.2.5.3 Vegetation types

In addition to vegetation coverage, some research suggested that different vegetation types, vegetation structure or plant species composition could also be expected to result in different hydrological behaviours (Tian et al., 2003). However, results from previous studies are not conclusive about the importance of plant types in controlling runoff. A 5-year record of discharge for the forest and grassland catchments at Puckapunyal showed a consistent pattern of forest producing lower peak discharges and significantly less runoff than grassland (Burch et al., 1987). Bochet et al. (2006) found that *Anthyllis cytisoides*, an open-canopy shrub, was significantly less efficient than the tussock grass *Stipa tenacissima* and *Rosmarinus officinalis* shrubs in reducing runoff volume under its canopy. On the contrary, Quinton et al. (1997) found few significant differences in the abilities of six vegetation types in controlling runoff in south-east Spain. The effects of vegetation types have been concluded by some researchers to be attributed to the differences in ground cover and plant morphologies which affect the redistribution of incident rainfall, as well as the extent of the amelioration of soil properties under different vegetation types (Bochet et al., 1999; Hidalgo et al., 1997).

2.2.6 Uncertainties in the affecting factors

Although a large number of studies have been carried out for many years in looking for the affecting factors of surface hydrologic processes and great improvement has been made, there are still many uncertainties and unsolved problems in this area due to the complexity and variability of the surface hydrology. Some of them are listed here for further discussion.

2.2.6.1 Inconsistent findings

Through the discussion in this section, it can be seen that some findings or conclusions from different researchers about which factors and how they affect the hydrological behaviours are not consistent or even contradictory. For example, whether rainfall intensity is positively or negatively related to infiltration rate, which parameters could best represent the effects of soil physical property, whether rock fragment will increase or decrease the runoff, if increased slope gradient could contribute to

increased runoff amount, how different slope shapes affect hydrological processes, what kind of relationship exist between vegetation cover and runoff, whether there is significant impact of vegetation types on infiltration-runoff processes, among others, remain unclear yet. This impedes the better understanding and predicting of the surface hydrological processes, and thus further efforts need to be made by pedologists, hydrologists and ecologists to answer these questions.

2.2.6.2 Interactions among different factors

Most of previous studies focused on the influence of a single factor or several separate factors, but in fact, these factors are not separated from each other, but closely correlated. For instance, rainfall characteristics have impacts on many other factors, such as sealing formation, soil moisture, vegetation cover and types. Soil properties could affect plant growth, while vegetation development could in turn change soil properties. The surface condition, like rock fragment, could influence the underlying soil. The slope gradient and aspect would cause the variation in soil water content and consequently the vegetation distribution. Vegetation could also prevent sealing, increase surface roughness and change the micro-topography. In addition to the interactions among these factors, their sub-factors are affecting each other as well. For example, the sub factors of soil properties, such as texture, bulk density and porosity, are related to each other, with clay usually having high bulk density and low porosity, while sand responds opposite. Rock fragments have great influence on crust formation, one other sub factor of surface condition. Different vegetation types may also have different effects on surface hydrology because of their differences in vegetation coverage. These interactions among the affecting factors would increase the complexity and difficulty in explaining the hydrological behaviours and thus partially contribute to some inconsistent findings from different studies.

2.2.6.3 Dominant factors at different spatial scales

The hydrological processes at different scales have been found to be dominated by different features. Some factors, dominant at large spatial scales, may become relatively unimportant at a small spatial scale (Haggett et al., 1965), while other features relevant at the small scale may become insignificant at larger scales (Schultz, 1994). At the small scale, there may be little heterogeneity of these affecting factors, and with an increase in scale, the heterogeneity may become obvious and random, but if the scale continues increasing, the heterogeneity will become more systematic. Specifically, at a small unit area (1 m^2), the soil, vegetation, topography and precipitation are considered homogeneous in space, and the hydrological process tends to be dominated by soil properties, vegetative characteristics, rainfall intensity and duration. At the hill-slope scale, soils and vegetation are likely to be variable over the area, and runoff tends to move in uneven rivulets controlled by micro-topography and vegetation

pattern, and the hydrologic response is dominated by soil properties, vegetation distribution, precipitation intensity and slope characteristics (inclination, profile and aspect). At the catchment scale, most of the affecting parameters are considered to be heterogeneous, even the spatial distribution of rainfall can be significant, and topographic and vegetative features start to have more impact on runoff distribution and catchment response. However, insufficient effort has been made towards the dominant parameters and their effects on the hydrological processes at different scales. Inconsistent conclusions from different studies may be due to the fact that they were carried out at different scales. These scale issues also lead to problems in hydrologic modelling that a model developed from a scale may produce unexpected errors when applied to a different scale.

2.2.6.4 Quantification of relationships

Most of the previous studies were limited in the qualitative description of the influence of affecting factors, such as "slope with greater gradient generates greater runoff", "vegetation patches increase infiltration", "stone cover changes the surface hydrology" and so forth. Just a few of them, such as that conducted by Li et al. (2011), have tried to develop linear regression equations for predicting runoff coefficients using data analysis methods like principle components analysis and stepwise linear regression analysis. The quantification of the impacts of these affecting factors is therefore very deficient, and considerable efforts need to be further made to quantify these relationships, which is essential for predicting the hydrological behaviours.

2.3 Infiltration Modelling

As mentioned before, infiltration of water into soils is one of the most important components of hydrological processes occurring at the soil-atmosphere interphase, since it determines how much water will enter the unsaturated soil zone, and how much will flow over the ground surface as runoff. Thus the ability to quantify infiltration is of great importance in water resource management. Prediction of flooding, erosion and pollutant transport all depend on the rate of runoff which is directly affected by the rate of infiltration. Therefore, accurate methods for characterizing infiltration are required.

2.3.1 Classical infiltration models

Numerous attempts have been made to model the infiltration process that a number of classical infiltration models have been developed through the past century. They can be basically categorized into physically based and empirical models.

2.3.1.1 Physically based models

Physically based models rely on the law of conservation of mass and the Darcy law, and assume the soil media as capillary tubes, infiltrating water into the whole porous media. The parameters of these infiltration models usually assign physical meanings, and can be obtained from soil physical properties such as soil hydraulic conductivity, soil porosity, soil water pressure head and soil water content. Examples of such models include the models of Green-Ampt, Philip, Mein and Larson, Smith and Parlange and Morel-Seytoux (Mishra et al., 2003), among which Green-Ampt model and Philip model have been used more frequently and will be discussed here because of their simplicity and wide spread use in hydrologic models.

Green-Ampt model

Green and Ampt (1911) developed the first physically based infiltration model for ponded and deep homogeneous soil profile conditions with uniform initial water content. It assumes a piston-type water content profile with a well-defined front, characterized by a constant pressure value. Using these hypotheses together with Darcy's law, the cumulative infiltration $I(t)$ can be expressed as equation (2-1):

$$I(t) = K_s t + (\theta_s - \theta_0)\psi_f \, ln\left[1 + \frac{I(t)}{(\theta_s - \theta_0)\psi_f}\right] \tag{2-1}$$

where t is time for infiltration (h), K_s is the hydraulic conductivity (mm h^{-1}) corresponding to the water content at natural saturation θ_s (cm^3 cm^{-3}), θ_0 is the initial water content (cm^3 cm^{-3}) considered to be uniformly distributed with depth, and ψ_f is the suction at wetting front (mm). Differentiating Eq. (2-1) yields the infiltration rate $i(t)$ (mm h^{-1}) at the soil surface:

$$i(t) = K_s\left[\frac{(\theta_s - \theta_0)\psi_f}{I(t)} + 1\right] \tag{2-2}$$

The values of K_s and $(\theta_s - \theta_0)$ in above equation could be derived from the hydraulic conductivity at natural saturation and the water-storage capacity, respectively. ψ_f cannot be measured directly, but it has been related in some theoretical way to soil characteristics or in a statistical way to textural soil properties. However, experience shows that such determination of ψ_f mostly generates large

imprecision on the calculated $I(t)$ values. Hence for field applications parameters are often estimated by empirical fitting. To that end, the equation can be rewritten as:

$$I(t) = K_s t + \lambda \, ln\left[1 + \frac{I(t)}{\lambda}\right] \quad \text{and} \quad i(t) = K_s\left[\frac{\lambda}{I(t)} + 1\right] \tag{2-3}$$

where $\lambda = (\theta_s - \theta_0)\psi_f$. Both parameters K_s and λ (mm) are considered as fitting parameter, and are free of any physical significance in such a case.

In spite of the many assumptions under which the Green-Ampt equation was originally developed, it has been adapted for use under a much wider variety of conditions. It produced reasonably good predictions for non-uniform soil profiles (Childs and Bybordi, 1969), and for soils with partially sealed surfaces (Hillel and Gardner, 1970). Its simplicity and adaptability to varying scenarios makes it a popular and widely used method for field applications. The physical significance of parameters and the ability to obtain their values from soil properties increases the attraction for this model. The Green-Ampt equation has been chosen for infiltration estimation in many physically based hydrologic models, such as WEPP (Laflen et al., 1991), SWAT (Tuppad et al., 2011), SWMM (Rossman, 2010), LISEM (De Roo et al., 1996), HEC-1 (Feldman, 1995) and ANSWERS-2000 (Bouraoui and Dillaha, 1996).

Philip model

Philip (1957a) developed an infinite-series solution to solve the non-linear partial differential Richards' equation (Richards, 1931) for a homogeneous deep soil with uniform initial water content under ponded conditions. The two-term Philip infiltration equations (Philip, 1957b) are:

$$i(t) = \frac{1}{2} S t^{-\frac{1}{2}} + A \quad \text{and} \quad I(t) = S t^{\frac{1}{2}} + At \tag{2-4}$$

where parameter S is referred to as the soil sorptivity (mm $h^{-0.5}$), and A is the soil water transmissivity (mm h^{-1}). Both S and A have physical meaning, with S indicating the initial capacity of the soil to absorb water and A controlling the equilibrium infiltration rate. They are both dependent on the soil properties and the initial water content, and can be determined from some soil physical properties. For example, S can be expressed in terms of saturated hydraulic conductivity, effective capillary drive and the difference between saturated and initial soil water content (Nachabe et al., 1997). Philip (1969) showed that A may take values between $0.38K_s$ and $0.66K_s$, and as time approaches infinity, A should approach K_s for a saturated soil. They can also be evaluated numerically using procedures provided by Philip (1957a), however, these solutions are too cumbersome for practical applications. Whisler and Bouwer (1970) found that determining their values from physical soil properties was very time consuming and yielded results that were not in agreement with the experimental curve. So in many

cases, the values of S and A are obtained by curve-fitting of Philip's model to infiltration data, but the physical significance of these parameters is lost by using this approach.

A shortcoming of the Philip infiltration model is that the assumptions for which the equation is applicable are rarely found in the field. Field soils are seldom homogeneous, but vary both spatially and with depth, and so do the vegetation and surface conditions. Consequently its reliability may reduce in practice, especially for larger areas such as catchments. Nevertheless, the Philip model has often been integrated in hydrologic models, including WATFLOOD (Kouwen, 2012) and HYSIM (Manley, 1993).

2.3.1.2 Empirical models

Another group of infiltration models are empirically based, as they do not give a physical insight into the infiltration process, but try to model the shape of the infiltration curve as well as possible (Van De Genachte et al., 1996). Empirical models are usually in the form of simple equations, the parameters of which do not have a physical meaning, and are derived by means of curve-fitting the equation to actual field or laboratory measurements of cumulative water infiltration. Examples of such models are the Horton, Holtan, SCS-CN, Kostiakov, Huggins and Monke, Mezencev and Collis-George models, among others (Mishra et al., 2003). Horton and Holtan models are the two most popular models.

Horton model

Horton model (Horton, 1940) is one of the most widely-used empirical infiltration models. It considers infiltration as a natural "exhaustion process", during which infiltration rate decreases exponentially with time from a finite initial value i_0 (mm h^{-1}) to a final constant value i_f (mm h^{-1}), as shown in the following equations:

$$i(t) = i_f + (i_0 - i_f)e^{-kt} \quad \text{and} \quad I(t) = i_f t + \frac{1}{k}(i_0 - i_f)(1 - e^{-kt}) \tag{2-5}$$

where k is the infiltration decay factor (h^{-1}). Although the Horton model is empirical in nature, it does reflect the laws and basic equations of soil physics. i_f refers to the same soil characteristic as the saturated hydraulic conductivity (K_s), and i_0 can be related to the initial soil moisture condition using a simple linear relation (Chahinian et al., 2005). Morel-Seytoux (1989) also related these parameters to the physically based parameters of the Green-Ampt model. However, for field applications, their values are often obtained from curve-fitting with the experimental data.

The Horton model has been employed in some hydrology models such as MARINE and SWMM (Chahinian et al., 2005) because it generally provides a good fit to data. However, it is somewhat

cumbersome in practice since it contains three constants that must be evaluated experimentally, and it does not adequately represent the rapid decrease of infiltration rate from very high values at a short period (Philip, 1957b). A further limitation would be that it is applicable only when rainfall intensity exceeds i_f.

Holtan model

Using a storage exhaustion concept, Holtan (1961) derived an infiltration equation expressed as:

$$i(t) = i_f + a(S_0 - I_t)^{1.4} \tag{2-6}$$

where S_0 is the storage potential of the soil above the impeding layer (mm) and a is a constant ($\mathrm{mm}^{-0.4}\ \mathrm{h}^{-1}$) dependent on soil type, surface condition and vegetation. S_0 can be computed from:

$$S_0 = (\phi - \theta_0)D \tag{2-7}$$

where ϕ is the total porosity ($\mathrm{cm}^3\ \mathrm{cm}^{-3}$) and D is the control zone depth (mm).

This model has been found to be suitable for inclusion in catchment models, such as LISEM, HEC-1 and ANSWERS (Beasley et al., 1980), and satisfactory progress has been reported for runoff predictions (Dunin, 1976) because of its soil water dependence. Nevertheless, a serious obstacle with this model is the determination of the control zone depth, D. Holtan and Creitz recommended using the depth to the plow layer or to the first impeding layer or depth of A-horizon, but Huggins and Monke found that the effective control zone depth varied depending on both the surface condition and the farming practices used for seedbed preparation (Turner, 2006). Therefore, in practical application this parameter is often determined by model calibration process.

2.3.2 Modified infiltration models for complex rainfall

Although various aforementioned infiltration models have been developed, a major limitation of them is that they were all developed from the ponding conditions, and thus are expected to be only valid for the single continuous rainfall events when the water supply rate is always larger than the infiltration capacity, in other words, when ponding occurs at all times. However, the natural rainfall events are not always constant and continuous, but often featured by temporally varied intensities and even several hiatus periods. Since these models express the infiltration capacity as a function of time or cumulative infiltration amount, they could only describe the decrease of infiltration capacity. In reality, however, the infiltration capacity would be also gradually recovered during dry periods because of the redistribution of soil moisture caused by the soil drainage or percolation to deeper layers and

evaporation. The inability of these classical infiltration models in describing the increase or recovery of infiltration capacity has constrained the application of many hydrologic models to event-based or short-term simulations, only. Some modification or improvement to the classical infiltration models is therefore required to make them applicable to more complex rainfall conditions. Some typical examples of the modified infiltration models are shown as follows.

2.3.3.1 Modified Horton model

To make the Horton equation applicable to complex rainfall conditions, Bauer (1974) introduced a soil drainage component to the original Horton model based on the concept that as the soil wets up, the rate of infiltration declines and the rate of percolation or drainage rises and minimum infiltration rate approximates to maximum drainage rate (Figure 2.3a). The drainage equation was then developed as:

$$d = i_f - i_f e^{-kt} \tag{2-8}$$

where d is the drainage rate (mm h^{-1}), i_f is the final steady infiltration rate (mm h^{-1}), and k is the infiltration decay factor (h^{-1}).

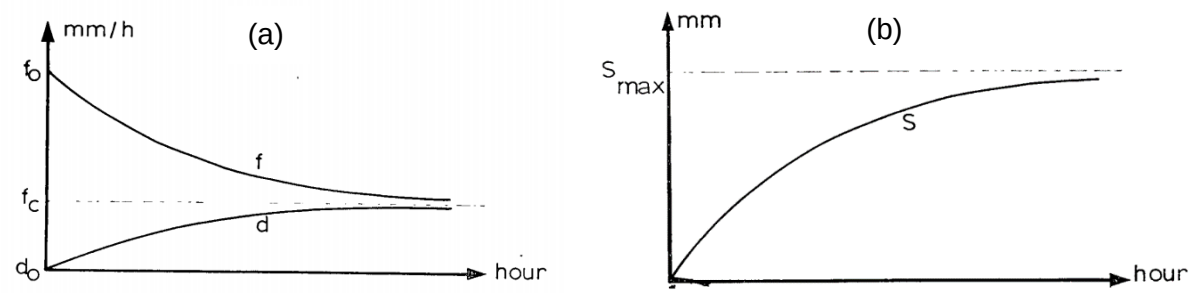

Figure 2.3 Infiltration and drainage capacity as a function of time (a) and soil water accumulation with time (b) in the modified Horton model (Bauer, 1974).

By expressing the change of soil water storage as the difference between the input infiltration and output drainage, the cumulative amount of soil water S_t' (mm) at time t (h) could be calculated as:

$$S_t' = \frac{i_0}{k}\left(1 - e^{-kt}\right) \tag{2-9}$$

where i_0 is the initial infiltration rate (mm h^{-1}). The resulting S_t' curve with time is shown in Figure 2.3b, from which it can be seen that as t approaches infinity, the soil gets saturated and the maximum soil water storage capacity S_{max} (mm) is:

$$S_{max} = \frac{i_0}{k} \tag{2-10}$$

Based on this concept, Aron (1992) further combined equation (2-8) and (2-9) and expressed the drainage rate as:

$$d = \frac{i_f}{i_0} k S_t' \tag{2-11}$$

Expressing the potential infiltration rate (infiltration capacity) i_p (mm h^{-1}) by combining equation (2-5), (2-8) and (2-9) results in:

$$i_p = i_0 + d - kS_t' \tag{2-12}$$

However, the actual/effective infiltration rate i_t (mm h^{-1}) does not always equal to i_p, as it is also determined by the water supply rate/available infiltration rate i_a (mm h^{-1}), which can be calculated based on the available water depth, consisting of both ponding depth and rainfall intensity:

$$i_a = \frac{R_t \Delta t + h_t}{\Delta t} \tag{2-13}$$

where R_t (mm h^{-1}) is rainfall intensity at time t, h_t (mm) is surface water depth at time t, and Δt (h) is the time increment. If the water supply rate exceeds the infiltration capacity, i_t will equal to i_p, otherwise it will equal to i_a.

Consequently, it can be seen that the major contribution of Bauer to the Horton model is introducing a drainage equation for water draining to deeper lying strata to allow the recovery of infiltration capacity, while that of Aron is further expressing both the infiltration and drainage rate as a function of soil water storage instead of time to make the model applicable at any time during a rainfall event, even when the water supply rate does not at all times exceed the infiltration capacity.

2.3.3.2 Modified Holtan model

In a similar way, Huggins & Monke (1966; 1968) introduced a soil water drainage component to the original Holtan model based on the assumptions that in the case of the soil water content being less than the its field capacity FC, no water will drain from the control zone, while when soil moisture exceeds FC, the water will move from the control zone at a drainage rate related to current soil storage potential S_t (mm), as expressed in equation (2-14):

$$d_t = i_f \left[1 - \frac{S_t}{(\phi - FC)D}\right]^3 \tag{2-14}$$

where ϕ is the total porosity. According to equation (2-7), S_t can be expressed as a function of current soil moisture θ_t: $S_t = (\phi - \theta_t)D$. Combining this formula and (2-14) and assuming ϕ equals to saturated soil water content θ_s, d_t can also be expressed by equation (2-15).

$$d_t = i_f \left[\frac{\theta_t - FC}{\theta_s - FC}\right]^3 \tag{2-15}$$

This equation shows that under the condition of saturation ($\theta_t = \theta_s$), water will move from the control zone at a drainage rate equal to the final steady state infiltration rate i_f. Thereafter the drainage rate will gradually decrease as the soil dries from the saturated state and finally reaches zero when the soil moisture equals to field capacity FC. As a result, the recovery of infiltration capacity can be described.

2.3.3.2 Modified Green-Ampt model

The original Green-Ampt model was modified to relate infiltration capacity to the cumulative soil water amount S_t' in ANSWERS-2000 (Bouraoui and Dillaha, 1996), where the equations developed by Savabi et al. (1989) were employed to calculate drainage rate when the soil moisture exceeds the field capacity. The drainage rate is calculated as:

$$d_t = D(\theta - FC)\left(1 - e^{-\Delta t / t_d}\right) \tag{2-16}$$

where Δt is time increment (h) and t_d (h) is time required for water to drain from an infiltration control depth:

$$t_d = \frac{\theta - FC}{K_A}\phi D \tag{2-17}$$

where K_A is the adjusted hydraulic conductivity rate (mm h^{-1}) which is calculated from:

$$K_A = K_s(\theta/\phi)^{-2.655/\log(FC/\phi)} \tag{2-18}$$

The incorporation of this soil drainage component enables the modified Green-Ampt model to describe both the decrease and increase in the infiltration capacity.

It can be seen that these modified infiltration models were basically developed from their original forms by expressing the infiltration capacity as a function of a soil storage condition related parameter that was not constrained by time. A soil drainage component was also employed in these models to take into account the recovery of infiltration capacity during dry periods. Despite of the similar conceptual basis and model structure, the specific formulas and parameters used in these models are totally different from each other. Therefore, they are expected to have varied performance and accuracies which need to be evaluated and compared by systematic tests.

2.3.3 Comparison of infiltration models

Numerous studies have been carried out to evaluate and compare the existing classical infiltration models. Swartzendruber and Youngs (1974) compared different physically based infiltration models and concluded that Philip's two-term equation was preferred over Green and Ampt's. Various empirical infiltration equations were evaluated by Parlange and Haverkamp (1989), and a best performance for Horton's equation was reported. Rawls et al. (1976) examined the infiltration models of Green and Ampt, Philip, Horton, and Hotlan, and found that the Horton model best represented the infiltration capacity curves. A similar result was observed in Chahinian's (2005) study, which showed that the Horton model had better overall performance over the Philip model. However, when Singh et al. (1992) evaluated the Horton and Philip models for determining the optimum slope of graded check borders, they revealed that the Philip model yielded values of slope closer to the observed field values than did the Horton model.

The above discussion shows that different results were obtained in different studies, thus there is no clear evidence which model is better and under what conditions. Basically, the physically based infiltration models usually apply the physical principles governing infiltration for simplified boundary and initial conditions, and are based on assumptions of uniform movement of water from the ponded surface downwards through deep homogenous soil with a well-defined wetting front. This physical basis on one hand enables the parameters to be obtained from soil water properties without measured infiltration data, but on the other hand, would also limit their applicability when the assumptions are not met in reality. For example, Mishra et al. (2003) found that the physically based models performed better on the soils tested in the laboratory than those tested in the field. The Philip model also performed worst in Ghorbani's (2009) study because a number of its pre-assumptions were violated when used in the field.

Empirical models tend to be less restricted by assumptions of soil surface and soil profile conditions. Their initial parameters are determined based on actual field-measured infiltration data, thus on heterogeneous field soils, empirical models may potentially provide more accurate predictions, as long as they are used under similar conditions to those under which they were developed. An example is that Gosh (1983) found the empirically based Kostiakov model to be better than the Philip model in fields with wide spatial variability in infiltration data. However, these models have less value as predictive tools when the parameter values are obtained from a site that differs significantly from the

site of application. Actual field measurements of infiltration are also required to determine these parameters, making these models less versatile.

While most of previous studies focused on the testing and comparison of the classical infiltration models using ponded water in infiltrometers or continuous rainfall, the systematic evaluation of the modified infiltration models under complex rainfall conditions is extremely lacked. This has greatly limited their application in the hydrologic models for the long-term simulation of the surface runoff behaviours.

2.3.4 Determination of infiltration parameters

As previously discussed, the developed infiltration models, especially some classical models, have been widely incorporated in hydrologic models for the determination of the infiltration process. Most of these hydrologic models have shown great sensitivity to the input parameter values in these infiltration models (Bingeman et al., 2006; De Roo and Jetten, 1999; Kannan et al., 2007; Nearing et al., 1990; Ritter, 1992; Zaghloul, 1983). Therefore, the precise determination of these infiltration parameters is essential for generating accurate prediction results.

The problem for the determination of infiltration parameters is the lack of any physical meaning of some fitting parameters in the empirical infiltration models and that they cannot be measured directly. They have to be determined through calibration with the actual infiltration data or from the suggested values from literature. The calibration process is time-consuming and the actual infiltration data is often unavailable in practice. Most of those suggested values, for example, the empirical parameter values in the Holtan model as suggested by Musgrave (1955) and Frere et al. (1975), were found to be very rough estimates that may lead to a large bias in an application (Turner, 2006). Even though some infiltration parameters with physical meaning can be obtained from direct laboratory or field measurements, they are always subject to measurement errors and uncertainty caused by the different measuring methods and the scaling effect. For example, the laboratory determined values of the saturated hydraulic conductivity, a common parameter for many infiltration models, have been found to vary significantly from field measured values (Mohanty et al., 1994; Reynolds et al., 2000). In addition, the distributed hydrologic models often require the inputs for each of a series of small spatial hydrologic elements. Due to the large spatial variability of the infiltration behaviour, it is time-consuming, costly and often impractical to directly measure the infiltration parameters as a large number of samples are required to be taken and analysed, and/or numerous *in situ* measurements are required to be conducted.

As an alternative, these infiltration parameters can be indirectly estimated from some more easily available or measurable controlling factors. Numerous studies have revealed that the infiltration process is influenced by various factors, however, most of them only qualitatively analysed the effects of these factors. A quantitative estimation for the parameters of infiltration models is very deficient, except for the Green-Ampt model. Some pedotransfer functions (PTF) have been developed to relate its parameters with soil texture and other simple soil properties (Ahuja et al., 1989; Brakensiek and Onstad, 1977; McCuen et al., 1981; Van den Putte et al., 2013; Zhang et al., 1995). These PTFs show great advantage in estimating the desired parameter values from already available basic soil data. However, they do not take into account other factors such as vegetation, topography and rainfall which also have great impact on infiltration parameters and bear some degree of uncertainty. Therefore, further efforts are required to explore the effects of other factors on the infiltration parameters and to quantify the relationships between them for the estimation of these parameter values.

2.4 Surface Runoff Modelling

2.4.1 Model classification

Various models have been developed for the prediction of the surface hydrological processes. They can be classified into different categories based on specific criteria. One important criterion is the ability of the model to describe the different components of surface hydrology conceptually or physically, another is the capacity to define the spatial description of large scale (e.g., catchment) hydrological processes as lumped or distributed (Refsgaard, 1996). In this respect, two typical model types are the lumped conceptual model and the distributed physically based model, as shown in Figure 2.4.

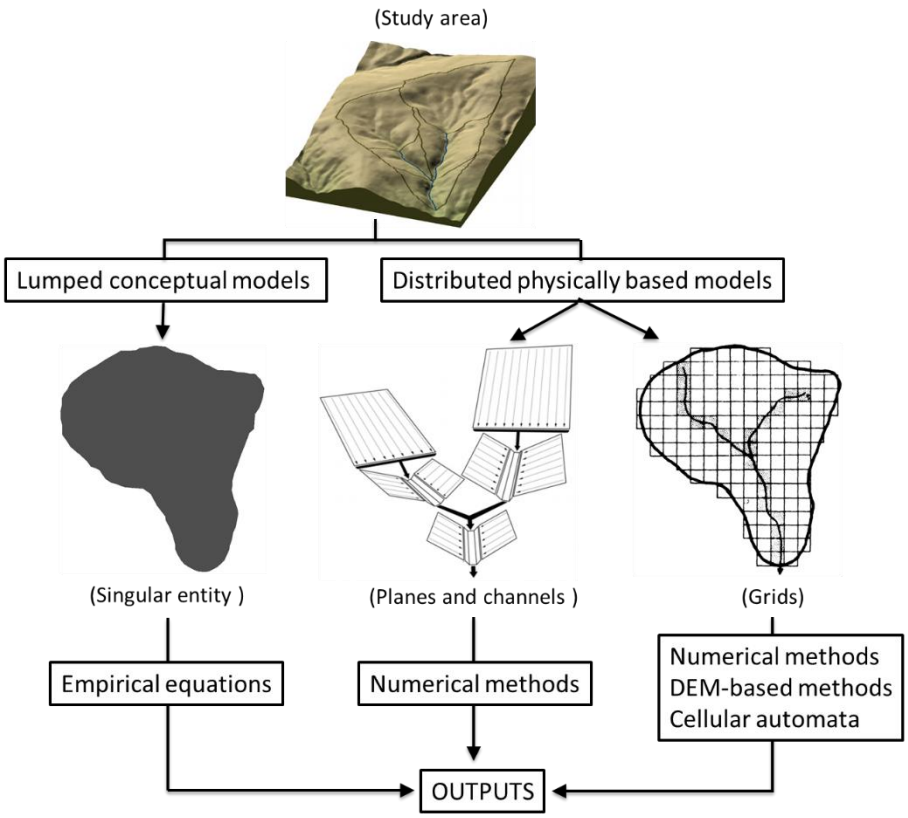

Figure 2.4 Schematic diagram for the structures of different types of hydrologic models.

2.4.1.1 Lumped conceptual model

Lumped conceptual models treat the study area as a spatially singular entity (Figure 2.4), use state variables that represent averages over the entire area, and produce output at a single point (Haan et al., 1982). This modelling procedure is based on establishing mathematical relationships or empirical equations between the input (precipitation) and the output (runoff) variables, usually by fitting the model to hydrologic data with an optimization technique. Typical examples of lumped conceptual runoff models (or erosion models that incorporate a runoff component) are the Stanford Watershed Model, the Sacramento (Jens Christian, 1997), SCS curve number (U.S. Department of Agriculture, 1972) and CREAMS (Knisel, 1980). Since they do not consider the complex physical processes, the primary advantage of this group of models is the computational efficiency, with relatively few input parameters required. However, the main disadvantage is clearly the loss of the spatial distribution information, and thus they do not have the capability of assessing the sensitivity of internal distributions of land use on runoff. Moreover, the parameters derived in this way can only be used to estimate the area that the model is calibrated with, and if the same set of parameters were to be used for time periods outside the calibration period, the prediction made by the model would be uncertain.

So great effort would be needed in model calibration if these models are applied to regions different from the location of first development.

2.4.1.2 Distributed physically based model

To better describe the extent of spatial and temporal variability of runoff processes, some distributed physically based models have emerged. They have a theoretical structure based upon physical laws, and usually make predictions by partitioning the target area into a number of hydrologic units supposed to be homogeneous in terms of their physical characteristics. For example, some of these models, including KINEROS (Smith, 1981), WEPP (Laflen et al., 1991), EUROSEM (Morgan et al., 1998b) and HEC-1 (Feldman, 1995), partition the target area (e.g., a catchment) using a network of elemental sections, such as a cascade of planes and channels (Figure 2.4). These elements are always simplified geometries with large sizes, which can provide a representation of the gross topographic features but may lose some local topography details and complexities. Defining these elements is sometimes an arbitrary process and requires professional experience, as different definitions may lead to large variations in the results. With the development of remote sensing, digital elevation models (DEM) and geographic information systems (GIS), grid structures (Figure 2.4) are more frequently used in the distributed models, with examples being ANSWERS (Beasley et al., 1980), AGNPS (Young et al., 1989), LISEM (De Roo et al., 1996) and SHE (Abbott et al., 1986). These grids usually have much smaller sizes than the geometric elements and provide an easier way to represent the study area. These models attempt to incorporate data concerning the areal distribution of controlling parameter variations in conjunction with computational algorithms to evaluate the influence of this distribution on simulated behaviour. Some of them would require development of many partial differential equations governing various physical processes and equations of continuity for surface water flow. A major advantage of this type of models is the ability to incorporate component relationships developed from small-scale studies to yield predictions on larger scales. Thus, distributed models are much less dependent on calibration data to adapt the model to widely differing geographic regions than are lumped models. Such models could increase the accuracy of the simulation, but this usually comes at the expense of increased computational and data preparation effort. So the main disadvantage of this strategy is the increase in model complexity and parameters parallel to the increase in partitioning. Nevertheless, since the various factors influencing the surface runoff, such as precipitation, soil, topography and vegetation, all have great spatial variations, a distributed physically based model is considered to be a better choice for describing and quantifying the complex, unsteady and non-uniform runoff processes occurring on a natural hill-slope or catchment.

In order to precisely simulate the surface runoff, two essential processes are required to be accurately determined. One is the runoff production process in each hydrologic element that determines how much of rainfall will become surface runoff, and the other one is the runoff distribution process among these elements that determines the movement of the excess precipitation over the land surface. These two components may appear in many different forms and degrees of complexity in different models, but they are always there in any distributed runoff model, together with the difficulty of clearly separating one component from each other.

2.4.2 Prediction of runoff production

The direct runoff is produced from the effective rainfall (sometimes called excess rainfall) which is neither retained on the land surface nor infiltrated into the soil. The difference between the input rainfall and the effective rainfall hyetographs is termed the abstractions or rainfall losses, which include: (1) Infiltration losses into soil; (2) Interception losses by vegetation or tree canopy; (3) Depression or hollow storage and (4) Evapotranspiration losses. In order to obtain a prediction of surface runoff it is necessary to quantitatively characterize all the components mentioned above.

2.3.2.1 Infiltration

Infiltration is the most important and also complicated component of the rainfall loss in many occasions. Its determination is therefore very essential and has been discussed in details in section 2.3.

2.3.2.2 Interception

The rainfall which is caught by vegetation prior to reaching the ground is referred to as interception losses. There are several factors influencing the amount of interception. The first one is the species, growth stage, and density of the vegetation. Interception is relatively important for the areas with dense vegetative canopies (e.g. forest covers), but plays a rather insignificant role in any areas barren of vegetation. Then the rainfall characteristics would also impact the interception that the relative effect of interception can be quite significant when runoff-producing events are rather small. In addition, the canopy is capable of holding a smaller interception volume as wind velocity increases (Donald and Michael, 1976; Haan et al., 1982).

To quantify the interception amount, Chow (1964) has developed an interception model which is of the form:

$$L = S + KEt \tag{2-19}$$

where L is the volume of water intercepted in inches, S the interception storage retained against the forces of wind and gravity, K the ratio of surface area of intercepting leaves to horizontal projection of the area, E the amount of water evaporated per hour during the rain period, and t the time in hours.

Aston (1979) also developed an equation to estimate the cumulative interception during a rainfall event:

$$P_{cum} = P_{max}\left[1 - exp\left(-0.046LAI\frac{R_{cum}}{P_{max}}\right)\right] \quad (2\text{-}20)$$

where P_{cum} is the cumulative interception (mm), R_{cum} is the cumulative rainfall (mm), LAI is the leaf area index, and P_{max} is the maximum interception storage capacity (mm) that can be estimated from LAI using the equation developed by Von Hoyningen-Huene (1981):

$$P_{max} = 0.935 + 0.498LAI + 0.00575LAI^2 \quad (2\text{-}21)$$

2.3.2.3 Depression storage/ Surface retention

Water caught in the small voids or swales on the ground surface which is held until it infiltrates or evaporates is called depression storage or surface retention. Factors which control the amount of surface retention are micro-topography, surface macro-slope and rainfall characteristics. Rough ground can store large amounts of rainfall which results in smaller amounts of water being available for surface runoff and larger amounts of water being infiltrated and/or evaporated. As the average macro-slope of a surface increases for a given roughness, the volume of surface retention will usually decrease. The larger the rainfall, the less significant depression storage will be in runoff model calculations.

Because of the wide variability of the depressions and the general lack of experimental data, a generalized relation or model of the process does not exist. However, Linsley et al. (1949) reported that the volume of water stored by depressions, V, at any given instant of time after the beginning of rainfall could be approximated by equation (2-22):

$$V = S_d[1 - exp(-kP_e)] \quad (2\text{-}22)$$

Where S_d is the maximum storage capacity of the depressions, P_e is the rainfall minus infiltration, interception and evaporation, and k is the constant equivalent to $1/S_d$.

2.3.2.4 Evapotranspiration

Evapotranspiration is a process by which water is returned to the atmosphere. It consists of evaporation from open water surface, bare soil surface, and water intercepted by plant surfaces, as well as transpiration by plants from their root zone. Since it is difficult to quantify evaporation and

transpiration separately, they are considered together as evapotranspiration. The process of evaporation is influenced by different meteorological variables, the nature of the evaporating surface, and availability of water. The amount and rate of transpiration depends on the type of vegetation cover and their stage of growth, season of the year, time of the day, availability of water in the root zone and the same meteorological factors that affect evaporation.

There are different methods available for the estimation of potential evapotranspiration. Several intensive physical approaches such as the Penman-Monteith equation (Monteith, 1965) have been developed, which require a large amount of input information. Because of the complexity of the process, many less demanding empirical approaches have been presented in the literature, including the Hamon (1961) and the Blaney and Criddle (1950) methods. However, many of the empirical methods are developed for specific climate regions and should not be used for conditions different from those they are developed for.

It can be seen that each of the four components shown above can be determined to calculate the effective rainfall and thus runoff production. Alternatively, sometimes a single model could be developed in a lumped fashion. For instance, the U.S. Soil Conservation Service (SCS) (1972) suggested an empirical model for rainfall abstractions based on the potential for the soil to absorb a certain amount of moisture. On the basis of field observations, this potential storage S (millimetres or inches) is related to a "curve number" CN which is a characteristic of the soil type, land use and the initial degree of saturation known as the antecedent moisture condition. The value of S is defined by the empirical expressions below depending on the units being used.

$$S = \frac{1000}{CN} - 10 \ \ (inches), \qquad S = \frac{25400}{CN} - 254 \ \ (millimetres) \tag{2-23}$$

2.4.3 Simulation of runoff distribution

After determining the amount of runoff produced in each hydrologic element, a further runoff distribution component is required to route the generated runoff among different hydrologic elements and from the source areas to the outlet. Different methods have been developed and incorporated in the distributed runoff models to determine this process.

2.3.3.1 Numerical techniques

Numerical techniques have been widely employed in the distributed runoff models to simulate the runoff routing processes. Typically, the overland flow and channel flow are described by solving the Saint-Venant equations of continuity and momentum. To make these complex equations solvable,

simplifying assumptions need to be made and different methods are produced by neglecting various terms of the momentum equation.

Kinematic wave method

The kinematic wave method is simplest and also the most popular method. Although it has been shown to be a valid approximation for some flow scenarios, it is based on various simplifying assumptions that the influences of local acceleration and pressure forces are neglected, the flow is one dimensional and its characteristics such as depth and velocity are considered to vary only in the direction of principle slope, and the land surface slope is approximately equal to the friction slope. As a consequence, neither the backwater effects nor the depression storage can be accounted for, and the peak flows are also tended to be over-estimated as this theory does not provide for attenuation of the waves (MacArthur and DeVries, 1993; Swensson, 2003). The finite difference numerical techniques are often employed to solve the kinematic wave equations, but they have low computational efficiency and would become unstable when the selection of space and time increments dissatisfy the Courant condition (Chow et al., 1988).

Diffusion wave method

The diffusion wave method is a more complete form of the momentum equation. In the rainfall-runoff model developed by Jain et al. (2004), a one-dimensional solution based on the diffusion wave method is used, with the advantages of accounting for backwater effects and including the acceleration and differences in pressure. However, like the kinematic wave method, it does not consider the spatial variation in the direction perpendicular to the principle slope due to its one-dimensional nature. CASC2D (Rojas et al., 2003) employed a more advanced two-dimensional diffusion wave method to make it capable of describing the overland flow process in both x- and y-axis directions. While it could better describe the spatial variation of the flow behaviours, one limitation of this model is that it produces the calculations in a sequence from the grid located at the top left corner to that at the bottom right corner in a study area. This would cause a problem when the update of states (e.g., water depth) for a grid depends on the previously updated neighbouring grids, which however, cannot be affected by this grid. This is obviously in disagreement with reality, in which water depth changes everywhere at the same time and the flows at different points are interacting with each other. Furthermore, the computational efficiency would be further reduced in these diffusion wave methods because of the increased complexity in solving the mathematical equations

2.3.3.2 Elevation-based methods

Alternative to the complex numerical methods, the more straightforward elevation-based methods have been developed to determine the runoff distributions simply according to the differences in the elevations among hydrologic elements. These methods are generally based on the digital elevation map (DEM), which appears to be a very suitable tool for the distributed runoff modelling due to its raster or grid based data structure. As a result, some DEM-based runoff routing algorithms were proposed for the derivation of flow directions. They are generally categorized into two groups, including the single-direction algorithms that transfer all flow from the centre grid to one downslope neighbour, and the multiple-direction algorithms that partition flow to multiple downslope neighbours.

Single-direction algorithms

D8 is the earliest and simplest method for specifying flow directions. It assigns all flow from each grid to one of its eight neighbours, either adjacent or diagonal, in the direction with steepest downward slope. This method was introduced by O'Callaghan and Mark (1984) and has been widely used (Jenson, 1991; Martz and Garbrecht, 1992). The *D8* method is computationally efficient due to its simplicity, but one major limitation is that flow which originates over a two-dimensional grid is treated as a point source (non-dimensional) and is projected downslope by a line (one dimensional) (Moore and Grayson, 1991).

The *ρ8* algorithm (Fairfield and Leymarie, 1991) attempts to overcome the problem of straight flow paths by introducing a stochastic component into method *D8*. This algorithm randomly assigns flow from the centre grid cell to one of its downslope neighbours with the probability proportional to slope. It maintains the simplicity of single-direction algorithm, and the randomness creates flow paths that reflect more closely the true processes than *D8*. However, this randomness does not ensure reproducible results, and in locations of parallel flow, adjacent flow paths are not parallel but wiggle randomly and therefore often converge laterally with one another.

Multiple-direction algorithms

MFD (Multiple flow direction methods) attempts to solve the major limitation of single-direction method, the one-dimensional representation of flow, by distributing flow fractionally from a grid among all of its lower-elevation neighbour grids according to some specified rules (Freeman, 1991; Quinn et al., 1991). However, *MFD* methods have the potential disadvantage that flow from a grid is dispersed to all neighbouring grids with lower elevation, thus it tends to produce wider flow pathways due to excessive flow divergence (Erskine et al., 2006).

The *DEMON* (digital elevation model networks) algorithm (Costa-Cabral and Burges, 1994) is an extension of the method of Lea (1992), where grid elevation values are taken as grid corners, rather than block centred, and flow directions are based on the aspect of a plane surface fit to each grid. Flow is assumed to be uniform over the grid area and partitioned to two downslope neighbours in cardinal directions. Flow is generated over an area, not at point sources, and is projected downslope over a two-dimensional flow strip, analogous to a flow tube. This procedure also has the advantage of specifying flow direction continuously (as an angle between 0 and 2π) and without dispersion.

The $D\infty$ algorithm (Tarboton, 1997) recognizes the advantages of *DEMON*, and makes some development through the assignment of a single flow direction to each grid. This single flow direction is determined in the direction of the steepest downwards slope on the eight triangular facets formed in a 3 x 3 grid cell window centred on the grid of interest. The flow from each grid either all drains to one neighbour (if the angle falls along a cardinal or diagonal direction) or is on an angle falling between the direct angle to two adjacent neighbours. In the latter case the flow is proportioned between these two neighbour grids according to how close the flow direction angle is to the direct angle to those grids. So it is a combination of single-direction and multiple-direction method to some extent. Similar to *DEMON*, the dispersion is minimized since flow is never proportioned between more than two downslope grids.

Several studies have shown differences between these different runoff routing algorithms based on predicted channel networks (Endreny and Wood, 2003) and the location of ephemeral gullies (Desmet and Govers, 1996), with better results derived from the algorithms with multiple directions and limited flow divergence (*DEMON* and $D\infty$). Erskine (2006) compared these algorithms in computing upslope contributing area based on different grid sizes, and concluded that multiple-direction algorithms, allowing for flow divergence, are recommended on the undulating terrains.

These elevation-based methods are very straightforward and computationally efficient, compared to those numerical methods; however, a major limitation is that they tend to be oversimplified as the water component in the elements is not taken into account. In reality, the water does not always flow according to the elevation differences because of the different water depths among the elements. Thus it is actually the relative water surface heights, rather than the relative element elevations, that determine the flow patterns. Moreover, since the elevation of each element is consistent and independent, flow directions derived from these methods are pre-determined and fixed, thus neither the dynamic flow behaviours nor the interactions between elements can be captured.

Therefore, currently available methods, either the numerical techniques or the elevation-based methods, all have their limitations in accuracy and/or computational efficiency for the simulation of surface runoff. Besides, most of existing runoff models were developed from the catchment scale in the natural environment, and thus they may be not applicable to the rehabilitated landforms, where the soil properties, vegetation covers, topography features, spatial complexities and runoff generation mechanisms could be significantly altered from their original natural conditions. Consequently, more effective and robust runoff models are required to be developed for the rehabilitated landforms on the basis of new methods with both high reliability and reduced complexity. Cellular Automata (CA) is one of such promising approach worthy of investigation, and it will be introduced and discussed in details in the following section.

2.5 Cellular Automata (CA) as a Possible Method for Runoff Simulation

2.5.1 Introduction

For many years it has been very difficult to explain and simulate the behaviour of complex phenomena because the traditional methods describing them were mainly based on the systems of differential equations, which could not be easily solved without making substantial simplifications, thus causing the models intractable even using powerful computers. The advent and development of novel parallel computing showed the significant potential in representing a valid alternative modelling technique to the classical numerical models in description of complex phenomena, especially when the differential equations cannot be efficiently solved because of their complexity. In particular, Cellular Automata (CA) provides such an alternative approach for some complex natural systems, whose behaviour can be described in terms of local interactions of its constituent parts (Tommaso, 1984).

Cellular Automata (CA) is a discrete dynamic system composed of a set of cells in a one-dimensional or multi-dimensional lattice. Each cell in the regular spatial lattice can have any one of a finite number of states, and the states of the cells are updated according to local transition rules. In CA, the state of a cell at a given time depends only on its own state and the states of its neighbours at the previous time step. All cells are updated synchronously, and thus the state of the entire automata advances in discrete time steps. The global behaviour of the system is determined by the evolution of the states of all cells as a result of multiple interactions (Figure 2.5). Consequently CA is very effective in solving scientific problems because it can capture the essential features of systems in which the global behaviour arises from the collective effect of large numbers of locally interacting simple components (Wolfram, 1984a).

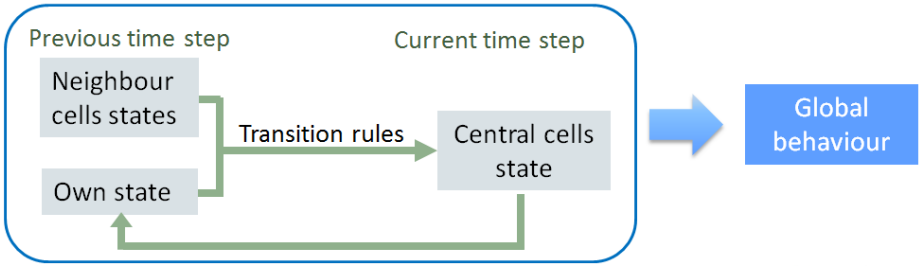

Figure 2.5 Evolution of cell states in CA.

2.5.2 CA components and theoretical background

Models based on CA theory consist of four primary components: a lattice space, the definition of a local neighbourhood area, transition rules determining the changes in cell properties, and boundary conditions (Parsons and Fonstad, 2007). Each of these components could influence the state of an individual cell and in turn the overall behaviour of the system.

2.5.2.1 Lattice space

A lattice space covers the whole study area and consists of a series of spatial cells. Theoretically, a cellular space can have any dimension from 1 to N. However, the majority of research so far has been on one-dimensional (Wolfram, 1984b) or two-dimensional CA. There is no restriction to the tessellation of a lattice space, which means that the shape of each cell can be any of the three regular polygons which tile the plane: triangle, square, or hexagon (Figure 2.6). Hexagons are often used in lattice gas model that deal with diffusion of gases and turbulent flow of liquids, and one of their advantages is that they maintain a constant distance from centre to edge of the hexagon. However, square cells are the most common form in CA applications due to their inherent convenience of implementation in computers.

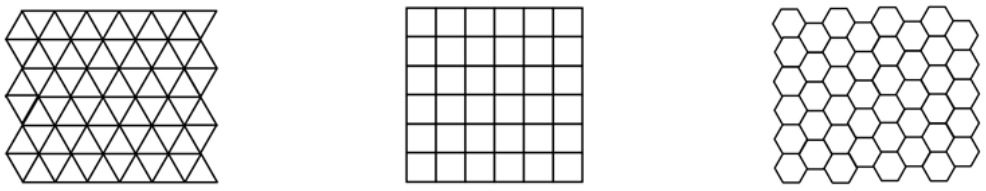

Figure 2.6 Examples of different types of CA lattice space.

2.5.2.2 Neighbourhood

A neighbourhood is the group of cells around a cell of interest that affect the centre cell's properties at each time step. The neighbourhoods can be either symmetrical or asymmetrical, with no limitation to the size of a neighbourhood, and thus there are numerous ways to define a neighbourhood for CA. The simplest choice is "nearest neighbours", in which only cells directly adjacent to a given cell are considered. Frequently used neighbourhood templates for two-dimensional square grids are the von Neumann-neighbourhood (Figure 2.7-a) and the Moore-neighbourhood (Figure 2.7-b). The von Neumann-neighbourhood is the group of four cells in the four cardinal directions from the centre cell, whereas the Moore-neighbourhood also includes the diagonal neighbours. Unlike the von Neumann-neighbourhood, in Moore-neighbourhood the centre cell is fully surrounded by neighbour cells, but the distance from the diagonal neighbours to the centre cell is different from that from cardinal neighbours, causing some potential difficulties in model application. The hexagonal grids employ the most symmetric two-dimensional neighbourhood (Figure 2.7-d), where each neighbour is the same distance around the centre cell and totally surrounds each part of the centre cell. In addition, neighbourhoods including a wider radius than these simple neighbourhoods may also be employed, termed the extended von Neumann and extended Moore neighbourhoods (Figure 2.7-c). Unfortunately, these hexagonal and extended neighbourhoods can be much more difficult to integrate with known physical laws and/or with computers than simple neighbourhoods. So the von Neumann and Moore neighbourhoods are most adopted in present studies.

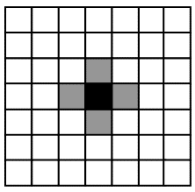

a) von Neumann neighbourhood

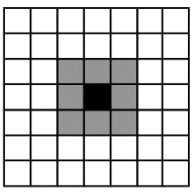

b) Moore neighbourhood

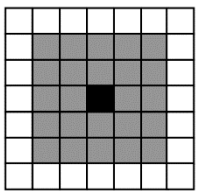

c) Extended Moore neighbourhoods

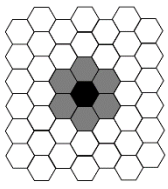

d) Hexagonal neighbourhood

Figure 2.7 Examples of CA neighbourhoods.

2.5.2.3 Transition rules

Transition rules specify how the state of each cell is updated according to the defined neighbourhood and current states of cells. One example is the famous transition rules in John Conway's Game of Life (Gardner, 1970), where cells are considered to be “alive” (their state is coded as “alive”) or “dead”. In each time step of the model, the transition rules are applied to the cells' states: a “live” cell in one time step remains “alive” in the next time step if its neighbourhood contains either two or three other alive cells, otherwise its state is coded as “dead”; while a “dead” cell in one time step can become “alive” in the next if its neighbourhood contains exactly three “live” cells. In concept, transition rules are applied to each cell in the lattice space uniformly and synchronously, so all the spatial cells change their states simultaneously according to the same transition rules during model execution.

For modelling and simulating the complex macroscopic phenomena by CA, a transition rule known as the minimisation-of-differences algorithm was proposed by Gregorio and Serra (1999). It is a very straightforward transition rule that a dynamic system tends to evolve towards equilibrium conditions by flow of some conserved quantity in the central cell to its neighbours, with an example demonstrated in Figure 2.8. This transition rule has been applied to simulate the lava flows, debris flows, bioremediation and soil erosion (D'Ambrosio et al., 2001; Gregorio and Serra, 1999).

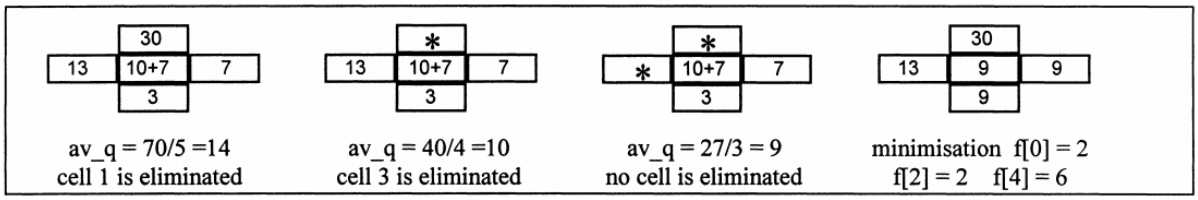

Figure 2.8 Example of distribution process by minimisation-of-differences algorithm (Gregorio and Serra, 1999).

2.5.2.4 Boundary conditions

The final component of a CA model is the boundary condition that describes what happens at the outer cells of the lattice. Since these outer cells do not have a complete neighbourhood, special conditions require to be applied to their behaviour. CA models may incorporate several different types of boundaries, including “reflective” boundary that prevents, for example, fluid from flowing off the edges, “periodic” boundary that allows it flowing off one edge to re-enter the grid on the opposite side from where it left, or “absorbing” boundary that absorbs any fluid moving into them (Parsons and

Fonstad, 2007). Sometimes, an auxiliary border consisting of several lines of cells could be added at the edge of study area to eliminate the boundary effects.

2.5.3 Application of CA

CA was invented by John von Neumann in the early fifties with the contribution of his colleague Stanislaw Ulam when they were investigating self-reproduction (Von Neumann, 1966). However, until 1970, CA had been studied by only a few researchers. With the advent and popularity of the "Game of Life" in 1970 developed by John Conway (Gardner, 1970), science research communities were introduced to and fascinated by the idea of CA, and researchers started to conduct a wide range of CA experiments in numerous fields. To date CA has been widely applied in a large number of science branches, such as urban development (Deadman et al., 1993; Itami, 1988; Kirtland et al., 1994), traffic flow simulation (Wahle et al., 2001), biological modelling (Ermentrout and Edelstein-Keshet, 1993), vegetation growth (Aassine and El Jaï, 2002; Silvertown et al., 1992), forest fire dynamics (Clarke et al., 1994), and so on.

While CA has become a major tool for discovering the processes and structures of many complex natural systems, only in the recent decade a few studies have emerged to relate its application to surface hydrologic modelling. Rinaldi et al. (2007) and Ma et al. (2009) developed CA based models for simulating runoff in large plains and on hill-slopes, respectively. Both models have shown the capacity of CA, however, a spatially uniform flow velocity was assumed and simply applied over the entire study area, leading them to be only used for simulating the steady flow conditions. Parsons and Fonstad (2007) developed a more complex CA model capable of simulating the unsteady flow conditions by delaying the water from one cell to the next until the correct timing is reached. Although this is a large progress, unfortunately in their model the flow directions were restricted to only four cardinal directions due to the difficulties in producing accurate timed water flows. Uncertainty also existed in selecting an appropriate time step for simulation. In addition, calculation of the rainfall excess is rather simple and empirical in this model as it does not include any related hydrologic principles. Some other CA models, such as RillGrow (Favis-Mortlock, 1998), EROSION-3D (Schmidt et al., 1999) and CAESAR (Coulthard et al., 2000), incorporate a surface hydrology component, but it is usually simplified because these models were primarily developed to study soil erosion or landform evolution. Larger errors are expected if they are used to quantitatively predict surface runoff yields. For instance, Mike Saynor (2012a) used CAESAR to simulate the runoff performance of field plots (30 m × 30 m) at rehabilitated mine sites in Australia, but the predicted discharge was 3.5 times greater than measured

values because some basic hydrological processes (e.g., infiltration) were not considered in the model. Consequently, a more effective and specialised CA-based model is required to be developed for the quantitative prediction of the dynamic surface runoff processes, by integrating fundamental hydrological principles and basic CA theories.

2.6 Summary of research gaps in the literature

The literature analysis in the previous sections aimed to overview the principles in surface hydrology and the current methods for the modelling of this process, specifically targeting issues on their application in the rehabilitated landforms. The main research gaps identified from the literature review relate to:

- There is a lack of understanding on the surface hydrological processes in the disturbed and rehabilitated landforms (section 2.1.3).
- There is no persistent conclusion about the influences of various affecting factors on the surface hydrology (section 2.2.6).
- The performance of the infiltration models modified for complex rainfall conditions has not been systematically evaluated, which has limited their application and value in hydrologic modelling (section 2.3.3).
- The determination of input parameters for infiltration models has been hampered by the difficulties and inaccuracies in the direct measurement; the quantitative estimation of their values from related controlling factors is required (section 2.3.4).
- Currently available methods for runoff simulation all have limitations in the accuracy of the prediction, computational efficiency and/or scale flexibility, and may produce unexpected errors if applied in rehabilitated landforms (section 2.4.3).
- Cellular Automata, an effective and well-accepted approach for describing the dynamic and complex processes in many disciplines, has been rarely applied to surface hydrologic modelling (section 2.5.3).

The understanding and simulation of the surface hydrological processes in the rehabilitated landforms are constrained by above mentioned research gaps. The study in this thesis aims to address these impediments.

Chapter 3 Estimating Input Parameters for Four Infiltration Models from Basic Soil, Vegetation and Rainfall Properties

3.1 Introduction

Infiltration process is one of the most important components in the hydrologic cycle as it determines the quantity of incoming precipitation which becomes surface runoff or contributes to soil moisture or groundwater (Dunne, 1978). Predictions of flooding, erosion and pollutant transport all depend on the rate of infiltration. Infiltration is also a very complex process to measure as it varies both temporally and spatially. To accurately characterize and quantify this process, considerable effort has been made to develop various infiltration models. Among these models, some physically based models including Philip (Philip, 1957b) and Green-Ampt (Green and Ampt, 1911) models, and some empirical models including Horton (Horton, 1940) and Holtan (Holtan, 1961) models are frequently used due to their simplicity, good fit to measured data and reduced number of parameters. These infiltration models have been incorporated in many distributed physically based hydrologic models to improve their prediction accuracy. For example, the Green-Ampt model is widely used in models such as WEPP (Laflen et al., 1991), SWAT (Tuppad et al., 2011), SWMM (Rossman, 2010), LISEM (De Roo et al., 1996), HEC-1 (Feldman, 1995) and ANSWERS-2000 (Bouraoui and Dillaha, 1996), Philip model is integrated in WATFLOOD (Kouwen, 2012) and HYSIM (Manley, 1993), Horton model is incorporated in MARINE (Estupina-Borrell et al., 2002) and SWMM, and Holtan model is used in LISEM, HEC-1 and ANSWERS (Beasley et al., 1980). Most of these hydrological models have shown great sensitivity to the input parameter values in these infiltration models (Bingeman et al., 2006; De Roo and Jetten, 1999; Kannan et al., 2007; Nearing et al., 1990; Ritter, 1992; Zaghloul, 1983). Therefore, the precise determination of these infiltration parameters is essential for generating accurate prediction results.

Problem for the determination of infiltration parameters is the lack of any physical meaning of some fitting parameters in the empirical infiltration models and that they cannot be measured directly. They have to be determined through calibration with the actual infiltration data or from the suggested values from literature. The calibration process is time-consuming and the actual infiltration data is often unavailable in practice. Most of those suggested values, for example, the empirical parameter values in the Holtan model as suggested by Musgrave (1955) and Frere et al. (1975), were found to be very rough estimates that may lead to a large bias in an application (Turner, 2006). Even though some infiltration parameters with physical meaning can be obtained from direct laboratory or field

measurements, they are always subject to measurement errors and uncertainty caused by the different measuring methods and the scaling effect. For example, the laboratory determined values of the saturated hydraulic conductivity, a common parameter for many infiltration models, have been found to vary significantly from the field measured values (Mohanty et al., 1994; Reynolds et al., 2000). In addition, the distributed hydrologic models often require the inputs for each of a series of small spatial hydrologic elements. Due to the large spatial variability of the infiltration behaviour, it is time-consuming, costly and often impractical to directly measure the infiltration parameters as a large number of samples are required to be taken and analysed, and/or numerous *in situ* measurements are required to be conducted.

As an alternative, these infiltration parameters can be indirectly estimated from some more easily available or measurable controlling factors. Numerous studies have revealed that the infiltration process is influenced by various factors, including soil properties (Mayor et al., 2009; Meek et al., 1992), surface conditions (Fattah and Upadhyaya, 1996; Lavee and Poesen, 1991; Li et al., 2011), vegetation covers (Puigdef ábregas, 2005; Wilcox et al., 1988), topography features (Fox et al., 1997; Poesen, 1984) and rainfall characteristics (Dunne et al., 1991; Foley et al., 1991). Most of previous studies have only qualitatively analysed the effects of these controlling factors. Just a few of them, such as that conducted by Li et al. (2011), have developed regression equations for predicting the steady-state infiltration rate. The quantitative estimation for the parameters of infiltration models, however, is very deficient, except for the Green-Ampt model. Some pedotransfer functions (PTF) have been developed to relate its parameters with soil texture and other simple soil properties (Ahuja et al., 1989; Brakensiek and Onstad, 1977; McCuen et al., 1981; Van den Putte et al., 2013; Zhang et al., 1995). These PTFs show great advantage in estimating the desired parameter values from already available basic soil data. However, they do not take into account other factors such as vegetation, topography and rainfall which also have great impact on infiltration parameters. Reason for this neglect is that in most of these studies the actual infiltration was measured by the single ring or double ring infiltrometer method, which was often applied on soil removed of vegetation and levelled ground surface by ponding the water inside. This ponded water is also different from the rainfall as the rain drop may compact the soil and cause surface sealing that could affect the infiltration rate (Bradford et al., 1987). Using a rainfall simulator or sprinkling infiltrometer may overcome these problems, and at the same time provide a larger spatial coverage. Therefore, the objectives of this study are (1) to measure and compare the infiltration rates under different soil, vegetation, topography and rainfall conditions using a field rainfall simulator; (2) to determine the input parameters for four popular infiltration models (i.e., Philip, Green-Ampt, Horton and Holtan model) for all rainfall events; (3) to

investigate various soil, vegetation, topography and rainfall related factors that have potential impacts on the infiltration parameters; and (4) to identify the major controlling factors for each infiltration parameter and quantify their relationships by developing predictive regression equations.

3.2 Materials and methods

3.2.1 Infiltration models

The Green-Ampt and Philip model used in this study are both physically based models. They assume the soil media as capillary tubes with water infiltrating into the porous media. Green and Ampt (1911) proposed this first physically based infiltration model based on Darcy's law, and expressed the infiltration rate as:

$$i_t = K_s \left[\frac{(\theta_s - \theta_0)\psi_f}{I_t} + 1\right] \tag{3.1}$$

where i_t is the infiltration rate (mm h^{-1}) at time t (h), K_s is the saturated hydraulic conductivity ($mm\ h^{-1}$), θ_s and θ_0 is the saturated and initial water content ($cm^3\ cm^{-3}$) respectively, ψ_f is the suction at the wetting front (mm), and I_t is the cumulative infiltration (mm) at time t.

Philip (1957b) developed a time series to solve the Richards' flow equation (Richards, 1931), and a two-term Philip infiltration equation was derived by neglecting the higher order terms:

$$i_t = 0.5 S_0 t^{-0.5} + A \tag{3.2}$$

where S_0 is the sorptivity (mm $h^{-0.5}$) and A is a parameter reflecting the steady infiltration rate ($mm\ h^{-1}$).

Another group of infiltration models are empirically based. They do not give a physical insight into the infiltration process, but try to model the shape of the infiltration curve as well as possible (Van De Genachte et al., 1996). The Horton model (Horton, 1940) is one of the most widely-used empirical infiltration models. It considers infiltration as a natural "exhaustion process", during which infiltration rate decreases exponentially with time, as shown in the following equation:

$$i_t = i_f + (i_0 - i_f)e^{-kt} \tag{3.3}$$

where i_0 and i_f is the initial and final steady infiltration rate (mm h^{-1}) respectively, and k is the infiltration decay coefficient (h^{-1}).

Using a storage exhaustion concept, Holtan (1961) derived an infiltration model expressed as:

$$i_t = i_f + a(S - I_t)^{1.4} \quad (3.4)$$

where a is a constant ($mm^{-0.4}\ h^{-1}$) dependent on soil type, surface and cropping conditions, and S is the soil water storage potential (mm).

As shown in Table 3.1, some parameters with physical meaning in these infiltration models can be directly measured from field experiments or laboratory analysis. However, some other parameters do not have any physical meaning or are very difficult to measure. These parameters are unmeasurable and need to be indirectly determined by curve-fitting the infiltration models to the measured infiltration rates.

Table 3.1 Measurable and unmeasurable input parameters for four infiltration models

Infiltration model	Directly measured Parameters[1]	Indirectly determined unmeasurable parameters[a]
Green-Ampt	K_s, θ_s, θ_0	ψ_f
Philip		S_0, A
Horton	i_f	i_0, k
Holtan	i_f	a, S

[a] K_s is the saturated hydraulic conductivity, θ_s and θ_0 is the saturated and initial water content respectively, ψ_f is the suction at the wetting front, S_0 is the sorptivity, A is the soil water transmissivity, i_f and i_0 is the final and initial infiltration rate respectively, k is the infiltration decay coefficient, a is a constant in Holtan model, and S is the soil water storage potential.

3.2.2 Experimental procedure

Rainfall simulation experiments were conducted in the field to measure the temporal changes of infiltration rates at different spatial plots. Both field investigations and laboratory analysis were conducted to measure the measurable infiltration parameters, as well as the factors that have potential impacts on the infiltration (Table 3.2), including rainfall intensity, slope gradient, soil physical and hydraulic properties, soil textural parameters and the vegetation related factors. They were selected because they are easily accessible and measurable factors that represent rainfall, topography and vegetation features.

Table 3.2 Potential controlling factors for the infiltration parameters

Controlling factors	Abbr.	Units	Controlling factors	Abbr.	Units
Rainfall intensity	*Rain*	mm h^{-1}	Stone content (>5.3 mm)	*Stone*	g g^{-1}
Slope gradient	*Slope*	%	Gravel content (2.0-5.3 mm)	*Gravel*	g g^{-1}
Top soil depth	*Depth*	m	Sand content (0.02-2.0 mm)	*Sand*	g g^{-1}
Bulk density	ρ_b	g cm^{-3}	Silt content (0.002-0.02 mm)	*Silt*	g g^{-1}
Porosity (saturated water content)	$\phi(\theta_s)$	m^3 m^{-3}	Clay content (<0.002 mm)	*Clay*	g g^{-1}
Field capacity	θ_{FC}	m^3 m^{-3}	Root content	*Root*	g/100cm^3
Initial soil moisture	θ_0	m^3 m^{-3}	Vegetation cover	*Cover*	m^2 m^{-2}
Initial saturation degree	*SAT%*	-	Vegetation height	*Height*	m

Field experiments

This study was carried out at the Veterinary Science Farm of the University of Queensland, which is located at Pinjarra Hills, Queensland, Eastern Australia. The climate is humid subtropical with an average annual rainfall of 1000 mm of which 66% occurs during the wet season from October to March. Monthly mean temperatures vary from 15 ℃ in July to 25 ℃ in January.

Small plots of 1 m^2 (1 m long and 1 m wide) were set up in an area of about 5 km^2. Specifically, plots 1 to 6 were randomly distributed on a lawn, which was in large parts compacted by vehicle traffic; plots 7 to 13 were randomly selected in a restored area, which was previously disturbed by construction work; while plots 14 to 22 were randomly set up in an undisturbed paddock (previously used for grazing and fallow since >5 years) with natural conditions. This selection of plots maximized the ranges of site features in terms of soil properties, slope gradients and vegetation characteristics. Furthermore, each of the last three plots, which were fully covered by vegetation, was further mowed into a partially covered plot and a bare plot to better investigate the influences of vegetation. This lead to six additional plots (Fig. 1). The 1 m^2 plot was used because they have been widely applied in field measurements of infiltration under either simulated (Dos Reis Castro et al., 1999; Leonard and Andrieux, 1998) or natural rainfalls (Le Bissonnais et al., 1998; Patin et al., 2012). The measured results in this size of plots are found to represent the local infiltration characteristics in this unit area, and the controlling factors are also relatively spatially homogenous in such a small plot. Each small

plot was defined by a 1 m ×1 m metal runoff frame sunk into the ground to a depth of 5 cm, allowing a 10 cm extension above the ground to separate runoff produced within the plot area from that produced outside the plot. A V-shape runoff collector was installed at the bottom of each plot for collecting and measuring runoff (Figure 3.2). Before the start of experiments an orthogonal top view picture of every plot was taken to make an assessment of the vegetation coverage. A mean vegetation height was determined by averaging 10 measured heights in each plot. The depth of the top soil was obtained by measuring the depth to the first impeding layer in the soil profile that was dug next to the plot. The slope gradient for each plot was also measured.

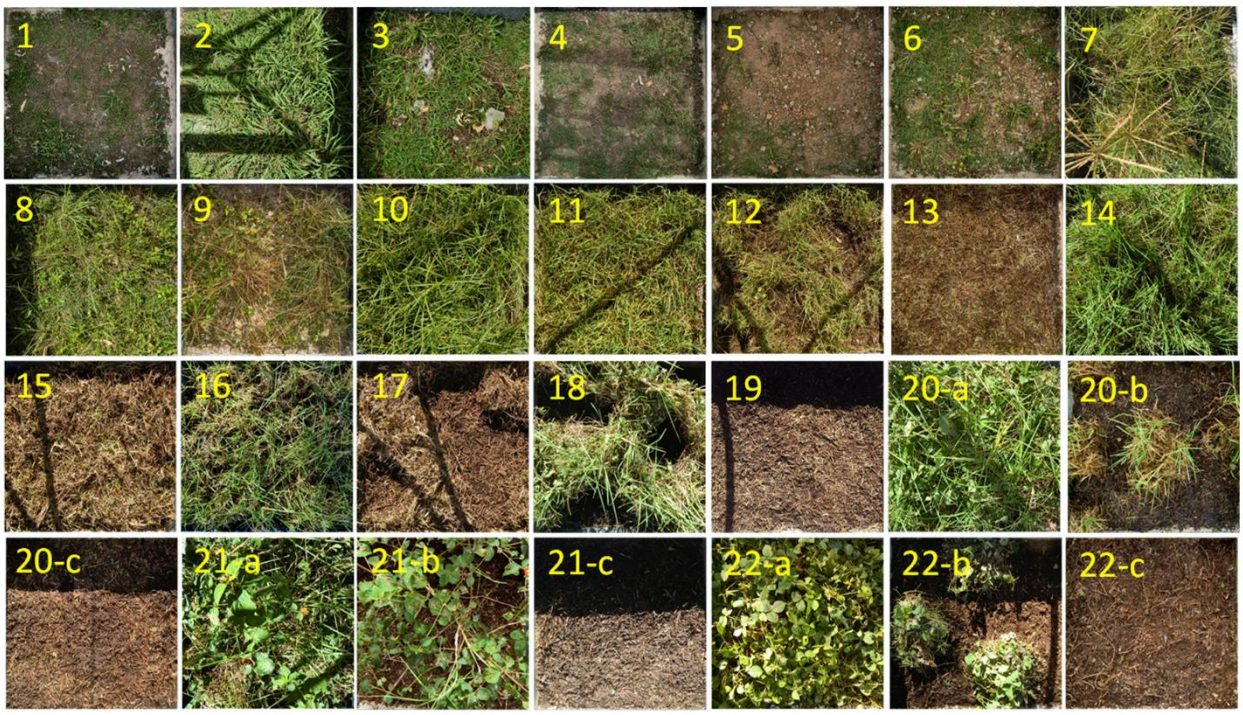

Figure 3.1 Orthogonal top view photos of all plots. Plot 20, 21 and 22 were mowed into plots with different vegetation covers.

Simulated rainfall was produced by a field rainfall simulator (Figure 3.2) which uses Veejet 80100 nozzles mounted on a manifold, with the nozzles controlled to sweep to and from across a plot. The more detailed information of this type of rainfall simulator is given by Loch et al. (2001), who has proven its ability in giving reasonable simulation of kinetic energies of intense natural rain and producing the rainfall intensity with a small coefficient of variation (8-10%) in its spatial distribution. For each plot, three runs were conducted based on different initial soil moisture conditions: a first dry run on the initially dry soil, a second wet run on the wet soil 24 hours after the first run, and a third moist run on the very wet soil just 2 hours after the second run. The rainfall intensity was controlled

by the frequency with which the nozzles sweep. In order to investigate the influence of rainfall intensity on infiltration, one of three sweeping frequencies was randomly selected for each rainfall event. The actual rainfall intensity was measured by four measuring cups distributed across the plot. During each rainfall simulation run, after the appearance of runoff, the runoff generated in 30 seconds was collected and measured at the outlet of the runoff collector using collecting bottles every minute in the first 15 minutes and every two minutes in the remaining period. Based on these measured runoff rates, the infiltration rates at different time points were calculated by subtracting them from the measured rainfall intensity. Each rainfall event lasted until the runoff equilibrium was reached. Since the final steady infiltration rate and the field saturated hydraulic conductivity represent the same physical phenomenon – the final water intake rate of a soil under saturated conditions, they were assumed to be equal in this study and were both determined by averaging the last 5 measured infiltration rates.

Figure 3.2 Photo of the field rainfall simulator.

Laboratory measurements

In order to avoid the disturbance of plots, soil was sampled from the area immediately adjacent to the plots. Three undisturbed soil core samples were taken at the depth of 0-5 cm before the start of each rainfall event with metal sampling rings (100 cm^3) for the measurement of basic soil properties. The initial and saturated soil water contents, as well as the field capacity of collected soil samples, were

determined by weighing them before and after oven-drying at 105 ℃ for 24 h. Specifically, the saturated condition was reached by leaving the core samples in a tray filled with shallow water for 2-4 days, and the field capacity was achieved by leaving the saturated core samples on a suction plate with 33 kPa (0.33 bar) suction pressure for 7 days. The total porosity of the soil sample was assumed to be equal to the saturated water content. The dry bulk density was calculated by dividing the oven-dried soil weight by the soil volume. For the particle size distribution analysis, both stone content (> 5.3 mm) and gravel content (2.0 - 5.3 mm) were determined by the sieving method, while the sand, silt and clay contents were measured using the hydrometer method. The root content was measured by weighing the roots in each soil sample and expressed as g/100cm^3.

3.2.3 Statistical analysis

Parameterization of infiltration models

The unmeasurable parameters in the four infiltration models were determined by curve-fitting the infiltration models to the observed infiltration rates after runoff generation by a non-linear least-squares optimization using the method of Marquardt in SAS (2008). The goodness of fit of each model was tested by both the coefficient of determination (R^2) and the root mean square error (*RMSE*) to evaluate how closely each model describes the measured infiltration. The R^2values indicate the degree to which data variations are explained by each model, while *RMSE* shows the amount of divergence of the model values from the observed values. Therefore, a high R^2 close to 1 and a low *RMSE* value close to 0 both indicate a good agreement between the predicted and observed infiltration curves.

Development of predictive regression equations

After deriving all the infiltration parameters and controlling factors, the entire data set was split into a calibration and validation subset using the method introduced by Van den Putte et al. (2013): the 66 rainfall events in total for the 22 natural plots (no mowing) were ranked based on the value of the runoff coefficient, and subsequently every rainfall event with an odd rank number was assigned to the calibration subset and that with an even rank number was assigned to the validation subset. The calibration subset was used to develop the predictive regression equations for the infiltration parameters. Four different factor sets were used in the regression analysis. The first one was a full factor set that consists of all the investigated soil, vegetation, rainfall and topography factors. The second factor set used soil related factors, only, as is the case in most existing pedotransfer functions. A simplified third factor set included only *Rain*, θ_0, *Cover* and *Height*, which are the factors easily obtainable from either field measurement or some quick methods such as remote sensing (RS) and

Geographic Information System (GIS) techniques. The fourth set further included K_s on the basis of the former factor set.

The correlation analysis was performed to reduce the number of variables for regression analysis in the first and second factor sets. The Pearson correlation coefficient (*r*) between each controlling factor and each infiltration parameter was calculated using SPSS Statistics 22. The *r* values range from -1 to +1, with the sign indicating the direction of the relationship, and its absolute value indicating the strength of the relationship. The controlling factors that had significant correlations ($P<0.05$) with one infiltration parameter were defined as the major controlling factors of this infiltration parameter. Only these identified major controlling factors were further used in the regression analysis in these two factor sets. For the other two factor sets, all the factors were included due to the small number of factors.

If the controlling factors to be included in the regression analysis were correlated with each other, they cannot be directly used due to the multicollinearity among the predictor variables, which has been found to have negative effects on the regression analysis (Gunst and Mason, 1980; Vereecken, 1988). In this case, a principle components analysis (PCA) was performed in SPSS prior to the regression analysis to find a smaller number of principle components (PCs) that are linear combinations of the original variables and can explain a large percentage of variability within samples (Lin et al., 1999). Since these PCs are orthogonal and thus uncorrelated, the problem of multicollinearity can be avoided by using them as the independent variables in the regression analysis.

Then the predictive regression equation for each infiltration parameter was developed by a multiple linear regression analysis performed in SPSS, using the standardized infiltration parameter as the dependent variable and the PCs or standardized controlling factors as the independent variables. These developed regression equations were further transformed into equations that were expressed in terms of the original infiltration parameters and controlling factors. The performance of these equations was measured by the coefficient of determination (R^2), which represents the proportion of variance in the dependent variable that can be explained by the independent variables. Thus the equation with the highest R^2 is expected to perform best.

Validation procedure

In order to validate the developed regression equations from each factor set, the unmeasurable infiltration parameters for all the rainfall events were predicted using these equations. The predicting accuracies were evaluated by the coefficient of determination (R^2) for fitting the one-to-one diagram to the scatter plots showing the observed versus predicted values. Then both the observed (measured

or curve-fitting determined) and predicted (based on different factor sets) parameter values were used as inputs for the infiltration models to generate the infiltration curves for each rainfall event. The performance of these predicted curves were evaluated and compared against the observed infiltration rates by the respective *RMSE* values. According to Wösten et al. (2001), the accuracy and reliability of the regression equations were assessed by the results in the calibration subset and in the validation subset, respectively.

3.3 Results

3.3.1 Potential controlling factors

Initial soil moisture conditions were found to affect the time to runoff from start of rainfall. The mean time to runoff generation was 7.86±4.31 min, 4.12±3.38 min and 2.53±1.78 min for the dry (first), wet (second) and moist (third) run, respectively, while the mean time to reach the runoff equilibrium was 93.46±13.87 min, 62.50±11.57 min and 36.18±4.83 min, respectively. Obviously it took longer time for the initially drier soil to generate runoff and to reach a steady infiltration rate. Table 3.3 summarizes the results of measured potential controlling factors for all the rainfall events. It can be seen that most of these controlling factors had a large range of values, except for the slope gradient with its maximum value of only 5%, due to the difficulty in setting up the rainfall simulator at steep slopes. Relatively large rainfall intensities (66.8-103.6 mm h^{-1}) were applied in order to ensure the occurrence of runoff which was necessary for determining the infiltration rates and also to reduce the time to runoff generation. This approach reduced the effect of delays as a consequence of sorptive buffering prior to the starting of runoff. The soil texture for different plots ranged from clay loam to sandy loam according to the results of particle size analysis. With respect to the vegetation parameters, the plots varied from bare soil without vegetation to those fully covered by vegetation (as also shown in Figure 3.1). These large variations in various controlling factors resulted in significantly different runoff behaviours for different rainfall events applied on different plots, with the runoff coefficient ranging from 1.5% to 87.0%.

3.3.2 Infiltration parameters

Except for the K_s, i_f, θ_s and θ_0 which were measured directly, all the other infiltration parameters were determined by fitting the four infiltration models to the measured infiltration rates. Figure 3.3, describing the infiltration curves for plot 12 and demonstrating an example for the curve-fitting results,

shows that these infiltration models seemed to be able to well fit the observed infiltration values. Statistical analysis showed that the mean R^2 for the dry, wet and moist run on all the plots was 0.887±0.088, 0.884±0.070 and 0.885±0.083 respectively, and the mean *RMSE* was 5.319±3.264 mm h^{-1}, 4.512±2.737 mm h^{-1} and 4.647±3.440 mm h^{-1} respectively. These large R^2 values and small *RMSE* values both indicate that the infiltration models were capable to well describe the temporally varied infiltration process, and no significant differences existed among their performance under different initial soil moisture conditions. Comparisons between infiltration models showed that the goodness of fit of empirical models including Horton (R^2=0.921, *RMSE*=3.769 mm h^{-1}) and Holtan (R^2=0.901, *RMSE*=4.221 mm h^{-1}) model was better than that of physically based models including Philip (R^2=0.893, *RMSE*=5.767 mm h^{-1}) and Green-Ampt model (R^2=0.826, *RMSE*=6.905 mm h^{-1}). This may be due to the fact that the physically based models were initially developed from bare soil and rely heavily on the soil hydraulic and physical properties within the profile (Turner, 2006), but do not take into account the surface conditions, such as vegetation factors which had a large influence on infiltration in this study. The performance of the Green-Ampt model was significant (P<0.05) worse than the other three models, probably because it had only one fitting parameter, while all the other models allow two parameters to be calibrated. Nevertheless, the four infiltration models all had large R^2 values greater than 0.8, indicating their good performance in this study**.**

The curve-fitting derived values for the infiltration parameters were summarized in Table 3.3. Due to the large variances in various controlling factors, their values also varied significantly, but at the same time were all physically meaningful and remained in reasonable ranges.

Table 3.3 Summary of results for the potential controlling factors and infiltration parameters.

Controlling factor /Infiltration parameter[a]	Min.	Max.	Range	Mean	Std. Deviation
Controlling factors					
Rain (mm h^{-1})	66.8	103.6	36.8	89.2	9.3
Slope (%)	1	5	4	2.54	1.07
Depth (m)	0.05	0.40	0.35	0.22	0.10
ρ_b (g cm^{-3})	0.53	1.17	0.64	0.78	0.20
ϕ (m^3 m^{-3})	0.33	0.55	0.22	0.45	0.07
θ_{FC} (m^3 m^{-3})	0.18	0.37	0.20	0.29	0.06
SAT%	0.28	0.98	0.70	0.77	0.18
Stone (g g^{-1})	0.01	0.36	0.36	0.11	0.10
Gravel (g g^{-1})	0.06	0.25	0.19	0.16	0.07
Sand (g g^{-1})	0.26	0.52	0.26	0.41	0.09
Silt (g g^{-1})	0.06	0.25	0.20	0.17	0.06
Clay (g g^{-1})	0.08	0.19	0.11	0.14	0.03
Root (g/100cm^3)	0.01	1.03	1.02	0.38	0.27
Cover (m^2 m^{-2})	0	1.00	1.00	0.62	0.37
Height (m)	0	0.87	0.87	0.28	0.27
Infiltration parameters					
$K_s(i_f)$ (mm h^{-1})	2.64	85.29	82.65	40.33	27.07
θ_s (m^3 m^{-3})	0.33	0.55	0.22	0.45	0.07
θ_0 (m^3 m^{-3})	0.11	0.53	0.42	0.36	0.12
ψ_f (mm) [b]	0.80	4706.77	4705.96	443.93	840.42
A (mm h^{-1}) [b]	1.01	84.85	83.84	27.83	24.80
S_0 (mm $h^{-0.5}$) [b]	0.42	107.19	106.77	37.39	24.84
i_0 (mm h^{-1}) [b]	62.02	391.80	329.78	113.83	41.35
k (h^{-1}) [b]	1.49	30.31	28.81	5.55	5.21
a ($mm^{-0.4}$ h^{-1}) [b]	0.00	4.57	4.57	0.44	0.77
S (mm) [b]	5.92	187.23	181.31	67.47	45.26

[a] Refer to Table 3.1 for the meaning of the symbols

[b] Infiltration parameters determined by curve-fitting procedure

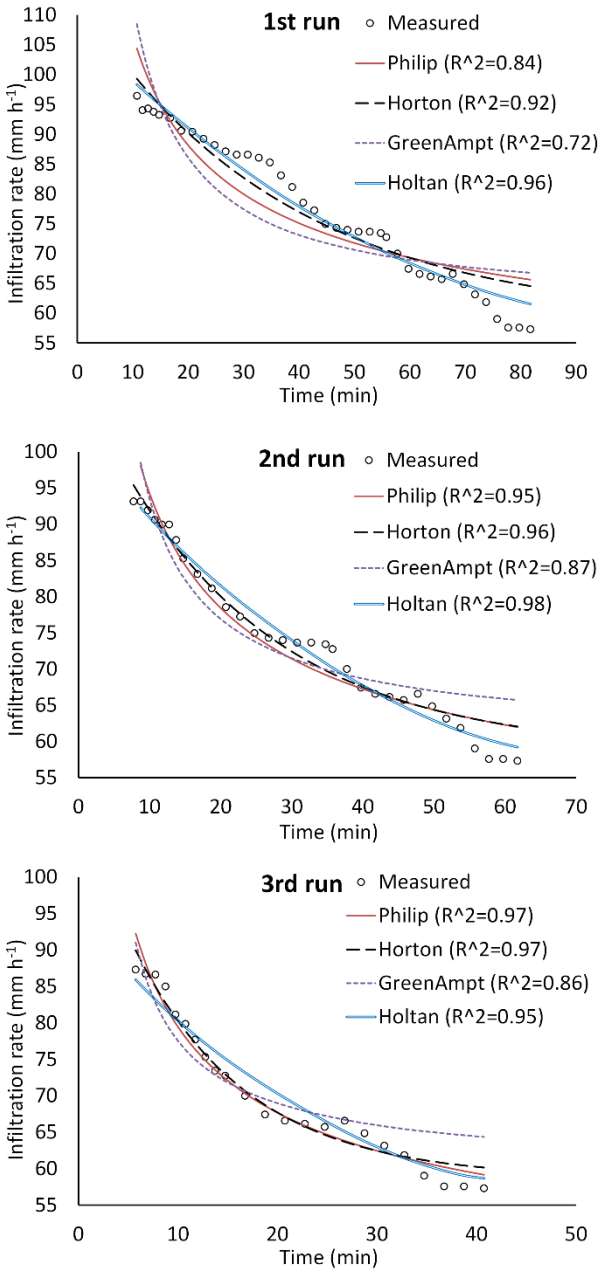

Figure 3.3 Curve-fitting of four infiltration models to the measured infiltration data on plot 12.

3.3.3 Predictive regression equations

The predictive regression equations were developed for all the unmeasurable infiltration parameters, based on four different factor sets in the calibration dataset.

The predictive regression equations were developed for all the unmeasurable infiltration parameters, based on four different factor sets in the calibration dataset.

1st factor set

Correlation analysis results showed that the number of identified major controlling factors for different infiltration parameters ranged from 3 to 11, and they were highly correlated with each other. The significant correlations existed not only within the group of soil texture variables (i.e., *Stone*, *Gravel*, *Sand*, *Silt*, *Clay*) and that of variables reflecting the soil physical properties (i.e., ρ_b, ϕ, θ_{FC}), but also between these two groups. The three vegetation factors, *Cover*, *Height* and *Root*, also showed strong correlations. Therefore, PCA was performed on these major controlling factors prior to the regression analysis. Table 3.4 shows the factor loading matrix for the parameter *k* which was controlled by the largest number of factors. The numbers in the table represent the correlations between the calculated PCs and the original factors, and only those factors with correlation values greater than 0.5 were defined as the major loading factors for each PC. It can be seen that PC1 is heavily loaded (either positively or negatively) on various soil related factors, while PC2 and PC3 is only highly correlated with *Cover* and *Rain* respecitvely. In the same way, PCs were determined for all the other infiltration parameters and the results are summarised in Table 3.5. It can be seen that PC1 representing the soil properties was identified for all these parameters, PC2 refering to vegetation features was built for all the parameter except for S_0, while PC3 reflecting rainfall intensity was only applied for some of these parameters, including S_0, i_0, *k* and *a*. In spite of the similar PCs, the major factors loaded on each PC varied for different parameters.

A multiple linear regression analysis was performed for each standardized infiltration parameter based on the identified PCs. The derived regression equations are demonstrated in Table 3.5. These equations were further transformed to the final predictive equations expressed as the original infiltration parameter and controlling factors, as shown in Table 3.6. The large R^2 values (ranging from 0.459 to 0.750) indicated the good performance of these developed equations.

Table 3.4 Component loading matrix for infiltration decay factor *k* based on 1st factor set.

Controlling factors	**Principle component**		
	PC1	**PC2**	**PC3**
ϕ	0.964[a]	0.040	0.134
θ_{FC}	0.957[a]	0.077	0.145
ρ_b	-0.944[a]	0.045	-0.117
Silt	0.934[a]	0.238	0.114
Depth	0.905[a]	-0.083	-0.119
Stone	-0.888[a]	-0.234	-0.153

K_s	0.871[a]	0.293	0.161
Clay	0.721[a]	0.162	0.135
SAT%	0.715[a]	.000	-0.466
Cover	-0.085	0.904[a]	-0.087
Rain	0.200	0.035	0.933[a]

[a] major loading factors for each principle component

Table 3.5 Prediction regression equations based PCs developed from 1st factor set.

Prediction equation based on PCs[a]	**Major loading factors**			
	PC1		**PC2**	**PC3**
	+	-	+	+
$Zscore(\psi_f) = 0.309 \times PC1 - 0.626 \times PC2 - 1.876 \times 10^{-16}$	ϕ, *Depth*, θ_0, K_s	ρ_b	*Root Cover*	
$Zscore(A) = 0.368 \times PC1 + 0.670 \times PC2 - 2.386 \times 10^{-16}$	*Sand*, *Silt Clay*, θ_{FC}, K_s	*Stone Gravel*	*Root Cover*	
$Zscore(S_0) = 0.018 \times PC1 + 0.646 \times PC3 - 2.619 \times 10^{-15}$	*Clay*,	*SAT%*		*Rain*
$Zscore(i_0) = 0.127 \times PC1 + 0.116 \times PC2 + 0.473 \times PC3 + 0.035$	*Sand*, *Clay*	ρ_b *Gravel*	*Height*	*Rain*
$Zscore(k) = -0.177 \times PC1 - 0.241 \times PC2 + 0.677 \times PC3 + 1.499 \times 10^{-15}$	*Silt*, *Clay*, ϕ, θ_{FC}, *Depth*, K_s	*Stone* ρ_b *SAT%*	*Cover*	*Rain*
$Zscore(a) = -0.474 \times PC1 - 0.243 \times PC2 - 0.442 \times PC3 + 1.262 \times 10^{-15}$	K_s		*Root Cover*	*Rain*
$Zscore(S) = 0.364 \times PC1 + 0.456 \times PC2 + 3.565 \times 10^{-16}$	*Silt*, *Clay*, ϕ, θ_{FC}, K_s	*Stone* ρ_b	*Cover*	

[a] *'Zscore'* means the standardized parameter.

2nd factor set

Only the factors reflecting soil properties were included in this factor set to determine whether they were sufficient to predict the infiltration parameters. A similar data processing procedure to that in the previous factor set was applied, and the resulted predictive regression equations are shown in Table 3.6. It can be seen that different major controlling factors were identified and included in the regression equations for different infiltration parameters. However, none of these equations had R^2 value greater

than 0.5, indicating that the regression equations developed from only soil related factors may not be able to well predict the target infiltration parameters in this study.

3rd factor set

Only four controlling factors, θ_0, *Cover*, *Height* and *Rain*, which can be easily and quickly measured in the field without taking any soil samples or conducting any laboratory analysis, were included in this factor set. Three PCs representing vegetation features (*Cover* and *Height*), initial soil moisture and rainfall intensity were derived from these controlling factors. The infiltration parameters were related to these PCs using a multiple regression analysis, with the resulted regression equations based on the original factors shown in Table 3.6. However, due to the small R^2 values (ranging from 0.173 to 0.473), these equations are not expected to perform well in predicting the infiltration parameter.

Table 3.6 Predictive regression equations based on original variables and developed from different factor sets.

Predictive regression equation based on original variables†	R^2
1st factor set (full factor set)	
$\varphi_f = 675.167 \times Depth - 295.769 \times \rho_b + 690.039 \times \varphi + 589.126 \times \theta_0 - 5.297 \times K_s - 660.432 \times Root - 564.907 \times Cover + 788.476$	0.698
$A = 14.596 \times \theta_{FC} - 18.516 \times Stone - 10.156 \times Gravel + 14.077 \times Sand + 29.771 \times Silt + 34.596 \times Clay + 0.200 \times K_s + 25.053 \times Root + 19.101 \times Cover - 15.067$	0.765
$S_0 = 1.408 \times Rain + 160.611 \times Clay - 23.502 \times SAT\% - 94.083$	0.646
$i_0 = 1.197 \times Rain - 6.966 \times \rho_b + 43.588 \times Gravel - 30.685 \times Sand + 70.571 \times Clay + 20.561 \times Height - 3.56$	0.459
$k = -0.287 \times Rain + 5.302 \times Depth + 0.945 \times \rho_b - 3.942 \times \varphi - 5.120 \times \theta_{FC} + 4.053 \times Stone - 4.997 \times Silt - 12.151 \times Clay - 0.480 \times Cover - 0.030 \times K_s + 7.775 \times SAT\% + 29.828$	0.740
$a = -0.040 \times Rain - 0.396 \times Root - 0.414 \times Cover - 0.010 \times K_s + 4.851$	0.692
$S = -4.413 \times \rho_b + 27.233 \times \varphi + 35.052 \times \theta_{FC} - 37.246 \times Stone + 65.712 \times Silt + 0.376 \times K_s + 86.342 \times Clay + 27.595 \times Cover - 0.885$	0.583
2nd factor set (soil factor set)	
$\varphi_f = 380.879 \times Depth - 196.690 \times \rho_b + 564.622 \times \varphi + 305.386 \times \theta_0 + 0.468 \times K_s + 118.525$	0.215
$A = 35.160 \times \theta_{FC} - 21.230 \times Stone - 31.344 \times Gravel + 23.862 \times Sand + 37.358 \times Silt + 57.576 \times Clay + 0.047 \times K_s + 1.254$	0.483
$S_0 = 252.427 \times Clay - 39.023 \times SAT\% + 31.035$	0.356
$i_0 = -5.312 \times \rho_b - 16.466 \times Gravel + 11.89 \times Sand + 28.608 \times Clay + 104.261$	0.135

$k = 4.361 \times Depth - 0.677 \times \rho_b + 0.184 \times \varphi - 2.403 \times \theta_{FC} + 3.914 \times Stone - 5.738 \times Silt - 20.499 \times Clay + 0.949 \times SAT\% - 0.053 \times K_s + 10.296$	0.410
$a = -0.019 \times K_s + 1.262$	0.455
$S = -17.782 \times \rho_b + 52.429 \times \varphi + 57.992 \times \theta_{FC} - 33.605 \times Stone + 59.298 \times Silt + 98.968 \times Clay + 0.066 \times K_s + 20.511$	0.442
3rd factor set (simplified factor set)	
$\varphi_f = -1.586 \times Rain + 1930.522 \times \theta_0 - 604.085 \times Cover - 582.258 \times Height + 390.380$	0.348
$A = 0.044 \times Rain + 22.097 \times \theta_0 + 18.552 \times Cover + 32.552 \times Height - 1.365$	0.315
$S_0 = -0.015 \times Rain - 1.063 \times \theta_0 - 6.109 \times Cover - 9.599 \times Height + 43.134$	0.175
$i_0 = 0.972 \times Rain + 32.223 \times \theta_0 - 3.409 \times Cover - 2.686 \times Height + 10.642$	0.173
$k = -0.383 \times Rain + 4.594 \times \theta_0 - 2.023 \times Cover - 1.039 \times Height + 39.375$	0.473
$a = -0.002 \times Rain + 2.102 \times \theta_0 - 0.572 \times Cover - 0.502 \times Height + 0.366$	0.436
$S = 0.044 \times Rain + 17.861 \times \theta_0 + 18.489 \times Cover + 31.692 \times Height + 39.514$	0.296
4th factor set (simplified factor set + K_s)	
$\varphi_f = 1983.973 \times \theta_0 - 708.477 \times Cover + 237.718 \times Height + 2.943 \times Rain - 10.069 \times K_s + 257.199$	0.726
$A = 18.586 \times \theta_0 + 24.956 \times Cover - 21.096 \times Height - 0.318 \times Rain + 0.655 \times K_s + 13.530$	0.932
$S_0 = -8.779 \times \theta_0 - 10.033 \times Cover + 6.354 \times Height + 0.166 \times Rain - 0.098 \times K_s - 101.302$	0.654
$i_0 = 27.186 \times \theta_0 - 8.659 \times Cover + 12.550 \times Height + 0.108 \times Rain - 0.079 \times K_s + 5.351$	0.440
$k = 6.432 \times \theta_0 - 0.853 \times Cover + 0.576 \times Height - 0.034 \times Rain - 0.038 \times K_s + 35.688$	0.695
$a = 2.177 \times \theta_0 - 0.769 \times Cover + 0.637 \times Height + 0.005 \times Rain - 0.013 \times K_s + 0.165$	0.623
$S = 10.628 \times \theta_0 + 27.305 \times Cover - 20.777 \times Height - 0.319 \times Rain + 0.678 \times K_s + 53.224$	0.528

[a] Refer to Table 3.1 and 3.2 for the meaning of the symbols.

4th factor set

The saturated hydraulic conductivity (K_s) describes functional hydraulic properties and is one of the most important and common soil hydraulic properties. It was added to the factors used in the 3rd factor set. This resulted in another PC that can be used as a measurement of K_s. After the regression analysis on these new PCs and the transformation procedure, the derived regression equations based on the original factors were summarized in Table 3.6. It can be seen that the R^2 values (ranging from 0.440

to 0.932) for these equations were much larger than those in the previous factor set, indicating that the performance of the predictive equations was much improved by incorporating K_s.

3.3.4 Validation results

The unmeasurable infiltration parameters in both calibration and validation subsets were calculated by the predictive regression equations developed from four different factor sets. Scatter plots showing the predicted versus observed (measured or curve-fitting determined) infiltration parameters are given in Figure 3.4. It can be seen that in general the dots lie closer to the 1:1 line in the 1st and 4th factor sets, while more scatter was observed for the 2nd and 3rd factor sets. This was as expected judging from the values for the R^2 shown in these figures. The average R^2 values for the 1st (0.653) and 4th (0.623) factor sets were significantly (P<0.05) larger than those for the 2nd (0.364) and 3rd (0.414) data sets. Only R^2 values for the parameter a were above 0.5 in the 2nd factor set, suggesting the potential failure of the predictive equations developed from this factor set. The equations developed from the 3rd factor set seemed to work well for k, but were obviously unsuccessful for S_0 and S, with R^2 values all smaller than 0.350. In the contrast, the parameter values predicted from the 1st and 4th factor sets all reasonably agreed with the observed values, with no significant differences existed in R^2 values between these two factor sets. In addition, the performance of the equations developed from these two factor sets did not vary significantly from the calibration subset to the validation subset, indicating that they had not only high accuracies but also high reliabilities.

The observed (measured or curve-fitting determined) and predicted infiltration parameter values (from four factor sets) were then used as the inputs for the infiltration models to simulate the infiltration rates for all the rainfall events. The resulted goodness of fit to the measured infiltration values was represented by *RMSE*. The mean *RMSE* values for all the rainfall events were summarized in Table 3.7. Not suprisingly, the observed infiltration parameter values led to the smallest *RMSE* values and thus the best model performance. In most cases the *RMSE* values based on the 1st and 4th factor sets were significantly (P<0.05) smaller than those based on the other two factor sets, but had no significant difference from the results based on the observed parameters. These results indicated that these infiltration models were able to accurately predict the actual infiltration processes on the basis of their parameter values estimated from the predictive regression equations developed from the 1st and 4th factor sets.

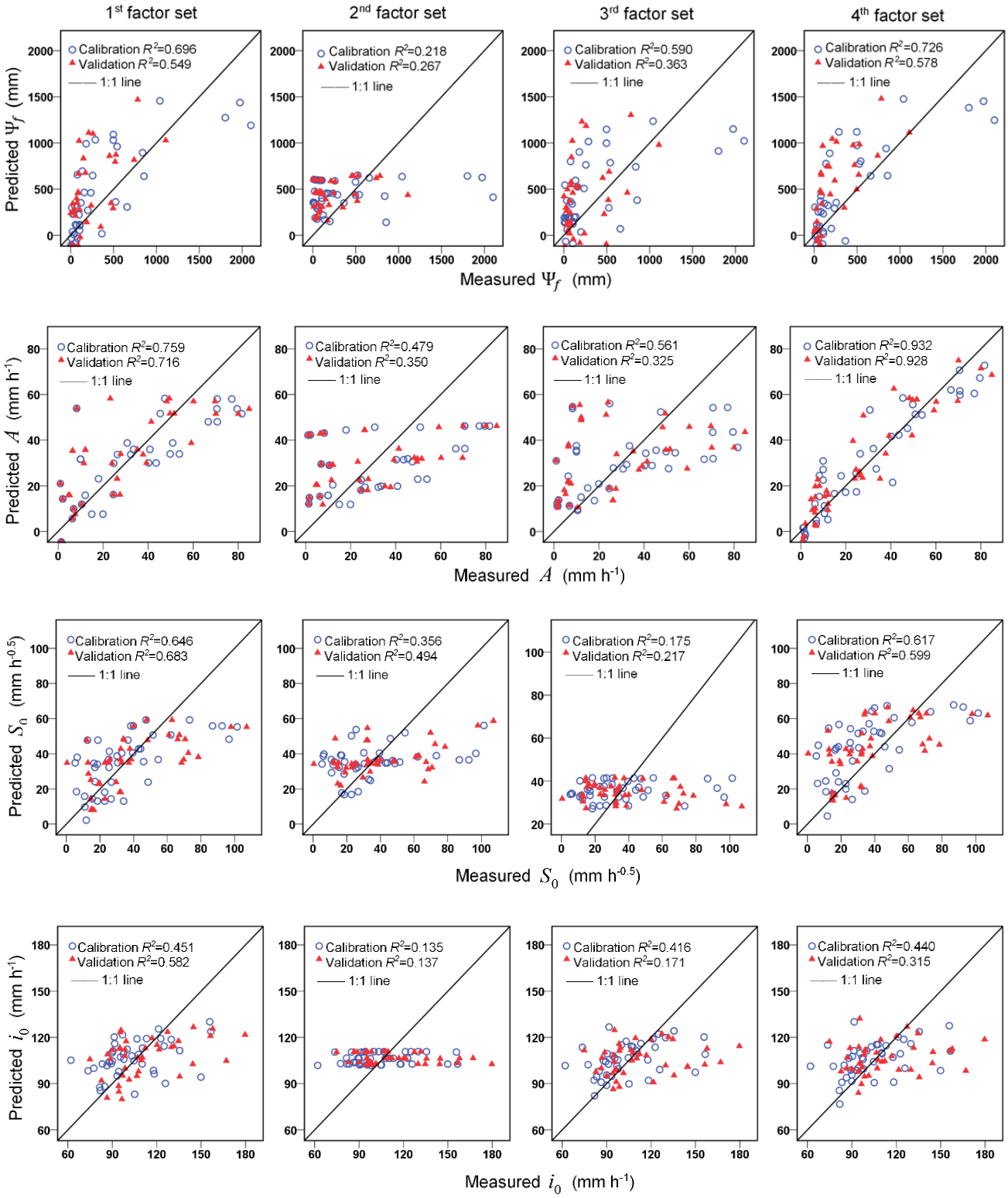
1st factor set
2nd factor set
3rd factor set
4th factor set
Calibration R^2=0.696
Validation R^2=0.549
1:1 line
Calibration R^2=0.218
Validation R^2=0.267
Calibration R^2=0.590
Validation R^2=0.363
Calibration R^2=0.726
Validation R^2=0.578
Predicted Ψ_f (mm)
Measured Ψ_f (mm)
Calibration R^2=0.759
Validation R^2=0.716
Calibration R^2=0.479
Validation R^2=0.350
Calibration R^2=0.561
Validation R^2=0.325
Calibration R^2=0.932
Validation R^2=0.928
Predicted A (mm h^{-1})
Measured A (mm h^{-1})
Calibration R^2=0.646
Validation R^2=0.683
Calibration R^2=0.356
Validation R^2=0.494
Calibration R^2=0.175
Validation R^2=0.217
Calibration R^2=0.617
Validation R^2=0.599
Predicted S_0 (mm h$^{-0.5}$)
Measured S_0 (mm h$^{-0.5}$)
Calibration R^2=0.451
Validation R^2=0.582
Calibration R^2=0.135
Validation R^2=0.137
Calibration R^2=0.416
Validation R^2=0.171
Calibration R^2=0.440
Validation R^2=0.315
Predicted i_0 (mm h^{-1})
Measured i_0 (mm h^{-1})

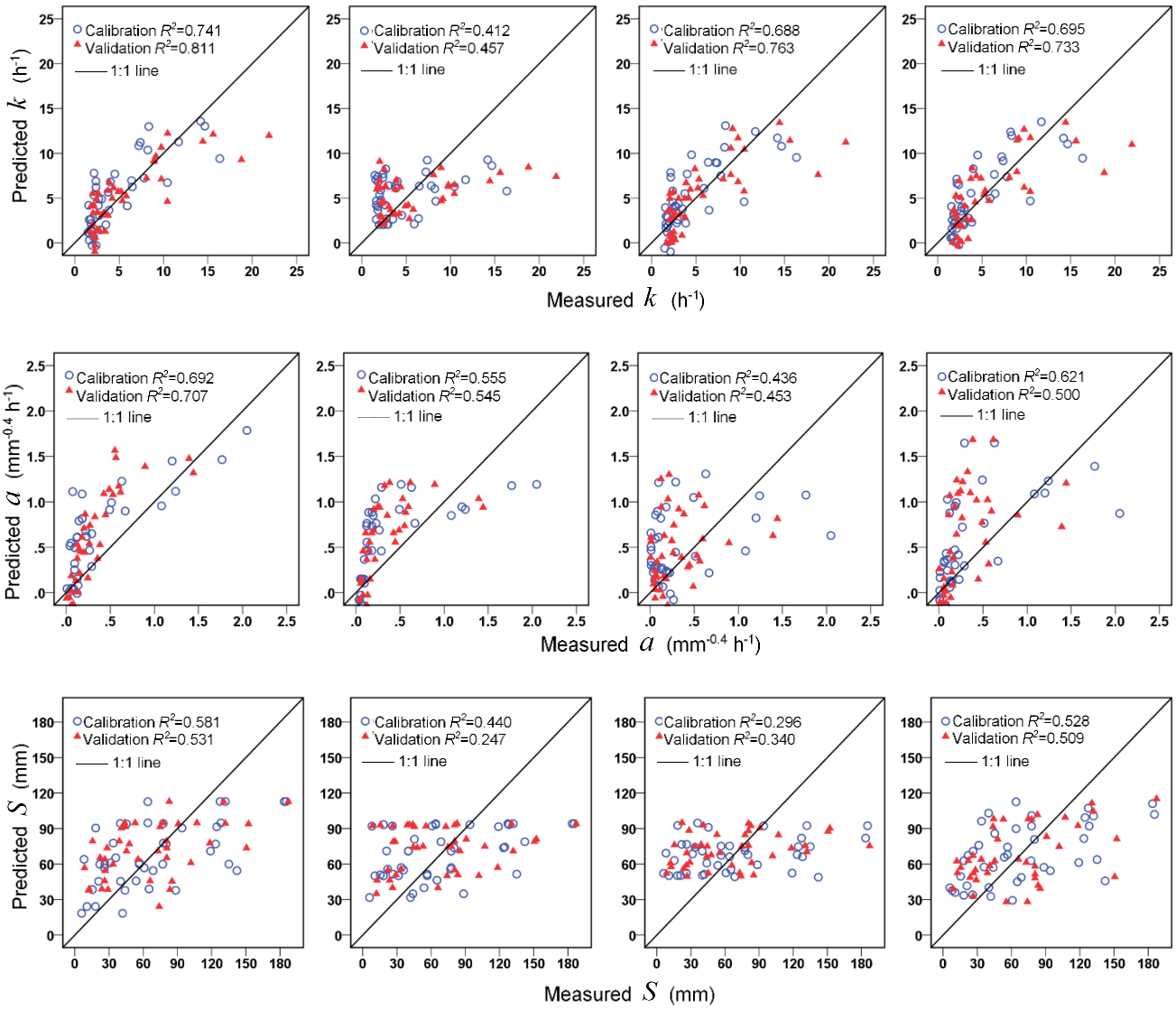

Figure 3.4 Predicted infiltration parameter values versus observed values for the four investigated factor sets. The symbols represent the same meaning as those in Table 3.1.

The response of the performance of the infiltration model to each of these infiltration parameters was also investigated, with the results shown in Figure 3.5. The linear fitting line for each parameter was able to reflect the sensitivity of *RMSE* to the predicting accuracy (R^2 in Figure 3.4) of this parameter. It can be seen that the fitting lines for ψ_f and a had the largest absolute values of slope in both calibration and validation subsets, indicating the greatest response of *RMSE* to them. These two parameters also led to the worst model performance (the largest *RMSE* values). The predicted results were more sensitive to k, S and A in the calibration subset than in the validation subset, while S_0 and i_0 both tended to produce the most accurate and consistent results.

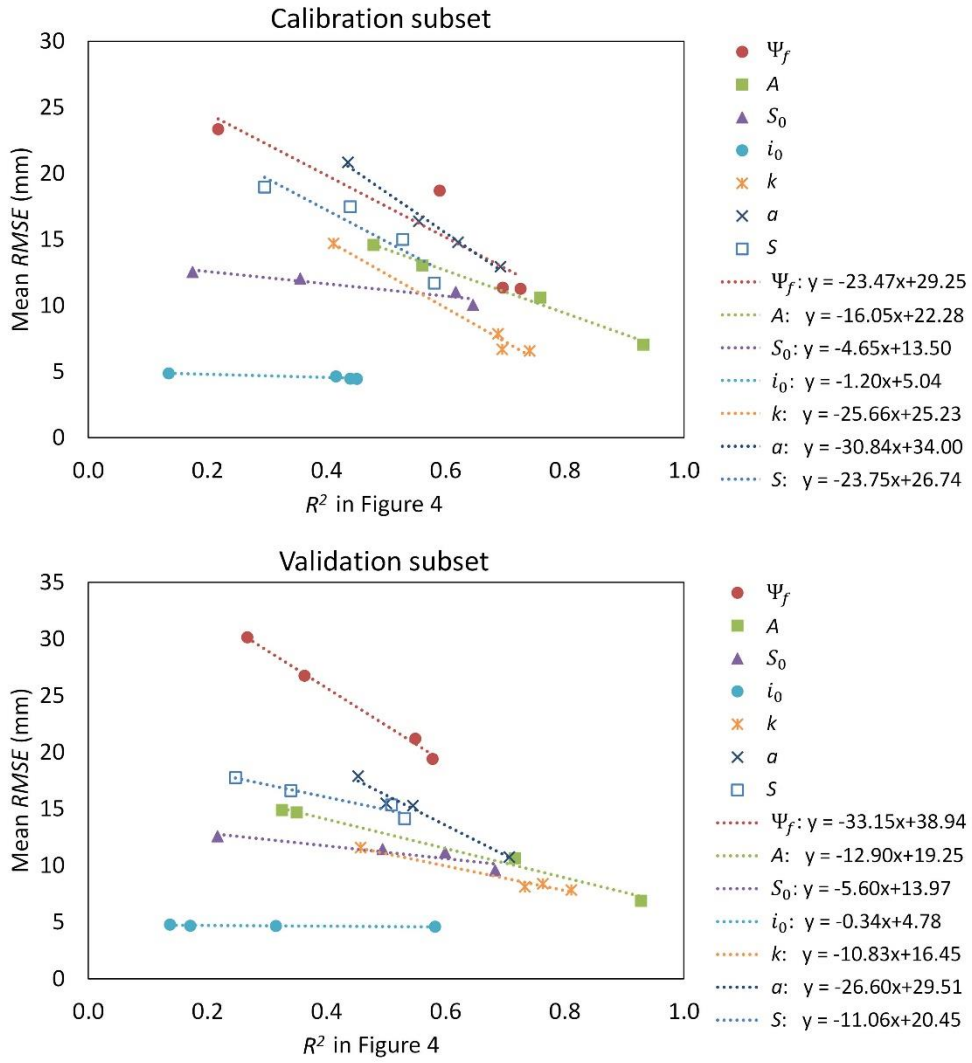

Figure 3.5 Response of infiltration model performance (*RMSE*) to the accuracy in determining the input parameters (R^2).

3.4 Discussion

3.4.1 Influences of different controlling factors on the infiltration parameters

In this study, four groups of potential controlling factors were investigated. Their effects on different infiltration parameters are discussed as follows:

Soil factors

The major controlling factors of each infiltration parameter and their relationships can be identified from Table 3.5, from which it can be seen that the group of soil related factors played the most

important role as they had significant influences on all these infiltration parameters. However, different soil factors were associated with different parameters.

The factors representing the soil texture were included in most of these regression equations. For example, the increased contents of *Stone* and *Gravel* could reduce *A* as these large fragments embedded in the soil may slow down the downward movement of water by reducing the hydraulic conductivity. On the contrary positive relations were found between *A* and the finer particle contents. These soil texture factors also had significant impacts on S_0, i_0, *k* and *S* due to their roles in affecting other soil properties.

While the increase of ρ_b is often associated with the reduction in ϕ, aeration and macro-porosity (Tekeste et al., 2006), in this study it was found to have an effect in reducing ψ_f, i_0 and *S*. However, it was positively associated with *k* as less time and water volume is required to fill the reduced pore space and smaller pores, which would result in a larger infiltration decay rate.

θ_0 and *SAT%* were both parameters reflecting the initial soil moisture conditions. A positive relationship between ψ_f and θ_0 was built in the regression equation, however, this is not in line with some other studies which suggested that a smaller θ_0 would result in a larger ψ_f due to the increased hydraulic gradient and the greater available storage capacity (Skaggs and Khaleel, 1982). This inconsistency may be due to the reason that θ_0 in this study was also significantly (P<0.01) and positively correlated with some other soil properties (e.g., ϕ, *Depth*, K_s) that have more important effects in increasing ψ_f. According to Philip (1957a), S_0, a parameter indicating the initial capacity of the soil to absorb water by capillary uptake, is a function of the initial soil moisture content. This was verified in this study that it had a negative relationship with *SAT%*. The increased *SAT%* would also increase *k* as the infiltration rate tended to drop more quickly to a steady rate in initially wetter soils.

In addition, *Depth* was found to be positively associated with ψ_f due to the increased hydraulic gradient, while negatively related to *k* because of the greater total pore space for water to fill. Although K_s was identified as a major controlling factor for most infiltration parameters in this study, its effect cannot be easily interpreted as it was significantly correlated with not only many other soil factors, but also the vegetation and rainfall factors.

Vegetation factors

The vegetation factors were included in six out of seven regression equations in Table 3.5, suggesting that they also played an important role in this study. To better analyse their effects, plot 20, 21 and 22 were mowed into different vegetation covers, with the same intensities of rainfall events applied. This

ensured the consistent soil and rainfall properties, thus allowing to investigate the impacts of above-ground vegetation solely.

The results for these three plots were demonstrated in Figure 3.6. It can be seen that the larger *Cover* would lead to larger *A*. This can be attributed to the role of vegetation in protecting the soil surface against the impact of raindrops, reducing their kinetic energy (Deuchars et al., 1999), preventing surface sealing (Foley et al., 1991), and consequently enhancing infiltration. A negative relationship was found between *Cove*r and *k*, probably because vegetation cover could delay the rainfall to reach the soil by intercepting and storing a portion of rainfall. The increased *S* with increased *Cove*r was also attributed to the fact that vegetation can serve as a water storage layer (by interception) and thus increase the total storage potential.

In addition to *Cove*r, *Root* also had great impacts on some of these infiltration parameters (Table 3.5). It could increase *A* as the roots in the soil have been found to increase soil aggregate stability (Blackburn, 1975), improve macropores (Bergkamp et al., 1996), and decrease bulk density (Greene, 1992), which all contribute to the increased infiltration rates. In this study *a* was largely associated with both *Cover* and *Root*, which is in line with the previous findings that this parameter is dependent on surface conditions and root density (Mishra et al., 2003; Turner, 2006).

Some parameters, however, were not obviously affected by the vegetation factors. Figure 3.6 showed that S_0 maintained a constant value for the same plot under different vegetation cover conditions. This agrees with the results in Table 3.5 that no vegetation factor was included in the regression equation for this parameter, which suggests that S_0 is vegetation independent. Although i_0 varied with different vegetation covers, its change did not show a consistent trend in different plots (Figure 3.6), probably due to the multiple effects of vegetation on this parameter. Vegetation played a role in increasing i_0 probably because of its capacity in preventing surface sealing at the beginning of rainfall event (Foley et al., 1991), but at the same time could decrease i_0 as it reduces the available rainfall for infiltration by its interception and storage functions.

Rainfall factors

Results in Table 3.5 also indicate the impacts of *Rain* on some of these infiltration parameters. Specifically, S_0 and i_0 were both positively related to *Rain* which to some extent determines the available water amount for the initial absorption and initial infiltration, respectively. The positive effect of *Rain* on *k* can be explained by the surface sealing introduced by raindrops, which would lead to a rapidly decreased infiltration rate and thus a large *k* value. Similarly, *Rain* negatively influenced *a* also due to its presumed role in changing surface conditions and soil properties via the impacts of raindrops.

Topography factors

Although the topography factor (i.e., slope gradient) was investigated as a potential controlling factor, it was not included in any of these regression equations shown in Table 3.5. One reason for this result may be that only a small range of slope gradients (0 - 5%) were tested in this study due to the difficulty to setup a rainfall simulator test on steeper slopes. Another reason could be the multiple and offsetting effects of slope gradient on infiltration under specific circumstances: with increased slope steepness greater runoff velocities would be expected, which on the one hand reduce the time for water to infiltrate and thus decrease the infiltration rate (Haggard et al., 2005; Huat et al., 2006), and on the other hand maintain a larger proportion of sediment particles in a suspended state resulting in reduced seal development and thus increased infiltration rate (Poesen, 1984; Römkens et al., 1985).

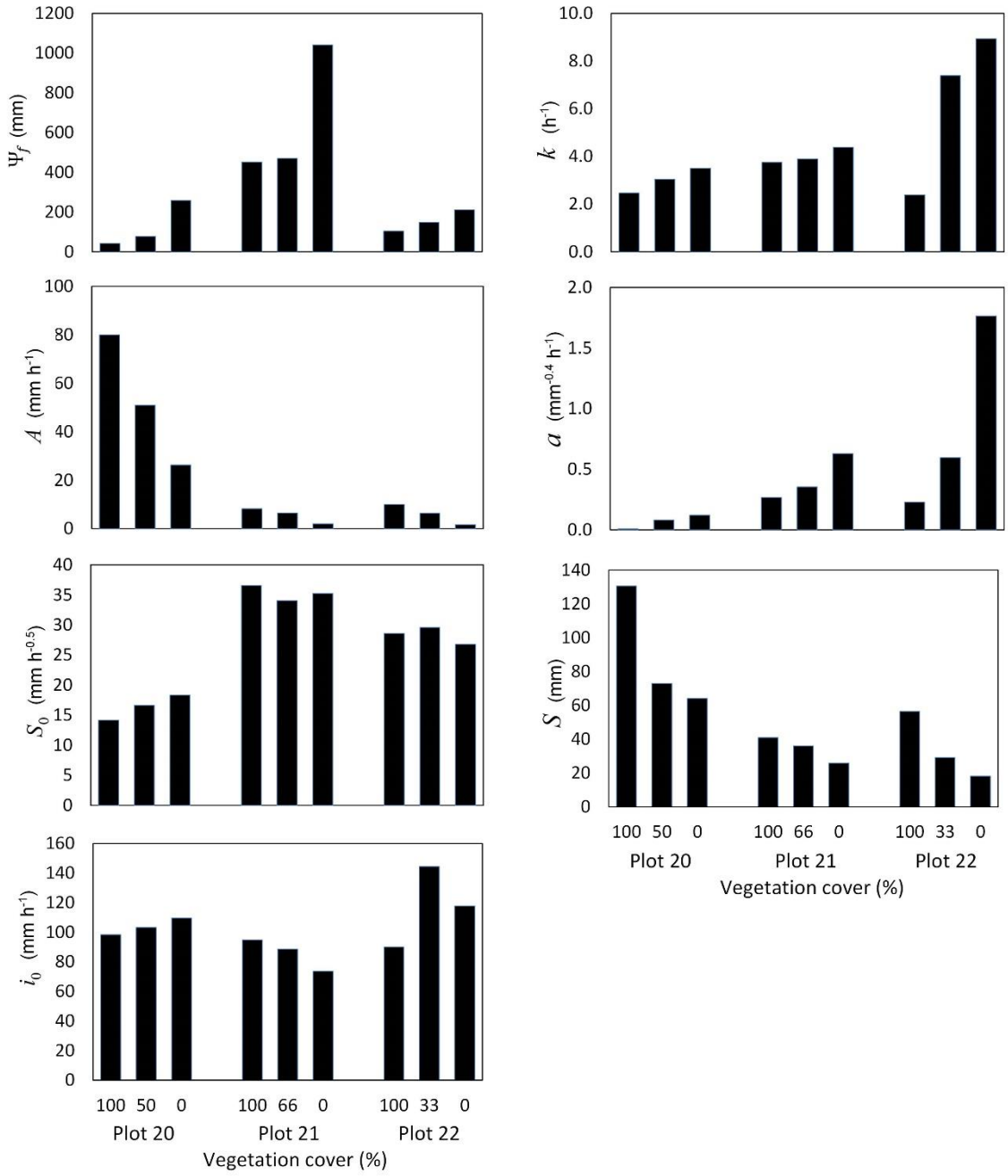

Figure 3.6 Comparison of Infiltration parameters under different vegetation covers in plot 20, 21 and 22. The symbols represent the same meaning as those in Table 3.1.

3.4.2 Insufficiency of soil factors in predicting infiltration parameters

Only the soil related factors were included in the 2nd factor set to evaluate whether they were sufficient to predict the infiltration parameters. Unfortunately, the predictive regression equations based on this factor set all failed (small R^2 values in Figure 3.4 and large *RMSE* values in Table 3.7). These results were not in accordance with some previous studies for developing the pedotransfer functions (PTF),

in which the functions developed from the basic soil data were proven quite effective. This inconsistency can be attributed to the fact that in these other studies the infiltration rates were measured by infiltrometers on bare soils or vegetation removed surfaces, while in our study they were measured by a field rainfall simulator on vegetation covered plots. Therefore, only soil factors were considered in their studies and the developed PTFs are only expected to be accurate for the bare soils under ponding conditions. In contrast, in our study the influences of many other factors, including the vegetation, topography and rainfall properties, were also investigated. The rainfall intensity and the vegetation features were found to have significant impacts on most infiltration parameters, which highlighted the important roles of these additional factors. Consequently, this explains why it was not sufficient to predict the infiltration parameters by considering the soil factors only, and why the accuracy of predictive equations was significantly improved by further including other controlling factors, as in the 1st factor set.

Table 3.7 Summary of mean *RMSE* values for the infiltration predictions based on observed and predicted parameter values from different factor sets.

	Green-Ampt	**Philip**	**Horton**	**Holtan**
	Calibration subset			
Observed	6.77a[a]	6.22a	4.82a	5.99a
1st factor set	11.35a	9.41a	6.56ab	10.01a
2nd factor set	23.34c	14.44b	12.27b	19.66b
3rd factor set	18.69b	16.69b	8.87b	23.47b
4th factor set	11.27a	9.36a	6.60ab	11.49a
	Validation subset			
Observed	6.60a	6.58a	4.75a	5.74a
1st factor set	14.19a	12.79a	7.07ab	13.74ab
2nd factor set	30.14b	23.31b	9.91b	22.24c
3rd factor set	26.75b	20.02b	9.53b	23.41c
4th factor set	14.41a	12.41a	7.66ab	15.46b

[a] Different letters in the same column indicate significant differences between *RMSE* values at $P<0.05$.

3.4.3 Readily obtainable factors for predicting infiltration parameters

The regression equations based on the 1st factor set, which includes all the potential controlling factors, have shown high efficacies in predicting the infiltration parameters (large R^2 values in Figure 3.4 and small *RMSE* values in Table 3.7). However, the determinations of some factors heavily rely on taking soil samples for laboratory analysis. When the spatially varied parameter values are requried for large scale studies, for example runoff simulations using distributed hydrologic models, much effort and

time is required for the measurements of these parameters. Therefore more practical and efficient solutions are requried. Attempts were made in this study by using only the easily measurable factors as variables (as shown in the 3rd factor set) to predict the infiltration parameters. These factors included θ_0, *Cover*, *Height* and *Rain*, which can be quickly and directly measured in the field without taking any samples or conducting any laboratory analysis. Another great advantage is that for large scale studies, the former three factors have been proven able to be effectively derived from RS and GIS techniques by various studies (Erik and Økland, 2002; Jackson, 1993; Stow et al., 2004), and the spatially and temporally varied rainfall information can also be readily obtained from rain gauge records or meteorological data. Nevertheless, the regression equations developed from these factors were found unsuccessful in predicting the infiltration parameters (small R^2 values in Figure 3.4 and large *RMSE* values in Table 3.7).The reason may be that the only soil related factor, θ_0, was not sufficient to represent the soil properties. Therefore another soil factor, K_s, was further included (as shown in the 4th factor set) with the intention to improve the performance of regression equations. K_s showed significant correlations with the largest number of other soil factors in this study, thus it was expected to best reflect the soil properties. This factor was selected also because it has been recognized as one of the most important and common soil hydraulic properties (Deb and Shukla, 2012; Klute and Dirksen, 1986; Mohanty et al., 1994). Various methods have been developed for its *in situ* measurement, including some quick methods such as the mini-infiltrometer (Decagon Devices, 2012), and some more accurate methods such as the disc infiltrometer (Perroux and White, 1988) and the hood infiltrometer which can be used on vegetation covered plots (Schwärzel and Punzel, 2007). In addition, an increasing number of studies have shown the potential to derive K_s from the RS data in recent years (Mohanty, 2013). As expected, the incorporation of K_s significantly improved the accuracies of the prediction equations (Figure 3.4 and Table 3.7). Since no significant difference (P<0.5) was found between the 1st and 4th factor sets either in R^2 values (Figure 3.4) or *RMSE* values (Table 3.7), we have successfully utilized these five relatively readily obtainable factors to replace the original 16 potential factors for predicting the infiltration parameters.

3.4.4 Sensitivity of infiltration models to their input parameters

The results in Figure 3.5 have shown the different extent of response of the infiltration models to their different input parameters. There is only one unmeasurable parameter, ψ_f, in the Green-Ampt model. The modelling results have shown great sensitivity to this parameter, and the inaccurcy in determining its value could also lead to large errors in the predicted infiltration rates. The physically based Philip model showed larger sensitivity to A than S_0, probably because A would have a consistent effect during

the entire infiltration process according to the second term of equation (2), while S_0 only has significant impact at the initial stage of infiltration as its effect would reduce with time, as shown in the first term of equation (2). Similarly, another two parameters reflecting the initial state for infiltration, i_0 and *S*, were also found to have little impact on the performance of the Horton model and the Holtan model, respectively. These two emprical models, however, were more greatly influenced by *k* and *a*, the parameters both controlling the decrease rate of infiltration. Therefore, more attention needs to be paid to those more 'sensitive' parameters when applying these infiltration models.

3.5 Conclusions

Infiltration experiments were carried out on 28 small plots with varied soil, vegetation and topography conditions, using a field rainfall simulator to identify the major controlling factors for the parameters in four popular infiltration models. The predictive regression equations were also developed for each infiltration parameter based on four factor sets that included different types and numbers of controlling factors. The results showed that the regression equations developed from the full factor set including all the factors were able to produce the parameter values for an accurate simulation of infiltration, while those based on soil related factors only failed in this study as they could not account for the great influences of other factors. The simplified factor set consisting of only θ_0, *Cover*, *Height* and *Rain*, four factors easily obtainable from either direct field measurement or RS and GIS techniques, did not achieve the expected success. However, the further incorporation of K_s significantly improved the efficacies of the regression equations. The results also showed that the performance of these infiltration models were more sensitive to the accuracy of their input parameters influencing the entire infiltration process than those affecting the initial stage of infiltration, only. Therefore, the results of this study have demonstrated that a better understanding of the effects of various factors - especially the vegetation and rainfall factors - on the different infiltration parameters is facilitating an improved estimation of the spatially varied infiltration parameter values for large scale studies by providing effective predictive equations. However, there are several limitations in this study. Firstly, a constant rainfall intensity was used for each rainfall event due to the constraint of the rainfall simulator, but the natural storm events are often featured by the temporally varied intensities. Thus the effects of the variations in a rainfall event (e.g., the peak intensity) on these infiltration parameters remain unclear. In addition, only a limited range of values for the controlling factors were investigated in this study (e.g., the soil texture only ranged from clay loam to sandy loam), and whether the developed predictive equations would be applicable to some other regions with different soil textures or other site features would require further investigation. Nevertheless, this study is expected to serve as a first approach to

explore the possibility of incorporating the vegetation and rainfall factors in estimating the parameters in the well-established infiltration models.

Chapter 4 Field Evaluation of Three Modified Infiltration Models for the Simulation of Rainfall Sequences

4.1 Introduction

Infiltration is one of the most important components in the surface hydrology cycle as it partitions the water entering the vadose zone from water running off on the ground surface. It is also a very complex process to determine as the infiltration rate varies both temporally and spatially. Various infiltration models have been developed for describing the dynamic infiltration process, and they have been widely incorporated in various hydrologic models. For example, the Green-Ampt model (Green and Ampt, 1911) is used in WEPP (Laflen et al., 1991), SWAT (Tuppad et al., 2011) and SWMM (Rossman, 2010), Philip model (Philip, 1957b) is integrated in WATFLOOD (Kouwen, 2012) and HYSIM (Manley, 1993), Horton model (Horton, 1940) is incorporated in MARINE (Estupina-Borrell et al., 2002) and SWMM, and Holtan model (Holtan, 1961) is used in LISEM (De Roo et al., 1996) and HEC-1 (Feldman, 1995).

A major limitation of these classical infiltration models is that most of them were developed from the ponding conditions, and thus are expected to be only valid for the single continuous rainfall events when the water supply rate is always larger than the infiltration capacity, in other words, when ponding occurs at all times. However, the natural rainfall events are not always constant and continuous, but often featured by temporally varied intensities and even several hiatus periods. This limitation is also reflected in the type of mathematical formulas used within these models. Some of them, such as Horton and Philip models, express the infiltration capacity as a function of time, and therefore resulting in the continuous decrease of infiltration with time during a simulation, even when the rainfall rate drops below the infiltration capacity or becomes zero. Some other models, such as Holtan and Green-Ampt models, determine the infiltration capacity on the basis of cumulative infiltration amount, and thus the infiltration capacity will decrease as the rainfall continues and become constant when no further infiltration occurs in the periods without rainfall. In reality, however, the infiltration capacity would be gradually recovered during the dry periods because of the redistribution of soil moisture caused by the soil drainage or percolation to deeper layers. The classical infiltration models could only describe the decrease of infiltration capacity, but not the increase or recovery of infiltration capacity. This has constrained the application of many hydrologic models to event-based or short-term simulations, only.

In order to make the hydrologic models applicable to more complex rainfall conditions or long term simulations, some modification or improvement to the classical infiltration models is required. Efforts for improvement have been made mainly along two different pathways. In the first pathway these models were improved by tracking the depth of penetration of an infiltration wetting front, with examples being the models proposed by Smith et al. (Smith et al., 1993), Corradini et al. (Corradini et al., 1994) and Corradini et al. (Corradini et al., 1997). While these wetting front models have a fundamental physical basis and have been found to be able to describe the soil water redistribution during the rainfall hiatus, they tend to be too complex and require too many input parameters. Considering that a distributed hydrologic model is in itself rather complex and requires considerable effort in preparing inputs due to the large spatial and temporal variations in the hydrological processes, the incorporation of these infiltration models would greatly increase the model complexity and reduce the computational efficiency, which is not desirable. Therefore, relatively simple representation of local infiltration is required.

A second pathway was the development of capacitance or bucket models which relate the fluxes to the soil storage values, according to Struthers et al. (Struthers et al., 2006). These models were basically developed from the improvement of some classical infiltration models by expressing the infiltration capacity as a function of a soil storage condition related parameter that was not constrained by time. A soil drainage component was also employed in these models to take into account the recovery of infiltration capacity during dry periods. Their typical examples are the modified Holtan model (Huggins and Monke, 1966; Huggins and Monke, 1968), modified Green-Ampt model (Bouraoui and Dillaha, 1996) and modified Horton model (Aron, 1992). Compared to the wetting front models, these capacitance models have the advantages in conceptual simplicity, simple parameterization and flexibility to various conditions. However, they have been rarely used in hydrologic models. In addition, despite of a similar conceptual basis and a similar model structure that includes both components for determining infiltration and soil drainage, the specific formulas and parameters used in different capacitance models are totally different from each other. Therefore, their performance and accuracies need to be evaluated and compared by systematic tests. While most of previous studies focused on testing the classical infiltration models on bare soils using ponded water in infiltrometers or continuous rainfall (Chahinian et al., 2005; Davidoff and Selim, 1986; Ghorbani Dashtaki et al., 2009; Mbagwu, 1995; Mishra et al., 2003), the evaluation of these modified models for rainfall sequences is lacking. Consequently, the main objective of this study was to evaluate the performance of three modified capacitance infiltration models (i.e., modified Holtan, Green-Ampt and Horton

models) on small field plots with different site conditions, using sequences of rainfall events produced by a rainfall simulator.

4.2 Materials and methods

4.2.1 Modified infiltration models

Three modified infiltration models for rainfall sequences were investigated for this study. Their specific formulas and calculation routines are as follows:

The initial Horton equation (Horton, 1940) considers infiltration as a natural "exhaustion process", during which infiltration capacity decreases exponentially with time, as shown in the following equation:

$$i_p = i_f + (i_0 - i_f)e^{-kt} \tag{4.1}$$

where i_p is the infiltration capacity (mm h^{-1}) at time t (h), i_0 and i_f is the initial and final steady infiltration rate (mm h^{-1}) respectively, and k is the infiltration decay coefficient (h^{-1}). Bauer (1974) introduced an equation to the original model to determine the soil drainage rate d_t (mm h^{-1}) on the basis of i_f, k and t, with the assumption that the rate of soil drainage rises as the soil wets up and the maximum drainage rate corresponds to the minimum infiltration rate. Then Aron (1992) further modified these equations by expressing the infiltration capacity and drainage rate as a function of cumulative soil water amount S_t' (mm) instead of time, and thus made the model applicable at any time during a rainfall event even when the rainfall rate drops below the infiltration capacity. The calculation routine and detailed formulas for the modified Horton model (MHR) are shown in Figure 4.1.

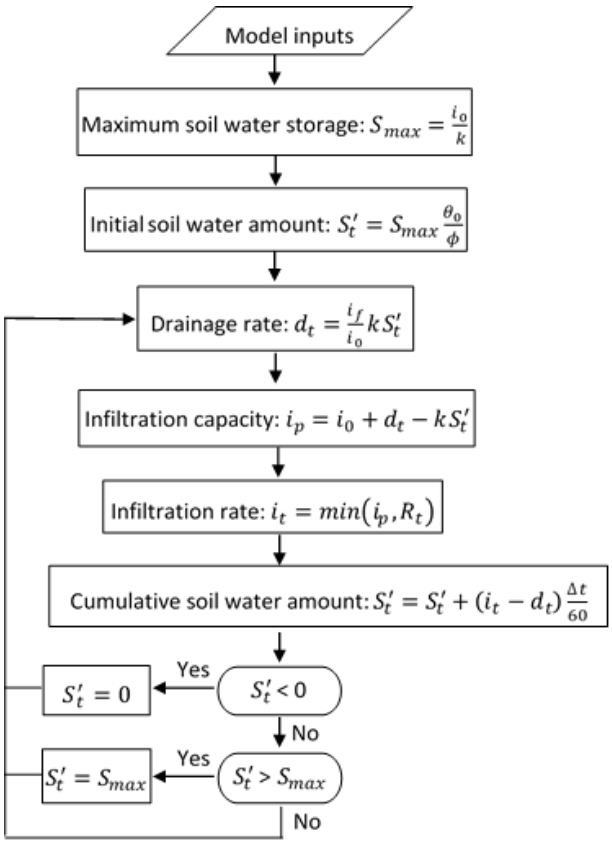

Figure 4.1 Calculation routine for the modified Horton Model. i_0 and i_f is the initial and final steady infiltration rate (mm h^{-1}) respectively, k is infiltration decay coefficient (h^{-1}), θ_0 is initial soil moisture (m^3 m^{-3}), ϕ is porosity (m^3 m^{-3}), R_t is rainfall intensity (mm h^{-1}) at time *t*, and Δt is time step (min) for calculation.

Green and Ampt (1911) proposed their original infiltration model based on Darcy's law, and expressed the infiltration capacity as:

$$i_p = K_s\left[1 + \frac{(\theta_s - \theta_0)\psi_f}{I_t}\right] \tag{4.2}$$

where K_s is the saturated hydraulic conductivity (mm h^{-1}), θ_s and θ_0 is the saturated and initial water content (cm^3 cm^{-3}) respectively, ψ_f is the suction at the wetting front (mm), and I_t is the cumulative infiltration (mm) at time *t*. The original model was modified to relate i_p to the cumulative soil water amount S_t' in ANSWERS-2000 (Bouraoui and Dillaha, 1996), where the equations developed by Savabi et al. (1989) were employed to calculate d_t when the soil moisture exceeds the field capacity. The calculation routine and detailed formulas for the modified Green-Ampt model (MGA) is shown in Figure 4.2.

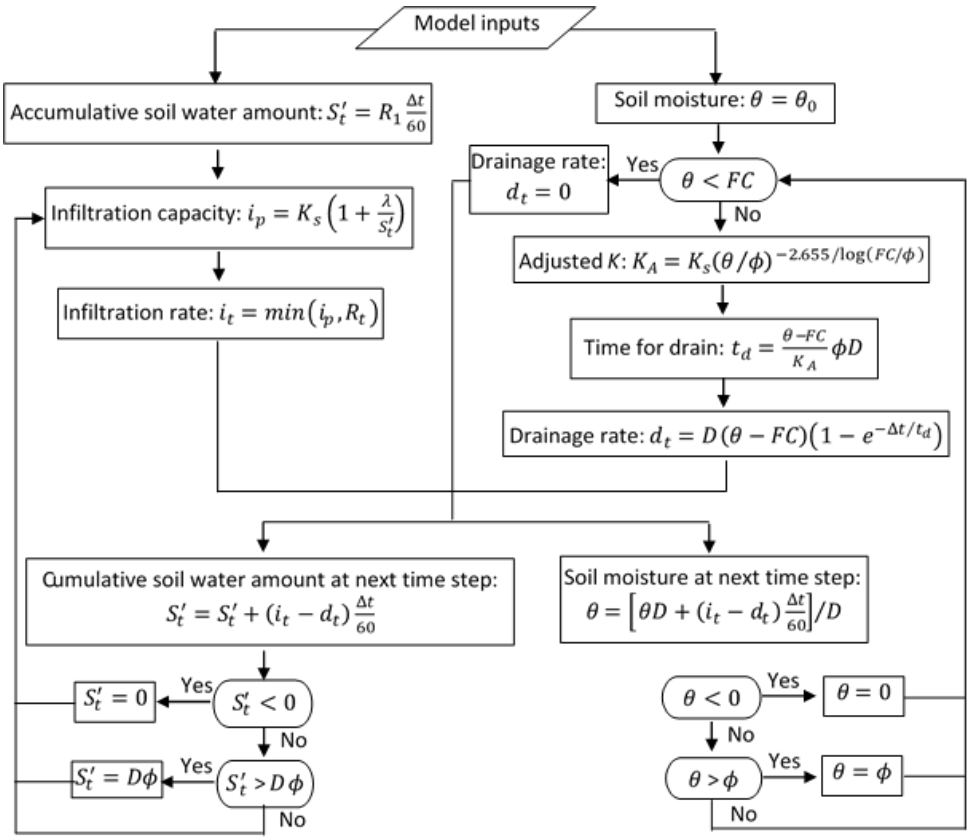

Figure 4.2 Calculation routine for the modified Green-Ampt Model. K_s is saturated hydraulic conductivity (mm h^{-1}), λ is a constant (mm), θ_0 is initial soil moisture (m^3 m^{-3}), FC is field capacity (m^3 m^{-3}), ϕ is porosity (m^3 m^{-3}), D is control zone depth (mm), R_1 is initial rainfall intensity (mm h^{-1}), R_t is rainfall intensity (mm h^{-1}) at time t, and Δt is time step (min) for calculation.

Using a storage exhaustion concept, Holtan (1961) derived an infiltration model expressed as:

$$i_p = i_f + a(S_0 - I_t)^{1.4} \tag{4.3}$$

where a is a constant ($mm^{-0.4}$ h^{-1}) dependent on soil type, surface and cropping conditions, and S_0 is the initial soil water storage potential (mm). Huggins & Monke (1966; Huggins and Monke, 1968) introduced a soil water drainage component to the original Holtan model based on the assumption that when soil moisture exceeds the field capacity, the water will move from the control zone at a drainage rate related to current soil storage potential S_t (mm). The calculation routine and detailed formulas for the modified Holtan model (MHL) is shown in Figure 4.3.

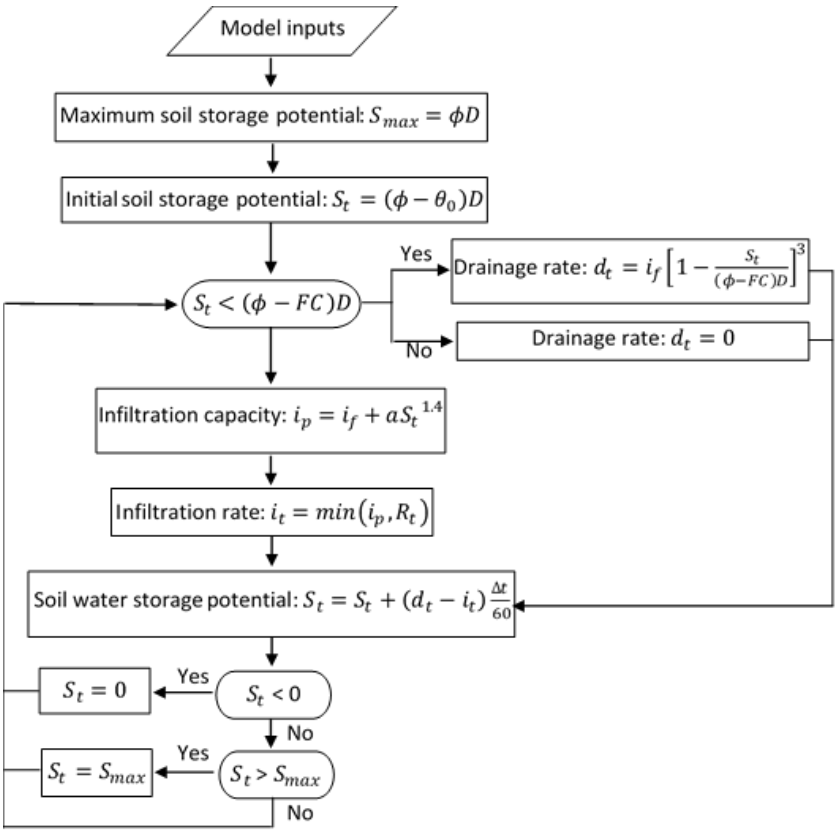

Figure 4.3 Calculation routine for modified Holtan Model. ϕ is porosity (m^3 m^{-3}), D is control zone depth (mm), θ_0 is initial soil moisture (m^3 m^{-3}), FC is field capacity (m^3 m^{-3}), i_f is final steady infiltration rate (mm h^{-1}), a is a constant ($mm^{-0.4}$ h^{-1}), R_t is rainfall intensity (mm h^{-1}) at time t, and Δt is time step (min) for calculation.

4.2.2 Experimental procedure

The study has been carried out at the experimental farm of The University of Queensland, Pinjarra Hills in Queensland, Eastern Australia, where the climate is humid subtropical. The average annual rainfall in this area is around 1000 mm, 66% of which occurs in the wet season from October to March. The minimum monthly mean temperature is 15 ℃ in July and the maximum value is 25 ℃ in January.

28 small plots, with the size of 1 m × 1 m, were randomly set up at the study site. These plots were featured by different soil, topography and vegetation characteristics (Figure 4.4), thus allowing the evaluation of infiltration models under different site conditions. A large number of previous studies have used 1 m^2 plots to field investigate the infiltration behaviours (Dos Reis Castro et al., 1999; Le Bissonnais et al., 1998; Leonard and Andrieux, 1998; Patin et al., 2012), and the infiltration characteristics and the site conditions have been found to be relatively spatially homogenous in such a small plot in this study area (Shao and Baumgartl, 2014). To set up the plot, a 1 m × 1 m metal frame

was sunk into the ground to 5 cm depth, with a 10 cm extension above the ground to prevent the runoff produced outside the frame from flowing into the plot. At the bottom of each plot, a V-shape runoff collector was installed to collect and measure runoff. The vegetation coverage, a mean vegetation height and the slope gradient were also investigated for each plot. Before the start of each rainfall event, three undisturbed soil core samples were taken at the depth of 0-5 cm in the area immediately adjacent to the plots for the laboratory measurement of input infiltration parameters and other basic soil properties. Specifically, the core samples were placed in a tray filled with shallow water for 2 to 4 days to reach the saturated condition. Then the saturated core samples were placed on a suction plate with a suction pressure of 33 kPa (0.33 bar) for 7 days to achieve field capacity. Values of the initial soil moisture, field capacity and saturated soil moisture of collected soil samples were calculated from their weights before and after oven-drying at 105 ℃ for 24 h. The total porosity was assumed to be equal to the saturated soil moisture in this study, and the dry bulk density was determined from the ratio of the oven-dried soil weight and the soil volume. With respect to the soil particle distribution analysis, the stone fraction (> 5.3 mm) and gravel fraction (2.0 - 5.3 mm) were both determined by the dry sieving method, the coarse sand fraction (0.2 – 2.0 mm) was derived by the wet sieving method, and the fine sand (0.02 – 0.2 mm), silt (0.002 – 0.02 mm) and clay (< 0.002mm) fractions were measured using the hydrometer method. In addition, the weight of roots in each soil sample was also measured.

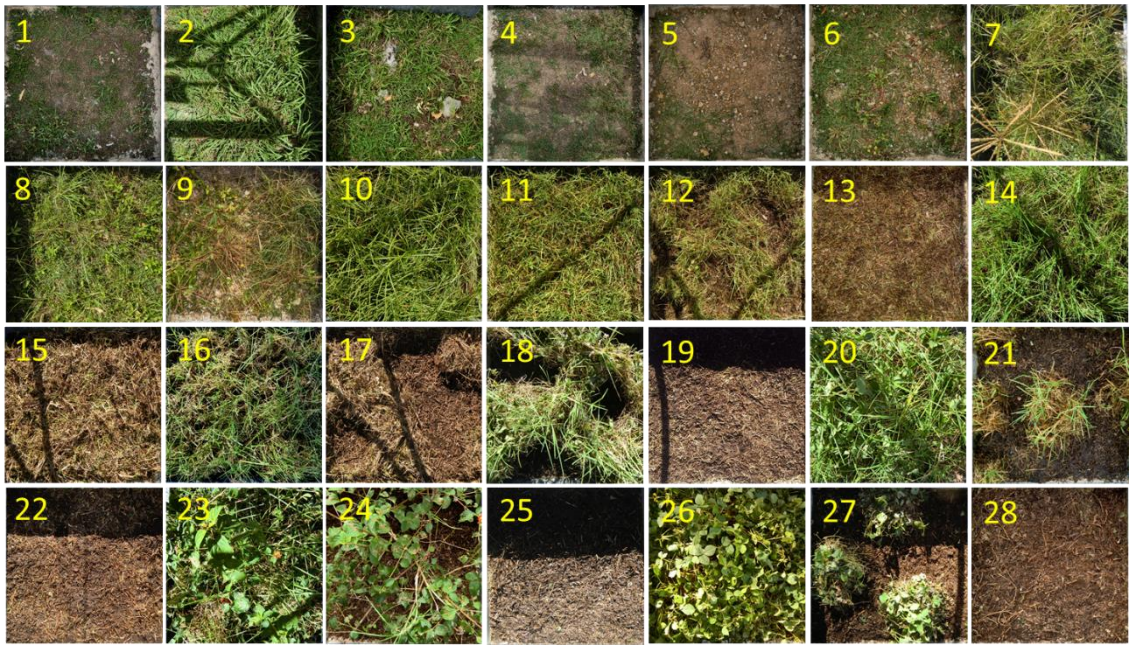

Figure 4.4. Orthogonal top view photos of 1 m × 1 m field plots.

A field rainfall simulator with Veejet 80100 nozzles, which are controlled to sweep to and from across a plot, was used to generate the rainfall. Loch (2001) provides more detailed information for this type of rainfall simulator and has proven its capability in producing the rainfall with the kinetic energies of intense natural rain and the intensity of a small coefficient of variation (8-10%) in its spatial distribution. For each plot, a continuous rainfall event was firstly applied until a stable runoff rate was reached, for the calibration of the target infiltration models. The field saturated hydraulic conductivity and the final steady state infiltration rate were assumed to be equal here and were both determined by the average values of the last five observed infiltration rates in this calibration rainfall event. A sequence of rainfall events were then applied 24 h after the first continuous rainfall event, for the validation purpose. This rainfall sequence consisted of four pulses of rainfall, with each duration of about 0.5 h, separated by three hiatuses. The first two hiatuses were relatively short and both had a duration of about 1 h, while the third one was much longer, with a duration of about 18 h. During each rainfall period, the intensity of the produced rainfall was measured by four measuring cups distributed across the plot, and the surface runoff was collected at the outlet of the runoff collector for 30 seconds in every one minute for the first 15 minutes and in every two minutes for the remaining period. The measured rainfall intensity varied in different rainfall events (66.8 - 103.6 mm h^{-1}) as shown in Table 4.2, because of the differences in the height of nozzles, water pressure or weather conditions (e.g., wind). Relatively large rainfall intensities were applied here in order to ensure the occurrence of runoff, which was necessary for determining the infiltration rates and also to reduce the time to runoff generation to minimize potential inaccuracies caused by missing infiltration information prior to the starting of runoff. The actual infiltration rates at different time points were then calculated by subtracting these measured runoff rates from the measured rainfall intensity.

Table 4.1 Measured and calibrated input parameters for three modified infiltration models.

Models [a]	**Measured parameters** [b]				**Calibrated parameters** [b]				
	$i_f(K_s)$	ϕ	θ_0	FC	i_0	k	a	D	λ
MHL	√	√	√	√			√	√	
MGA	√	√	√	√				√	√
MHR	√	√	√		√	√			

[a] MHL: modified Holtan model; MGA: modified Green-Ampt model; MHR: modified Horton model.

[b] i_f : final steady infiltration rate (mm h^{-1}); K_s : saturated hydraulic conductivity (mm h^{-1}); ϕ: soil porosity (m^3 m^{-3}); θ_0: initial soil moisture (m^3 m^{-3}); FC: field capacity (m^3 m^{-3}); i_0: initial infiltration rate (mm h^{-1}); k: infiltration decay coefficient (h^{-1}); a: a constant ($mm^{-0.4}$ h^{-1}) in modified Holtan model; D: control zone depth (mm); λ: a constant (mm) in modified Green-Ampt model.

4.2.3 Statistical Analysis

The required input parameters for each of the three modified infiltration models are summarised in Table 4.1. It can be seen that some of these parameters could be directly measured from field investigation or laboratory analysis, while others were very difficult to measure and had to be indirectly determined by calibration with the observed results in the first continuous rainfall event. The goodness of fit of the predicted infiltration curve to the observed infiltration rates was tested by both the coefficient of determination (R^2) and the root mean square error (*RMSE*). R^2 indicates how accurately the model tracks the variation of observed values, and its value can range from 0 to 1 (perfect fit). *RMSE* shows the amount of divergence of the model values from the observed values and its value close to 0 indicates good agreement. In addition, the percentage of error (*PE*) was used to assess the under- or over-prediction and the magnitude of prediction error in the total infiltration amount. The mathematical expressions used for these three statistical analysis measures are:

$$R^2 = \left(\frac{\sum_{i=1}^{n} \left(O_i - \bar{O}\right)\left(P_i - \bar{P}\right)}{\sqrt{\sum_{i=1}^{n} \left(O_i - \bar{O}\right)^2} \sqrt{\sum_{i=1}^{n} \left(P_i - \bar{P}\right)^2}} \right)^2 \tag{4.4}$$

$$RMSE = \sqrt{\frac{1}{n} \sum_{i=1}^{n} \left(O_i - P_i\right)^2} \tag{4.5}$$

$$PE = \frac{P_i - O_i}{O_i} \times 100\% \tag{4.6}$$

where n is number of observations during the prediction period; O_i and P_i are observed and predicted values at each comparison point i; $\bar{O}$ and $\bar{P}$ is arithmetic mean of the observed and predicted values, respectively.

Results from the four separated rainfall pulses in the rainfall sequence were used to validate the three modified infiltration models. The overall model performance during the entire sequence of rainfall was also evaluated. This led to five datasets in total for model validation. R^2 and *RMSE* were employed to assess the agreement of predicted and observed infiltration rates at various time points in each dataset, and *PE* was used to represent the prediction accuracies in total infiltration amount and the initial soil moisture. Correlation analysis was then performed to identify the relationships between model performance and different site conditions, by calculating the Pearson correlation coefficient (r) using

SPSS Statistics 22. The *r* values range from -1 to +1, with the sign indicating the direction of the relationship, and its absolute value indicating the strength of the relationship.

4.3 Results and discussion

4.3.1 Parameterisation of infiltration models

The investigated site conditions for the field plots were summarised in Table 4.2. It can be seen that most of the plot features had a large range of values, except for the slope gradient which had a maximum value of only 5% due to the difficulty in setting up the rainfall simulator on steeper slopes. The soil in the plots had various textures ranged from clay loam to sandy loam, as well as significantly different physical and hydraulic properties. For the vegetation features, the plots varied from totally bare soil conditions to those fully covered by vegetation (as also shown in Figure 4.4).

Table 4.2 Summary of results for the plot features and infiltration parameters.

Plot feature /infiltration parameter [a]	**Min.**	**Max.**	**Range**	**Mean**	**Std. Deviation**
		Plot features			
Rainfall intensity (mm h^{-1})	66.8	103.6	36.8	89.2	9.30
Slope gradient (%)	1	5	4	2.54	1.07
Bulk density (g cm^{-3})	0.53	1.17	0.64	0.78	0.20
Porosity (m^3 m^{-3})	0.33	0.55	0.22	0.45	0.07
Stone content (g g^{-1})	0.01	0.36	0.36	0.11	0.10
Gravel content (g g^{-1})	0.06	0.25	0.19	0.16	0.07
Sand content (g g^{-1})	0.26	0.52	0.26	0.41	0.09
Silt content (g g^{-1})	0.06	0.25	0.20	0.17	0.06
Clay content (g g^{-1})	0.08	0.19	0.11	0.14	0.03
Root content (kg/m^3)	0.10	10.30	10.20	3.80	2.70
Vegetation cover (m^2 m^{-2})	0	1.00	1.00	0.62	0.37
Plant height (m)	0	0.87	0.87	0.28	0.27
		Measured infiltration parameters			
$K_s(i_f)$ (mm h^{-1})	2.64	85.29	82.65	40.33	27.07
ϕ (m^3 m^{-3})	0.33	0.55	0.22	0.45	0.07
θ_0 (m^3 m^{-3})	0.11	0.53	0.42	0.36	0.12
FC (m^3 m^{-3})	0.18	0.37	0.20	0.29	0.06
		Calibrated infiltration parameters			
i_0 (mm h^{-1})	116.34	762.31	645.97	371.33	208.99

k (h^{-1})	1.49	3.09	1.60	2.11	0.44
a ($mm^{-0.4}$ h^{-1})	0.04	0.51	0.48	0.18	0.12
D (m)	0.23	1.96	1.73	0.76	0.40
λ (m)	0.18	200.52	200.34	21.29	46.36

[a] i_f : final steady infiltration rate; K_s: saturated hydraulic conductivity; ϕ: soil porosity; θ_0: initial soil moisture; *FC*: field capacity; i_0: initial infiltration rate; *k*: infiltration decay coefficient; *a*: a constant in modified Holtan model; *D*: control zone depth; λ: a constant of the modified Green-Ampt model.

The greatly varied site conditions resulted in large variations in the rainfall duration (72 - 123 min) and runoff coefficient (8.8% - 70.8%) of the calibration rainfall events. The measured and calibrated input parameter values for the investigated infiltration models also had large ranges (Table 4.2). Figure 4.5 shows the parameterisation results on plot 10, 9 and 22, which were selected for demonstration because they were representative for the conditions of low (9.0%), medium (35.1%) and high (59.7%) runoff coefficient in sequence. It can be seen that the predicted infiltration curves by the three modified infiltration models all fit the observed infiltration rates well on the three plots. Statistical analysis on the whole range of plots further showed that the mean R^2 in the calibration process of all the plots was 0.960 ± 0.014, 0.941 ± 0.029 and 0.961 ± 0.017 for MHL, MGA and MHR respectively, the mean *RMSE* was 4.985 ± 1.919 mm h^{-1}, 6.659 ± 2.620 mm h^{-1} and 4.577 ± 1.991 mm h^{-1} respectively, and the mean percentage error in total infiltration amount (*PE-I*) was $3.034 \pm 1.839\%$, $3.554 \pm 3.865\%$ and $1.598 \pm 2.255\%$ respectively. These large R^2 values and small *RMSE* and *PE-I* values indicated that the three modified infiltration models were able to describe the infiltration process in the continuous calibration rainfall events very well, with no significant difference among their performance. It can be also concluded that the values of the calibrated infiltration parameters had high accuracy and reliability.

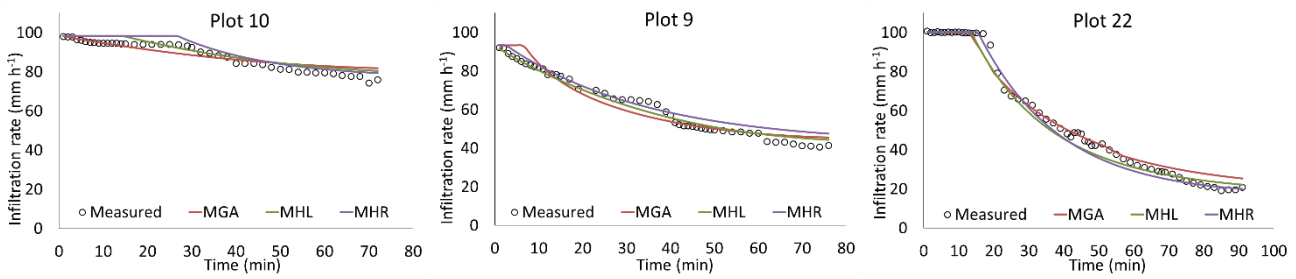

Figure 4.5 Calibration of three modified infiltration models on three representative plots using the continuous rainfall events. Plot 10, 9 and 22 is featured with low (9.0%), medium (35.1%) and high (59.7%) runoff coefficient, respectively. MGA, MHL, MHR represents modified Green-Ampt, Holtan and Horton model, respectively.

4.3.2 Evaluation of infiltration models

The evaluation results of the three modified infiltration models, which document an independent validation of the model, using the five different datasets are summarised in Table 4.4. It can be seen that in the dataset of the first rainfall pulse (R1) in the rainfall sequence, all three models performed well, with high R^2 and low *RMSE* and *PE-I* values. No significant difference was found between their performances.

In the dataset of the second rainfall pulse (R2), the performance of MHL and MGA was significantly (P<0.05) better than that of MHR. When comparing to the results in R1, a significant decrease in R^2 and significant increases in both *RMSE* and *PE-I* were observed for MHR (P<0.05), indicating a significant reduction in the simulation accuracy. However, the performance of both MHL and MGA was maintained at a high level and was comparative to that in R1.

In the third rainfall pulse (R3), MHL had the best performance which was not significantly different from that in the previous rainfall periods. MGA had comparative R^2 with MHL, however, its *RMSE* was significantly larger (P<0.05), indicating a reduced accuracy. Horton produced significant errors, with small R^2 and large *RMSE* and *PE-I* values.

In the fourth rainfall pulse (R4), which followed a long dry period, the R^2 values of both MHL and MGA were only slightly decreased. However, their *RMSE* values were significantly increased (P<0.05) when compared to those in the previous rainfall pulses. MHR was totally failed in this dataset, as reflected by the extremely small R^2 and large *RMSE* and *PE-I*.

It can be observed that the simulation accuracy of the three models all decreased from R1 to R4, probably attributed to the accumulation of errors in the predicted initial soil moisture. Results in the

dataset of the entire sequence of rainfall suggested the overall good performance of MHL and MGA, but a significantly (P<0.05) poorer performance of MHR.

Table 4.3 Summary of statistic values for the evaluation of different infiltration models during the rainfall sequences.

Models [a]	R1 [b]	R2 [b]	R3 [b]	R4 [b]	Entire [b]
			R^2 [c]		
MHL	0.81±0.23 Aa	0.82±0.12 Aa	0.84±0.09 Aa	0.78±0.23 Aa	0.86±0.06 Aa
MGA	0.82±0.23 Aa	0.82±0.12 Aa	0.81±0.14 Aa	0.77±0.27 Aa	0.83±0.06 Aa
MHR	0.74±0.31 Aa	0.52±0.35 Bb	0.58±0.36 Bb	0.09±0.19 Bc	0.64±0.22 Bab
IMHR	0.78±0.36 Aa	0.79±0.14 Aa	0.80±0.17 Aa	0.71±0.26 Ab	0.85±0.09 Aa
			RMSE (mm/h) [c]		
MHL	4.44±2.33 Aa	4.41±2.35 Aa	6.65±3.63 Aa	15.60±9.58 Ac	9.59±5.08 Ab
MGA	5.60±3.02 Aa	5.62±3.36 Aa	9.34±5.02 Ab	15.14±11.98 Ac	10.46±6.88 Ab
MHR	4.75±2.90 Aa	13.21±7.91 Bb	16.72±9.54 Bb	26.04±20.98 Bc	18.52±11.16 Bb
IMHR	4.68±2.68 Aa	5.65±2.49 Aa	5.42±2.36 Aa	16.13±12.44 Ac	10.07±6.37 Ab
			PE-I (%) [c]		
MHL	0.16±1.46 Ba	1.98±10.02 Ab	5.06±18.06 Bc	6.54±24.60 Ac	3.85±8.74 Abc
MGA	-1.57±3.79 Aa	6.28±14.20 Bb	8.76±22.73 Bbc	9.99±29.46 Ac	5.56±11.66 Ab
MHR	0.51±3.36 Ba	24.21±20.38 Cb	52.05±31.91 Cd	34.75±33.71 Bc	18.81±12.27 Bb
IMHR	1.92±2.43 Cc	-2.73±11.14 Ab	-9.15±9.11 Aa	10.69±28.72 Ad	2.84±8.43 Ac
			PE-θ_0 (%) [c]		
MHL	-	14.03±17.79 Bc	7.16±12.70 Bb	0.92±13.88 Ba	-
MGA	-	12.62±16.69 Bc	4.74±11.71 Bb	-2.88±13.82 Ba	-
MHR	-	-4.66±22.52 Ac	-14.92±25.30 Ab	-86.60±22.32 Aa	-
IMHR	-	16.74±18.15 Bc	8.38±12.67 Bb	-4.47±9.29 Ba	-

[a] MHL: modified Holtan model; MGA: modified Green-Ampt model; MHR: modified Horton model; IMHR: improved modified Horton model.

[b] R1, R2, R3 and R4 represents the first, second, third and fourth rainfall pulse in the rainfall sequence, respectively; 'Entire' represents the entire rainfall sequence.

[c] R^2: coefficient of determination; *RMSE*: root mean square error; *PE-I*: percentage error in total infiltration volume; *PE-θ_0*: percentage error in initial soil moisture.

Figure 4.6, describing the predicted infiltration curves on plot 10, 9 and 22, showed some examples of the validation results through visual assessment of the model performance. It can be seen that for all three plots, both MHL and MGA performed well in all the four rainfall pulses of the rainfall sequence, while MHR only had satisfactory performance during R1, but produced significant errors in the other rainfall pulses.

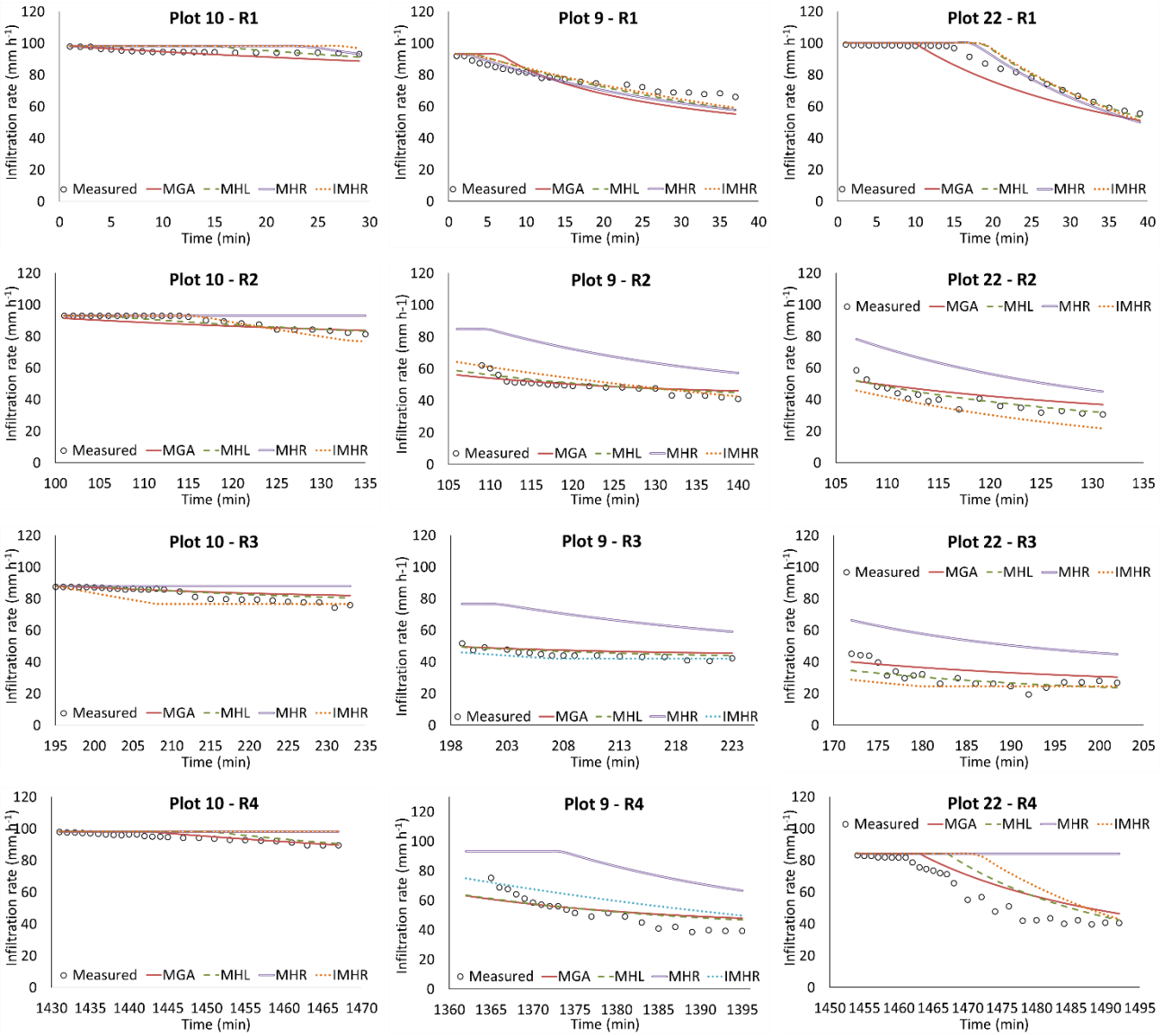

Figure 4.6 Evaluation of modified infiltration models on representative plots using different datasets. Plot 10, 9 and 22 is featured with low (9.0%), medium (35.1%) and high (59.7%) runoff coefficient, respectively. R1, R2, R3 and R4 represents the first, second, third and fourth rainfall pulse in the rainfall sequence, respectively. MGA, MHL, MHR represent the modified Green-Ampt, Holtan and Horton model, respectively, and IMHR represents the improved modified Horton model.

4.3.3 Improvement of the modified Horton model

Aforementioned evaluation results have shown that among the three investigated infiltration models, only MHR failed in describing the infiltration behaviour during the rainfall sequences. The reasons for the poor performance of MHR can be identified from the values of *PE-I* and *PE-*θ_0 (percentage error in initial soil moisture) in Table 4.3, which indicated that MHR significantly overestimated the total

infiltration amount, while it significantly underestimated the initial soil moistures ($P<0.05$). Figure 4.7 also demonstrated that MHR tended to overestimate the soil drainage rate and thus the recovery of infiltration capacity. This was further verified by comparing the predicted soil drainage coefficient, the ratio of total soil drainage volume to the total rainfall volume during the rainfall sequence. The results showed that the mean drainage coefficient predicted by MHR (0.984 ± 0.260) was significantly ($P<0.05$) larger than those predicted by MHL (0.422 ± 0.141) and MGA (0.459 ± 0.136). The overestimation of soil drainage by MHR can be attributed to two possible reasons. Firstly, MHR calculates soil drainage at any time even when the soil moisture is smaller than the field capacity (Figure 4.1), while in both the other two models there is a constraint that the soil only drains water when the soil moisture exceeds the field capacity (Figure 4.2 and 4.3). The second reason might be that the formula used for determining soil drainage rate in MHR tended to calculate too large drainage rate values.

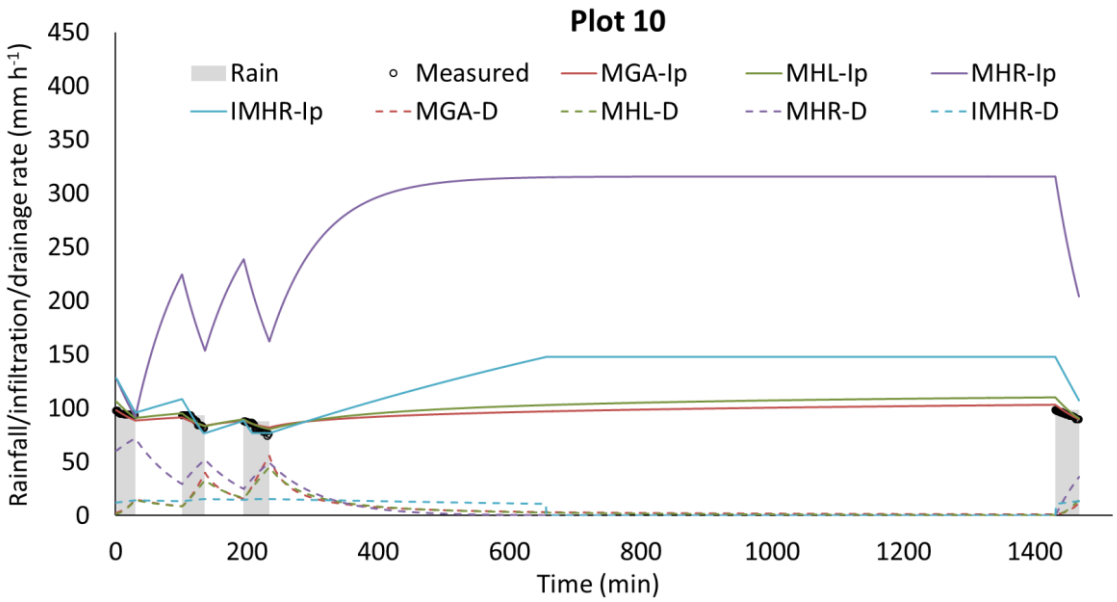

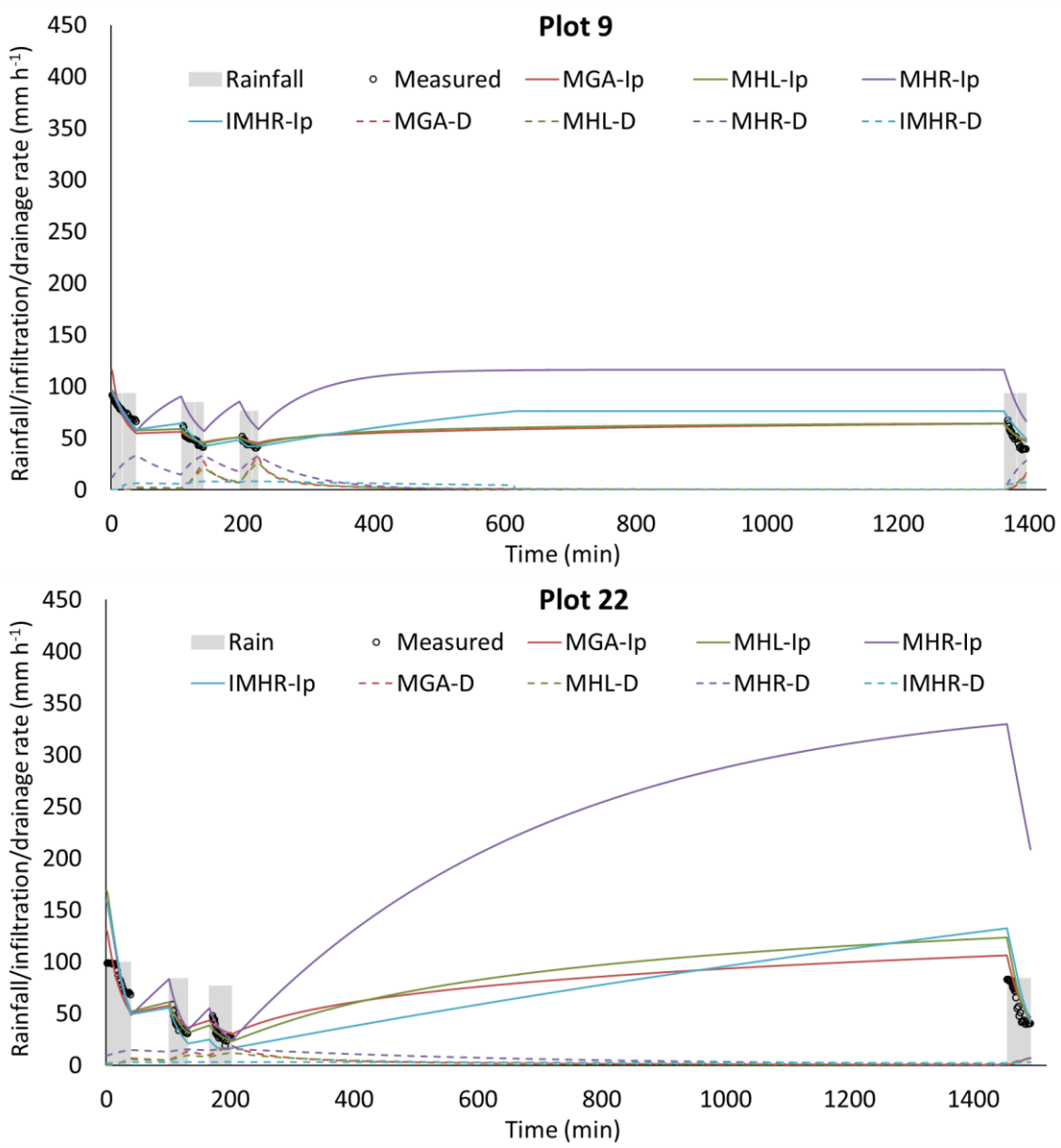

Figure 4.7 Predicted infiltration capacity curves (Ip) and soil drainage rate curves (D) by different modified infiltration models during the rainfall sequence applied on representative plots. Plot 10, 9 and 22 is featured with low (9.0%), medium (35.1%) and high (59.7%) runoff coefficient, respectively. MGA, MHL, MHR represents the modified Green-Ampt, Holtan and Horton model, respectively, and IMHR represents the improved modified Horton model.

Therefore, attempts have been made in this study to further improve the accuracy of the original MHR, by introducing a constraint of field capacity and applying a reduction coefficient β to the soil drainage formula. By testing different values of β ranged from 1 to 0, the highest simulation accuracies were achieved when β equalled to 0.2. The resultant calculation routine and detailed formulas for the

improved MHR (IMHR) were shown in Figure 4.8. From Table 4.3, it can be seen IMHR had significantly larger R^2 values while significantly smaller *RMSE*, *PE-I* and *PE-*θ_0 values than MHR ($P<0.05$), indicating the greatly improved model performance. Furthermore, there was no significant difference between the results of IMHR and those of MHL or MGA, suggesting a comparative performance of IMHR with the latter two models. These findings were further verified in Figure 4.6, where the predicted infiltration curves by IMHR agreed well with the observed values in all rainfall pulses. Results of the drainage coefficients indicated that IMHR (0.437 ± 0.163) estimated significantly less soil drainage than MHR (0.437 ± 0.163), and its results were very close to those of MHL (0.422 ± 0.141) and MGA (0.459 ± 0.136). However, Figure 4.7 showed that while their drainage coefficients were very similar, they had different shapes of drainage curves. IMHR tended to produce a flat drainage curve with a long duration, while the curves produced MHL and MGA were both fluctuant and more sensitive to the changes of rainfall intensities.

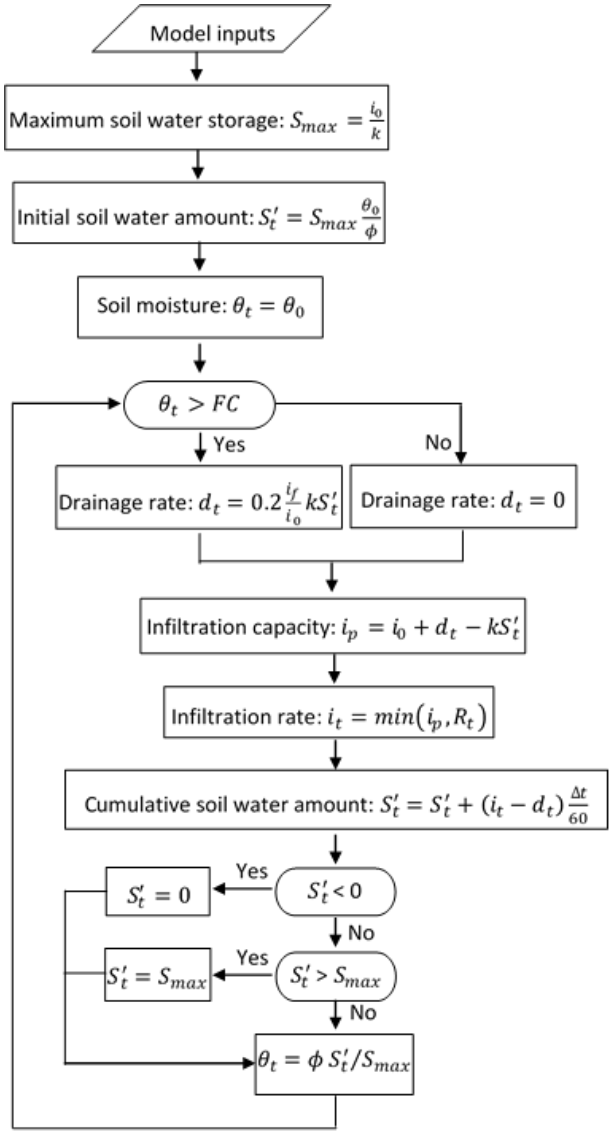

Figure 4.8 Calculation routine for improved modified Horton Model (IMHR). i_0 and i_f is the initial and final steady infiltration rate (mm h^{-1}) respectively, k is infiltration decay coefficient (h^{-1}), θ_0 is initial soil moisture (m^3 m^{-3}), ϕ is porosity (m^3 m^{-3}), FC is field capacity (m^3 m^{-3}), R_t is rainfall intensity (mm h^{-1}) at time t, Δt is time step (min) for calculation, and θ_t is soil moisture at time t (m^3 m^{-3}).

4.3.4 Effects of site conditions on model performance

In spite of the overall high simulation accuracies of MHL, MGA and IMHR, the relatively large standard error values shown in Table 4.3 suggested the possible varied model performance on different plots and under different site conditions. Therefore, correlation analysis was further conducted to identify which factors would have great influences on the model performance. The factors selected for analysis included various topography, soil and vegetation related plot features as listed in Table 4.2,

as well as the rainfall intensity and runoff coefficient for each rainfall event. In addition, the accuracies of the input parameter values were also taken into account, by including R^2, *RMSE*, *PE-I* and *PE-*θ_0 values for the model calibration.

Correlation analysis showed that in all validation datasets, R^2 values of the three models had significant (P<0.05) and negative correlations with the vegetation cover and root content. This result suggests that the simulation accuracy could be affected by the presence of vegetation, probably due to the fact that these infiltration models were primarily developed for bare soils and that vegetation would affect the infiltration process by intercepting and storing rainfall, protecting the soil surface against the impact of raindrops, and changing the soil properties and thus the infiltration characteristic (Deuchars et al., 1999; Foley et al., 1991; Puigdefábregas, 2005; Wilcox et al., 1988). In addition, in all datasets except for R1, *PE-I* of three models were all significantly (P<0.05) and positively correlated with the runoff coefficient, suggesting that these models tended to produce relatively large biases in total infiltration when the infiltration rates were low. However, no significant correlation was found between simulation accuracy and slope gradient or any soil related factor, indicating that the model performance was not affected by either soil properties or topography conditions. Further, it was found that in all rainfall pulses, R^2, *RMSE* and *PE-I* for the model validations were significantly (P<0.05) and positively correlated to those for model calibration, highlighting the importance of the accurate determination of input parameter values.

4.3.5 Model sensitivity analysis

The performance of the investigated infiltration models has been found to be closely associated with the accuracy of their input parameters. It is therefore essential to understand which parameters have the most prominent impact on the modelling results. For this purpose, a model sensitivity analysis was carried out. The rainfall sequence applied on plot 9 was selected as a representative for this analysis. Then four 20% decrements and four 20% increments from the base infiltration parameter values (measured or calibrated results) were applied. Two output parameters, total infiltration volume (*INF*) and total soil drainage volume (*DR*), were used to evaluate the model responses.

Figure 4.9 shows that *INF* and *DR* predicted by MHL, MGA and IMHR were both most sensitive to K_s or i_f, demonstrating the importance of these two parameters which reflect the steady or minimum infiltration capacity of the soil. *INF* was also largely influenced by some other input parameters. Specifically, both ϕ and *D*, the two parameters determining the soil storage capacity, had large impacts on *INF* predicted by MHL, while only ϕ had obvious impacts on *INF* in MGA. MHR showed great

sensitivity to i_0 and *k* in *INF*. Compared to *INF*, greater variations were found in *DR* in both MHL and MGA, where *DR* was largely sensitive to all of their parameters. In IMHR, however, *DR* was only sensitive to some of its parameters, including i_f, *FC* and *k*.

From the results, it can be seen that *DR* tended to be more sensitive to the changes in input parameters than *INF*. This may be attributed to the fact that in these models the actual infiltration rate was determined by the smaller value between the rainfall intensity and the soil infiltration capacity, while the soil drainage rate was solely dependent on the soil conditions. Moreover, the input parameters influencing the entire infiltration process, such as K_s, i_f, ϕ, *D*, *FC* and *k*, were found to have larger impacts on the modelling results than the parameters that only had significant influences at the initial stage of infiltration, such as *a*, θ_0, λ and i_0. In addition, the three infiltration models showed some differences in their responses to different input parameters. On the whole, MHL and MGA showed greater parameter sensitivity than IMHR. This agrees with the correlation analysis results that MHL and MGA had larger correlations (0.752 and 0.724 respectively) between *PE-I* and *RMSE* for calibration than IMHR (0.564). It can be concluded from this comparative study that the prediction accuracy of MHL and MGA tended to be influenced to a greater extent by the errors in their input parameter values than IMHR, and more attention needs to be paid to those more sensitive input parameters when applying these infiltration models.

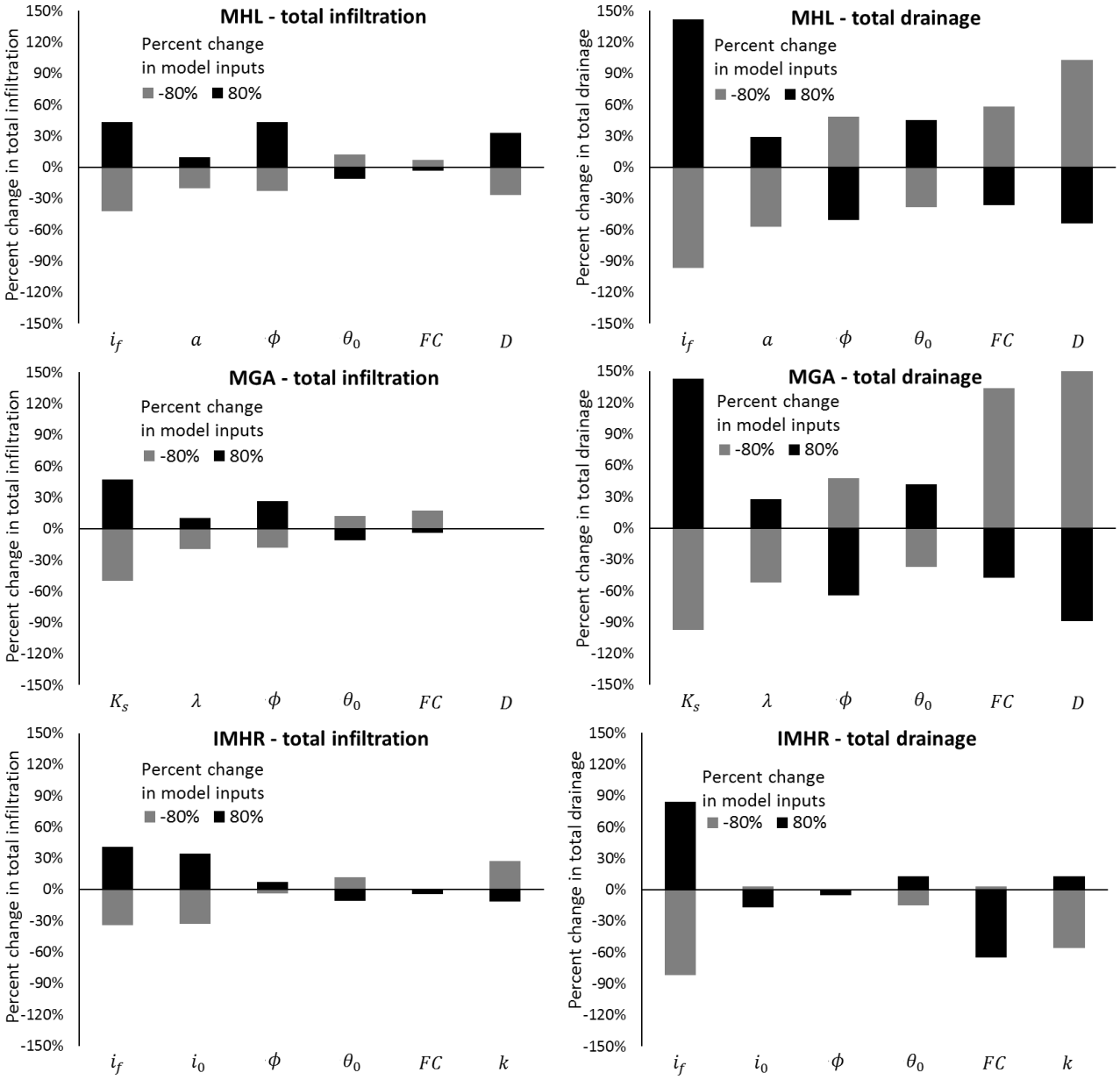

Figure 4.9 Results for model sensitivity analysis on plot 9 during the rainfall sequence. MGA, MHL and IMHR represents the modified Green-Ampt model, modified Horton model and the improved modified Horton model, respectively. i_0 and i_f is initial and final steady infiltration rate (mm h^{-1}), respectively, K_s is saturated hydraulic conductivity (mm h^{-1}), ϕ is soil porosity (m^3 m^{-3}), θ_0 is initial soil moisture (m^3 m^{-3}), FC is field capacity (m^3 m^{-3}), k is infiltration decay coefficient (h^{-1}), D is control zone depth (mm), and a ($mm^{-0.4}$ h^{-1}) and λ (mm) are both constant.

4.4 Conclusions

Performance of three infiltration models modified for sequences of rainfall were evaluated on small field plots with varied site conditions, using simulated rainfall sequences which consisted of four

rainfall pulses and three hiatus. Despite of the gradually reducing simulation accuracy from the first rainfall pulse to the last one, both MHL and MGA had satisfactory and comparative performance during the entire rainfall sequence, with large R^2 values and small *RMSE* and *PE-I* values when comparing the predicted results to observed values. MHR, however, failed in accurately describing the infiltration processes due to its overestimation of soil drainage rate. MHR could be improved by applying a constraint that soil only drains water when soil moisture exceeds field capacity and introducing a reduction coefficient which equalled to 0.2 to the formula for calculating soil drainage rate. IMHR was found to significantly improve the simulation accuracy of MHR, and its performance was comparative to that of MHL and MGA. Correlation analysis showed that the performance of MHL, MGA and IMHR did not vary significantly under different soil, topography or rainfall conditions, but was negatively related to vegetation cover because of the role of vegetation in influencing the infiltration process. Model performance was also found to be greatly impacted by the accuracy in determining the input parameters. Sensitivity analysis was conducted for these three models. The results showed that the models were mostly sensitive to the input parameters representing the final steady infiltration capacity. Furthermore, they tended to be more sensitive to the parameters affecting the entire infiltration process compared to those which only had significant impacts at the initial stage of infiltration. In addition, MHL and MGA showed greater sensitivity to the errors in input parameters values than IMHR.

Based on all results from this study, MHL, MGA and IMHR have been proven to be able to well describe the infiltration processes during the sequences of rainfall events. They also have simple calculation routines and formulas and thus are expected to be computationally efficient. Therefore, by incorporating these modified infiltration models, the applications of many hydrologic models are expected to be extended from the predictions of single continuous rainfall events to more complex rainfall sequences, and from short-term simulations to long-term simulations. Since these three models had comparative performance and the same complexity in their input parameters (i.e, four measurable and two calibrated parameters), no direct preference among them could be derived from this study. However, prior to implementation of these models in hydrologic models for the simulation of more complex hydrological processes at larger scales, their performance in terms of simulation accuracy and computational efficiency should be further tested.

Chapter 5 Development of a Surface Runoff Model Based on Cellular Automata (RunCA)

5.1 Introduction

Surface runoff and associated soil erosion are subjects of continuous concern around the world, as they may have serious environmental consequences, including flood, landform instability (e.g., landslide and debris flow), loss of top soil and fertilizer leading to plant death or crop failure, and the transport of pollutants to surrounding areas and water courses. A quantitative evaluation of the extent and magnitude of runoff problems is consequently required to find, implement or improve land management strategies. For this purpose, some lumped conceptual runoff models (or erosion models that incorporate a runoff model) have been developed since the 1970s, typical examples being the SCS curve number (U.S. Department of Agriculture, 1972), USLE (Wischmeier and Smith, 1978), CREAMS (Knisel, 1980) and RUSLE (Renard et al., 1997). These models usually treat the study area as a spatially singular entity, use state variables that represent averages over the entire area, and produce outputs at a single point according to empirical relationships (Haan et al., 1982). These models are computationally very efficient in calculating runoff and have relatively few input parameters. However, they are not able to capture the spatial or temporal variations in hydrological processes, and require calibration if applied to regions different from the location of first development.

To better describe the extent of spatial and temporal variability of runoff processes, some distributed physically based hydrologic/erosion models have emerged. Some of these models, including KINEROS (Smith, 1981), WEPP (Laflen et al., 1991), EUROSEM (Morgan et al., 1998b) and HEC-1 (Feldman, 1995), partition the target area (e.g., a catchment) using a network of elemental sections, such as a cascade of planes and channels. These elements are always simplified geometries with large sizes, which can provide a representation of the gross topographic features but may lose some local topography details and complexities. With the development of remote sensing, digital elevation models (DEM) and geographic information systems (GIS), grid structures are more frequently used in hydrologic models, with examples being ANSWERS (Beasley et al., 1980), AGNPS (Young et al., 1989), LISEM (De Roo et al., 1996) and SHE (Abbott et al., 1986). These grids usually have much smaller sizes than the geometric elements and provide an easier way to represent the study area.

Numerical techniques have been widely employed in these distributed models to simulate the runoff routing processes. Typically, the overland flow and channel flow are described by solving the Saint-

Venant equations of continuity and momentum. To make these complex equations solvable, simplifying assumptions need to be made and different methods are produced by neglecting various terms of the momentum equation. The kinematic wave model is the simplest method that neglects both acceleration and pressure terms, while the diffusion wave model is a more complete form that includes the influence of the pressure force. Therefore, the diffusion wave method is expected to be more accurate when slopes are low and the diffusion term in the equation overwhelms the kinematic term. These two models only simulate the one-dimensional flow, while the spatial variation in the direction perpendicular to the principle slope could not be captured. The more advanced 2-D diffusion wave method, such as that used in CASC2D (Rojas et al., 2003), could better describe the spatial variation of the flow behaviours, but this would further increase the complexity and hence may lead to low computational efficiency.

Alternatively, several simpler methods have been developed for determining the water flows based on the elevation differences of the elements. For example, in AGNPS flow directions are determined from the DEM. The DEM-based runoff routing algorithms include both single-direction algorithms (e.g., D8 (O'Callaghan and Mark, 1984) and ρ8 (Fairfield and Leymarie, 1991)) that transfer all flow from the centre grid to one downslope neighbour, and multiple-direction algorithms (e.g., MFD (Quinn et al., 1991), DEMON (Costa-Cabral and Burges, 1994) and D∞ (Tarboton, 1997)) that partition flow to multiple downslope neighbours. These elevation-based methods are very straightforward and computationally efficient; however, a major limitation is that they tend to be oversimplified as the water component in the elements is not taken into account. In reality, the water does not always flow according to the elevation differences because of the different water depths among the elements. Moreover, flow directions derived from these methods are pre-determined and fixed, thus nor the dynamic flow behaviours or the interactions between elements can be captured.

Therefore, alternative methods that have both high reliability and reduced complexity are required for more efficient hydrologic modelling. Cellular Automata (CA), a discrete dynamic system composed of a set of cells in a regular spatial lattice, is one of such promising approach worthy of investigation. Since the states of each cell depend only on the states of its neighbours and the global behaviour of the whole system is determined by the synchronous evolution of all the cells in discrete time steps, CA is very effective in simulating dynamic complex natural phenomena from local to global according to simple transition rules (Wolfram, 1984a). Unlike some other disciplines where CA has been widely applied and accepted, CA was not introduced into surface hydrology until Murray and Paola (1994) developed the first cellular braided river model about 40 years after CA was first proposed in the 1950s (Von Neumann, 1966). Only in the recent six years a few studies have emerged to relate its application

to hydrologic modelling. Rinaldi et al. (2007) and Ma et al. (2009) developed CA based algorithms for simulating runoff in large plains and on hill-slopes, respectively. Both models have shown the capacity of CA, however, a spatially uniform flow velocity was assumed and simply applied over the entire study area, leading them to be only used for simulating the steady flow conditions. Parsons and Fonstad (2007) developed a more complex CA model capable of simulating the unsteady flow conditions by delaying the water from one cell to the next until the correct timing is reached. Although this is a large progress, unfortunately in their model the flow directions were restricted to only four cardinal directions due to the difficulties in producing accurate timed water flows. Uncertainty also existed in selecting an appropriate time step for simulation. In addition, calculation of the rainfall excess is rather simple and empirical in this model as it does not include any related hydrologic principles. Some other CA models, such as RillGrow (Favis-Mortlock, 1998), EROSION-3D (Schmidt et al., 1999) and CAESAR (Coulthard et al., 2000), incorporate a surface hydrology component, but it is usually simplified because these models were primarily developed to study soil erosion or landform evolution. Consequently, in this study a CA-based model, which integrates measurable hydrologic parameters, is developed for quantitatively predicting the dynamic surface runoff processes under complex conditions at different scales.

5.2 Definition of lattice space and spatial cells: partition process

A typical CA based model *A* can be expressed as a quadruple (Gregorio and Serra, 1999):

$$A = (Z^d, X, S, \sigma) \tag{5.1}$$

where Z^d represents a lattice of cells covering the study area, X is the definition of the local neighbourhood, S is the set of cell states, and σ is the transition rule determining the changes in cell properties. Based on this structure and integrated with the physical processes involved in runoff production and distribution, the RunCA (Runoff Model Based on Cellular Automata) has been developed and is described as follows.

As illustrated in Figure 5.1, in this model the study area is partitioned into small hydrologic elements by a two-dimensional lattice consisting of square cells. This discretization is selected for its simplicity, broad application and convenience of implementation in computers. The model uses the Moore-neighbourhood, which consists of eight adjacent cells in the four cardinal directions and the four diagonal directions from the centre cell. The spatial cells located on the borders of the lattice space are treated as "closed and reflective" cells that simulate virtual plot boundaries. No water flows beyond

these boundary cells. The cells located at the outlet are treated as "open and absorbing" cells, which means they will absorb any water flowing into them by moving the water into a storage value. These values can then be used to track the volume of water leaving the study area and thus record the runoff amount as a virtual runoff collector.

The simulation accuracy and computational complexity of CA models are largely determined by the size of their spatial cells, which is affected by various factors, including the size and spatial homogeneity of the study area, model accuracy requirements and the resolution of available spatial data (e.g., resolution of DEM/GIS maps and density of rain gauges). Normally, the accuracy of results can be improved by reducing the cell size, however, at the expense of increased time and labour required to run the model.

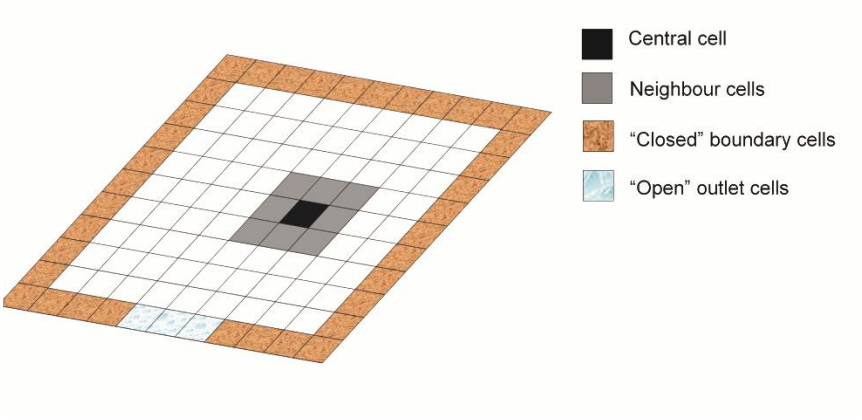

Figure 5.1 Lattice space and spatial cells in the RunCA model.

5.3 Determination of cell state: runoff production process

At each time step, the simulation of the runoff production process is based on the determination of the cell state, expressed as the cell height, which consists of both cell elevation and water depth. The cell elevation is derived from field measurements, topographic maps or DEM, and remains constant during a rainfall event. The determination of water depth is relatively complex, as it varies both temporally and spatially, and is controlled by both the effective rainfall at the current time step and the balance between inflows and outflows at the last time step, derived from transition rules described later. The effective rainfall (R_e) is determined by three components in equation (5.2):

$$R_e = R_i - P - I \tag{5.2}$$

where R_i is input rainfall, P is interception by vegetation, and I is infiltration. Here the evapotranspiration is neglected because it is negligible during runoff-producing rainfall events. In order to obtain the effective rainfall, it is necessary to quantitatively characterize all three components.

5.3.1 Input rainfall

The input rainfall information at each time step can be derived from local measurements using rain gauges and/or records from nearby meteorological stations. For small scale simulation (e.g., small hill-slopes), rainfall can be assumed to be uniformly distributed over the study area. For large scales, the spatial distribution of rainfall needs to be considered and different rainfall inputs should be applied to different cells, for which spatial interpolation methods may be employed.

5.3.2 Interception

Interception refers to the portion of input rainfall collected, stored and evaporated from vegetation. In the areas barren of vegetation, interception is negligible. However, its relative effect can be significant when the vegetation cover is high and the rainfall intensity is small. In this model, interception is determined by the method used in LISEM (De Roo et al., 1996), where the cumulative interception during a rainfall event is estimated using an equation developed by Aston (1979):

$$P_{cum} = P_{max}\left[1 - exp\left(-0.046LAI\frac{R_{cum}}{P_{max}}\right)\right] \tag{5.3}$$

where P_{cum} is the cumulative interception (mm), R_{cum} is the cumulative rainfall (mm), *LAI* is the leaf area index, and P_{max} is the maximum interception storage capacity (mm) that can be estimated from *LAI* using the equation developed by Von Hoyningen-Huene (1981):

$$P_{max} = 0.935 + 0.468LAI + 0.00575LAI^2 \tag{5.4}$$

From the cumulative interception, the interception increment at each time step (P) is calculated by subtracting the P_{cum} at a previous time step from that at the current time step.

5.3.3 Infiltration

In many cases, infiltration prediction directly determines the accuracy of a hydrologic model, as it controls how much water will enter the unsaturated soil zone, and how much will flow on the ground surface as runoff. It is difficult to quantitatively analyse the infiltration process due to its various affecting factors and its changing characteristics with time, but several physically based and empirical infiltration models have been developed. Among these models, the Philip (1957a), Green-Ampt

(1911), Horton (1940) and Holtan (1961) equations are frequently used due to their simplicity, good fit to data and the ability to obtain their parameter values. These four infiltration models have been implemented in the RunCA model, permitting investigation of their relative efficacy for runoff prediction during single consecutive rainfall events (Table 5.1). However, these models are only valid when the water supply rate at all times exceeds the soil infiltration capacity as they were primarily developed for describing the infiltration processes under ponding conditions. They cannot be used for intermittent or multiple rainfall events, where the recovery of infiltration capacity during dry periods needs to be considered. To make the RunCA model applicable to complex rainfall conditions and long-term simulations, three improved infiltration models, including the modified Horton equation (Aron, 1992; Bauer, 1974), modified Holtan equation (Huggins and Monke, 1966; Huggins and Monke, 1968) and modified Green-Ampt equation (Bouraoui and Dillaha, 1996), are incorporated to allow soil drainage and infiltration recovery (Table 5.1).

Table 5.1 Infiltration Equations Integrated in RunCA [a]

Single continuous rainfall events		Intermittent/multiple rainfall events	
Philip equation	$i_t = 0.5S_0 t^{-0.5} + A$	Modified Horton equation	$i_t = i_0 + d_t - kS_t$ $d_t = \frac{i_f}{i_0} kS_t$
Green-Ampt equation	$i_t = K_s(\lambda / I_t + 1)$		
Horton equation	$i_t = i_f + (i_0 - i_f)e^{-kt}$		
Holtan equation	$i_t = i_f + (i_0 - i_f)\left(\frac{S - I_t}{\phi D}\right)^P$	Modified Holtan equation	$i_t = i_f + (i_0 - i_f)\left(\frac{S_t'}{\phi D}\right)^P$ $d_t = i_f \left[1 - \frac{S_t'}{(\phi - FC)D}\right]^3$
		Modified Green-Ampt equation	$i_t = K_s(\lambda / I_t + 1)$ $d_t = D(\theta - FC)\left(1 - e^{-\Delta t / t_d}\right)$

[a] i_t: infiltration capacity at time *t*, mm h^{-1} ; S_0: sorptivity, mm h$^{-0.5}$; A: soil water transmissivity, mm h^{-1}; K_s: hydraulic conductivity at natural saturation, mm h^{-1}; λ: fitting parameter in Green-Ampt equation, mm; I_t: cumulative infiltration at time *t*, mm; i_f: final steady infiltration rate, mm h^{-1}; i_0: initial infiltration rate, mm h^{-1}; *k*: infiltration decay factor in Horton equation, h^{-1}; *S*: soil water storage potential, mm; ϕ: total porosity, m^3 m^{-3}; *D*: control zone depth, mm; *P*: dimensionless coefficient

relating decrease rate of infiltration capacity in Holtan equation; d_t: soil drainage rate at time *t*, mm h^{-1}; S_t: cumulative soil water at time *t*, mm; S'_t: soil water storage potential at time *t*, mm; θ: soil moisture at time *t*, m^3 m^{-3}; FC: field capacity, m^3 m^{-3}; t_d: time for drain, min; Δt: time step (min) for calculation.

5.4 Application of transition rules: runoff distribution process

At each time step and after determining the states (i.e., water depth and cell height) of each cell, the redistribution of water amongst the spatial cells is then derived by applying three CA transition rules to all these cells.

5.4.1 First transition rule for identifying flowing neighbours

This first transition rule determines at each time step to which neighbour cells the water in each central cell will flow, on the basis of the minimization of differences algorithm. This algorithm was first proposed by Gregorio and Serra (1999), and is based on a very straightforward principle that a dynamic system tends to evolve towards equilibrium conditions by flow of some conserved quantity in the central cell to its neighbours. Specific to this runoff model, the water always flows from the central cell to its lower-height neighbour cells, in order to minimize the height differences among cells to reach equilibrium conditions. To implement this algorithm in RunCA, the average cell height in a local neighbourhood area is firstly determined and compared to the height of each neighbour cell to eliminate the neighbours with larger height values. Then a new average height is calculated and again compared to the remaining neighbours for further elimination. This process repeats until no neighbour could be eliminated, and then the remaining neighbours are identified as the flowing neighbours that will receive water flows from the central cell. The more detailed procedure and the equations for calculation are shown in Figure 5.2.

Three different flow-direction options are included in this model. The first one (4N) only allows the water in the central cell to flow to four cardinal neighbours, while the second option (8N) allows eight flow directions by including the four diagonal neighbours. However, according to the previous findings on the MFD (Multiple flow direction) DEM-based runoff routing algorithm, the 4N and 8N type tends to cause under flow divergence and over flow divergence, respectively (Erskine et al., 2006). Therefore, a third flow-direction option (4+4N) is proposed, which gives the water in a cell the priority to flow to its four cardinal neighbours, and only allows it to flow to the four diagonal neighbours when there is no cardinal neighbour to flow to (i.e., all the cardinal neighbours are higher than the central cell). This is a compromise between the former two options, and is expected to be more realistic by controlling

the flow dispersion and at the same time keeping the eight possible flow directions. Their performance will be evaluated and compared later in the model testing sections.

5.4.2 Second transition rule for calculating flow amount to flowing neighbours

According to the minimization of differences algorithm, the potential flow amount f_p from the central cell to each identified flowing neighbour is determined by the difference of its height and the average height. However, this calculation is based on the assumption of a constant velocity for all the flows. In reality the water flow velocity on a hill-slope or in a catchment is highly spatially and temporally variable due to various conditions, such as local elevation gradient, surface roughness and water depth. These variations are essential for the runoff distribution, and thus are considered in RunCA by calculating the travel time for all the flows. Specifically, the Manning's equation is employed to determine the velocity *V* for the outflow from the central cell to each flowing neighbour:

$$V = \frac{h^{2/3} s^{1/2}}{n} \tag{5.5}$$

where *h* is water depth in the central cell, *n* is Manning's roughness coefficient, and *s* is water surface slope which is calculated from dividing the flow travel distance *D* by the height difference of the central cell and its flowing neighbour. Then the time *T* required for water to travel from the central cell to its flowing neighbour can be calculated from dividing the flow travel distance by the flow velocity, as shown in equation (5.6):

$$T = \frac{D}{V} = \frac{nD}{h^{2/3} s^{1/2}} \tag{5.6}$$

If *L* represents the cell side length, then *D* equals to *L* and $\sqrt{2}L$, respectively for the cardinal flowing neighbour and the diagonal flowing neighbour.

The calculated flow travel time is then compared to the time step *t* used in the simulation. If *t* is larger than *T*, which means that there is enough time for the calculated f_p to finish travelling, then the actual flow amount *f* will be equal to f_p; when *t* is smaller than *T*, which means f_p cannot finish travelling in a time step, then only part of f_p can flow and *f* is further calculated by multiplying f_p by the ratio between *t* and *T*. Based on this consideration, a small time step which is less than most of the calculated flow travel times is demanded. To estimate a suitable time step value, the potential flow travel times are calculated prior to the simulation, by assuming *s* equal to the land surface slope gradient and *h* equal to the elevation differences between cells. These calculated potential flow travel times are further

sorted from largest to smallest and their percentiles are given, which provide a reference for the selection of time step. Normally a time step smaller than the 99% percentile is recommended to guarantee the simulation accuracy.

After determining the amount of each flow, the total outflow from each central cell f_0 is then calculated by the sum of f to all its flowing neighbours. When f_0 is larger than its water depth h_0, which means that the water in the central cell is not sufficient for all the calculated outflows, f to each flowing neighbour needs to be further modified by timing a ratio of h_0 and f_0. In this case the final f_0 is equal to h_0.

The detailed calculation process and equations used for this transition rule is demonstrated in the flowchart shown in Figure 5.2.

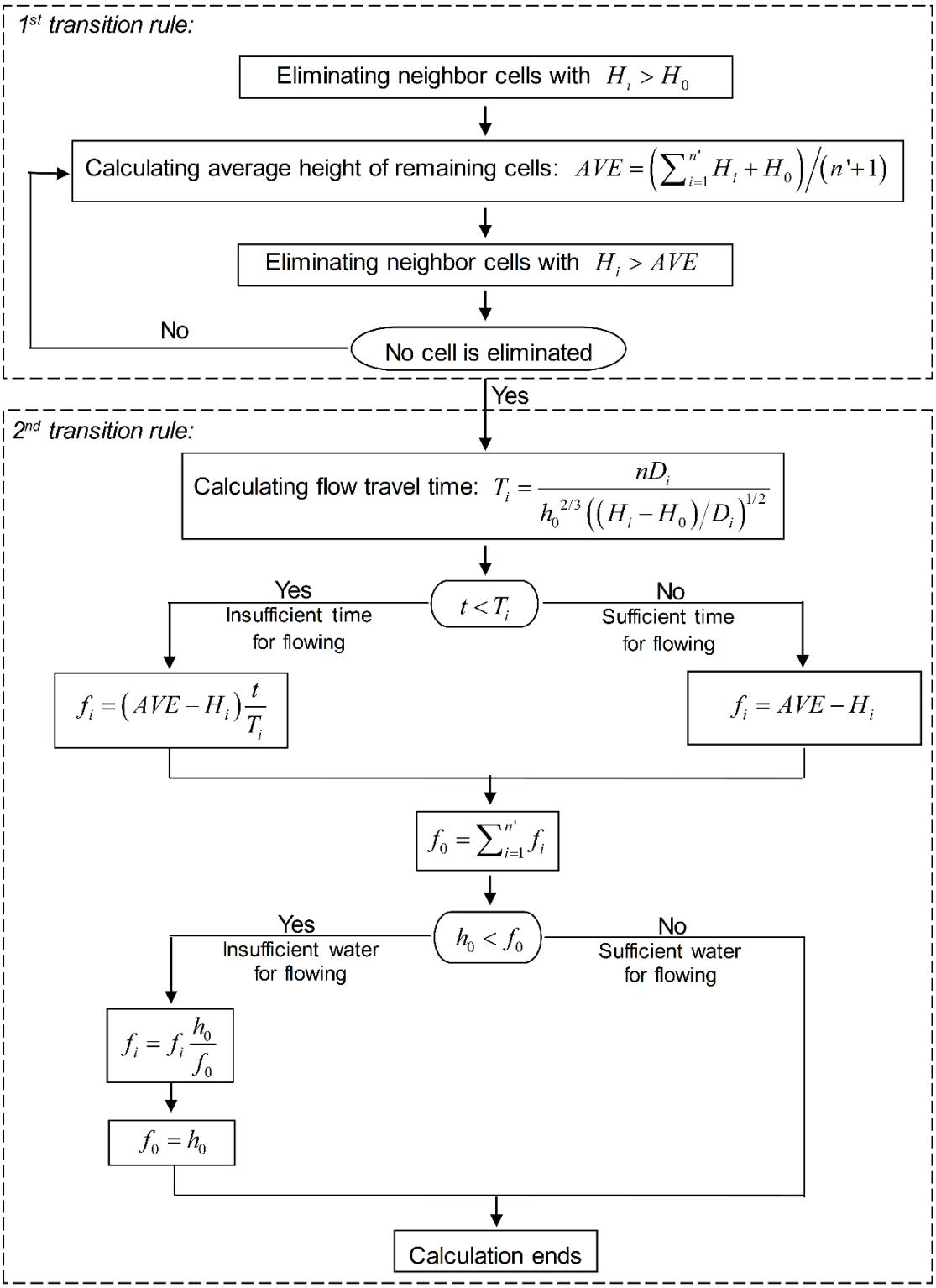

Figure 5.2 Flowchart for calculating water flows from central cell to neighbours. H_i and H_0 represents neighbour heights and central cell height, respectively; n' is the number of remaining neighbours after each elimination; T_i and D_i represents flow travel time and distance from central cell to each flowing neighbour, respectively; n is Manning's coefficient; h_0 is the water depth in central cell; t is time step;

f_i represents the flow amount from central cell to each flowing neighbour, while f_0 is the total outflow from central cell.

5.4.3 Third transition rule for determining total flows

At each time step the former two transition rules are applied to all the spatial cells in the lattice space, thus the outflow *f* from each central cell to each of its neighbours can be determined and stored in a buffer. However in the global view, each central cell is also one neighbour of its adjacent cells, thus it not only flows water out, but also receives water from the surrounding cells at the same time. Consequently a third transition rule needs to be applied to calculate the total flow *F* (the balance between outflow and inflows) for each cell. This transition rule is based on the consideration that the inflows from the neighbours to each cell can be derived from the according outflows of these neighbours. More specifically, if *i* and *j* represent the row number and column number respectively, and the arrows represents the flow directions, then the total flow for the cell (*i*, *j*) can be determined by equation (5.7) for 4N option, and equation (5.8) for both 8N and 4+4N options:

$$F(i,j) = f(i-1,j)(\downarrow) + f(i,j-1)(\rightarrow) + f(i,j+1)(\leftarrow) + f(i+1,j)(\uparrow) - f_0(i,j) \tag{5.7}$$

$$\begin{aligned} F(i,j) = {} & f(i-1,j-1)(\searrow) + f(i-1,j)(\downarrow) + f(i-1,j+1)(\swarrow) + f(i,j-1)(\rightarrow) + \\ & f(i,j+1)(\leftarrow) + f(i+1,j-1)(\nearrow) + f(i+1,j)(\uparrow) + f(i+1,j+1)(\nwarrow) - f_0(i,j) \end{aligned} \tag{5.8}$$

The calculated total flow could be positive if the sum of inflows is larger than the total outflow, or reversely negative. Then the new water depth and cell height are updated by adding this total flow to the current water depth for the calculation of the next time step. This allows the simultaneous update of the states of all the cells.

Based on all the components discussed above, RunCA has been implemented in C++ using the object-oriented paradigm for the sake of flexibility and reusability. The model structure and modelling procedure is summarized in Figure 5.3.

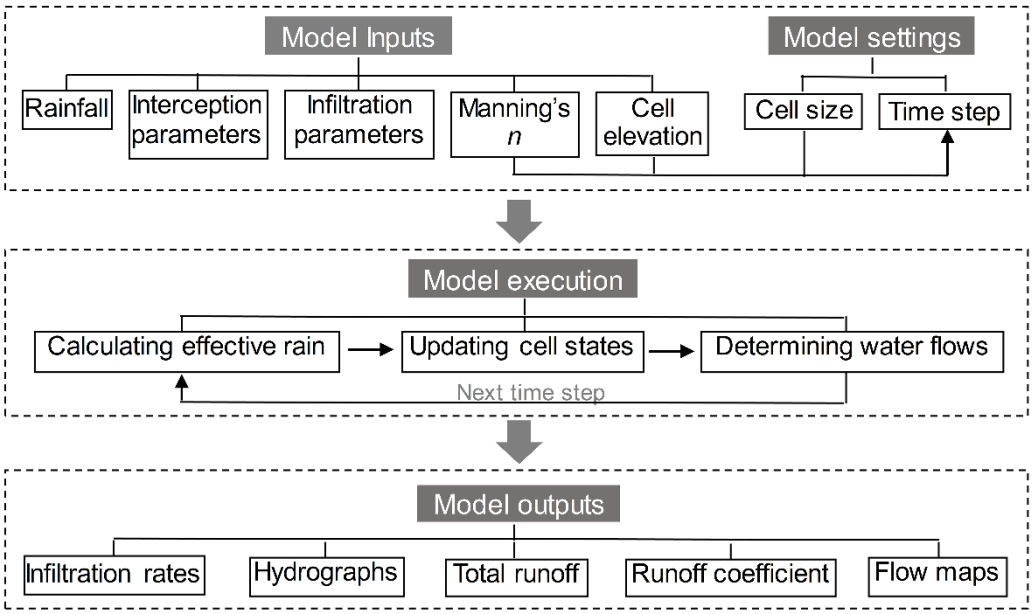

Figure 5.3 Flowchart for RunCA modelling procedure.

5.5 Conclusions

The Runoff Model Based on Cellular Automata (RunCA) has been developed to simulate surface runoff at different scales by integrating basic cellular automata (CA) rules with fundamental measureable hydraulic properties. In this model, a two-dimensional lattice composed of a series of rectangular cells was employed to cover the study area. Runoff production within each cell was simulated by determining the cell state (height) that consists of both cell elevation and water depth. The distribution of water flow among cells was determined by applying CA transition rules based on the minimization-of-difference algorithm and the calculated spatially varied flow velocities.

This study applied a new technique, Cellular Automata, for runoff modelling. The cell structure of RunCA, which enables its integration with GIS, can provide an accurate and easy representation of the study area. Linking ground-truthed data of hydrological properties with remote sensed data as model inputs broadens the range of options of applications for this model. The simultaneous update of states of all the spatial cells at multiple time steps enables the model to describe the spatially and temporally varied runoff behaviours. Compared to the numerical techniques employed in most traditional distributed hydrologic models, the transition rules used in RunCA are expected to reduce the complexity in computation as there is no need to solve any complex equations of continuity or momentum. These CA transition rules are also considered to be more realistic than the DEM-based routing algorithms as they determine the water distribution based on the water surface elevations

instead of the land surface elevations. This model would be a further step based on the existing CA runoff models by considering the spatially varied flow velocities, introducing a more realistic 4+4N flow-direction algorithm and incorporating physically measurable hydrologic principles (e.g., infiltration characteristic) when determining the runoff production. Besides, instead of restricting to a certain spatial or temporal scale, RunCA is developed as a universal tool to be applied in different spatial scales for both event-based and long-term simulations. The performance of RunCA, however, needs to be further verified and validated by systematic analysis, which would be discussed in the following chapter.

Chapter 6 Systematic Validation of RunCA at Different Spatial Scales

6.1 Introduction

A Cellular Automata based surface runoff model, RunCA, has been developed in the previous chapter. Before applying this developed model to real cases, it must be tested and verified to ensure that the model indeed represents the physical world adequately. Therefore, a systematic verification and validation procedure consisting of three steps (Wang et al., 2009) was employed in this chapter: (1) verification by analytical solution under simplified conditions to test the physical basis of the model and to ensure the validity of computer coding and calculation algorithm; (2) validation by laboratory experiments to evaluate the model's capacity in reproducing the basic physical processes of surface runoff; and (3) validation by field measurements to prove that the model has the capability of predicting the behaviour of the natural phenomenon.

Two standard statistical metrics, including Nash-Sutcliffe efficiency or modelling efficiency (*EF*) (Nash and Sutcliffe, 1970) and root mean square error (*RMSE*), were used to evaluate the performance of RunCA. *EF* describes the proportion of the variance of the observed values that is accounted for by the model, and its value can vary from 1 (perfect fit) to negative infinity. *RMSE* shows the amount of divergence of the model values from the observed values and its value close to 0 indicates good agreement. The mathematical expressions used for these two statistical analysis measures are:

$$EF = 1 - \frac{\sum_{i=1}^{n}\left(O_i - P_i\right)^2}{\sum_{i=1}^{n}\left(O_i - \overline{O}\right)^2} \tag{6.1}$$

$$RMSE = \sqrt{\frac{1}{n}\sum_{i=1}^{n}\left(O_i - P_i\right)^2} \tag{6.2}$$

where n is number of observations during the simulation period; O_i and P_i are observed and simulated values at each comparison point i; $\bar{O}$ is arithmetic mean of the observed values.

6.2 Model verification by analytical solution under simplified conditions

RunCA was firstly tested against the analytical solution for the idealized overland flow over a uniform plane using the kinematic wave modelling, as suggested by Singh (1996). A 500 m long and 100 m wide hypothetical flow plane at a uniform slope of 5% was considered, where the surface roughness, slope, and rainfall regime were assumed invariant in space and time. A Manning's *n* of 0.01, a cell size of 1 m and a time step of 1 s were set for all the simulations by RunCA in this section.

The effective rainfall of 100 mm h^{-1} was applied on an impervious plane with no infiltration, and the hydrographs predicted by both the analytical solution (derived from Figure 12.13 and 12.26 in Singh (1996)) and RunCA are shown in Figure 6.1. Figure 6.1a represents the equilibrium hydrograph where the rainfall duration is 25 min and is larger than the time of concentration, i.e., the time when flow from the farthest point reaches the outlet, while Figure 6.1b shows the partial equilibrium hydrograph where the rainfall duration is 5 min and is smaller than the time of concentration. Both figures show that compared to the results derived from the analytical solution, RunCA predicted slightly higher values of runoff rates during the rising limbs while slightly lower values during the recession limbs of the hydrographs. However, they had very similar crest segments where the peak discharge rate values were almost the same. The large *EF* values (0.964 and 0.923) and small *RMSE* values (8.054 mm h^{-1} and 6.414 mm h^{-1}) indicated the good agreement between analytical solution and RunCA.

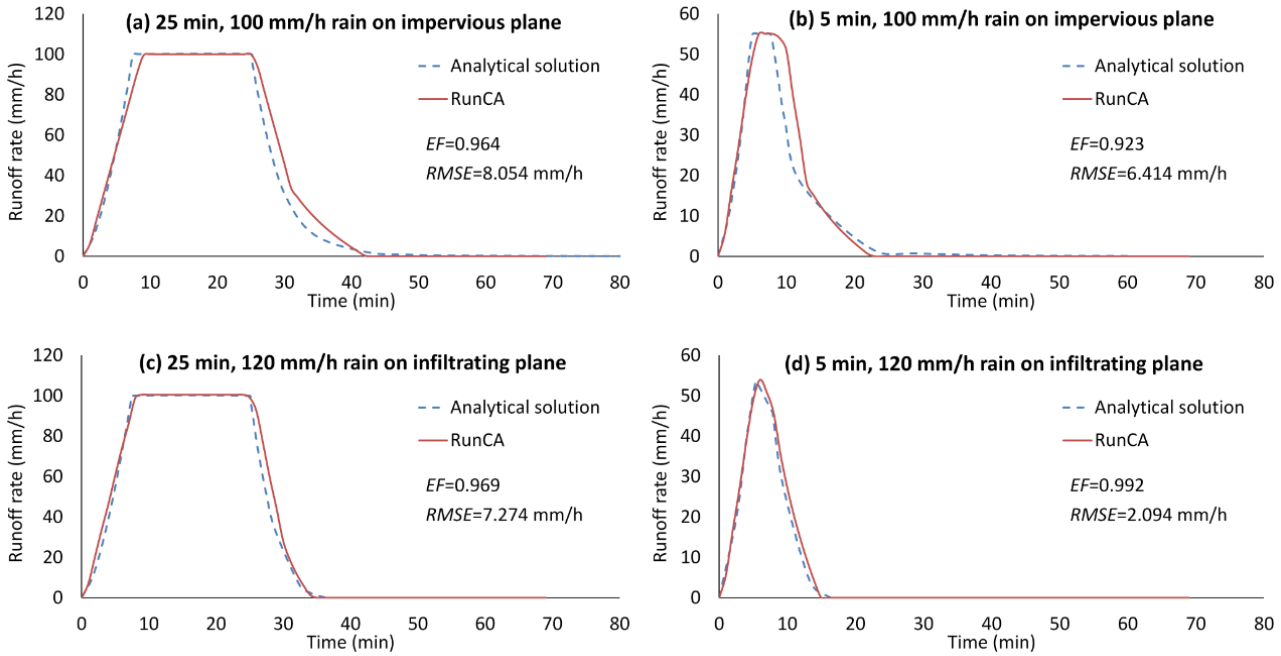

Figure 6.1 Simulated hydrographs based on the analytical solution and RunCA, for both the impervious plane (a, b) with no infiltration and the infiltrating plane (c, d) with a constant infiltration rate of 20 mm h^{-1}.

Figure 6.1c and 4d show the results for another case where the 120 mm h^{-1} of rainfall was applied on the infiltrating plane with a constant infiltration rate of 20 mm h^{-1}. Similarly, both equilibrium and partial equilibrium conditions were considered using the 25 min and 5 min rainfall durations. Again, good fit between the hydrographs based on the analytical solution (derived from Figure 13.10 and 13.18 in Singh (1996)) and RunCA was achieved. Hence, the model verification by the analytical solution of the equation of continuity and momentum verifies the transition rules for runoff distribution in RunCA and the correctness of the software code, and at the same time suggests the model ability in reflecting the basic physical processes involved in surface water flows.

6.3 Model validation with laboratory experiments at small plot scale

Laboratory experiments are often conducted in a controllable and repeatable environment, smaller in scale and less costly to measure more properties at higher resolution of the measuring points. Therefore, the comparison between the measured values with modelled results is more meaningful to test the model's capability in reproducing the most fundamental physical processes of the system tested (Wang et al., 2009; Wang and Wu, 2004). In this study, the performance of RunCA was tested by using the results of runoff experiments previously carried out at small plot scale in the rainfall simulation laboratory of Beijing Normal University, China.

6.3.1 Experimental data

Small laboratory plots (2 m × 1 m) were established by spraying the substrate, consisting of a mixture of natural soil and soil adhesive, onto a platform using the soil-spray technique applied by a high hydraulic pressure machine to form a stabilized soil layer with a thickness of 30 cm. Six treatments were set up based on two different types (inorganic and polymer) and three contents (0.3%, 0.5%, 0.7%) of soil adhesives to achieve different infiltration characteristics among plots. Simulated rainfall was produced by a group of rainfall simulators, which use Veejet 80100 nozzles, with a water pressure of 0.04 MPa, height of 5 m, target area of 2.2 m × 3 m, and coefficient of uniformity of 95%. Steady rainfalls with three different intensities (20 mm/h, 44 mm/h and 70 mm/h) were applied to the plots at three different slope gradients (10%, 20% and 30%), with a duration of 2 hours for each rainfall event.

Surface runoff has been collected and measured every five minutes during all the rainfall events. Results showed that total runoff increased with increasing adhesive content within both groups of plots treated by inorganic and polymer adhesive, with the latter group tending to generate more runoff. In

addition, larger runoff amount has been produced at steeper slopes and during higher intensity rainfall events.

6.3.2 Model inputs and settings

Before running RunCA for runoff simulation, five groups of input parameters needed to be determined, as well as two basic model settings (Figure 5.3):

***Cell elevation**:* Due to the straight slope profile and the relative smooth surface, the elevation of each line of cells on the plot could be easily calculated based on the slope length and angle. After applying the rainfall using the simulator, some rills were observed on some plots. The elevation of the cells located on these rills were determined by subtracting the measured rill depths.

Rainfall: actual rainfall intensity was measured by tipping buckets for each rainfall event, and was considered homogeneously distributed on the plot because of the high coefficient of uniformity of rainfall simulators and the small size of the runoff plot.

Interception: this part was ignored since no vegetation cover existed on any plot.

Manning's n: This roughness coefficient was derived empirically from the guide values in EUROSEM (Morgan et al., 1998a). The resulted values varied from 0.026 for plot 1 treated with lowest content of inorganic adhesive to 0.016 for plot 6 treated with highest content of polymer adhesive.

Infiltration: infiltration rate of each plot varied temporally and the four infiltration equations for single rainfall events (Table 5.1) were selected due to the continuous rainfall applied. Since the input parameter values for these infiltration equations were not measured in this experiment, they were derived indirectly by calibration with the actual infiltration values, which were determined by subtracting measured runoff amount from rainfall amount every five minutes. For each plot at each slope gradient, infiltration parameters were calibrated by curve-fitting with the experimental data in the 44 mm h^{-1} rainfall event, and the calibrated values were then used for runoff simulations in both 20 mm h^{-1} and 70 mm h^{-1} rainfall events. Table 6.1 summarizes the derived parameter values, with the mean coefficient of determination (R^2) of four infiltration equations ranging from 0.84 to 0.96, indicating that these selected infiltration equations were able to well describe the infiltration process and the determined parameter values were accurate and reliable.

Model settings: For the plots with smooth and homogenous surfaces, the side length of each cell was set as 0.1 m, with 20 × 10 cells in total covering the whole plot. While for the more heterogeneous

surfaces where rills developed, smaller cell size (0.01m × 0.01m) was used in order to capture the rill characteristics. The potential flow travel times were then calculated based on equation (6) using the method described in section 2.3. The value of the 99% percentile was selected here as the time step for simulation. The resultant time step ranged from 0.044 s for plot 1 at 20 °slope to 0.013 s for plot 6 at 40 °slope.

Table 6.1 Calibrated Infiltration Parameter Values and Coefficients of Determination (R^2) for Curve-fitting Results at Small Plot Scale [a]

Plot	Slope	Philip			Horton				Green-Ampt			Holtan			
	(%)	A	S_o	R^2	i_f	i_0	k	R^2	K	a	R^2	i_f	i_0	P	R^2
1	10	1.34	0.44	0.85	1.33	2.50	1.65	0.97	1.50	0.05	0.79	1.24	2.62	1.03	0.96
	20	1.14	0.39	0.99	1.33	2.74	6.77	0.95	1.30	0.04	0.98	1.04	2.12	1.45	0.91
	30	0.83	0.35	0.91	0.98	2.79	7.48	0.94	1.03	0.04	0.87	0.82	3.68	2.53	0.94
2	10	1.24	0.44	0.73	0.98	2.37	1.38	0.99	1.41	0.05	0.59	1.02	3.02	1.20	0.99
	20	0.92	0.37	0.98	1.07	2.49	5.26	0.97	1.08	0.05	0.96	0.94	3.79	2.98	0.94
	30	0.69	0.34	0.91	0.88	2.63	9.29	0.95	0.87	0.04	0.88	0.69	3.51	2.72	0.93
3	10	0.92	0.46	0.76	0.49	2.30	1.58	0.99	1.12	0.06	0.62	0.59	5.77	2.29	0.99
	20	0.64	0.40	0.93	0.65	2.24	3.06	0.99	0.83	0.06	0.90	0.45	3.99	2.87	0.99
	30	0.44	0.35	0.92	0.64	2.42	8.57	0.98	0.60	0.05	0.88	0.30	4.21	3.28	0.94
4	10	1.26	0.44	0.84	1.36	2.30	1.24	0.93	1.41	0.05	0.78	1.12	2.12	0.71	0.90
	20	0.97	0.39	0.98	1.14	2.56	4.64	0.96	1.14	0.05	0.97	0.82	3.02	2.35	0.93
	30	0.69	0.35	0.88	0.80	2.67	6.90	0.94	0.89	0.05	0.85	0.71	3.58	2.55	0.94
5	10	1.24	0.45	0.55	1.00	2.20	0.97	0.98	1.38	0.29	0.74	0.94	2.45	0.83	0.97
	20	0.74	0.37	0.93	0.77	2.30	3.51	0.96	0.92	0.05	0.90	0.89	3.21	2.75	0.95
	30	0.52	0.33	0.86	0.62	2.45	6.55	0.94	0.72	0.05	0.81	0.80	3.24	2.72	0.94
6	10	0.89	0.43	0.83	0.79	1.95	1.16	0.96	1.04	0.06	0.75	0.82	2.63	1.42	0.95
	20	0.58	0.38	0.94	0.61	2.07	2.73	0.97	0.76	0.06	0.92	0.59	2.91	2.53	0.96
	30	0.31	0.33	0.87	0.49	2.30	7.74	0.97	0.47	0.05	0.83	0.49	3.14	3.06	0.94
Mean				0.87				0.96			0.84				0.94

[a] All the symbols representing infiltration parameters are the same as those in Table 5.1.

6.3.3 Model validation

RunCA was performed for the 20 mm h^{-1} and 70 mm h^{-1} rainfall events applied on all the plots at different slope gradients. The model performance was evaluated through the comparison of the predicted hydrographs with the measured runoff rates at certain time points, using both *EF* and *RMSE*. The resultant *EF* was on average 0.795 (0.033) for the 20 mm h^{-1} rainfall events, and was significantly

correlated (r=0.446, P<0.001) to the R^2 for curve-fitting the infiltration equations, suggesting that a large portion of error in the simulated runoff rates was attributed to the error in estimating the infiltration parameters, instead of the inherent error of model itself. This is confirmed by the fact that when simulating runoff for the larger intensity (70 mm h^{-1}) rainfall events where infiltration played a less important role, the model performed much better, with the *EF* values significantly (P<0.01) increased to 0.995 (0.001). Among all the simulations, the largest *RMSE* value was only 2.62 mm h^{-1}, and 80% of these values were less than 1.5 mm h^{-1}, suggesting a good model efficacy in predicting the runoff rates with time.

Correlation analysis showed that neither *EF* nor *RMSE* had significant correlation with the plot or slope gradient, indicating that the model performance did not vary much under different soil or topographic conditions. Three different flow-direction options were also compared, but no obvious difference was found, probably due to the relative simple slope profiles and homogenous surface conditions.

Figure 6.2 shows the simulated flow maps at different time steps on a plot with rills development (plot 4 at 30% slope), during the 20 mm h^{-1}rainfall event and based on the Horton infiltration equation. It can be clearly seen that most water was flowing in the rills, while on the surface without rills, the water depth increased from the top to the bottom of the plot due to the accumulation of runoff water downslope. Besides, the runoff gradually expanded to a larger area and grew deeper with time due to the decreasing infiltration rate. All these results have indicated that the RunCA is able to describe both the spatial distribution and the temporal variation in the runoff process in this study.

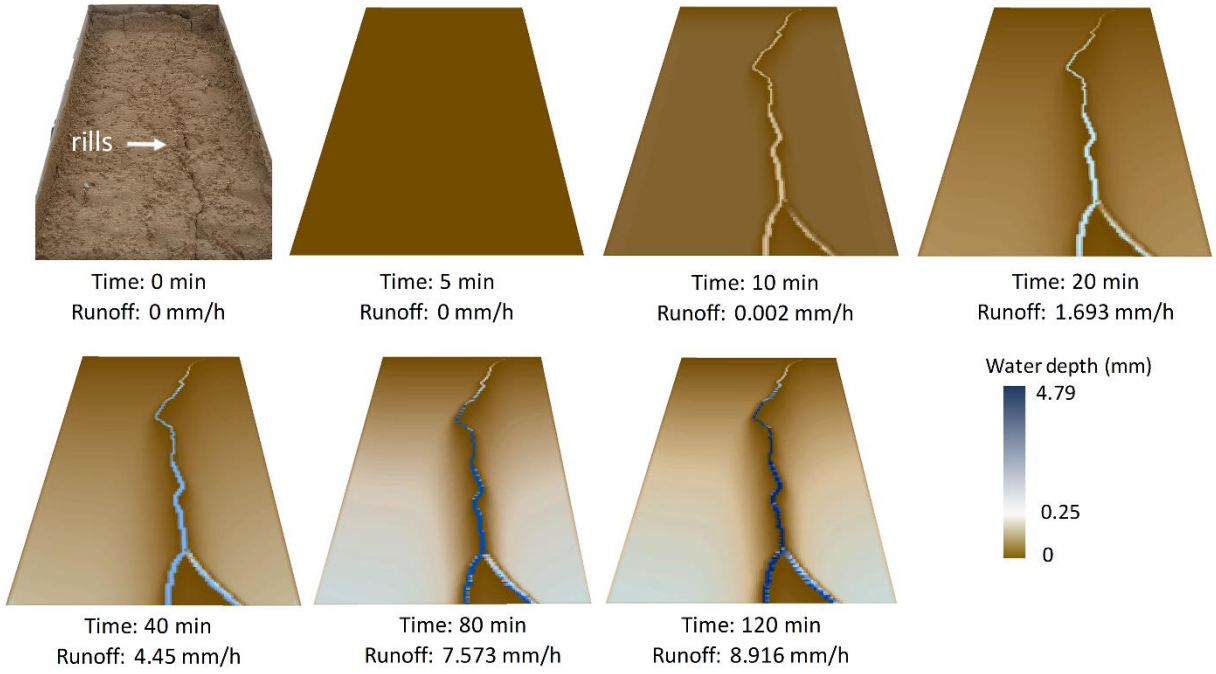

Figure 6.2 Simulated flow maps (plan views) at different time steps on laboratory plot 4 at 30% slope, 20 mm h^{-1} rainfall and based on Horton infiltration equation. The first flow map is a photo of plot surface at the initial condition.

6.3.4 Model sensitivity analysis

The above modelling results have suggested a close association between the simulated runoff and the infiltration parameters. To better understand the model response to the change in each of these parameters, sensitivity analysis was further performed. The 44 mm h^{-1} rainfall event applied on plot 2 at 30% slope was selected as a representative for this analysis. Then four 20% decrements and four 20% increments from the base infiltration parameter values (curve-fitting results) and the base Manning's *n* value were applied. In addition, the simulations based on eight cell sizes ranged from 0.01 m to 0.25 m were also performed, to evaluate the model sensitivity to the spatial resolution.

Two output parameters, total runoff Q_t and total infiltration amount INF_t, were used to evaluate the model responses. Figure 6.3 shows that both Q_t and INF_t were more sensitive to A, K_s and i_f, which are all the parameters reflecting the steady infiltration rate, than the other infiltration parameters. Manning's *n*, the parameter influencing the flow velocity and thus time step, had almost no impact on the results. The model also showed very little response to the change of cell size (results are not shown here), probably due to the fact that the plot in this test was small and homogeneous.

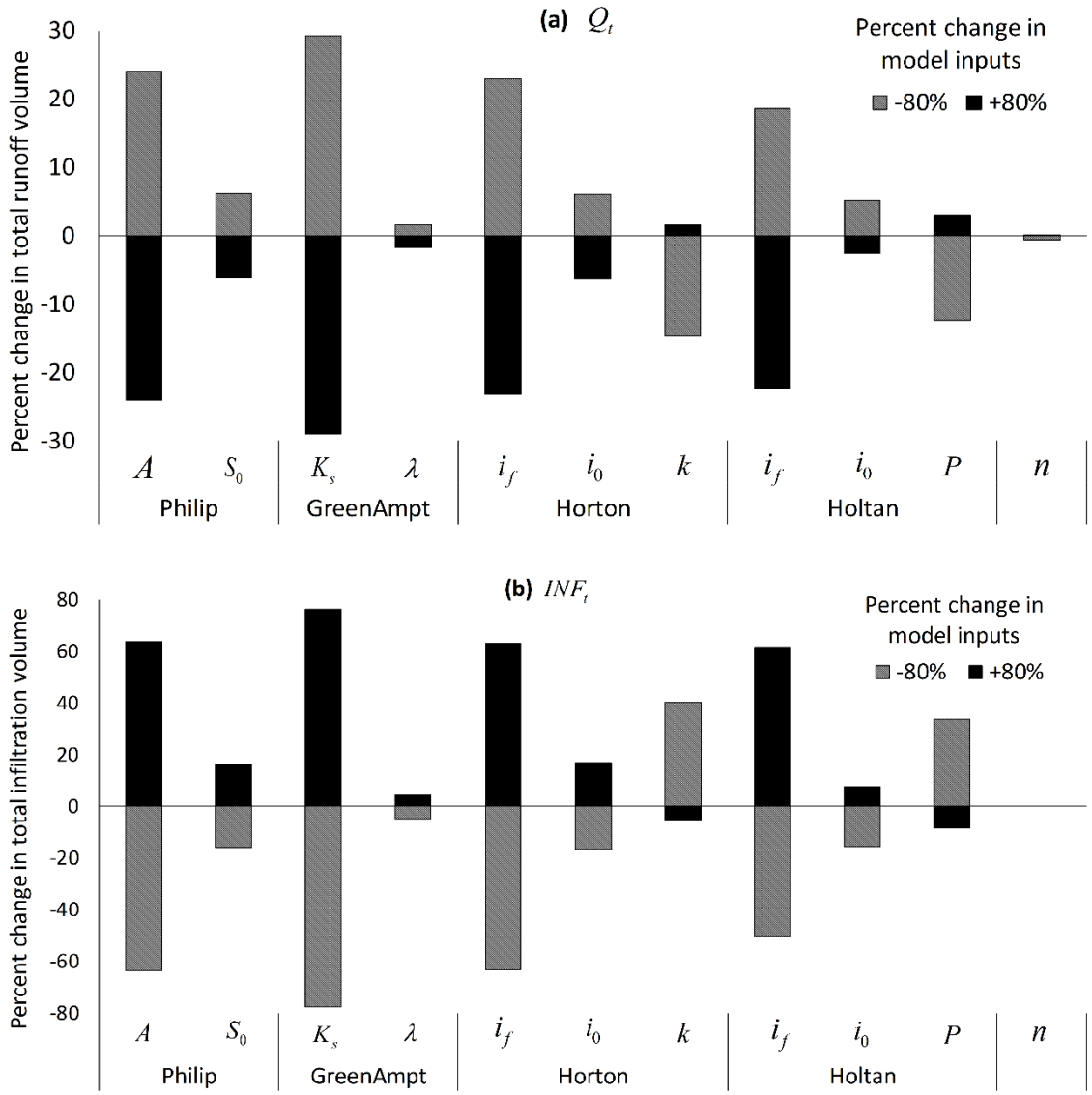

Figure 6.3 Results for model sensitivity analysis performed on plot 2 at 30% slope and 44 mm h^{-1} rainfall intensity. Q_t and INF_t represents total runoff and total infiltration amount respectively, n represents Manning's roughness coefficient, while all the other symbols representing infiltration parameters are the same as those in Table 5.1.

6.4 Model validation with field measurements at the basin scale

Previous model validations by analytical solution and laboratory experiments have demonstrated the efficacy of the model in reproducing the basic runoff processes. Before applying it to the investigation of a real-world problem, one more step is required to test the model by field data under the natural conditions. Therefore the model performance was further evaluated by applying it to a representative natural basin.

6.4.1 Field data

Field data reported by Ritter (1992) were taken from the Pine Glen drainage basin located on rehabilitated surface mines in central Pennsylvania, to investigate its surface hydrology using our model RunCA. This basin (10.6 ha) was selected because it had well identified heterogeneous topographic and surface properties, which allowed the test of the model accuracy under complex conditions. A complete hydrology data set available in this basin is another advantage for model application. On the basis of vegetation type, land use, soil thickness and property, the basin could be divided into 5 different land units (Figure 6.4a). For each unit, infiltration parameters were measured by infiltration tests conducted by Jorgensen and Gardner (1987) on 0.4 m ×0.1 m plots with a dripping-rainfall infiltrometer. In addition, a recording rain gauge and a water-level recorder housed in a cut-throat flume were installed to continuously measure the rainfall and runoff rates (Ritter, 1990).

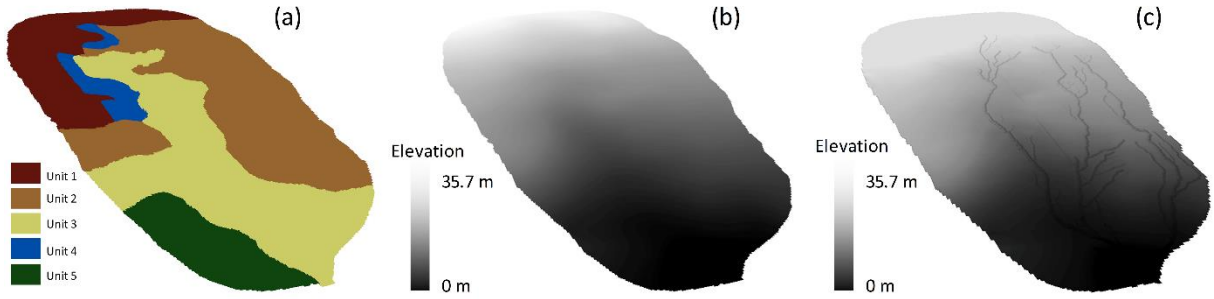

Figure 6.4 Distribution of land units (a) of Pine Glen Basin, DEM in the year 1 (b) and the year 6 (c) after the rehabilitation.

6.4.2 Model inputs and settings

Cell elevation: the elevation values of spatial cells were derived from the basin DEMs (Figure 6.4b and 6.4c), which were created from an original topography maps (Ritter, 1992) using ArcMap 10. The DEMs in different years after the rehabilitation showed different extents of the channel network development in this basin.

Rainfall: two observed rainfall events, with each in year 1 and 6 after the rehabilitation, were selected for model application. These rainfall events had temporally varied rainfall intensities, and thus were ideal for testing the model performance during complex rainfall conditions.

Interception: due to the lack of *LAI* information for this basin, the interception could not be calculated. However, since the average vegetation cover in this basin was low (< 20%), the maximum interception

would be only 0.4 mm with an *LAI* of 2 according to Equation (5.3). Compared to the total rainfall amount (8.4 mm and 12.7 mm), this part was negligible and thus not included in this simulation.

Infiltration: Based on the intermittent rainfall type and the available data, the modified Holtan infiltration equation (Table 5.1) was used in this simulation, with its measured input parameter values for each unit at different years shown in Table 6.2.

Manning's n: Different Manning's *n* values were used for the different land units and the channels, as suggested by Ritter (1990) and shown in Table 6.2.

Model settings: 1 m × 1 m cell size was set for the simulation, with 1.01×10^5 cells in total covering the whole basin. Based on the method introduced in section 2.3, an estimated time step value of 1.37 s and 0.33 s, which equals to the calculated 99% percentile, was selected for the simulation in the year 1 and 6, respectively. The latter smaller value can be explained by the larger flow velocity in the developed channels.

Table 6.2 Measured Infiltration Input Parameters and Manning's n for Runoff Simulation in Pine Glen Basin [a]

Unit	i_f (mm h^{-1})	i_0 (mm h^{-1})	P	φ (%)	θ_0 (%)	FC (%)	D (mm)	Manning's n
				Year 1				
1	60.00	64.50	0.55	43.00	6.45	21.50	100.00	0.25
2	10.00	64.50	1.00	30.00	4.50	15.00	25.00	0.10
3	10.00	64.50	1.00	30.00	4.50	15.00	25.00	0.10
4	10.00	64.50	1.00	30.00	4.50	15.00	25.00	0.10
5	10.00	64.50	1.00	30.00	4.50	15.00	25.00	0.10
				Year 6				
1	60.00	64.50	0.55	43.00	6.45	21.50	100.00	0.25
2	9.00	63.50	10.00	27.00	4.05	13.50	25.00	0.05
3	20.00	70.40	1.00	30.00	4.50	15.00	25.00	0.075
4	22.00	62.00	4.00	43.00	6.45	21.50	25.00	0.05
5	13.20	71.00	10.00	28.00	4.20	14.00	25.00	0.25
Channels								0.05

[a] θ_0 represents the initial soil moisture, and all the other symbols are the same as those in Table 5.1.

6.4.3 Model validation

The observed hydrograph for the chosen rainfall events, together with the simulated hydrographs based on the different flow-direction options, are demonstrated in Figure 6.5. It can be seen that the predicted hydrographs based on the 4+4N option agree best with the measured hydrographs in both runoff events, with the *EF* values greater than 0.913 and *RMSE* values less than 0.183 mm h^{-1}. The

hydrographs derived from the 4N option showed similar trends, however, they tend to underestimate the runoff rates. The reason for this can be found from the close examination of the flow maps as shown in Figure 6.7. It can be seen that after 30 min of the rainfall event in year 6, there was still a portion of excess runoff trapped in the channels or small pits instead of flowing to the outlet, due to the limited flow directions to the cardinal neighbours of the 4N option. On the contrary, much less trapped water flow was observed in the according flow map derived from the 4+4N option. The 8N flow-direction option failed here (EF<0.124) in describing the shapes of the hydrographs, by overestimating the discharge rates and underestimating the durations of the runoff process. This may be attributed to the excessive flow divergence and unrealistic broadened flow pathways introduced by requiring water flow from a cell to all neighbour cells with smaller heights. These results are in line with our expectation that the 4+4N option is more accurate and realistic than the other two options as it controls the flow dispersion and at the same time maintains the eight possible flow directions. Therefore all the following model validation and sensitivity analysis are based on the results derived from this preferred option.

Event 1 occurred in the first year after the rehabilitation work, when no channel network was developed and relative low infiltration rates were observed on the newly established mine soils. Figure 6.6 shows the simulated flow maps at different time steps in this runoff event. It can be seen that with the increasing rainfall intensity, runoff was generated in an expanding area and tended to flow to and accumulated in the central lower part of the basin, from where it further travelled to the outlet at the bottom of the basin. The runoff then disappeared gradually after the rainfall stopped. Due to the dominant overland flow process in this basin, the resultant hydrograph was characterized by low peak discharge rate, long lag time and gradual rising and recession limbs (Figure 6.5a). All these characteristics were captured by the predicted hydrograph, indicating the model capacity in describing the overland flow.

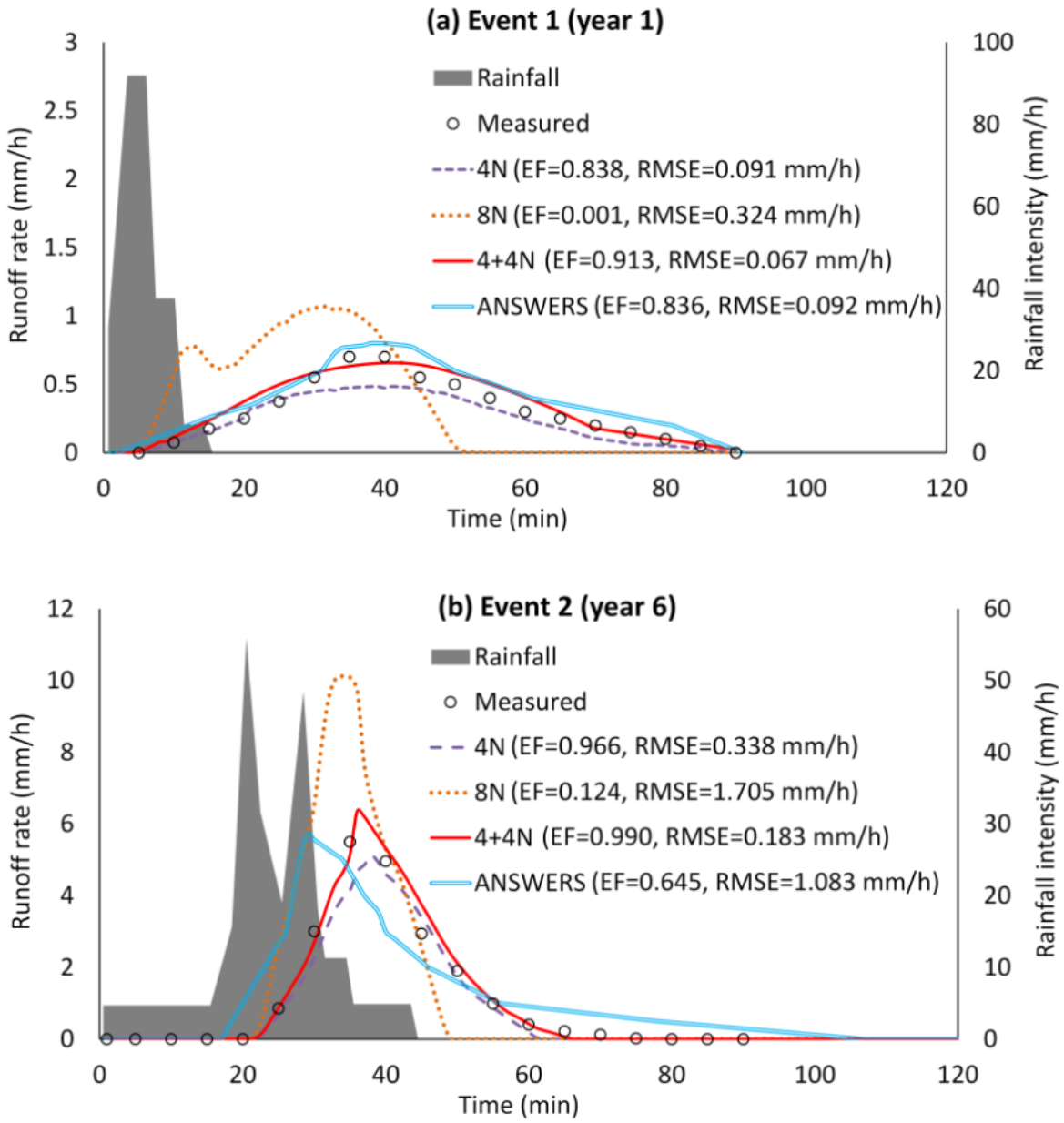

Figure 6.5 Observed discharge rates and simulated hydrographs based on ANSWERS and different flow-direction options of RunCA for two rainfall events in the year 1 and 6 after rehabilitation.

The infiltration capacity of mine soil recovered gradually within six years following rehabilitation, and in the meantime the channel network initiation and maximum expansion in this basin occurred. The resultant simulated flow maps in the year 6 are shown in Figure 6.7. It can be observed that the changes in runoff area and depth both responded quickly to the changes of rainfall intensity, and the channels captured and transmitted a majority of the produced runoff. Due to the dominant channelized flow process, which has higher efficiency for removal of surface runoff from the basin than the overland flow process, the observed hydrograph for this rainfall event exhibits a short lag time and time to peak,

steep rising and recession limbs and high instantaneous peak discharge (Figure 6.5b). Comparison of the hydrographs shows that the predicted and measured slopes of the rising limbs matched well, as well as the peak discharge values and the times to peak discharge. The observed falling limbs, however, showed a slightly longer lag time than the predicted one, probably due to the contribution of the sub-surface flow which is not considered in the current model, with the recovered infiltration capacity. Nevertheless, the general agreement of predicted and observed results demonstrated the model capacity in simulating the channelized flow.

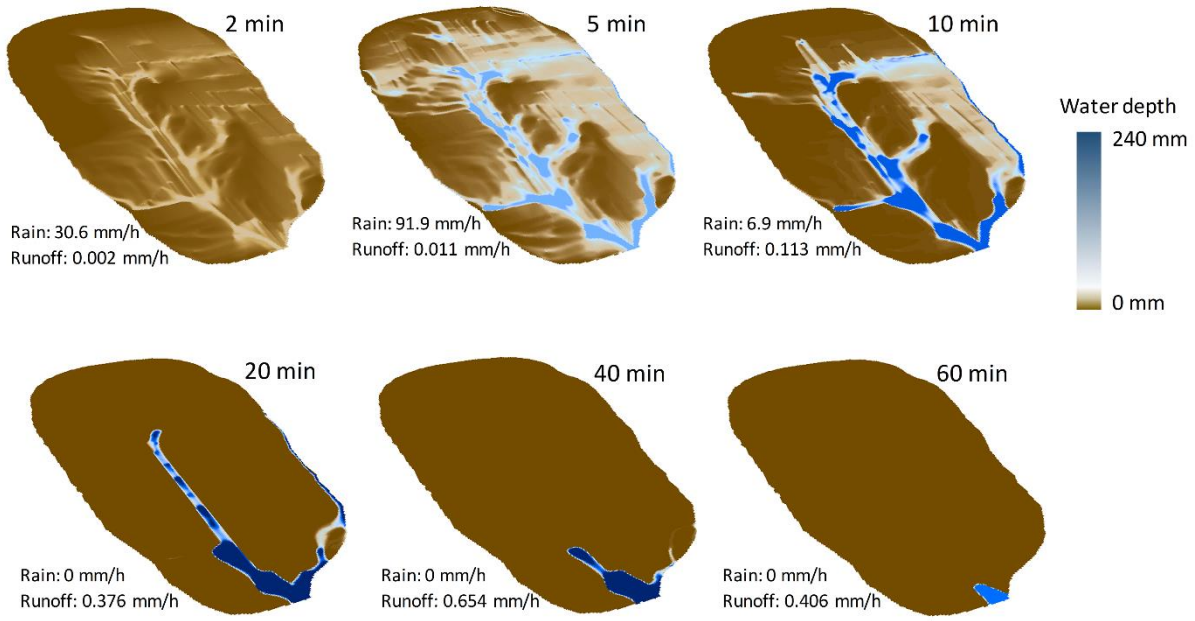

Figure 6.6 Simulated flow maps at different time steps for rainfall event 1 in the year 1.

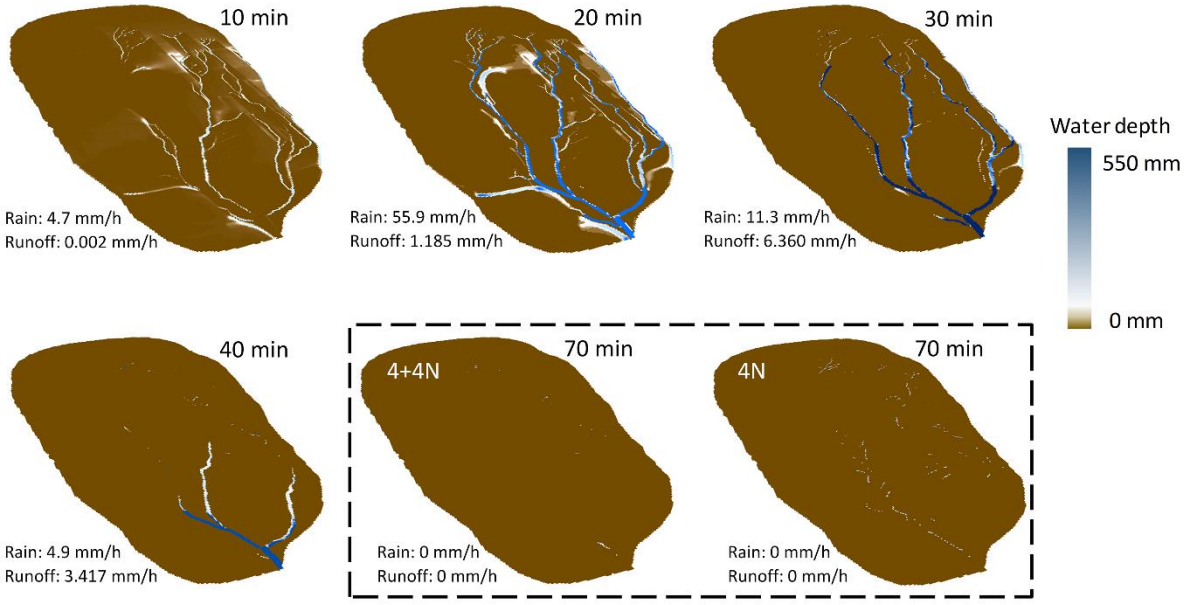

Figure 6.7 Simulated flow maps at different time steps for rainfall event 2 in the year 6. The last two flow maps demonstrate the comparison of results derived from 4+4N and 4N flow direction options.

The performance of RunCA were also compared to that of a well-known distributed physically based hydrologic model, ANSWERS (Beasley et al., 1980), in which the hydrologic response of any element in the basin is computed by an explicit, backward difference solution of the continuity equation, using Manning's equation as a stage-discharge relationship for both overland and channelized flow (Beasley and Huggins, 1981). The model ANSWERS was chosen as its effectiveness in predicting surface runoff has been proven in a wide range of applications (Amin, 1982; Razavian, 1990; Sichani and Engel, 1990; Singh et al., 2006). Its performance was also found comparable to some other hydrologic models (Bhuyan et al., 2002; Borah et al., 2004; Walling et al., 2003). This model was also selected for its similarity of input parameters (e.g., infiltration parameters and Manning's *n*) with RunCA, thus allowing the comparison of model performance by excluding the influence of errors in deriving the parameter values. The detailed information related to the input parameters and simulation process of ANSWERS for these two rainfall events can be found in Ritter (1990) and Ritter (1992). Comparison of simulation results showed that there was no significant difference in the performance of ANSWERS and RunCA in the simulation of the hydrograph of rainfall event 1, although RunCA had a slightly larger *EF* value a smaller *RMSE* value (Figure 6.5a). However, ANSWERS produced obvious bias in simulating the hydrograph of rainfall event 2 by underestimating the lag time of runoff production following the rainfall (Figure 6.5b), while RunCA agreed much better with the observed discharge

rates. These results indicated an improvement of simulation accuracy by using RunCA instead of ANSWERS in this case study.

6.4.4 Model sensitivity analysis

To better understand the model response to the change in each input parameter and model setting, sensitivity analysis was performed, using runoff event 2. Three runoff output parameters that describe hydrographs and two infiltration output parameters (Figure 6.8) were used to evaluate the model responses. The infiltration parameter and Manning's *n* values for year 6 in Table 6.2 were selected as the base values. Then four 20% decrements and four 20% increments from these base values were applied for the sensitivity analysis. In addition, the simulations based on eight cell sizes ranged from 0.1 to 10 times of its original value were also performed.

Figure 6.8 shows the model sensitivity analysis results, which are expressed as the percentage changes from the base output values. It can be found that the output parameters were all significantly sensitive to the change in the final steady infiltration rate i_f, indicating the importance of i_f in this model. In addition, both peak discharge rate Q_p and time to peak T_p, the parameters determining the hydrograph shapes, were greatly influenced by the Manning's *n*, due to its role in changing the flow velocity according to equation (5). The total drainage amount DR_t was also very sensitive to ϕ, FC and D, which is not surprising because they are all parameters for the modified Holtan equation as shown in Table 5.1. The change of spatial resolution to different directions had different impacts on the outputs. When reducing the cell side length to 0.1 m, the results were not significantly affected. But when increasing it gradually to 10 m, the total discharge Q_t and Q_p were greatly reduced, while T_p and the total infiltration INF_t were increased. This can be due to the reason that large cell sizes lead to the loss of micro-topographic details and the channel information, and thus result in inaccurate outputs.

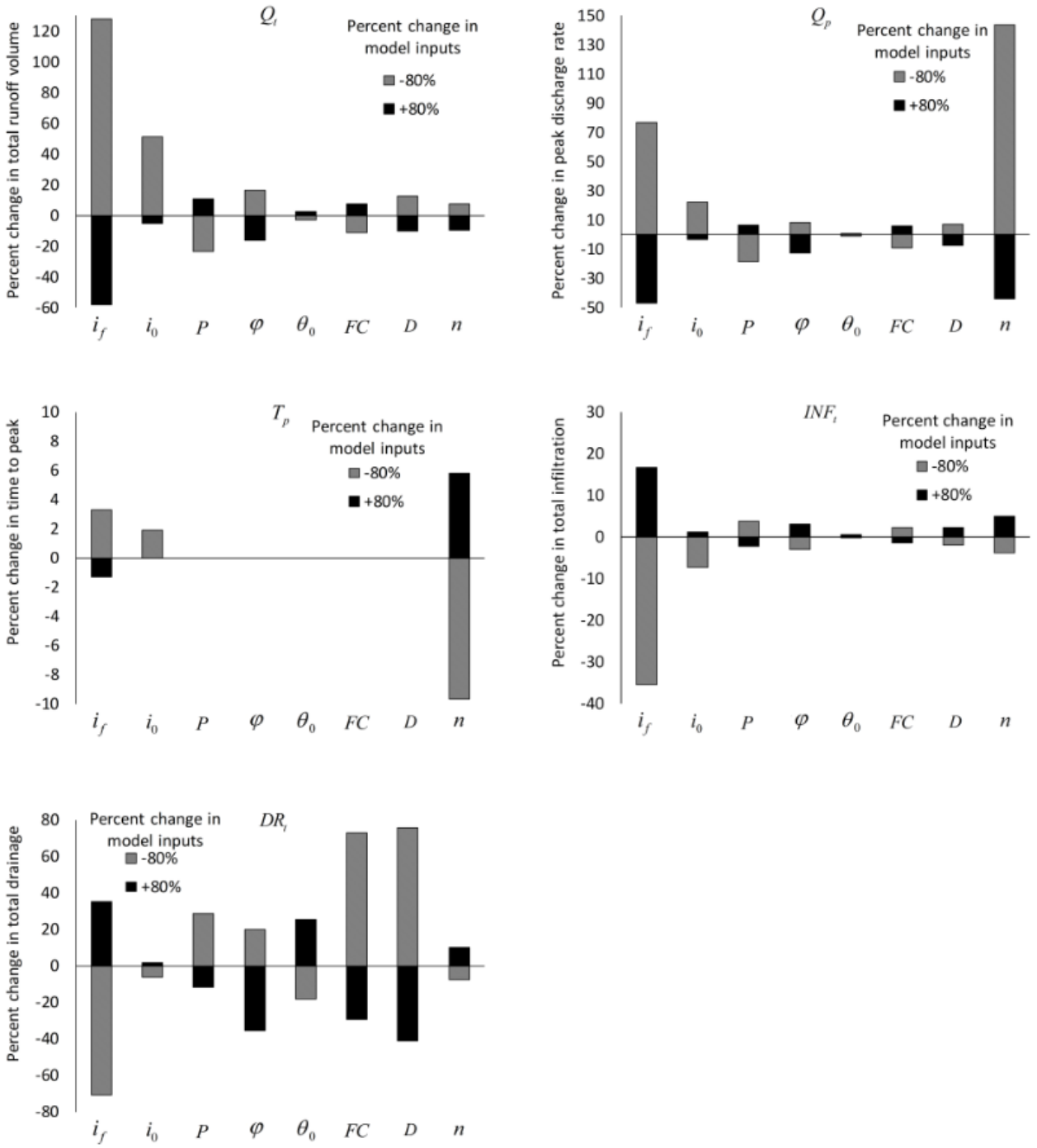

Figure 6.8 Model sensitivity analysis results at the basin scale. Q_t, Q_p and T_p represents total discharge, peak discharge and time to peak discharge respectively, INF_t and DR_t represents total infiltration and total drainage respectively, *n* represents Manning's roughness coefficient, while all the other symbols representing infiltration parameters are the same as those in Table 6.2.

6.5 Conclusions

The efficacy of a CA-based runoff model (RunCA) was systematically validated by three steps. The comparison with the analytical solution proved the effectiveness of the calculation algorithms of RunCA in simulating the runoff distribution. The results of laboratory experiments on small plots showed that the model predicted the hydrographs with the average *EF* above 0.90 and *RMSE* below 0.50 mm h^{-1}. Its performance was not affected by varied soil or topographic conditions, but was most sensitive to the input final steady infiltration rate of soil, which could be measured directly in the field. Validation by field measurements at a basin showed that the 4+4N flow-direction option provided the best agreement between the simulated and measured hydrographs. The spatial distribution and temporal variation of the runoff process could also be described by RunCA, as reflected in the flow maps. RunCA showed better performance compared to ANSWERS in predicting the hydrographs in this case study. In addition to the steady infiltration rate, the modelling results at this large scale were sensitive to the Manning's *n* because of the changed flow velocity, as well as to the setting of cell size due to the loss of topographic details.

At current stage RunCA focuses only on the simulation of infiltration-excess runoff (Hortonian runoff) processes, thus it may produce some inaccurate results when applying it to the large scale study area where different runoff generation mechanisms (e.g., saturation-excess runoff or subsurface runoff) are dominant. For the validations in this study, the impacts of vegetation (e.g. interception) on surface runoff were not included due to lack of appropriate information or type of test. This needs to be further evaluated. As the main purpose of this chapter was to focus on the initial validation of the model, RunCA was only tested in limited case studies using limited rainfall events. Nevertheless, based on the results there is promising potential for successfully applying this model and evaluating its performance to other spatial or temporal scales and under more complex conditions.

Chapter 7 Assessing Runoff Performance in a Rehabilitated Landform Using RunCA: a Case Study in Ranger Uranium Mine

7.1 Introduction

Surface runoff is recognized as a major contributor to many environmental issues, including soil erosion, flood, debris flow, landslide and pollutant transport. Whilst many previous studies have been conducted to understand and predict the runoff processes in the agricultural and other natural systems, limited effort has been made to the disturbed environment such as the mining areas, where the consequences of the excessive runoff could also be serious. At mine closure, rehabilitation work is often carried out to minimise the harmful impacts of mining and to restore the ecological functions of the environment. However, due to the extensive disturbance during the mining activities in terms of excavation, stacking and rebuilding, the rehabilitated landforms are often greatly altered from their original conditions and tend to be more vulnerable to the instability caused by surface runoff. In case of the use of covers for the encapsulation of contaminants, as a consequence erosion may expose hazardous material and deteriorate the water quality downstream by the sediment delivery, and even worse, a large amount of waste materials could be released to environment because of the destruction of the waste containment facilities (e.g., collapse of waste rock dumps and breakage of tailings dams). To prevent these detrimental consequences, optimised rehabilitation design and water management strategies are required to be developed on the basis of well predicted and assessed runoff behaviours.

Various hydrologic models (or erosion models that incorporate a hydrologic component) have been developed over the past few decades and are available for the prediction of surface runoff. These models are basically classified into two groups. The first group is the lumped conceptual models which treat the study area as a spatially singular entity (Figure 7.1) and calculates runoff on the basis of lumped parameters according to some empirical relationships (Haan et al., 1982). Typical examples are SCS curve number (U.S. Department of Agriculture, 1972) and CREAMS (Knisel, 1980). While these models are computationally efficient and widely applied, they are not able to capture the spatial information in the runoff processes. Besides, the empirical relationships developed for the natural environment cannot necessarily be applied to the mining context, where the substrates are often significantly different from natural conditions.

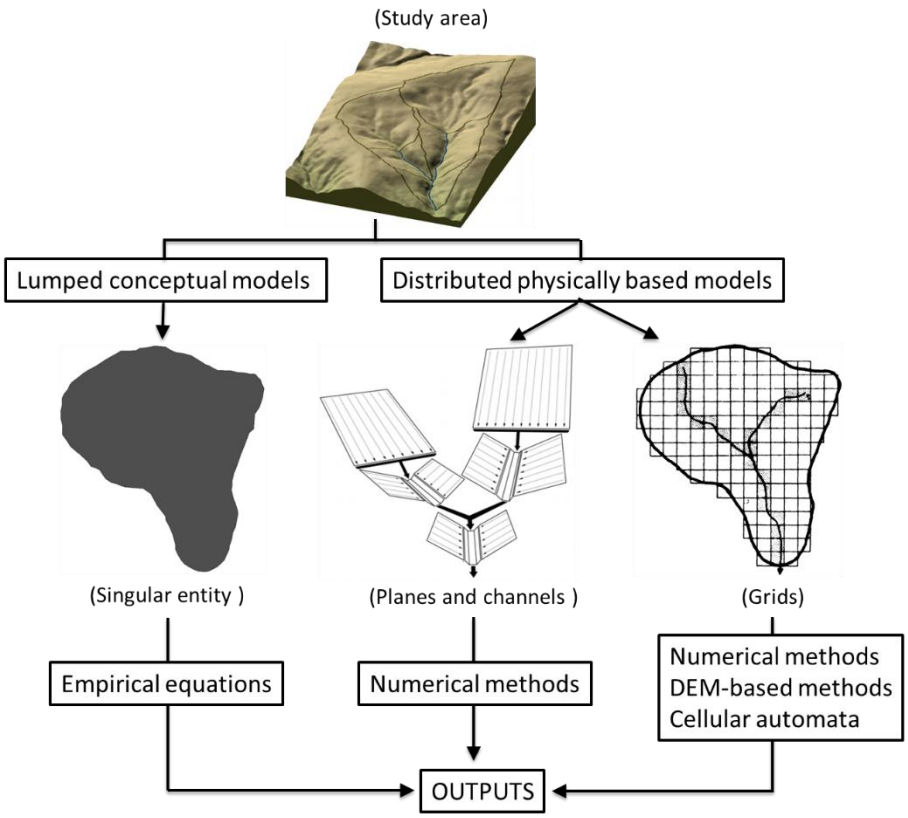

Figure 7.1 Schematic diagram for the structures of different types of hydrologic models.

Another popular group of models are distributed physically based models. In some of these models the target area (usually the catchment) is represented by a network of hydrologic elements, such as a cascade of planes and channels (Figure 7.1) as in KINEROS (Smith, 1981), WEPP (Laflen et al., 1991) and EUROSEM (Morgan et al., 1998b). Since these elements are always simplified geometries with large size, they can only reflect the gross topographic features without local details, and thus may be not suitable for some small scale studies where the spatial heterogeneity needs to be considered, as in most mining areas. Numerical techniques, on the basis of solving the equations of continuity and momentum, are employed in these models to simulate the overland flows and channel flows. Some simplifying assumptions made to these complex equations led to the kinematic wave method and diffusion wave method, which both assume a uniform slope and a one-dimensional flow along the slope direction. Therefore, they tend to produce unexpected errors when these assumptions are not met under more complex topography conditions.

With the development of remote sensing and GIS techniques, grid structures (Figure 7.1) are more frequently used in many distributed hydrologic models. These grids usually have much smaller sizes and therefore are expected to better represent the study area. More advanced numerical methods, such

as the two-dimensional diffusion wave method used in CASC2D (Rojas et al., 2003), have been developed to determine the runoff distribution among the grids. While these methods are able to describe the spatial variations in the runoff behaviours, the computational efficiency is greatly reduced because of the increased complexity in solving the mathematical equations and the larger number of hydrologic elements in these models. Alternative ways are the more straightforward elevation-based methods which determine the flow distributions simply according to the differences in the elevations among grids. These methods are generally based on the digital elevation maps (DEM), using different runoff routing algorithms to transfer the flow from a centre grid to one downslope neighbour (Fairfield and Leymarie, 1991; O'Callaghan and Mark, 1984) or multiple downslope neighbours (Costa-Cabral and Burges, 1994; Quinn et al., 1991; Tarboton, 1997). Despite of the great computational efficiency, these elevation-based methods tend to be oversimplified as they do not take into account the water component in the grids, and therefore they can only generate the fixed flow directions but cannot capture the dynamic flow behaviours.

More recently, Cellular Automata (CA) has been employed for distributed hydrologic models. CA also has a cell/grid based structure, but different from DEM, it is a dynamic system that evolves at discrete time steps on the basis of the synchronous updates of the states of all the spatial cells. It is able to well capture the interactions among cells as the state of each cell depends on the states of its surrounding neighbour cells. Therefore, CA has been found very effective in simulating dynamic complex phenomena from local to global scale according to simple transition rules (Wolfram, 1984a), without solving any complex mathematical equations. Despite of a long history since it was first proposed in the 1950s (Von Neumann, 1966) and wide applications in many areas, CA has not been introduced to surface hydrologic modelling until the recent decade. Some CA based soil erosion and landform evolution models, such as RillGrow (Favis-Mortlock, 1998), EROSION-3D (Schmidt et al., 1999), SIBERIA (Willgoose et al., 1991) and CAESAR (Coulthard et al., 2000), were firstly proposed. They all incorporate a surface hydrology component, which however, is often simplified and only empirically based. Two more specific models were then developed by Rinaldi et al. (2007) and Ma et al. (2009) to simulate the steady state runoff in large plains and on hill-slopes, respectively, by assuming a spatially uniform flow velocity. Parsons and Fonstad (2007) proposed a more advanced CA model capable of simulating the unsteady flow conditions by introducing a timing to control the release of water stored in the cells. However, the performance of this algorithm was found to be largely dependent on the selection of the time step. The accuracy of this model is also restricted by the empirical calculation of runoff production and the four flow directions to cardinal neighbours that may cause the underestimation of flow divergence (Erskine et al., 2006).

To further improve the simulation accuracy, RunCA (Runoff Model Based on Cellular Automata) was proposed by Shao et al. (Shao et al., Under review) to simulate surface runoff at different scales. Since well-established infiltration models are incorporated in RunCA to calculate the runoff production and effective transition rules are developed to determine the unsteady state runoff process on the basis of cardinal-direction-priority principle, minimisation-of-difference algorithm and spatially varied flow velocities, RunCA is expected to be a large progress to the previous CA runoff models. Satisfactory performance of RunCA has been achieved when initially evaluating the model by analytical solution under simplified conditions, laboratory experiments at small plot scale and literature data in a natural basin (Shao et al., Under review). However, a detailed calibration and validation process for this model has not been reported. It also remains unclear whether the model would have the comparative performance under more complex conditions at the field scale and whether it would be applicable to the conditions of rehabilitated landforms in e.g. mining. In this study RunCA was further applied to simulate the surface runoff on a rehabilitated landform at a mine site in northern Australia. This landform was selected as it had a great extent of surface roughness caused by surface ripping and coarse waste rock materials, as well as complete sets of hydrologic data observed in multiple years with high measurement accuracies. The previous successful applications of the landform evolution models of CAESAR and CAESAR-Lisflood on this landform (Coulthard et al., 2012; Lowry J.B.C. et al., 2011; Saynor et al., 2012a) also laid a solid foundation for the runoff simulations by RunCA. The objectives of this study are (1) investigate how RunCA performs at the field scale for both event-based and long-term simulations through the calibration with the observed data and (2) assess the effectiveness of the proposed landform designs in controlling surface runoff by the simulation results.

7.2 Materials and method

7.2.1 Description of RunCA model

RunCA is a surface runoff model developed based on the theory of Cellular Automata. It uses a two-dimensional lattice consisting of square cells to partition the study area into small hydrologic elements. The cells located at the boundaries are treated as “closed” cells that prevent the runoff from flowing beyond the boundaries, while the cells at the outlet are “open” cells that allow the flow water to leave the study area and at the same time record the runoff amount. The Moore-neighbourhood type, which consists of eight adjacent cells in the four cardinal directions and the four diagonal directions from the centre cell, is employed in this model.

The state of each spatial cell in this model is expressed as the water depth, which varies both temporally and spatially, and is determined from the runoff production process. The amount of runoff produced in a cell at every time step is derived by subtracting the amount infiltrated into the soil and the amount intercepted by vegetation from the total input rainfall amount. Since infiltration is a very important component and also a rather complex process for partitioning the water entering the vadose zone from water running off on the ground surface, three infiltration routines are incorporated in RunCA on the basis of the modified Holtan model (Huggins and Monke, 1966; Huggins and Monke, 1968), modified Horton model (Aron, 1992) and modified Green-Ampt model (Bouraoui and Dillaha, 1996). These models have been proven very effective in simulating the infiltration processes during sequences of rainfall events (Shao and Baumgartl, Under review). They allow the infiltration recovery during the dry periods and thus enable RunCA to be applicable for both event-based and long-term simulations.

The flow distribution among these cells are controlled by three transition rules. The first transition rule is to calculate the potential flows from each cell to its neighbour cells. It is based on the cardinal-direction-priority principle, which means that the water has the priority to flow to its four cardinal neighbours, and it will flow to its diagonal neighbours only when there is no cardinal neighbour to flow. This helps to control the unexpected flow dispersion, and at the same time keep eight possible flow directions. The calculation of flow amount is based on the improved minimisation-of-differences algorithm. This means that the water always flows from the cells with greater heights (elevation + water depth) to those with lower heights to minimise their height differences to reach the most balanced conditions. No complex calculations are included in this process, which ensures the high computational efficiency of RunCA. Since in reality the actual flow amount is also determined by the spatially varied flow velocities, a second transition rule is then applied to incorporate the effects of flow velocity. The travel time for each flow is firstly calculated based on the Manning's equation, and then this value is compared to the time step used for the simulation. If the time step is smaller than the calculated flow travel time, the actual flow amount needs to be further adjusted by multiplying a ratio between time step and flow travel time. This transition rule enables the model to simulate the unsteady state runoff process. The former two transition rules are both applied to the local neighbourhood area, however, from a global view, one cell not only discharges water, but also receives water from its neighbour cells. Therefore a third transition rule is used to calculate the total flow for each cell by the balance between outflow and inflows. Then the new water depth in each cell is updated by adding this total flow to the current water depth for the calculation of the next time step. Through the synchronous and continuous updating of all the cells in the lattice space, the temporal and spatial runoff behaviours can be described. The model structure and modelling procedure of RunCA is summarized in Figure 7.2.

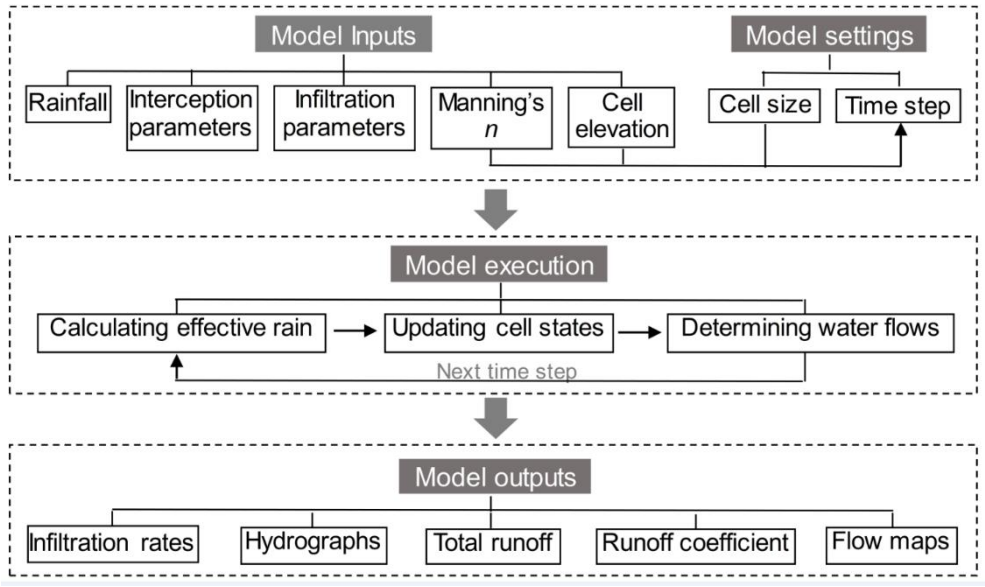

Figure 7.2 Flowchart for the structure and modelling procedure of RunCA (Shao et al., Under review).

7.2.2 Introduction to study site

The study site is at Ranger Uranium Mine, which is operated by Energy Resources of Australia Ltd (ERA). It is located in the wet-dry monsoonal tropics, approximately 250 km east of Darwin, Northern Territory, Australia (Saynor et al., 2012a) (Figure 7.3). The average annual rainfall in this area is 1584 mm (Meteorology, 2014), featured with high-intensity storms occurring between October and April (wet season) while virtually no rain falls during the remainder of the year (dry season). Therefore, high rates of runoff is expected in the wet seasons. The mine site is surrounded by the World Heritage-listed Kakadu National Park, and a broad expanse of floodplain and wetlands listed as 'Wetlands of International Importance' under the Ramsar Convention are located in its downstream area (Coulthard et al., 2012). Four surrounding catchments are potentially impacted by the surface runoff and associated erosion from the mine site (Figure 7.3). Given the aforementioned climate condition and regional significance, the current environmental requirements for Ranger Uranium Mine specify that "the rehabilitated site should have erosion characteristics which as far as can reasonably be achieved, do not vary significantly from those of comparable landforms in surrounding undisturbed areas" (Division, 1999). The rehabilitation design therefore must ensure that surface runoff and erosion from the mine site are well controlled to minimise the potential release of contaminants that would degrade the environment of surrounding areas.

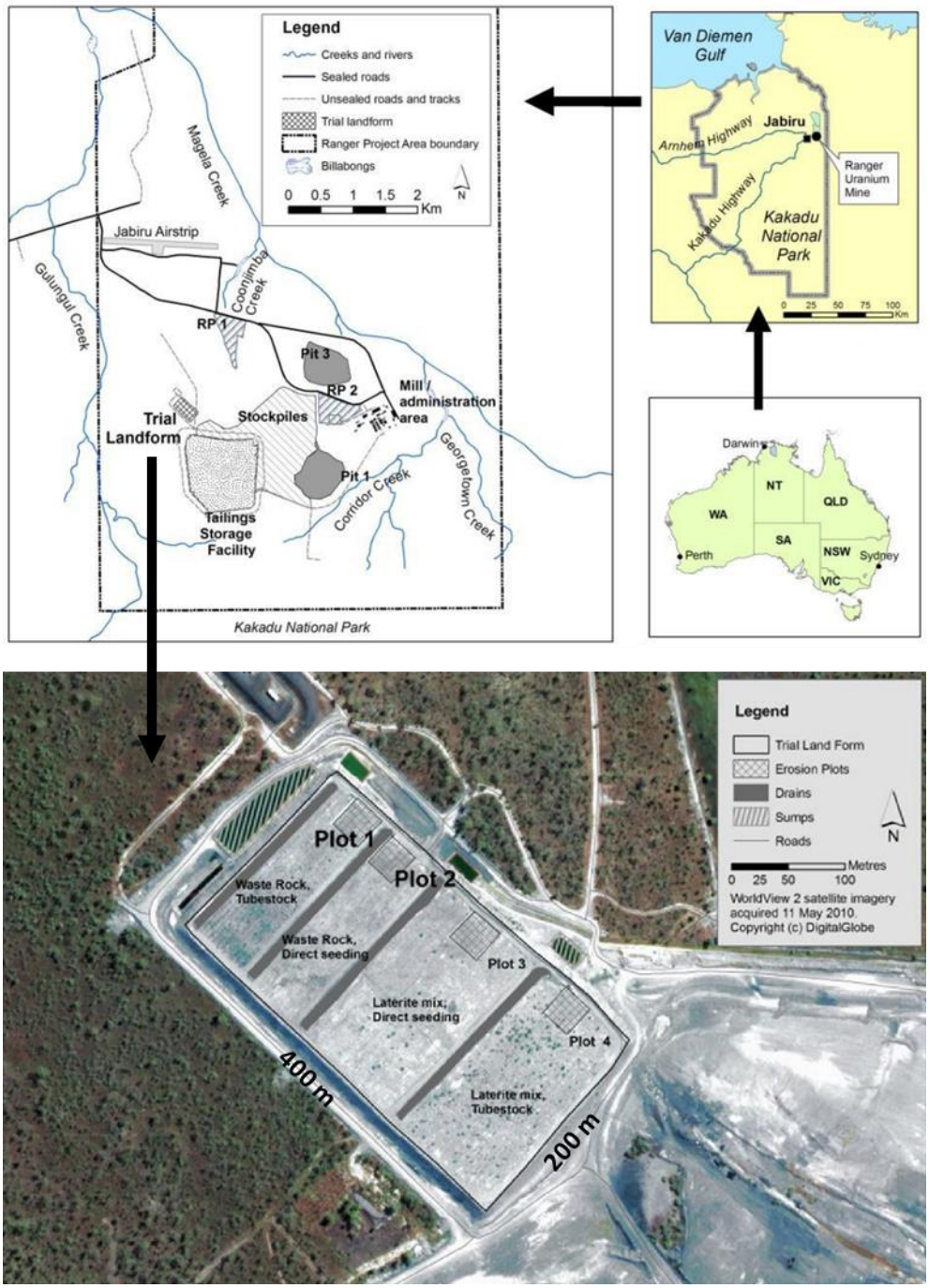

Figure 7.3 Location of Ranger Uranium Mine and satellite imagery of the trial landform (Lowry et al., 2014; Saynor et al., 2012a).

To assist with the evaluation of the proposed landform designs and revegetation strategies for the mine closure at the end of mine life, a trial landform with a footprint area of approximately 8 ha (200 m × 400 m), was constructed during late 2008 and early 2009 by ERA to the northwest of the tailings storage facility at Ranger mine (Figure 7.3). Two types of potential cover materials, waste rock alone

and waste rock blended with approximately 30% of laterite (a type of fine-grained weathered horizon material), were designed on this landform to test and compare their suitability as cap materials (Lowry et al., 2014; Saynor et al., 2012a). These materials were used because they were the main components of the uneconomic stockpiles at this mine site, while topsoil was not available as it was not stockpiled during mining (Saynor et al., 2012a). The constructed landform has a mean slope of 2%, and its surface was ripped along the contour using tynes attached to a large bulldozer (Figure 7.4a) (Lowry et al., 2014; Saynor et al., 2012a), with the expectation to reduce surface runoff, enhance infiltration and conserve water for revegetation. The vegetation was planted along the rip lines using two different methods, with half of the area planted by direct seeding and the other half with tubestocks, for each of those two cover types.

Four runoff plots, with each size of approximately 30 m × 30 m, were set up on the trial landform by the Supervising Scientist Division during the dry season of 2009. Two plots (plot 1 and 2) were constructed in the area of the waste rock cover, and the other two (plot 3 and 4) were in the area of mixed waste rock and laterite cover (Figure 7.3) (Coulthard et al., 2012; Lowry et al., 2014; Saynor et al., 2012a). Raised borders (Figure 7.6a) were built around these plots to prevent the runoff produced in the rest area of the landform from flowing into the plots. The purposes of setting up these runoff plots were to facilitate the measurement and assessment of the runoff and erosion performance of the proposed landform designs. Plot 1 and plot 2 (Figure 7.4), on the waste rock cover, were the focus of this study as they had the most complete sets of available measured and observed data.

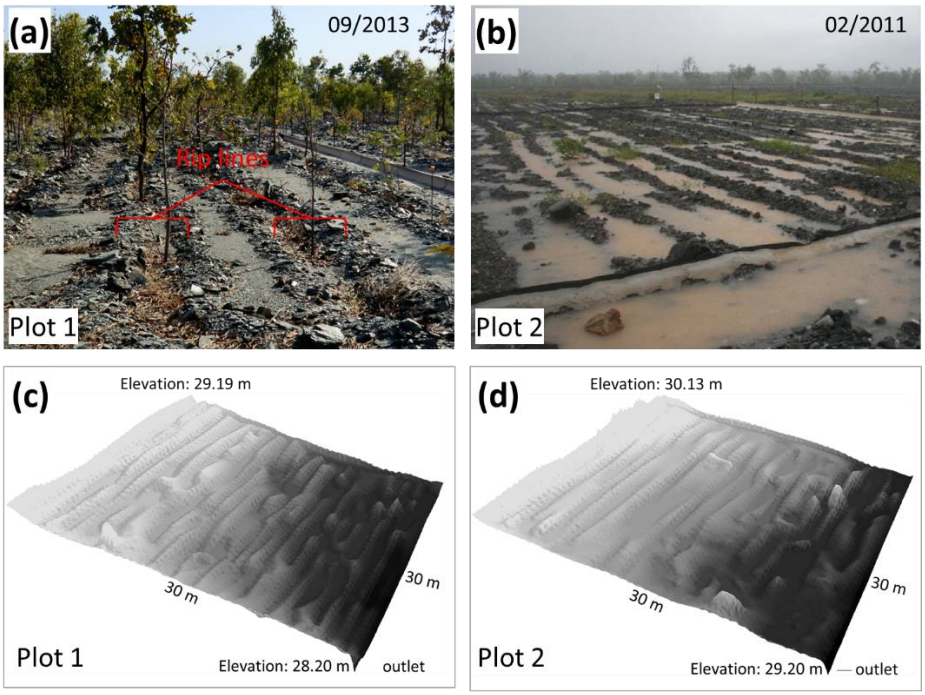

Figure 7.4 Photos (a, b) of runoff plot 1 (dry) and plot 2 (wet) and their digital elevation maps (c, d). Figure (b) from Saynor et al. (2012b).

7.2.3 Field observation and measurement

Bulk samples of surface material were collected by Saynor and Houghton (2011) across the waste rock surface of the trial landform, at both the non-ripped areas between the rip lines and the top of the mounds formed by ripping (Figure 7.5a). Grain size analysis was conducted on these samples by the combined hydrometer and sieve method (Gee and Bauder, 1986) and the results for the grain size distribution of the waste rock cover are demonstrated in Figure 7.5b, which shows that the large fractions (> 0.2 m) accounts for more than 40% of the total amount.

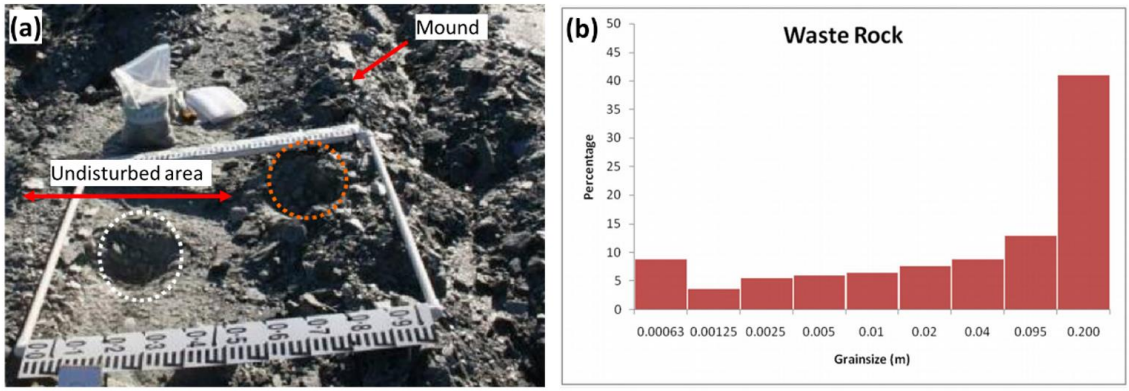

Figure 7.5 Bulk samples collection (a) (Saynor and Houghton, 2011) and grain size analysis results (b) for waste rock cover on trial landform (Lowry et al., 2014; Saynor et al., 2012a).

Digital elevation maps (DEM) of the runoff plots were produced by ***eriss*** (Environmental Research Institute of the Supervising Scientist) in June 2010 from the data collected by a Terrestrial Laser Scanner, with a horizontal resolution of 20 cm (Lowry et al., 2014; Saynor et al., 2012a). Then the DEMs were processed in ArcGIS 10.1 to remove the high points resulted from the capture of components of vegetation. Figure 7.4c and 7.4d show the final DEMs for plot 1 and 2, from which it can be seen that plot 1 has better defined rip lines than plot 2. Field survey of topography was also conducted and 14 rip lines were observed in each plot (a rip line consists of two mounds and a furrow created by ripping). The mean measured width of rip lines was 163 ± 20 cm for plot 1 and 171 ± 52 cm for plot 2, and the mean height (measured from the top of mounds to the bottom of furrows) was 15 ± 5 cm for plot 1 and 10 ± 4 cm for plot 2.

As described in Saynor et al. (2012a) and Lowry et al. (2014), an exposed PVC drain was installed at the downslope border of each plot to divert surface runoff to the outlet of the plot, where continuous measurements are made in a 200 mm RBC flume which has a trapezoidal broad-crested control section (Figure 7.6a). Water height was measured in the control section by both an optical shaft encoder (primary sensor) and a pressure transducer (backup sensor). According to Saynor et al. (2012a), the runoff rates were then calculated from these recorded water heights using the equations derived by Bos et al. (1984) and Evans and Riley (1993). A tipping bucket rain gauge was also installed adjacent to each runoff plot for the measurement of rainfall rates. All the above data are recorded and stored in a data logger with mobile phone telemetry connection (Saynor et al., 2012a). Data at one-minute intervals and over four water years from 2009 to 2013, monitored and provided by ***eriss***, was used in this study, with each water year defined as the period from 1 September to 31 August of the following year to facilitate the data analysis. In addition, the surface water content across the landform was measured by ERA continuously at 30-minute intervals with four Campbell scientific CS616 soil moisture probes horizontally buried at the depth of 5 cm, and another four vertically buried at 0-30 cm in plot 1. The soil moisture data was recorded by the Campbell data logger CR1000.

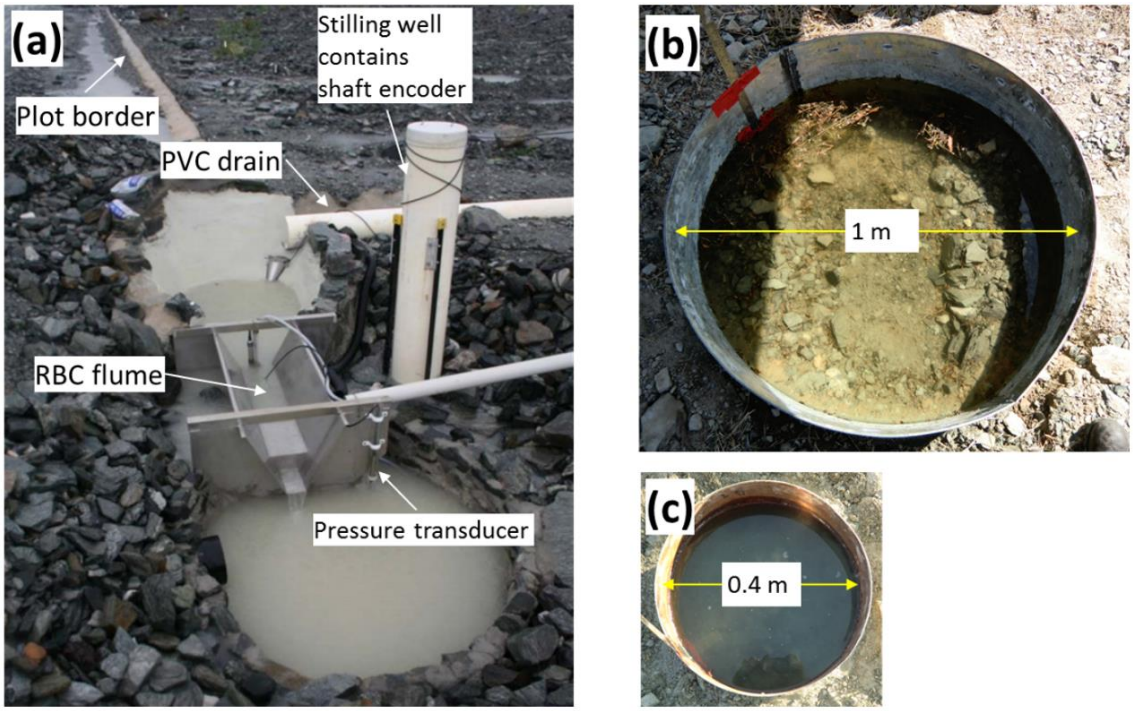

Figure 7.6 Runoff monitoring at outlet (a) and infiltration measurement using infiltrometers with large (b) and small (c) diameters on plot 1. Figure (a) from Saynor et al. (2012b), modified.

In order to determine the hydraulic properties of this landform and the infiltration input parameters for RunCA, field infiltration measurements were carried out across the landform in September 2013, with the joint effort of ERA, the University of Queensland and Charles Darwin University. Due to the large width of the rip lines, four measurements were conducted on the rip lines at randomly selected areas on the waste rock cover, using a ring infiltrometer with a large diameter of 1 m (Figure 7.6b). Another four measurement were also conducted randomly on the non-ripped areas between the rip lines, using a smaller ring infiltrometer with a diameter of 0.4 m (Figure 7.6c). The falling head method was employed in all these measurements. Each measurement lasted until a stable infiltration state was reached, and then the final steady infiltration rate i_f was calculated by averaging the last three measured infiltration rates. Core samples were also taken in the areas immediately adjacent to the infiltration measurements for the laboratory determination of various properties. Specifically, the total porosity *TP* was assumed to be equal to the saturated water content, which was reached by leaving the core samples in a tray filled with shallow water for 2-4 days, and field capacity θ_{FC} was achieved by leaving the saturated core samples on a suction plate with 33 kPa (0.33 bar) suction pressure for 7 days. Initial soil moisture θ_0, *TP* and θ_{FC} were then determined by weighing the core samples before and after oven-drying at 105 ℃ for 24 h in the laboratory.

7.2.4 Statistical analysis

As some of the infiltration parameters for RunCA are very difficult to measure directly, a curve-fitting procedure was used to derive their values on the basis of measured infiltration rates. The goodness of fit of the simulated infiltration curves to the observed data were assessed by both the coefficient of determination (R^2) and the root mean square error (*RMSE*). R^2 indicates how accurately the model tracks the variation of observed values, and its value can range from 0 to 1 (perfect fit). *RMSE* shows the amount of divergence of the model values from the observed values and its value close to 0 indicates good agreement. R^2 of the 1:1 fitting line in the scatter plots showing the predicted runoff volumes against the measured values was used to represent their agreement. Percentage error (*PE*) was also employed to reflect the under- or over-prediction and the magnitude of prediction error in the predicted runoff volume. In addition to *RMSE*, the Nash-Sutcliffe efficiency (*EF*) (Nash and Sutcliffe, 1970) was used to evaluate the performance of RunCA in simulating the event-based runoff curves. It describes the proportion of the variance of the observed values that is accounted for by the model, and its value can vary from 1 (perfect fit) to negative infinity. The mathematical expressions used for these statistical analysis measures are:

$$R^2 = \left(\frac{\sum_{i=1}^{n} \left(O_i - \overline{O}\right)\left(P_i - \overline{P}\right)}{\sqrt{\sum_{i=1}^{n} \left(O_i - \overline{O}\right)^2} \sqrt{\sum_{i=1}^{n} \left(P_i - \overline{P}\right)^2}} \right)^2 \tag{7.1}$$

$$RMSE = \sqrt{\frac{1}{n} \sum_{i=1}^{n} \left(O_i - P_i\right)^2} \tag{7.2}$$

$$PE = \frac{P_i - O_i}{O_i} \times 100\% \tag{7.3}$$

$$EF = 1 - \frac{\sum_{i=1}^{n} \left(O_i - P_i\right)^2}{\sum_{i=1}^{n} \left(O_i - \overline{O}\right)^2} \tag{7.4}$$

where n is number of observations during the prediction period; O_i and P_i are observed and predicted values at each comparison point i; $\overline{O}$ and $\overline{P}$ is arithmetic mean of the observed and predicted values, respectively.

7.3 Results and discussion

7.3.1 Observed rainfall and surface runoff

The data of rainfall rates and runoff rates for runoff plot 1 and plot 2 during the four water years from 2009 to 2013 was collected, processed and supplied by ***eriss***. The observed results are demonstrated in Figure 7.7. It can be seen that the majority of rainfall happened in the wet season of each water year from September to April, with great variations in the rainfall rates (ranging from 0 mm h^{-1} to 384 mm h^{-1}). The monitored surface runoff rates from both plots showed corresponding changes to the varied rainfall rates. While most of the produced runoff rates were less than 20 mm h^{-1}, a number of significantly higher rates were recorded in several extreme rainfall events, with the maximum runoff rate reaching 135 mm h^{-1} and 245 mm h^{-1} for plot 1 and plot 2, respectively.

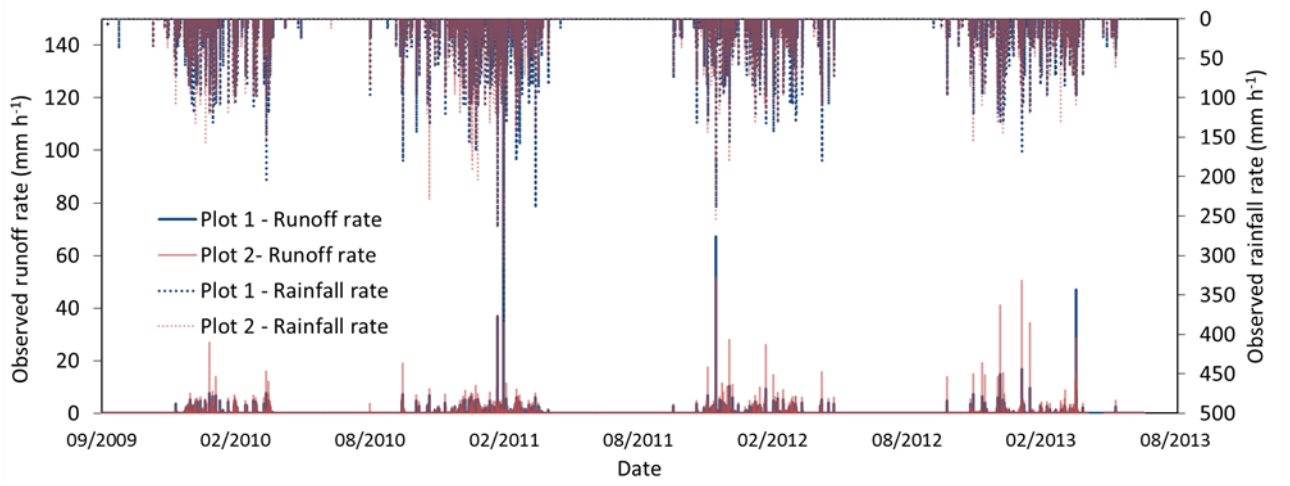

Figure 7.7 Observed rainfall and runoff rates for runoff plot 1 and 2 during four water years from 2009 to 2013.

Table 1 summarises the recorded annual rainfall and runoff for each water year. It can be seen that the two plots had very close annual rainfall values, with significantly larger rainfall amount observed in 2010-11 than in other water years. Correspondingly, the annual runoff was the largest in 2010-11 for both plots, with larger volume of runoff produced in plot 2 than in plot 1 in each water year. An interval of three hours was employed in this study to define and separate rainfall events, in other words, each rainfall event only consisted of rainfall hiatuses that were less than three hours. This resulted in 304 rainfall events in total for the four water years, with the number of events in each water year shown in Table 1. Plot 2 seemed to have larger mean event duration and runoff coefficient than plot 1, while

large ranges of values and standard deviations were derived for both plots (Table 1), demonstrating the varied characteristics of the observed rainfall events. According to the frequency analysis, more than 80% of the events had runoff coefficients less than 6% and 10% for plot 1 and plot 2, respectively. However, for some large events, the runoff coefficient could reach values as high as 80% for both plots. These large variations in the rainfall and runoff behaviours provided good opportunities to evaluate the accuracy of RunCA and assess the performance of the proposed landform designs under different conditions.

Table 7.1 Statistical values for the observed rainfall events in the four water years from 2009 to 2013.

Water year [a]	Annual rainfall (mm)	Annual runoff (mm)	Number of events	Event duration (min)		Runoff coefficient (%)	
				Range	Mean	Range	Mean
Plot 1							
2009-10	1528.1	77.7	68	15-534	113.1±104.2	0.7-14.2	5.6±2.5
2010-11	2205.4	300.2	96	15-631	139.0±140.3	2.6-88.2	6.0±9.1
2011-12	1481.0	101.2	78	16-713	87.5±127.6	2.2-40.3	5.4±4.4
2012-13	1283.0	121.8	62	8-2135	88.1±275.8	1.2-29.9	4.6±4.3
Plot 2							
2009-10	1531.5	132.0	68	26-543	156.2±114.3	1.1-22.3	8.0±4.0
2010-11	2293.6	328.5	96	31-760	177.5±148.5	3.7-78.2	8.7±7.9
2011-12	1531.4	166.3	78	26-1017	130.2±154.0	2.5-30.9	8.9±5.0
2012-13	1274.2	196.4	62	13-2154	127.8±270.8	2.2-57.9	11.7±9.7

[a] A water year is defined as the period from 1 September to 31 August of the following year

7.3.2 Measured infiltration characteristics

The results of infiltration measurements showed that the time to reach the steady infiltration rate ranged from 20 min to 35 min for rip lines, and 10 min to 22 min for non-ripped areas. These shorter time to equilibrium than those of most natural soils indicated a quicker decrease of infiltration rate on this waste rock cover, probably due to a relatively high proportion of large macropores in the coarse rock matrix.

Table 7.2 Summary of infiltration parameter values for field infiltration measurements conducted on waste rock cover.

Measurement No.	Infiltration parameters [a]						*RMSE* (mm h^{-1})	R^2
	i_f (mm h^{-1})	θ_{FC} (m^3 m^{-3})	θ_0 (m^3 m^{-3})	*TP* (m^3 m^{-3})	*a* [b] (mm)	*D* [b] (mm)		
Rip lines								
1	25.20	0.09	0.07	0.30	0.60	180	7.37	0.84
2	24.00	0.12	0.09	0.26	0.50	90	5.09	0.84
3	18.00	0.11	0.07	0.30	1.30	100	6.79	0.82
4	30.00	0.09	0.08	0.26	2.50	120	7.76	0.95
Mean	24.30	0.10	0.08	0.28	1.23	122.50	6.75	0.86
SD	4.94	0.02	0.01	0.02	0.92	40.31	3.35	0.03
Non-ripped areas								
5	7.50	0.08	0.06	0.23	0.75	100	9.38	0.83
6	19.20	0.08	0.07	0.23	1.50	150	6.23	0.96
7	12.00	0.06	0.06	0.21	1.50	50	5.00	0.96
8	14.00	0.11	0.07	0.25	1.00	80	7.73	0.85
Mean	13.18	0.08	0.07	0.23	1.19	95.00	7.08	0.90
SD	4.85	0.02	0.01	0.01	0.38	42.03	1.90	0.07

[a] i_f: final steady infiltration rate (mm h^{-1}); θ_0: initial soil moisture (m^3 m^{-3}); θ_{FC}: field capacity (m^3 m^{-3}); *TP*: soil porosity (m^3 m^{-3}); *a*: a constant (mm$^{-0.4}$ h^{-1}) in modified Holtan model; *D*: depth of control zone which affects the infiltration process (mm).

[b] unmeasurable parameters determined by curve-fitting with observed infiltration rates.

The three modified infiltration models employed in RunCA as introduced before were all used to describe the infiltration processes, and the modified Holtan model was found to best match the observed results and thus was selected for the further simulations in this study. Six input parameters are required to determine the modified Holtan model. Among these parameters, i_f, *TP*, θ_0 and θ_{FC} were all determined from field observations or laboratory analysis. The other two parameter (constant *a* and control zone depth *D*), however, are very difficult to be measured directly and thus were indirectly derived by a curve-fitting procedure to the modified Holtan model with the observed infiltration rates. Table 7.2 summarise all the determined parameter values. It can be seen that within the group of rip lines or non-ripped areas, there was a range of values for each derived parameter from different measurements, but the standard deviation was not significant. This suggests a relatively homogeneous distribution of infiltration characteristics within each group. However, there were obvious differences in the parameter values between these two groups, with all parameter values larger in the rip lines than in the non-ripped area. This can be attributed to the effects of surface ripping on

enhancing infiltration on rip lines, and also the washing of fine materials by runoff from rip lines to non-ripped area, where the infiltration capacity was reduced due to this sedimentation. The small *RMSE* and large R^2 values shown in the table indicate the capacity of the modified Holtan model in describing the infiltration processes, as well as the accuracy and reliability of the derived infiltration parameter values. Figure 7.8 also demonstrates that the simulated infiltration curves agreed well with the measured infiltration rates in two examples.

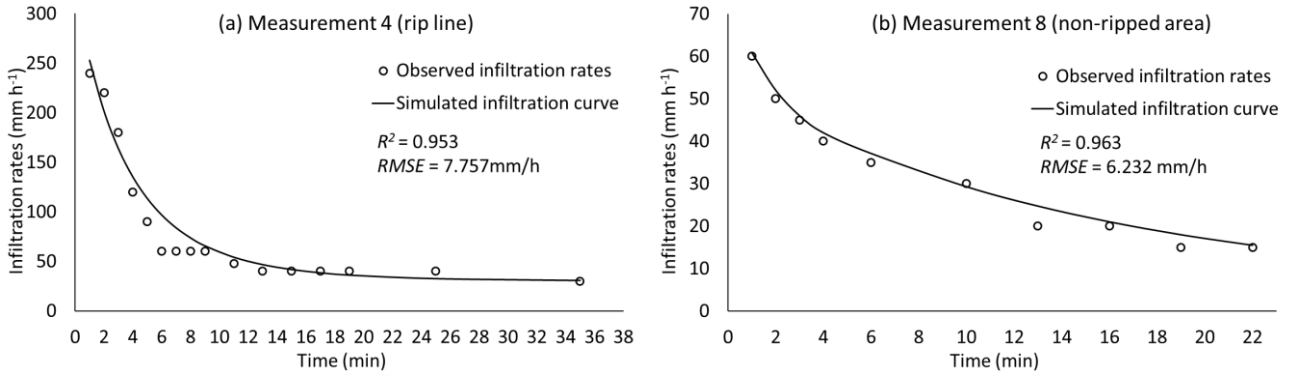

Figure 7.8 Examples showing the agreement of simulated infiltration curves to the observed infiltration rates in the measurements conducted in rip lines (a) and non-ripped areas (b).

7.3.3 Model sensitivity analysis

As there were a range of values for each input parameter from different measurements across the landform, model calibration needs to be further conducted to optimise a set of parameter values. Before the calibration procedure, the model sensitivity analysis is required to be performed in order to understand how the modelling results would respond to the changes in the parameters and which parameters would have more important influences on the results, so that the priority of parameters to be calibrated can be identified. In this study, seven input parameters, including the six aforementioned infiltration parameters and the Manning's roughness coefficient *n*, were included in the sensitivity analysis. Because of the observed differences between the rip lines and non-ripped areas, two different sets of input values were applied accordingly. The mean values of the infiltration parameters as shown in Table 7.2 were used as the base values. The base values for *n* were derived empirically from the guide values in EUROSEM (Morgan et al., 1998a), with 0.05 for the rip line areas and 0.03 for the non-ripped areas. Then five 10% increments and five 10% decrements were applied to these base values for runoff simulations. The total runoff volume was selected as the output parameter to evaluate the model responses. To investigate the model sensitivity under different rainfall conditions, all the observed rainfall events were ranked on the basis of rainfall intensity from the smallest to largest, and

then the three rainfall events at the 25%, 50% and 75% percentiles were selected to represent the small, medium and large rainfall events, respectively. The characteristics of the chosen events are summarised in Table 7.3.

Table 7.3 Characteristics of the rainfall events selected for model sensitivity analysis.

Event No.	Date	Rainfall intensity (mm/h)	Duration (min)	Total rain (mm)	Runoff coefficient (%)
208	29/1/2012	10.67	36	6.40	4.70
252	30/11/2013	20.36	33	11.2	4.67
73	28/10/2011	30.00	42	21.0	5.73

The sensitivity analysis results are demonstrated in Figure 7.9. In general the model showed larger responses under higher rainfall intensity, and the model sensitivity was greater on plot 2 than plot 1. The simulated total runoff volume was more sensitive to the input parameters in the non-ripped areas than those in the rip lines, probably because of the more important role of these non-ripped in contributing surface runoff in this landform. The figure also shows that the changes in the parameter values, either increments or decrements, tended to have more significant impacts on the increase of total runoff volume than its decrease. In addition, the importance of different parameters in influencing the modelling results can be identified. Specifically, the model was most sensitive to *TP* and *D*, both parameters determining the substrate water storage capacity. a, i_f and θ_0 had less significant impacts, while the modelling results were hardly impacted by *FC* or *n*.

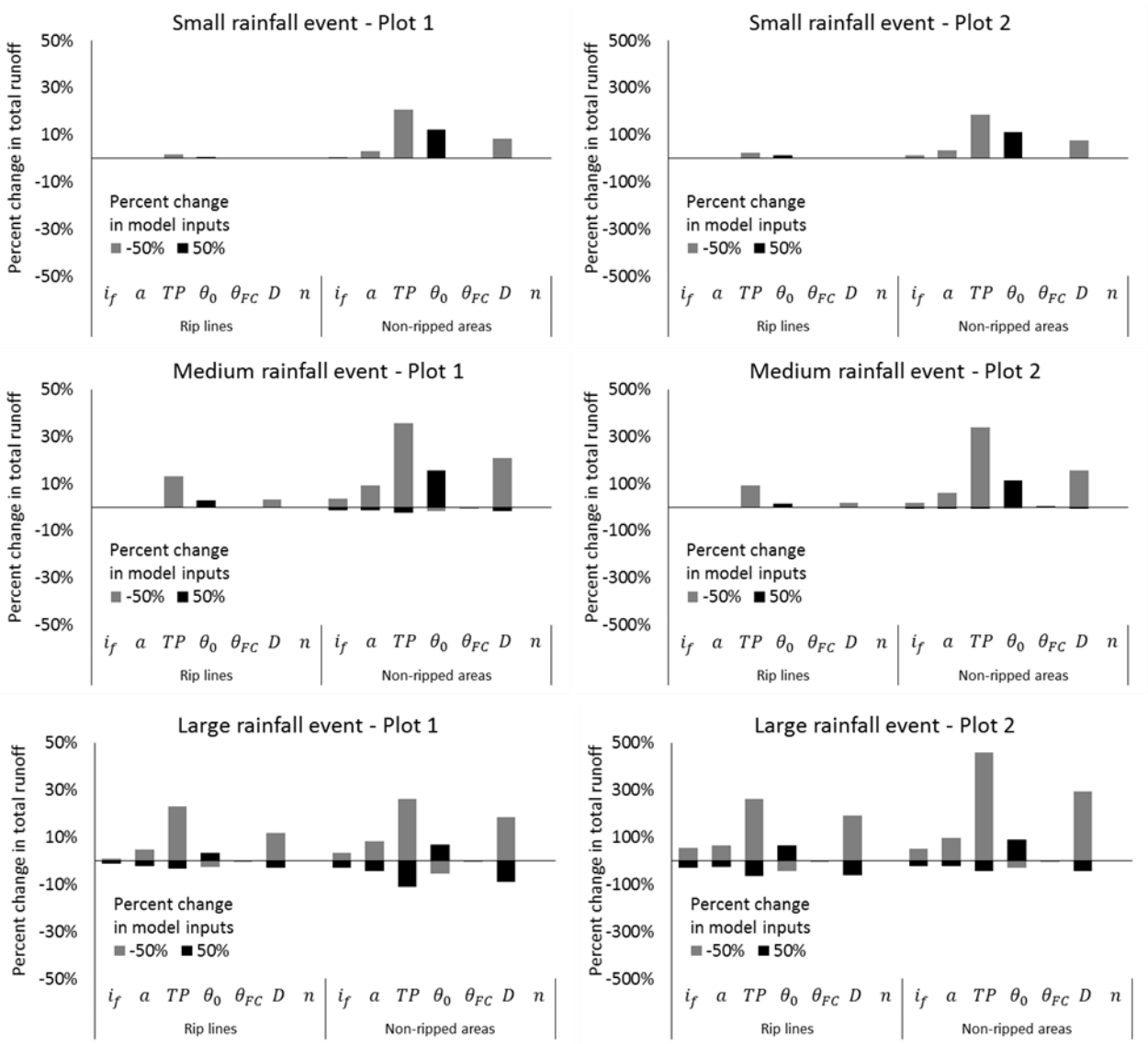

Figure 7.9 Results for model sensitivity analysis using three rainfall events. i_f is final steady infiltration rate (mm h^{-1}), θ_0 is initial soil moisture (m^3 m^{-3}), *FC* is field capacity (m^3 m^{-3}), *TP* is soil porosity (m^3 m^{-3}), *a* is a constant ($mm^{-0.4}$ h^{-1}), *D* is control zone depth (mm), and *n* is Manning's roughness coefficient.

7.3.4 Calibration of model input parameters

According to the sensitivity analysis results, the order of parameters for calibration can be determined on the basis of their influences from the largest to the smallest. With group I and II representing the rip line and the non-ripped area, respectively, then the model calibration was carried out in the order of *TP*(II), *D*(II), *TP*(I), *D*(I), *a*(II), i_f(II), *a*(I), i_f(I), θ_{FC}(II), θ_{FC}((I), *n*(II) and *n*(I). θ_0 was not included here as it varied among rainfall events and was determined from the measurements of TDRs. 30 rainfall events were randomly selected from the 303 events in the four water years for the calibration purpose.

Statistical analysis showed that these rainfall events had large ranges of characteristics and thus were expected to well represent the whole set of rainfall events. The predicted total runoff values for all the calibration rainfall events were plotted against the measured values, and the coefficient of determination R^2 of the 1:1 fitting line in the scatter plot was used to assess the results of calibration, with the larger R^2 representing the better agreement between the simulated and observed results. The calibration of each parameter started from its mean value shown in Table 7.2, and then 5% increment or decrement was applied each time according to the simulation results and the sensitivity analysis results, until a largest R^2 was reached or a minimum or maximum investigated value of this parameter in Table 7.2 was reached. This procedure optimised the parameter values and at the same time ensured that they remained in the ranges of the measurements, which made them reasonable.

Table 7.4 Calibrated values of input parameters for the runoff simulations by RunCA.

	i_f (mm h^{-1})	a (mm)	TP (m^3 m^{-3})	θ_{FC} (m^3 m^{-3})	D (mm)	n
			Plot 1			
Rip line	24.3	0.80	0.26	0.10	90	0.05
Non-ripped area	12.9	0.75	0.21	0.08	50	0.03
			Plot 2			
Rip line	29.2	1.48	0.28	0.10	135	0.05
Non-ripped area	7.9	0.75	0.21	0.08	50	0.03

[a] i_f: final steady infiltration rate (mm h^{-1}); θ_{FC}: field capacity (m^3 m^{-3}); TP: soil porosity (m^3 m^{-3}); a: a constant (mm$^{-0.4}$ h^{-1}) in modified Holtan model; D: control zone depth (mm); n: Manning's roughness coefficient.

The calibration results are displayed in Table 7.4, which shows that the calibrated values of parameters were larger in the rip lines than in the non-ripped areas on both plots. This indicates the larger infiltration capacities in the rip lines, which is in line with the investigated results in Table 7.2. Figure 10a and 10d demonstrate that the total runoff predicted from the calibrated parameters matched well with the observed values, with large R^2 values (0.981 for plot 1 and 0.980 for plot 2). Therefore, these calibrated parameter values are expected to lead to the highest simulation accuracies.

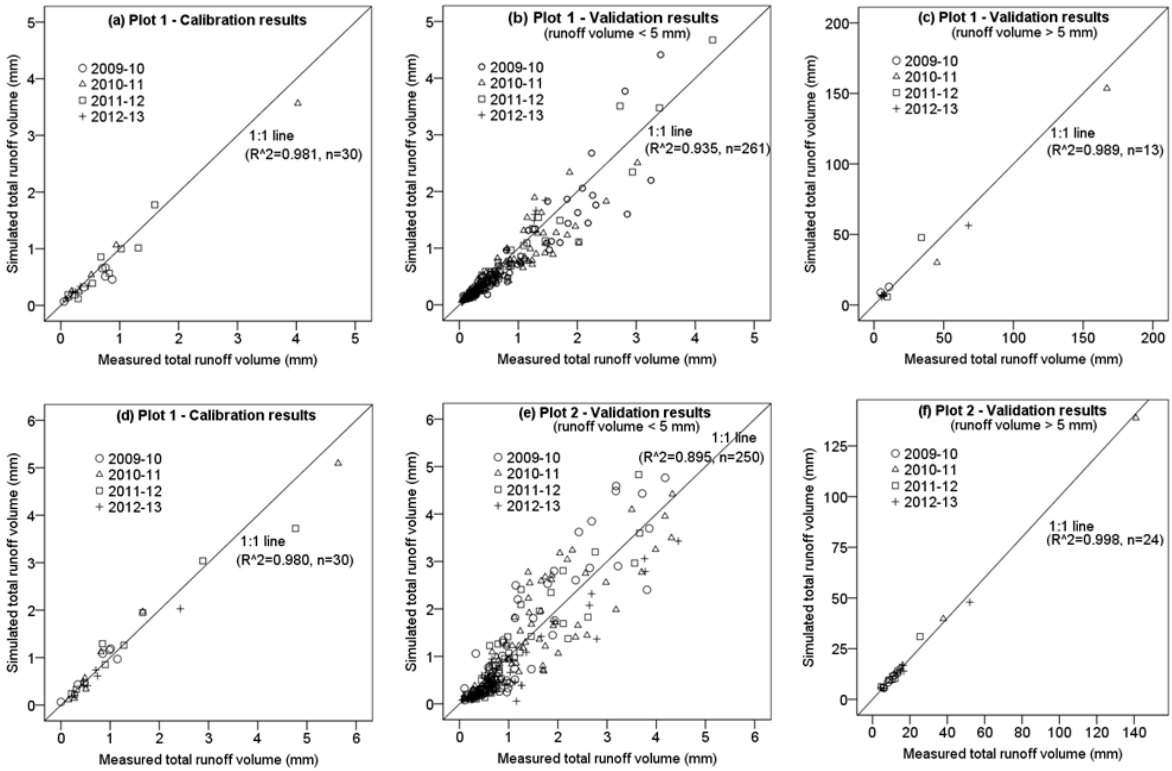

Figure 7.10 Scatter plots showing the simulated total runoff volumes against the observed values for calibration events (a) and validation events with runoff volumes less than 5 mm (b) and larger than 5 mm (c).

7.3.5 Runoff simulation using RunCA

7.3.5.1 Event runoff volume

On the basis of the calibrated input parameter values from the 30 calibration rainfall events and the measured antecedent soil moistures (ranging from 0.068 m^3 m^{-3} to 0.269 m^3 m^{-3}) by the TDRs, RunCA was performed to simulate the surface runoff for the remaining 273 rainfall events for the validation purpose. Figure 7.10 shows the scatter plots of the predicted total runoff volumes against the observed values for all the validation events. Due to the large range in the total runoff volumes, the results were displayed in two separated figures (Figure 7.10b and 7.10c for plot 1, Figure 7.10e and 7.10f for plot 2) for a better demonstration. It can be seen that the scatter plots all had high R^2 values which were above 0.895, indicating no obvious differences between years or between the calibration and validation events Statistical analysis showed that the mean percentage error in total runoff volume (*PE-TR*) of all validation events was only -5.24% for plot 1 and -8.18% for plot 2. No significant correlation (P<0.5) was found between *PE-TR* and any of the event features, such as rainfall duration, rainfall intensity, total rainfall, runoff coefficient or total runoff volume. These results indicate that the model was able

to predict the event-based runoff volume produced on these runoff plots with satisfactory accuracies for different rainfall conditions.

7.3.5.2 Event-based runoff curves

Apart from the total runoff volume, RunCA also describes the temporally changing runoff rates. Figure 7.11 shows some examples of the simulated runoff curves during the events with different rainfall conditions. Figure 7.11a demonstrates a rainfall event with relatively short duration and low rainfall intensity, where in general the simulated runoff curves agreed well with the observed runoff rates on both plots, with only minor differences during the recession limbs of the runoff curves. The rainfall event shown in Figure 7.11b also had a short duration but a higher mean rainfall intensity. As reflected in the large *EF* values and small *RMSE* values, the modelled runoff curves were able to capture the changes of the measured runoff rates on both plots, although the predicted values seemed to be more sensitive to the change of rainfall rates than the observed values. Figure 7.11c describes the results for a relatively long rainfall event which was featured by intermittent rainfall with low mean intensity. It can be seen that the runoff behaviours in the two plots were reasonably described by the model in the two major rain pulses and also in the major rain hiatus. The rainfall event displayed in Figure 7.11d had a similar duration with that in Figure 7.11c, but characterized by continuous rainfall with a larger mean intensity. The maximum rainfall rate reached values as high as 384 mm h^{-1} in this event, and this significant rainfall resulted in much larger runoff rates than those in most other rainfall events. While the peak discharge rates were slightly underestimated by the model in both plots, the simulated runoff curve was able to follow the overall trend of the observed results, especially during the runoff rising and falling (recession) phases. Comparison of simulated runoff curve with the measured runoff rates was conducted for all the validation rainfall events. The statistical analysis showed large mean *EF* values (0.693 ± 0.129 for plot 1 and 0.683 ± 0.140 for plot 2) and small mean *RMSE* values (0.548 ± 0.272 mm h^{-1} for plot 1 and 0.575 ± 0.378 for plot 2) of all these events. Consequently, all the results have demonstrated the capacity of RunCA in simulating the temporally varied runoff rates in both plots under various rainfall conditions.

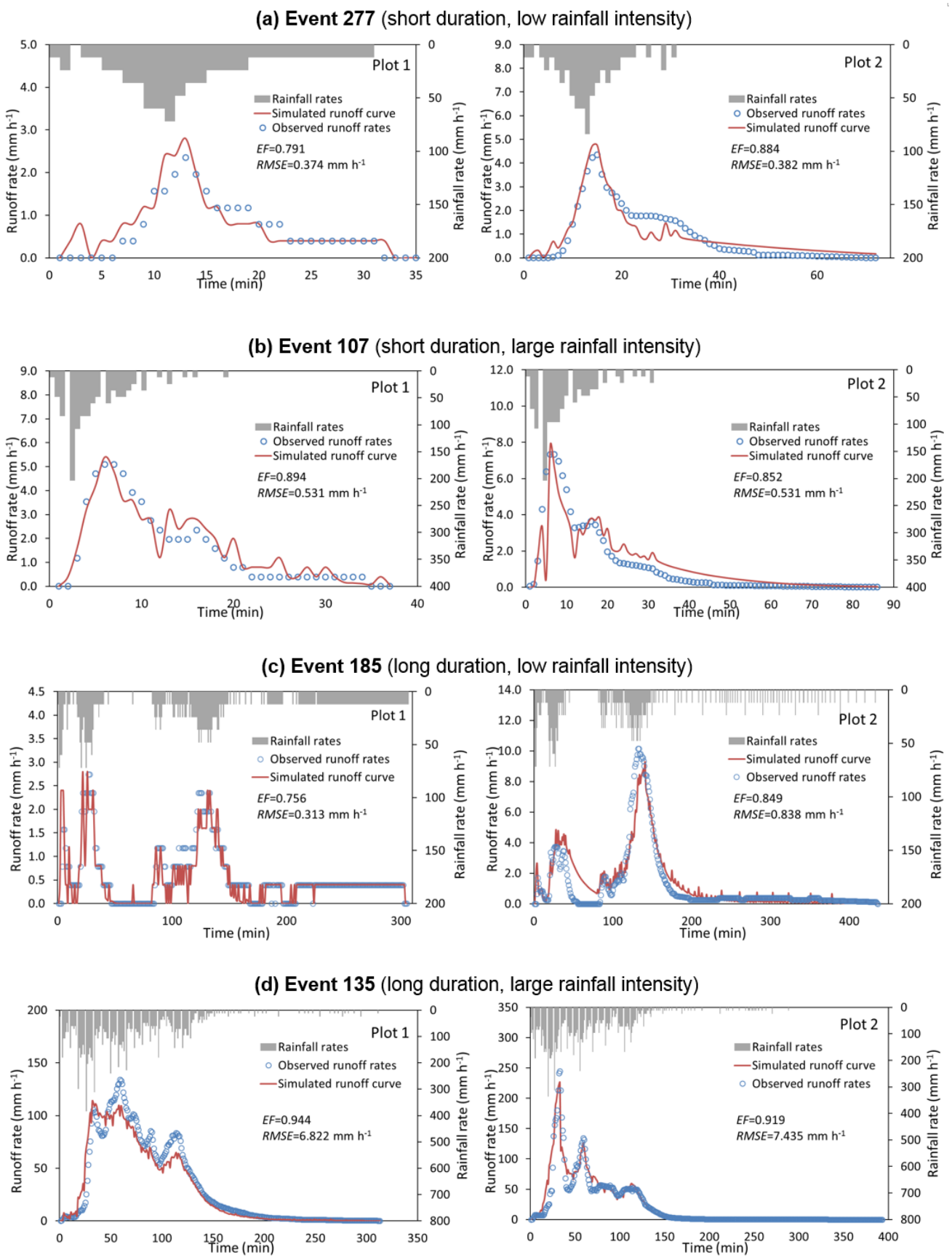

Figure 7.11 Simulated runoff curves and observed runoff rates for representative validation rainfall events with different durations and rainfall intensities.

7.3.5.3 Flow maps at different time steps

In addition to the runoff curves, RunCA also creates flow maps at different time steps to demonstrate the spatial distribution of runoff behaviours. Figure 7.12 illustrates an example of rainfall event 277, where it can be seen that runoff was produced in an expanding area with a growing water depth as the rainfall proceeded. The majority of overland flow was accumulated in the rip lines which served as the temporal water storages, and the stored water flow disappeared gradually through infiltration with diminishing rainfall. In this case where the rainfall amount was small (11 mm), the depth of the trapped water in the furrows was smaller than the height of the mounds. Therefore, the flow paths to the outlet at the bottom left corner of the flow maps were discontinued by the rip lines, and only the small non-ripped area at the bottom part of the plot became the major contributing area for runoff. This resulted in very low runoff rates ((< 3.2 mm h^{-1} for plot 1 and < 3.7 mm h^{-1} for plot 2) at the outlet. However, when a much more significant amount of rainfall was applied, as in the example of rainfall event 135 (189.4 mm) demonstrated in Figure 7.13, the water accumulated in the furrows would grow deep enough to exceed the maximum storage capacity of these furrows and thus render the overtopping. As a result, not only the rip lines but also most of the non-ripped areas were inundated by the water flow, as shown in the flow map at the time of 35 min in Figure 7.13. This led to the formation of continuous runoff paths to the outlet and thus the significant runoff rates which were as high as 118.4 mm h^{-1} for plot 1 and 137.3 mm h^{-1} for plot 2. These results indicated that while the rip lines were effective in capturing water and reducing runoff during most of the rainfall events, their effects would become insufficient when overtopping happened in some extremely large rainfall events. Meanwhile, the accurate responses of the flow distributions to the rainfall conditions, as well as the good agreement of the flow maps to the observed situations (Figure 7.4b), both reflect the capacity of RunCA in describing the spatial distribution of runoff on this landform which has great topographic complexity.

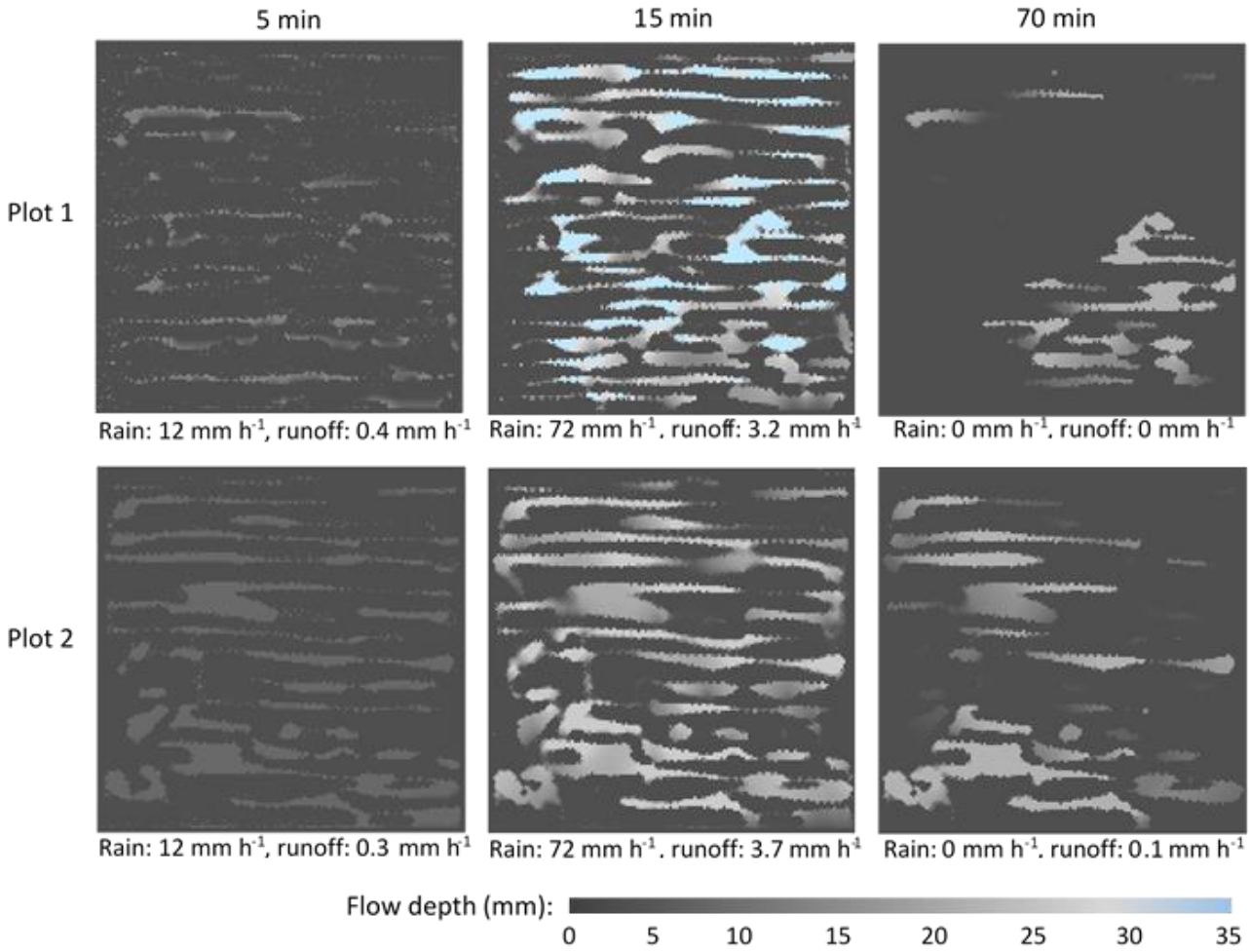

Figure 7.12 Simulated flow distribution maps at different time steps for event 277 with small rainfall amount.

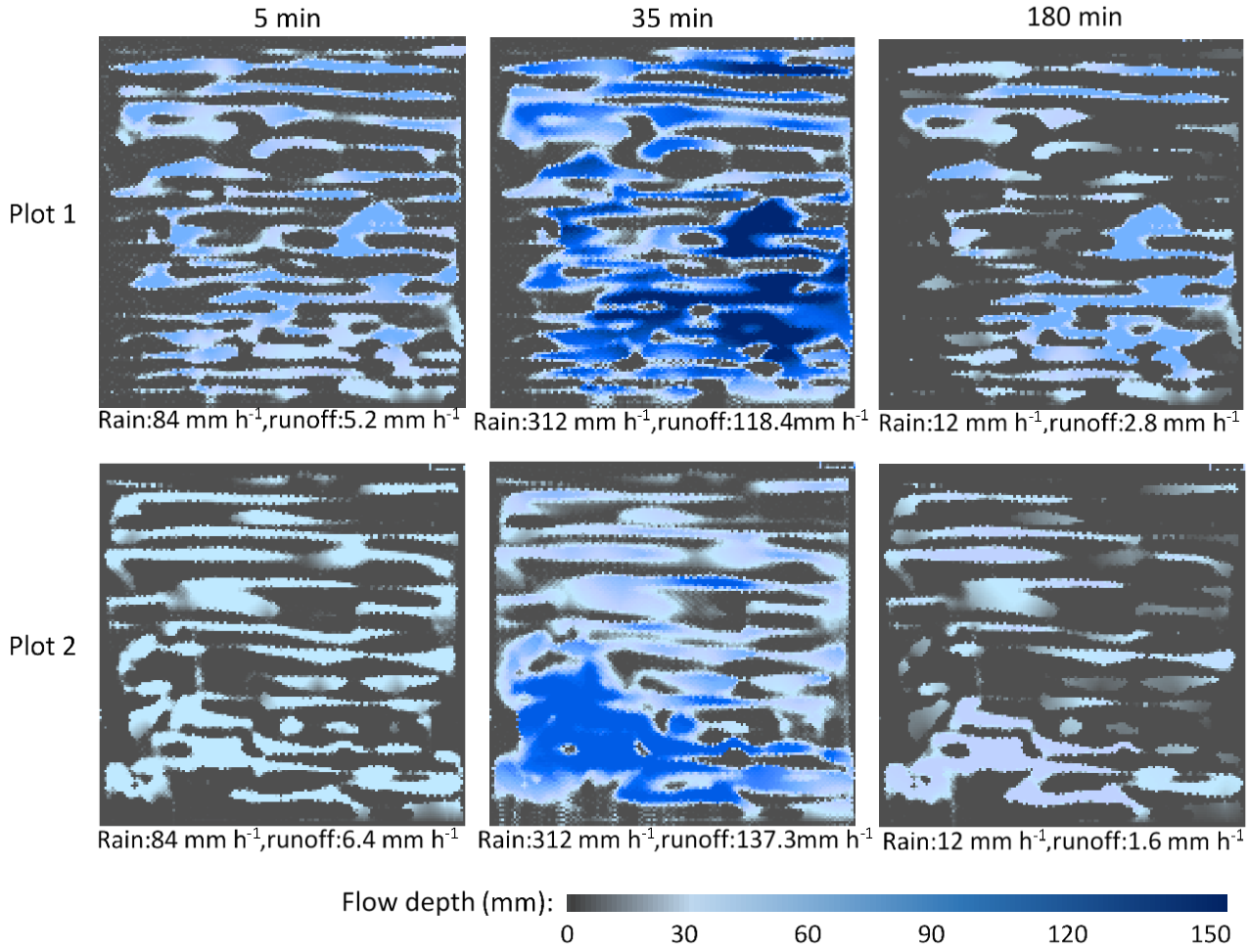

Figure 7.13 Simulated flow distribution maps at different time steps for event 135 with large rainfall amount.

7.3.5.4 Long-term runoff simulation

Abovementioned results have demonstrated the efficacy of RunCA in simulating event-based runoff. A continuous runoff simulation for the entire four water years was also conducted to predict the long-term runoff behaviour on this landform and to evaluate the model performance for long-term simulations. The simulation results are displayed in Figure 7.14, which shows that the simulated cumulative runoff curve well followed the overall trend of the measured cumulative runoff curve, where the runoff volume increased mainly in the wet seasons and tended to stabilise at certain levels in the dry seasons. While moderate increments were observed for most of the time, three major rainfall events, with each occurring in the water year 2010-11, 2011-12 and 2012-13, respectively, contributed to the majority of the increase in the cumulative runoff. Simulation errors were mainly produced in these large rainfall events, leading to an overall underestimation of 43.3 mm and 42.6 mm at the end

of simulation for plot 1 and plot 2, respectively. Nevertheless, compared to the overall large cumulative runoff volumes (600 mm for plot 1 and 800 mm for plot 2), these simulation errors were insignificant and the ability of RunCA in simulating multi-year runoff behaviours was well demonstrated.

Despite of the minor underestimation by RunCA, the accuracy of the simulated results was improved when compared to the results published by Saynor et al. (2012a), where the predicted cumulative runoff volume by CAESAR model for plot 1 was 3.5 times higher than the measured result. CAESAR is a landform evolution model primarily developed for the simulations at large spatial and temporal scales, and recently it has been downscaled to predict the runoff and erosion at this trial landform (Coulthard et al., 2012; Lowry J.B.C. et al., 2011). Its hydrologic component produces surface runoff when a lumped soil moisture storage exceeds an empirically calculated threshold value. This simplified runoff generation mechanism leads to some difficulties to account for the spatial or temporal changes in runoff production. This may be one of the causes for the significant prediction errors in the runoff volume. RunCA is based on well-established infiltration models for the description of the temporal variations (either decrease or increase) in infiltration capacity, which would contribute to the accurate prediction of runoff production. Different to CAESAR, which assumes a spatially uniform runoff velocity and thus only simulates the steady state runoff, RunCA is able to simulate the unsteady state runoff behaviours by calculating the velocity of flows from each of those spatial cells. In case of such complex landforms with great spatial variations in local topography, surface roughness and water depth, this is an advantage and improves the accuracy of prediction. However, the CAESAR-Lisflood model (Coulthard et al., 2013), an improved version of CAESAR by integrating the LISFLOOD-FP 2D hydrodynamic model, is currently used to assess the runoff and erosion behaviours on this trial landform. Since the LISFLOOD-FP 2D flow model simulates runoff by solving a reduced form of the shallow water equations using a simple numerical scheme, the new CAESAR-Lisflood model has a much more stronger physical basis than the previous CAESAR model, and is expected to be more computationally efficient and generate more accurate prediction outcomes. The performance of CAESAR-Lisflood and RunCA will to be further compared and evaluated when the simulation results of CAESAR-Lisflood for runoff plot 1 become available.

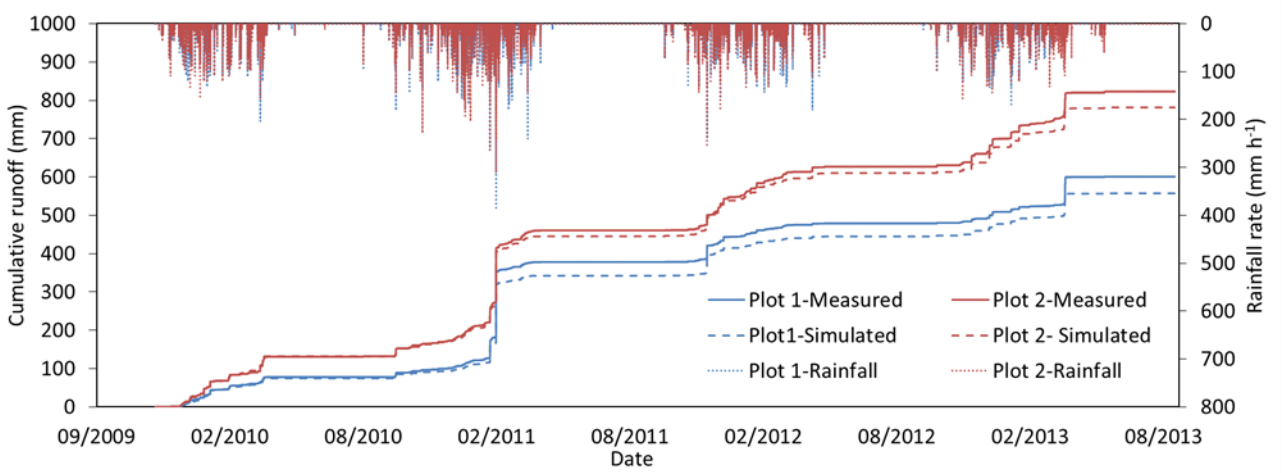

Figure 7.14 Simulated and measured cumulative runoff for runoff plot 1 and plot 2 during four water years from 2009 to 2013.

7.3.6 Landform optimization

Runoff simulation results by RunCA have shown that the runoff produced during most of the observed rainfall events in the four water years were not significant, with low runoff rates (<10 mm h^{-1}), small runoff coefficient (<10%) and thus low erosion risks. This can be attributed to the role of rip lines in capturing water flow and interrupting the runoff paths. Nevertheless, the three large rainfall events observed during this period still led to extremely high runoff rates and volumes, which reflects the insufficiency of the designed rip lines under these extreme conditions. As it is recognised that the majority of erosion typically occurs during a limited number of high-intensity events (Moliere et al., 2002), the expected high erosion rates may further lower the mounds and infill the furrows and the areas between the rip lines, which would in turn increase the runoff and erosion risks and thus cause the instability of this landform in long-term. Therefore, different landform designs were tested in this study by increasing the height of the rip lines, with the intention to reduce runoff rates during extreme rainfall events and improve the landform stability.

The mean height of the original rip lines (measured from the top of mounds to the bottom of furrows) were 15 cm for plot 1 and 10 cm for plot 2. Then their mean height was increased with a 15 cm increment at each time until the minimum runoff rates were reached. The recorded largest rainfall event in the four water years, event 135, was selected for the runoff simulations. Figure 7.15 shows the simulation results in the runoff plots with different landform designs. It can be clearly seen that for both plots the runoff rates decreased gradually with the raising rip line height. When the height increased to 90 cm at plot 1 and 85 cm at plot 2, a minimum runoff coefficient of only 7% and 15% was reached, respectively, which was a significant decrease from that of 81% and 77% on the original

landforms. This may be attributed to the reason that more water was captured and stored in the deeper furrows instead of flowing over the ground surface, leading to the decreased runoff rates. While these simulated elevated rip lines could help better control the surface runoff and thus erosion, it would not be physically or mechanically possible to achieve too high rip lines in practice, and it is also more costly to create higher rip lines due to the increased earthworks. It is therefore required to design the rip lines to a feasible height with an acceptable runoff rates during large rainfall events and also a minimised movement of materials. In this case, for example, a height from 45 cm to 60 cm would be recommended.

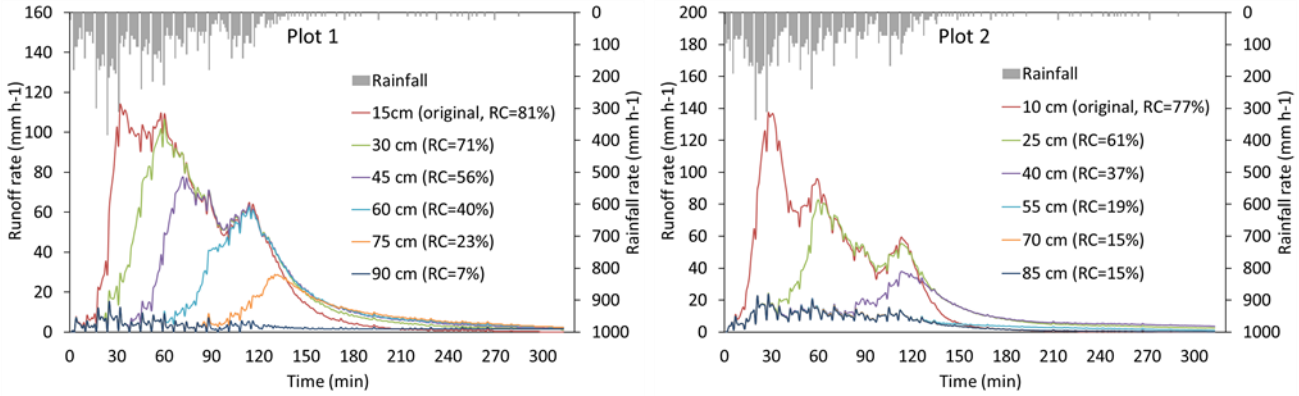

Figure 7.15 Simulated runoff curves for the runoff plots designed with different rip line heights. RC represent runoff coefficient.

7.4 Conclusions

The performance of a Cellular Automata based runoff model, RunCA, was evaluated by the simulation of surface runoff in two runoff plots built on a trial landform at Ranger Uranium Mine, northern Australia. Rainfall and runoff rates were observed continuously for these plots in four water years from 2009 to 2013. Infiltration measurements were also conducted on this landform using both large and regular ring infiltrometers to investigate the temporally and spatially varied infiltration rates, from which a range of infiltration parameter values were determined. RunCA was then parameterised by the model calibration process on the basis of the model sensitivity analysis results and the field derived parameter values. Runoff simulations for 273 observed individual rainfall events showed that RunCA was able to accurately predict the event-based total runoff volumes and well describe the temporally varied runoff rates under different rainfall conditions. The simulated water flow maps, which agreed with the observed situations, also demonstrated its ability in capturing the spatial variations in the runoff behaviours on this landform. The long-term simulation for the entire period of four water years indicated that the predicted cumulative runoff curve could well reflect the trend of the observed results,

although the model slightly underestimated the runoff volume in the largest observed rainfall event. All these results have proven the efficacy of RunCA in predicting the runoff performance on this complex rehabilitated mining landform.

This trial landform was built to assess the stability, in terms of runoff and erosion performance, of the proposed landform designs for the mine closure. The surface of the waste rock cover was ripped along the contour with the intention to reduce surface runoff, enhance infiltration and conserve water for revegetation. Field investigation indeed showed a higher infiltration capacity in the areas of these rip lines than the non-ripped areas between them, due to the disturbance to the surface. Both the monitored and simulated results demonstrated that these proposed landform designs were able to control the surface runoff to very low levels, with runoff coefficients less than 6% and 10% for 80% of the observed rainfall events on plot 1 and plot 2, respectively. This can be attributed to the roles of the furrows in capturing and storing flow water and the role of the mounds in discontinuing the runoff paths. However, when the maximum storage capacity of these furrows was exceeded during several large rainfall events, the runoff became much more significant that the runoff coefficient reached as high as 88.2% and the maximum runoff rate reached 135 mm h^{-1}. This contributed to the majority of cumulative runoff in these plots and led to high potentials for erosion and landform instability. To potentially address this issue, attempts have been made in this study to create virtual landforms by increasing the height of the rip lines. The resultant runoff was dramatically reduced with the elevating rip lines, according to the simulation results by RunCA. Therefore, it is suggested here that the current landforms may be subjected to great runoff and erosion risks under extreme rainfall events, and raising the rip line height can potentially solve this problem. RunCA can be used as a simulation tool to optimise the landform designs, however, field experiments are required to verify the predicted results.

In conclusion, the results of this study have proven the efficacy of RunCA in simulating the runoff performance on a rehabilitated landform. It therefore shows potential to be used as an effective simulation tool for various purposes, for example, the optimisation of landform designs.

Chapter 8 Application of RunCA in Mined Land Rehabilitation Designs

8.1 Introduction

Considerable effort has been made towards the rehabilitation of mined land in order to minimise serious and long-lasting environmental and social impacts. However, many rehabilitation projects have failed because of the landform instability caused by the altered surface hydrology. In order to minimise the 'footprint' of waste materials generated from the mining process, many man-made structures, such as waste rock dumps, are often built as elevated structures with steep and straight outer slopes which may result in high surface runoff rates. Due to the extensive disturbance during the rehabilitation process, the physical properties of the rehabilitated soils are dramatically altered from their natural condition, and exhibit increase in bulk density, loss of soil structure and reduction in porosity. Consequently, new rehabilitated soils have the infiltration capacities that can be an order of magnitude lower than those of surrounding undisturbed soils (Jorgensen and Gardner, 1987; Lemieux, 1987), and are considered to have high runoff potential (Ritter and Gardner, 1993). In addition, the reduced vegetation covers in rehabilitated landforms also contribute to the increase of runoff, especially at the early phases of rehabilitation. The resultant excessive surface runoff may cause intense water erosion which in turn results in exposure of encapsulated contaminants, elevated sediment delivery and subsequent degradation of downstream water quality which would have negative impacts on surrounding environment and communities (Evans, 2000). Accelerated runoff would also lead to the increased soil and nutrients loss, as well as the water deficit which may cause revegetation failure and biodiversity loss (Haigh, 1992; Kapolka and Dollhopf, 2001; Nicolau and Asensio, 2000). More seriously, elevated runoff could render catastrophic destruction of waste containment facilities, such as the collapse of waste rock dumps and breakage of tailings dams, and hence release of large amount of waste materials to the environment and pose profound threats to the safety of local residents.

Proper rehabilitation planning, including the landform designs and revegetation strategies, together with the suitable water management, could help minimize the potential harmful consequences brought by the runoff problems and thus improve the long-term landform stability. Hydrologic models are therefore required to predict and evaluate the hydrologic behaviours of different rehabilitation designs and strategies. Various models have been developed for this purpose, in which the lumped conceptual runoff models were first developed since the 1970s, typical examples being the SCS curve number (U.S. Department of Agriculture, 1972) and CREAMS (Knisel, 1980). These models usually treat

the study area as a spatially singular entity, use state variables that represent averages over the entire area, and produce outputs at a single point according to empirical relationships (Haan et al., 1982). These models are computationally very efficient in calculating runoff and have relatively few input parameters. However, they would not be applicable for rehabilitation designs as they are not able to describe the spatially or temporally varied hydrological processes in rehabilitated landforms. Besides, they may require great effort in calibration as the mined land is significantly different from the location of their first development.

To better describe the extent of spatial and temporal variability of runoff processes, some distributed physically based hydrologic models have emerged. These models are mechanistic models and usually make predictions by partitioning the target area into a series of small hydrologic elements. For example, the study area is represented by a cascade of planes and channels in KINEROS (Smith, 1981), WEPP (Laflen et al., 1991) and EUROSEM (Morgan et al., 1998b). In most distributed models, the collective behaviour of individual elements is simulated by integration of the continuity equation which treats outflow from an individual element as inflow into its adjacent elements, and the kinematic wave equation is widely used to simulate the movement of rainfall excess water. Although this has been shown to be a valid approximation for some overland flow scenarios, it is based on substantial simplifying assumptions and is rather complex to solve, leading to low computational stability and efficiency. Furthermore, most of these models were developed for catchment studies, therefore they may be inaccurate when simulating runoff at smaller scales, such as a waste rock dump or a tailings dam which are usually the basic units for rehabilitation designs.

Another group of hydrologic models are elevation-based models, which determine the runoff distribution based on the elevation differences between adjacent elements. For example, in ANSWERS (Beasley et al., 1980) the outflow from an element is directed to adjacent elements in the direction of the steepest slope. In AGNPS (Young et al., 1989) flow directions are determined from digital elevation models (DEM). These elevation-based methods are very straightforward and computationally efficient. However, a major limitation is that they do not take into account the water component in each element. In reality it is actually the relative water surface heights, rather than the land surface elevations, that determine runoff patterns. Since the flow directions derived from these models are pre-determined and fixed, the dynamic flow behaviours, such as the overtopping and backflows which are important for landform designs, cannot be captured.

Since the traditional hydrologic models all have their own limitations when applied to mined land rehabilitations, more advanced methods which can suit different spatial scales and at the same time

can simulate the spatially varied and dynamic runoff processes are required. Cellular Automata (CA), discrete dynamic systems composed of a set of cells in a regular spatial lattice, are promising approach worthy of investigation. Since the states of each cell depend only on the states of its neighbours and the global behaviour of the whole system is determined by the synchronous evolution of all the cells in discrete time steps, CA are very effective in simulating dynamic complex natural phenomena according to simple transition rules (Wolfram, 1984a). Proposed in the 1950s to investigate self-reproduction (Von Neumann, 1966), CA have been widely applied in a large number of disciplines, but were not introduced into hydrology until Murray and Paola (1994) developed the first cellular braided river model. Later it was successfully applied to other hydrological processes, such as water flow in unsaturated soil (Folino et al., 2006) and ground water modelling (Ravazzani et al., 2011). However, rare studies have been focused on the application of CA in surface runoff. Some CA based land evolution models, such as GOLEM (Tucker and Slingerland, 1994) and CAESAR (Coulthard et al., 2000), incorporate a surface hydrology component which is usually simplified. Through proper calibrations, these simplified hydrology models in the land evolution models may be sufficient for large temporal scale simulations of landform evolutions. However, they may cause large errors for short-term simulations of runoff. Furthermore, these models may be not suitable for mining industry as they were developed for larger temporal scale simulations (thousands of years) which largely exceeds the life of a mine (usually about 30 years). Consequently, in this study a CA-based runoff model (RunCA) is developed for quantitatively predicting the spatially and temporally surface runoff processes in rehabilitated landforms. The examples of its application in mined land rehabilitation planning in terms of landform designs, revegetation strategies and cover constructions are also demonstrated. In this paper only conceptual studies are conducted on virtual objects, further work needs to be carried out to verify these results in comparison to real cases.

8.2 Description of RunCA

RunCA uses a two-dimensional lattice consisting of square cells to represent the study area. The Moore-neighbourhood, which consists of eight adjacent cells is employed in this model for the local calculations. The water is only allowed to flow away from the study area at the defined outlet located at the lower boundary.

8.2.1 Cell states

The cell state is expressed as the water surface elevation of each cell, which consists of both cell elevation and water depth. The cell elevation is considered constant during a rainfall event, while the

water depth varies both temporally and spatially, and is determined by the effective rainfall which is calculated by subtracting interception and infiltration from the input rainfall.

Specifically, interception by vegetation is determined by both equation (1) developed by Aston (1979) and equation (2) developed by Von Hoyningen-Huene (1981) :

$$P_{cum} = P_{max}\left[1 - exp\left(-0.046LAI\frac{R_{cum}}{P_{max}}\right)\right] \quad (8.1)$$

$$P_{max} = 0.935 + 0.468LAI + 0.00575LAI^2 \quad (8.2)$$

where P_{cum} and R_{cum} is the cumulative interception (mm) and cumulative rainfall (mm) respectively, P_{max} is the maximum interception storage capacity (mm), and *LAI* is the leaf area index. From the cumulative interception, the interception increment at each time step is calculated by subtracting the P_{cum} at a previous time step from that at the current time step.

Infiltration controls the amount of water that will enter the unsaturated soil zone, and the amount that will flow on the ground surface as runoff, thus in many cases its prediction largely determines the accuracy of a hydrologic model. To make RunCA applicable to various rainfall conditions such as intermittent or multiple rainfall events, as well as various time scales including both short-term and long-term simulations, two improved infiltration models, the modified Horton equation (Aron, 1992; Bauer, 1974) and the modified Holtan equation (Huggins and Monke, 1966; Huggins and Monke, 1968), that both allow soil drainage and infiltration recovery are incorporated in RunCA (Table 8.1).

Table 8.1 Infiltration Equations Integrated in RunCA.

	Infiltration rate	**Soil drainage rate**
Modified Horton equation	$i_t = i_0 + d_t - kS_t$	$d_t = \frac{i_f}{i_0}kS_t$
Modified Holtan equation	$i_t = i_f + (i_0 - i_f)\left(\frac{S_t'}{\phi D}\right)^P$	$d_t = i_f\left[1 - \frac{S_t'}{(\phi - FC)D}\right]^3$

[a] i_t: infiltration capacity at time *t*, mm h^{-1}; i_0: initial infiltration rate, mm h^{-1}; d_t: soil drainage rate at time *t*, mm h^{-1}; *k*: infiltration decay factor in Horton equation, h^{-1}; S_t: cumulative soil water at time *t*, mm; i_f: final steady infiltration rate, mm/h; S_t': soil water storage potential at time *t*, mm; ϕ: total porosity, m^3 m^{-3}; *D*: control zone depth, mm; *P*: dimensionless coefficient relating decrease rate of infiltration capacity in Holtan equation.

8.2.2 Transition rules

At each time step two transition rules are applied to determine the redistribution of water amongst the spatial cells.

Transition rule A for allocating outflows to neighbours

This first transition rule regulates how the water in a central cell flows to its neighbours in a neighbourhood area, and is developed based on the cardinal-direction-priority principle, improved minimization-of-differences algorithm and the calculated flow travelling time.

Cardinal direction priority principle: The Moore-neighbourhood employed in this model allows the water in a cell to flow to eight different directions. However, the flow routing distance from the diagonal neighbours to the central cell is different from that from the cardinal neighbours (the neighbours in north, west, south and west directions), and it has been found to tend to produce wider flow pathways due to excessive flow divergence (Erskine et al., 2006). Therefore, a novel cardinal direction priority principle is proposed and used here, which means that the water in a cell has the priority to flow to its four cardinal neighbours, and it will flow to the four diagonal neighbours only when there is no cardinal neighbour to flow. This principle controls the flow dispersion and at the same time keeps the eight possible flow directions.

Improved minimization of differences algorithm: the original minimization of differences algorithm was proposed by Di Gregorio (1999), and is based on a very straightforward principle that a dynamic system tends to evolve towards equilibrium conditions by flow of some conserved quantity in the central cell to its neighbours. Specific to this runoff model, in a local neighbourhood area the water always flows from the central cell to its lower-height neighbour cells, as shown in Figure 8.1 in order to minimize the height differences among cells to reach equilibrium conditions. In RunCA an improvement of the original algorithm is that two different cases are considered, that is, whether the water amount in the central cell is sufficient (case 1 in Figure 8.1) or not (case 2 in Figure 8.1) for all the calculated flows.

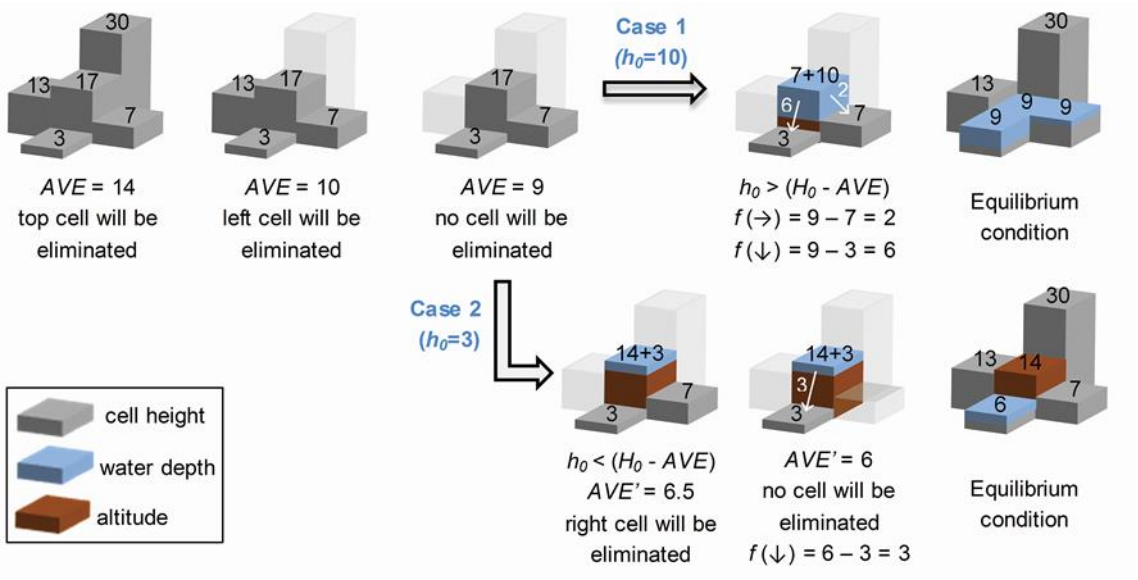

Figure 8.1 Illustration of the improved minimization-of-differences algorithm for calculating water flows from the central cell to its neighbour cells in a local neighbourhood area. *AVE* represents the average height of remaining cells; AVE' is calculated from dividing the sum of central cell water depth and total heights of remaining neighbours by the number of remaining neighbours; H_0 and h_0 represents the height and water depth of the central cell, respectively; and *f* is the outflow from the central cell.

Flow travelling time: the flow amount *f* calculated from the minimization-of-differences algorithm is based on the assumption of a constant velocity for all the flows. However, in reality the water flow velocity would be highly spatially and temporally variable due to the varied local elevation gradient, surface roughness and water depth. Therefore, the travelling time *T* for all the flows are calculated based on the Manning's equation:

$$T = \frac{D}{V} = \frac{nD}{h^{2/3} s^{1/2}} \tag{8.3}$$

where *D* is the flow travelling distance, *V* is flow velocity, *n* is Manning's roughness coefficient, *h* is water depth in the central cell, and *s* is water surface slope. Then the calculated *T* is compared to the time step used for simulation. If time step is larger than *T*, which means there is sufficient time for the flow to finish travelling, then the actual flow amount remains equal to *f*. On the contrary, if time step is smaller than *T*, which means *f* cannot finish travelling in a time step, then only part of *f* can flow and the actual flow amount is further calculated by multiplying a ratio between time step and *T*. This allows RunCA to simulate the unsteady state runoff with spatially and temporally varied flow velocities.

Transition rule B for determining total flows

At each time step transition rule A is applied to all the spatial cells, thus the outflow from each central cell to each of its neighbours can be determined. In the global view, each central cell is also one neighbour of its adjacent cells, thus it not only flows water out, but also receives water from the surrounding cells at the same time. Consequently a second transition rule is applied to calculate the total flow (the balance between outflow and inflows) for each cell. The calculated total flow could be positive if the sum of inflows is larger than the total outflow, or reversely negative. Then the new water depth and cell height are updated by adding this total flow to the current water depth for the calculation of the next time step. This allows the simultaneous update of the states of all the cells.

Based on all the components discussed above, RunCA has been implemented in C++. Then the developed RunCA model was applied to several aspects of mined land rehabilitation design, as discussed in the following sections.

8.3 Application of RunCA in mined land rehabilitation designs

The examples included in this study for applying RunCA were landform designs for both hill-slopes and tailings dams, revegetation strategies and cover designs. These case studies were selected because they are of major interest when planning landforms for mine closure. They are also subjected to the risks caused by surface runoff and may have severe environmental consequences if not well managed.

8.3.1 Hill-slope designs

Hill-slopes are major surface runoff contribution areas in rehabilitated landforms and are most unstable due to their relatively large steepness. Many harmful environmental consequences, such as water erosion, landslide, discharge of pollutants and revegetation failure, are most likely to happen here. Therefore, proper hill-slope designs that include both grading and shaping are essential for guaranteeing the long-term landform stability.

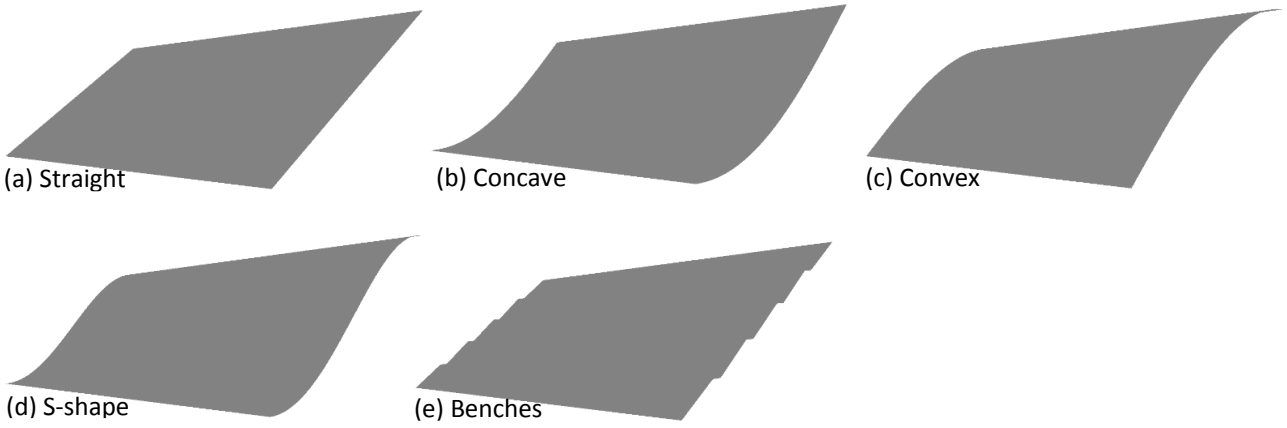

Figure 8.2 Different shapes of batter slopes.

In this study, four different slope shapes, including straight, concave, convex and S-shape profile, were created for a batter slope on a waste rock dump with a height of 40 m, a slope length of 200m, a width of 500 m and a gradient of 20% (Figure 8.2a-d). In addition, four 10 m wide benches were cut into the straight batter slope at a 2% gradient and a spacing of 40 m (Figure 8.2e). Then a 60 min rainfall event with a constant 30 mm h^{-1} rainfall intensity was applied to each of these batter slopes to simulate the surface runoff using RunCA. The resulted hydrographs (Figure 8.3a) showed that both the concave and S-shape slopes could reduce the runoff rates and increase the runoff duration when compared to the straight slope, while the convex slope did not have such effect. This can be explained by the fact that the runoff velocity may decrease downslope as the gradient decreases on a concave or S-shape hill-slope. The decreased flow velocity could reduce the risk for water erosion and thus increase the slope stability, as found by some previous studies showing that convex or linear slopes tended to have higher rates of erosion than concave slopes (Hancock, 2004; Toy and Chuse, 2005; Willard, 2010), and the concave and S-shape profiles were more stable than the convex and straight profile (Nicolau, 2003; Toy and Black, 2000). Furthermore, the reduced runoff velocity and increased runoff duration also allowed longer time for runoff to infiltrate into soil, which on one hand reduces the runoff rate, and on the other hand increases the water supply for plants. Despite of the advantages of concave and S-shape profiles, they are considerably more difficult and costly to construct than straight slopes because of the greater manoeuvring problems of earth-moving machinery (Hancock et al., 2003; Toy and Black, 2000). Placing benches is another popular option when reconstructing batter slopes. Simulation results in this study indicated that these benches could reduce the runoff rates as well as the runoff coefficient, probably attributed to their role in capturing and trapping runoff and thus reducing flow velocity and volume moving downslope. However, Gyasi-Agyei and Willgoose (1996)

pointed out that the potential risk of failure for these benches over the long term may channel water in concentrated flow paths and lead to severe gullying.

Five slope gradients were also evaluated for both concave and straight batter slopes, with results shown in Figure 8.3b and 8.3c. A gentlest hydrograph was produced on the flattest concave slope (10%), featured with the lowest peak runoff rate and the longest runoff duration. Runoff rates increased with the gradually increased slope gradient to 40%, while no obvious change was observed when further increasing gradient to 80%. Similar trends were found for the straight slopes, however, the responses were less significant. This can be explained by the reduced flow velocity on flatter slopes, which would increase the time for water to infiltrate and thus increase the infiltration rate (Haggard et al., 2005; Huat et al., 2006), and would also reduce the erosion rate and thus increase the slope stability (Silburn et al., 1991; Silburn et al., 1990; Toy and Chuse, 2005). Nevertheless, the reduced slope gradient could result in the undesired expanded waste pile footprints. Therefore, in practice it is required to reconstruct the batter slopes to a most suitable gradient with an acceptable stability and also a minimized occupied area. RunCA provided such a simulation tool for the slope designs.

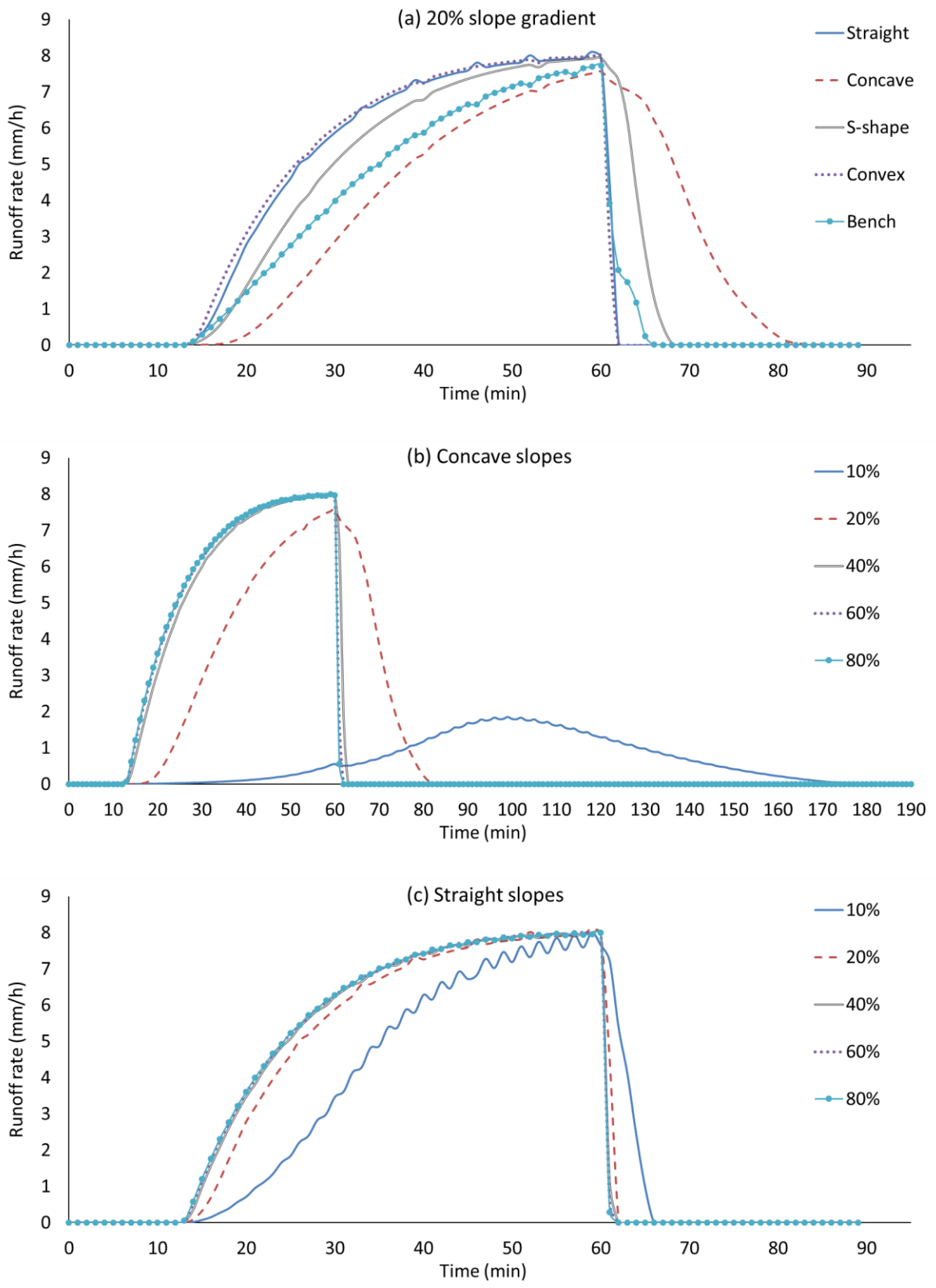

Figure 8.3 Hydrographs of (a) 20% gradient slopes with different shapes; (b) concave slopes with different gradients and (c) straight slopes with different gradients.

8.3.2 Tailings dam landform designs

Tailings dam is another common and important containment structure in the mine site that occupies a large area and contains contaminants such as metals (Carlsson and Bücchel, 2005) and radioactive materials (Bollhöfer et al., 2008; Lottermoser and Ashley, 2006). The surface cover is usually built in the rehabilitation process on the tailings dam to isolate the contaminants and prevent the degradation of downstream water quality. The stability of this facility, however, is threatened by heavy rainfall and the resultant high runoff rates, which may lead to serious issues, such as the exposure of encapsulated contaminants and the failure of tailings dams caused by landslide or collapse. Therefore, a suitable landform design and water management strategy is essential to prevent these detrimental consequences.

In this study a virtual 400 m × 400 m rehabilitated tailings dam (Figure 8.4a) was created at a gradient of 2% for evaluating the effectiveness of different landform designs. Embankments were built along the edges to prevent water flowing out of the tailings dam. An 8 m wide outlet was placed at the lowest corner to drain the runoff away. Then RunCA was performed on this tailings dam to simulate surface runoff during a 30 min storm with a constant intensity of 60 mm h^{-1}. The simulated flow map at the 30 min (Figure 8.4I) showed that large volume of flow water was accumulated and flowing along the two lower sides, which may increase the risk of dam failure, such as overtopping and the breakage of embankments which would release a significant quantity of waste (could be thousands of tons) to the natural environment. These concentrated flow pathways also resulted in a hydrograph with a high peak discharge rate (Figure 8.5), which requires a wide and deep drainage structure at the outlet and thus increase the construction costs. To potentially overcome these problems, different numbers of mounds were created on the flat dam surface. These mounds were 5 m high and their sizes and distribution were shown in Figure 8.4b and 8.4c. As expected, flow maps from these landforms showed that the existence of mounds could help reduce the surface water level along the embankments by trapping a portion of runoff (Figure 8.4II and 8.4III). The delay of flow to reach the outlet by these mounds also reduced the peak discharge rates and increased the runoff duration (Figure 8.5). The two landform designs with different numbers and sizes of mounds, however, did not show obvious differences in the flow maps or hydrographs, probably because they had the same total covering area (0.04 km^2) in this study.

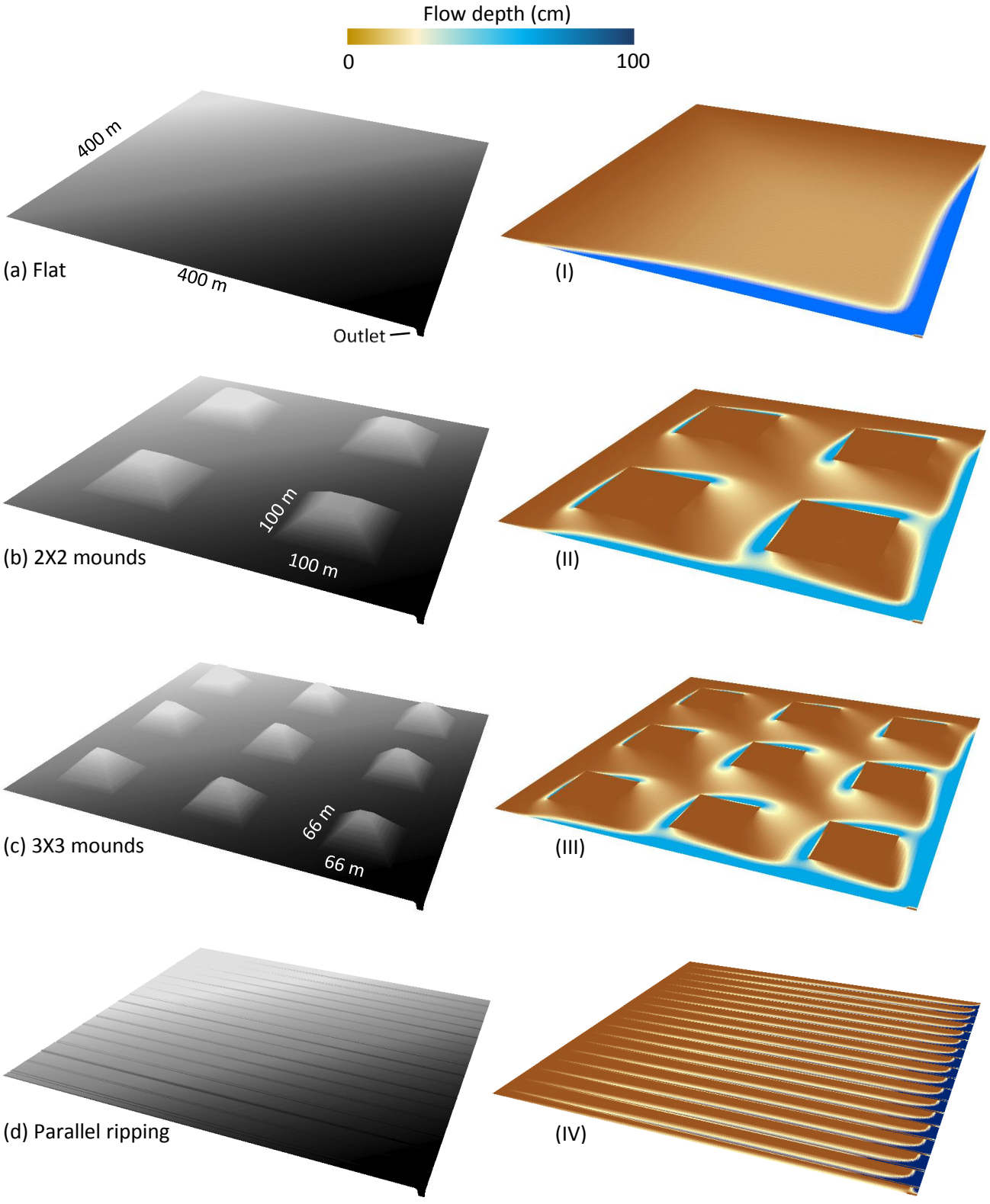
Flow depth (cm)
0
100
400 m
400 m
Outlet
(a) Flat
(I)
100 m
100 m
(b) 2X2 mounds
(II)
66 m
66 m
(c) 3X3 mounds
(III)
(d) Parallel ripping
(IV)

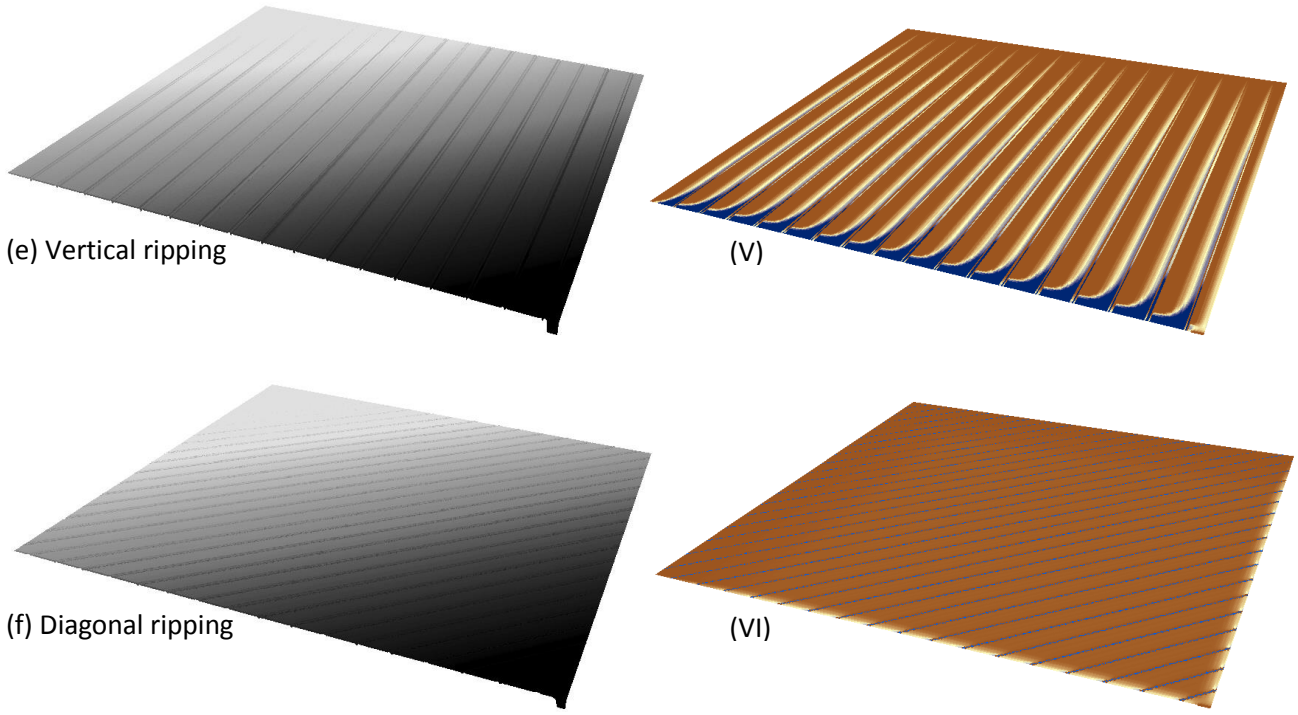

Figure 8.4 Tailings dams with different landform designs (a-f) and their simulated flow maps (I-VI) at 30 min.

Another type of landforms evaluated in this study were the ripped surfaces. Rip lines (profile shown in Figure 8.6) were created on the tailings dam surface at a spacing of 20 m. Three landforms with different rip lines distributions, namely parallel, vertical and diagonal directions as shown in Figure 8.4d-f, were included in the runoff simulations. The former two landforms generated similar flow maps, featured by runoff flowing along the rip lines and accumulated at the lower ends (Figure 8.4IV and 4V). The rip lines could catch and store a portion of runoff, thus resulting in gentle hydrographs with low runoff rates and long runoff durations (Figure 8.5). However, the large volume of water accumulated at the lower end would exert large pressures to the embankment at that side. This issue did not exist in the landform with rip lines at the diagonal direction. Since all these rip lines were parallel to the slope descending direction, the trapped water would not flow along the rip lines to either end, or flow out until the rips were filled up (Figure 8.4VI). The hydrograph produced from this landform displayed extremely low runoff rates, which on one hand would be benefit for reducing the erosion risk, but on the other hand would also lead to excessive water infiltrated downwards into the waste materials, thus increasing the risk for seepage and associated acid drainage issues.

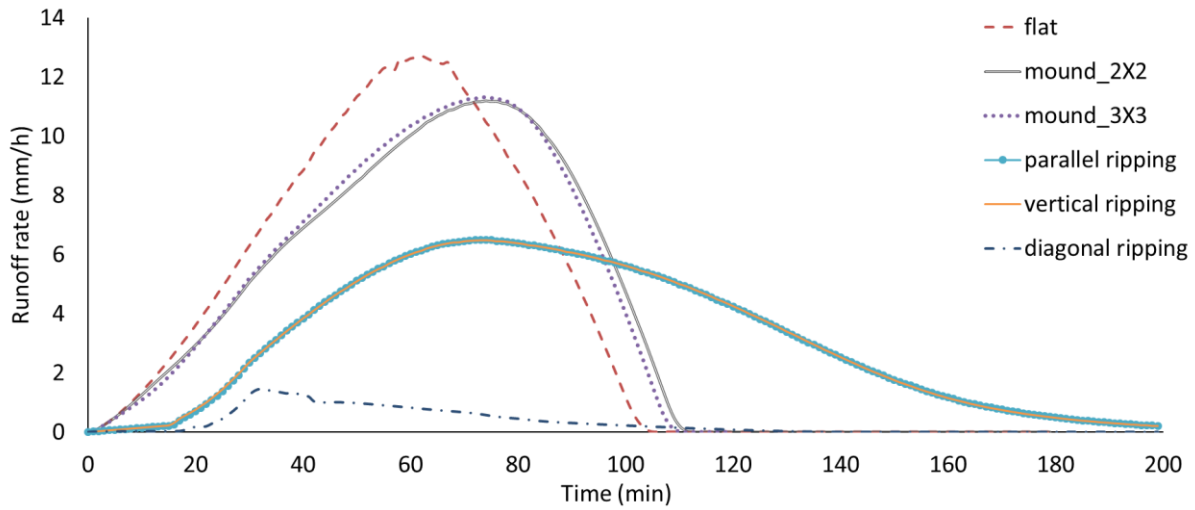

Figure 8.5 Hydrographs of tailings dams with different landform designs. The curves of parallel ripping and vertical ripping are overlapped due to their similar runoff behaviours.

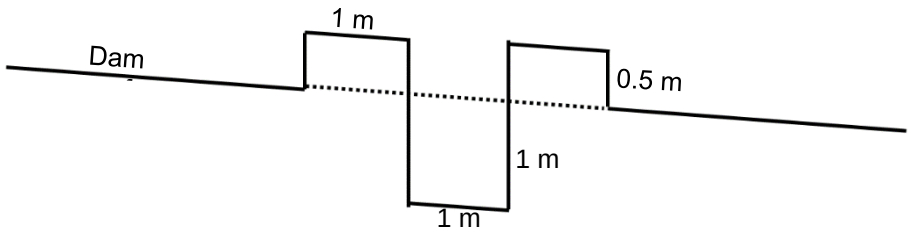

Figure 8.6 Profile of ripping lines on the tailings dam.

By comparing runoff simulation results from different tailings dam landform designs, the mounds, which can reduce runoff rates without trapping much water on the surface, are recommended to be used in humid regions where the principal objective is runoff control to minimize erosion and dam failure risks. The rip lines parallel to the slope descending direction, which can reduce runoff rates and at the same time accumulate large volume of runoff in them, are recommended to be used in arid and semiarid regions where the main purpose is water conservation to increase water supply for vegetation.

8.3.3 Revegetation strategies

In addition to the topography of landforms, vegetation has also been found to have influences on surface runoff by intercepting and storing rainfall (Owens et al., 2006), improving soil structure and thus infiltration (Puigdef ábregas, 2005), and increasing surface roughness and thus reducing the flow

velocity (Dunne and Dietrich, 1980). However, how revegetation designs, such as the vegetation coverage and distributions, would affect the runoff processes in rehabilitated landforms have been rarely studied.

Table 8.2 Modified Holtan infiltration equation parameter values for both bare areas and vegetation covered areas [a]

	i_f (mm h^{-1})	i_0 (mm h^{-1})	P	ϕ (%)	θ_0 (%)	FC (%)	Manning's n	D (mm)
Bare	20	60	4	40	5	20	0.05	80
Vegetated	60	100	4	50	5	25	0.1	100

[a] All the symbols representing infiltration parameters are the same as those in Table 8.1.

In this study a 200 m long, 500 m wide, 40 m high and 20% steep virtual batter slope was created for revegetation. Plants were designed on the slope in rows or columns, with their total coverage ranged from 0% to 80% (Figure 8.7). Rainfall events with a constant intensity of 40 mm h^{-1} and a duration of 60 min were applied for runoff simulation on these slopes. A larger set of infiltration, interception and Manning's roughness parameter values was applied to the 'vegetated' cells according to the previous findings (Table 8.2). Not surprisingly, simulation results showed that runoff coefficient decreased gradually with the increasing vegetation covers for both the vegetation planted in rows and columns (Figure 8.7). This confirms the role of vegetation in controlling the surface runoff. A further finding was that under the same vegetation coverage, runoff coefficient was smaller when plants were in rows than in columns, suggesting that the distribution of vegetation would also impact the runoff process.

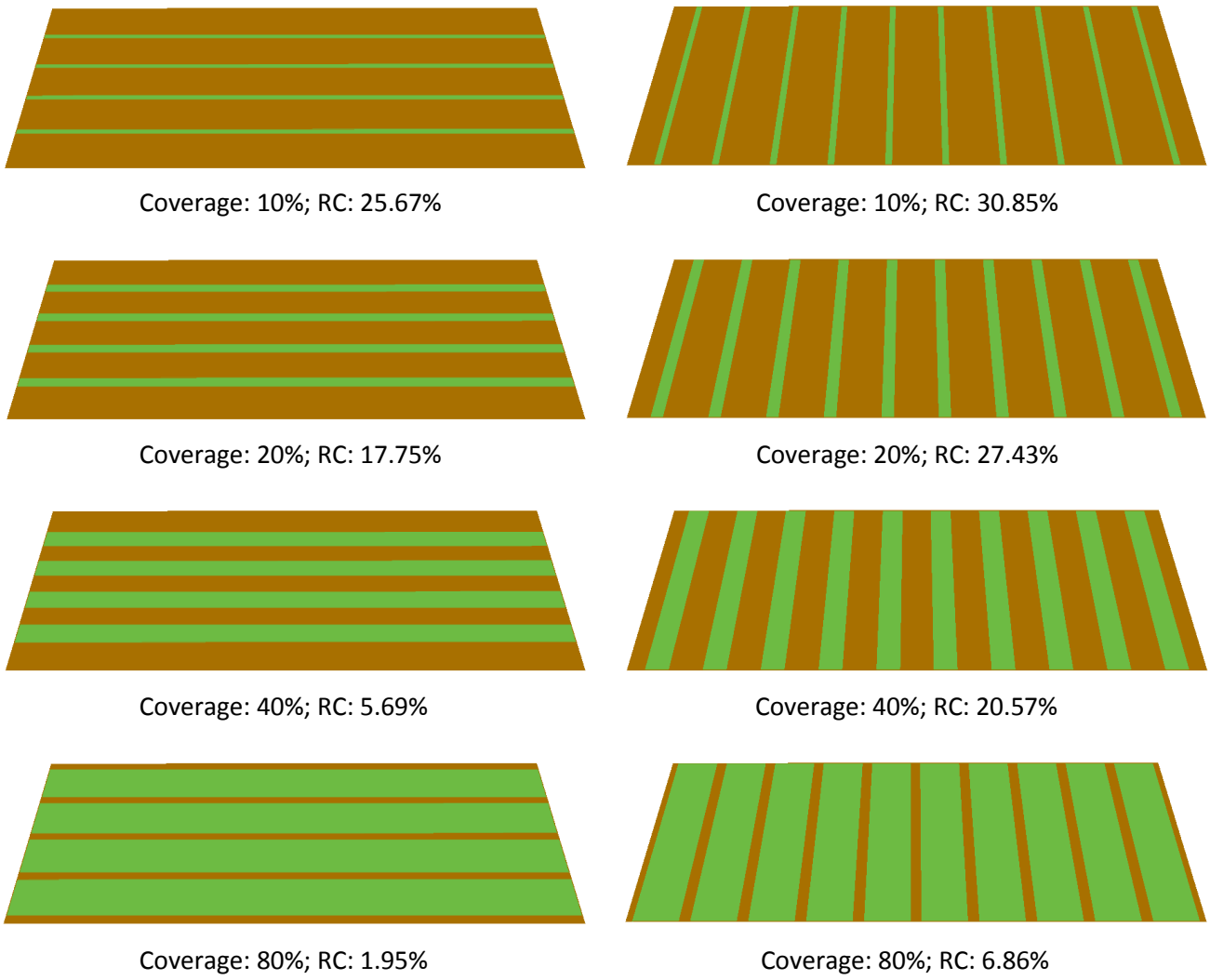

Figure 8.7 Batter slopes with different vegetation covers and their runoff coefficients (RC).

Therefore, more revegetation designs with different plants distributions were further assessed. As shown in Figure 8.8, all the slopes have the same 40% vegetation coverage but different distribution patterns in rows, columns or patches. Comparison between different vegetation positions (Figure 8.8a-c) indicated that the slope with vegetation distributed on the lower position had the smallest runoff coefficient. This may be explained by the positioning of the lower vegetation, which produces larger volume of runoff at the upslope bare area than what can infiltrate into the vegetated area or can be retained by the plants. Different numbers of vegetation rows were also compared, and the results showed less runoff was produced when increasing the number of rows from 1 to 8. This can be attributed to the fact that each row of vegetation could increase the slope surface roughness and performed as a 'decelerator' to reduce the flow velocity. Therefore, the increased number of vegetation rows would allow more time for the flow water infiltrating into soil and reduce the runoff volume. The

reduced flow velocity could also help reduce the erosion rate. The change of the number of vegetation columns, however, did not have any impact on the runoff results as most runoff was produced and flowing downslope on the bare area between vegetation columns. Different numbers of vegetation patches were also investigated. The increased patches had limited effect in reducing the runoff coefficient, and they tended to generate less runoff than the vegetation columns but more than the rows. Besides, it should be noted that the vegetation columns or patches could lead to concentrated flows between vegetated areas and thus increase the risk for soil erosion and slope instability.

(a) 1 row on upper slope; RC: 20.90%

(b) 1 row on lower slope; RC: 3.28%

(c) 1 row on middle slope; RC: 10.71%

(d) 1 column; RC: 20.57%

(e) 2 rows; RC: 7.35%

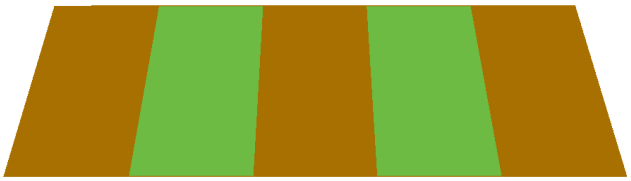

(f) 2 columns; RC: 20.57%

(g) 4 rows; RC: 5.07%

(h) 4 columns; RC: 20.57%

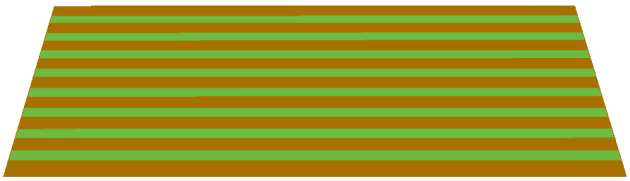

(i) 8 rows; RC: 4.70%

(j) 8 columns; RC: 20.57%

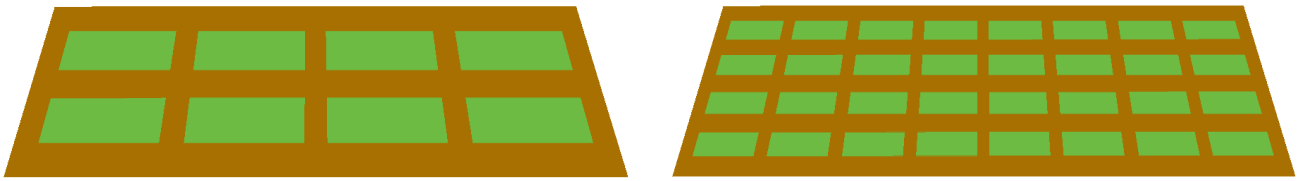

(k) 2X4 patches; RC: 11.89% (l) 4X8 patches; RC: 10.13%

Figure 8.8 Batter slopes with a vegetation coverage of 40%, but different vegetation distributions and their according runoff coefficients (RC).

Above results suggest that the increased vegetation cover can help control the surface runoff on the batter slopes. Large number of vegetation strips perpendicular to the slope descending direction are recommended as they are most effective in reducing the runoff coefficient, and are also expected to reduce the erosion rates by slowing down the runoff and preventing concentrated flows.

8.3.4 Cover constructions

In the rehabilitation process, surface covers are usually built on tailings dams or waste rock dumps to work as a physical barrier (Gatzweiler et al., 2001; Leoni et al., 2004; O'Kane and Wels, 2003), with the aim to isolate the contaminants, prevent the degradation of downstream water quality and provide the substrate for plant growth. The performance of covers would vary significantly according to their properties such as the component materials and thicknesses, and poor designs may cause the unbalanced hydrologic behaviours and thus the failure of a cover system. For example, elevated runoff and erosion rates could lead to the exposure of encapsulated contaminants or the failure of revegetation, while the excessive infiltrated water would result in contaminated seepage and acid drainage issues. Since RunCA simulates various hydrologic processes including surface runoff, infiltration process and soil drainage, it can be potentially used to access the hydrologic performance of different cover designs.

Table 8.3 Modified Holtan infiltration equation parameter values for different cover materials [a]

	i_f (mm h^{-1})	i_0 (mm h^{-1})	P	ϕ (%)	θ_0 (%)	FC (%)	Manning's n	D (mm)
Waste rock	40	70	2	30	5	15	0.1	
Soil	20	60	4	40	5	20	0.05	0.125 - 14
Spoil	10	30	8	30	5	15	0.025	

[a] All the symbols representing infiltration parameters are the same as those in Table 8.1.

In the study presented here, three types of covers constructed with waste rocks, soils and spoils, respectively, were built on a 200 m long, 500 m wide, 40 m high and 20% steep virtual batter slope. Nine different thicknesses varied from 0.125 m to 14 m were also evaluated for each type of cover. The Modified Holtan equation infiltration parameters (Table 8.1) for different materials, with their values empirically assumed to represent the infiltration characteristics of common waste rocks, soil and spoils, are shown in Table 8.3. Then a 60 min rainfall event with a constant 60 mm h^{-1} intensity was applied for runoff simulation using RunCA. The results are summarised in Figure 8.9. It can be seen that the covers constructed with waste rocks had the lowest runoff coefficient, due to their coarse texture and the resultant high infiltration capacities. On the contrary, the spoils, which consists of large amounts of fine particles, had very low infiltration capacity and produced the largest volume of runoff. With respect to runoff responses to the cover thickness, runoff coefficients of soil and spoil covers both decreased gradually with the increasing thickness. This can be attributed to the increased water storage capacity and in consequence the increased soil drainage rate according to the modified Holtan equation. However, less change in runoff coefficient can be observed after the thickness reached 2 m, indicating that the further increase of cover thickness had little effect on changing the hydrologic behaviours. The runoff coefficient of the spoil cover did not show a similar trend with the former two types, but stayed at a constant value when increasing the thickness. Reason may be that the spoil is very prone to superficial crusting (Nicolau, 2003) which may cause a large infiltration decrease rate (parameter *P*). As a result, most of rainfall (~80%) became surface runoff instead of infiltrating into cover or draining to deeper layers. Therefore, it is actually the top spoil layer, rather than the whole cover profile, that determines the hydrologic processes.

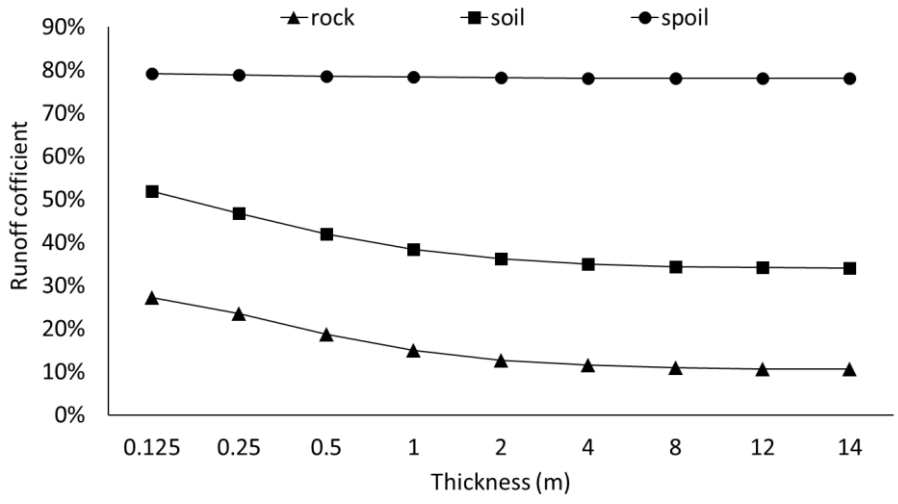

Figure 8.9 Runoff coefficients of waste rock, soil and spoil covers with different thicknesses.

In addition to the above covers with the constant thickness along the slope, we also evaluated the covers with an increasing thickness from 0.125 m at the top to 2 m at the bottom of the slope (Figure 8.10). Since this type of covers are very similar to the natural hill-slopes where the soil thickness is larger downslope because of the effect of deposition, they are expected to be more stable. Simulation results showed that the runoff coefficient for this type of waste rock cover and soil cover was 12.92% and 36.69%, respectively. These covers had an average thickness of 1.06 m, but their runoff coefficient values were smaller than those of 1 m constant thick covers (14.95% and 38.38%), and very close to those of 2 m constant thick covers (12.74% and 36.22%). This may be explained by two reasons. Firstly, the surface flow tends to accumulate downslope, and the larger infiltration capacity downslope (because of the larger depth) could allow more water to infiltrate and thus reduce runoff. Secondly, the reduced slope gradient would reduce the flow velocity and thus increase infiltration by allowing more time for flow to infiltrate. If using this type of cover instead of the cover with 2 m constant thickness, it can reduce the cost of earthworks for removing of about 93,750 m^3 of material in this study.

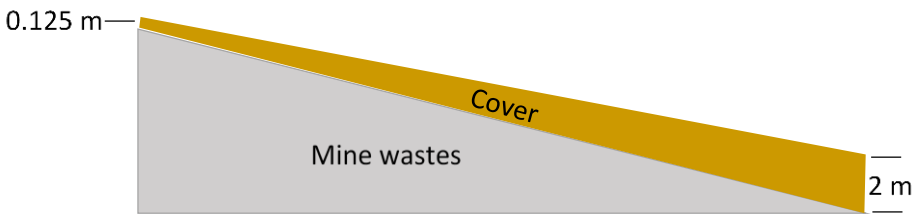

Figure 8.10 Schematic diagram of cover system with increasing thickness from top to bottom of slope.

Assessing the hydrologic performance of covers using RunCA can help select the construction materials for varied purposes under varied climate conditions. It also facilitates the decisions from a rainfall-infiltration-runoff point of view on an optimum cover thickness which on one hand controls the surface runoff and erosion rates to an acceptable level and on the other hand may reduce construction costs. Covers with increasing thickness downslope are worth further investigation as they were found to be more efficient than the traditional covers, and at the same time would be more stable and would require less earthwork.

8.4 Conclusions

RunCA is a novel hydrologic model that simulates the surface runoff by integrating cellular automata theories and basic hydrologic principles. It partitions the target area into a series of small spatial cells, and calculates the runoff production in each cell based on the balance of rainfall, interception and infiltration which is determined from various classical and modified equations. Flow distribution amongst these cells are regulated by three novel CA transition rules on the basis of the water surface elevations and the spatially varied flow velocities. The cell structure of RunCA can provide a better and easier representation of the study area than the elemental sections used in some distributed hydrologic models. The simultaneous update of states of all the cells at multiple time steps enables the model to capture the dynamic runoff behaviours. This model is also expected to be computationally more efficient than most traditional models as it does not need to solve any complex equations of continuity or momentum. Besides, instead of restricting to a certain spatial or temporal scale, RunCA can be applied in different spatial scales for both event-based and continuous simulations.

Proper rehabilitation planning is essential to minimize the harmful consequences brought by elevated runoff and the resultant landform instability, and RunCA provides a valuable simulation tool for such purpose. Several examples of rehabilitation designs, including hill-slope and tailings dam landform designs, revegetation strategies and cover constructions, were demonstrated and discussed in this paper. Some conclusions from the RunCA simulation results, such as the positive relationship between runoff and slope gradients, different runoff responses to the slope shapes, the decreased runoff coefficient with increasing vegetation cover, and the low runoff production on covers constructed with high infiltrability materials, were all in line with the previous findings. This agreement has proven the applicability and efficacy of RunCA in assessing the hydrologic performance of different rehabilitation designs. In addition to these conclusions, some new findings were also derived from the simulation results. For example, building mounds and ripping surface could both help decrease the runoff rates on tailings dams and also reduce the water pressures at the embankments. However, their functions are different and thus are recommended to be applied to specific climatic regions. Plants grown in rows were more effective than those in columns or patches in controlling runoff rates on the slopes, and the efficiency increased with the increasing number of rows. Enlarging the thickness had an effect in improving infiltration and thus reducing runoff for the waste rock and soil covers, but not for the spoil covers which were prone to the crust formation on the surface. Furthermore, the covers with an increasing thickness from top to bottom of the slope was found more effective than the covers with a constant thickness, and they had another advantage in reducing the required earthworks. All findings

match observations and can be supported by reasonable explanations. However, further investigations (for example, field experiments) are required to systematically verify the model results.

Chapter 9 Conclusions, Contributions and Recommendations

This chapter summarises the outcomes of this research and demonstrates how each of the research objectives has been addressed. The main research findings are presented and discussed in the context of how the thesis has contributed to our knowledge of critical aspects of surface hydrology. The chapter concludes with a summary of the limitations of this research and recommendations for future research.

9.1 Summary of thesis

The research problem identified in Chapter 1 stated that the stabilities of the rehabilitated landforms are often threatened by the excessive surface runoff due to the altered topography and surface hydraulic properties. The elevated runoff may be the cause for serious soil erosion, downstream contamination, revegetation failure and destruction of the waste containment facilities. It is therefore essential to minimise these environmental consequences through appropriate rehabilitation designs and water management. However, a review of literature in Chapter 2 recognised a deficiency in the understanding and estimation of the surface hydrological processes in the rehabilitated landforms. Typically, several research gaps have been identified in the affecting factors of surface hydrology, infiltration models and the determination of their parameters, as well as the methods for modelling surface runoff. To address these research problems and impediments, a research aim was proposed to "***provide supportive information to achieve long-term stability of rehabilitated landforms by improving rehabilitation designs and water management on the basis of well understood and predicted surface hydrological processes***". Four research objectives were set up to achieve this aim.

As soil infiltration is recognized as a major regulator of the surface hydrological behaviours, the first two objectives were both proposed to address the uncertainties in the determination of infiltration processes, with objective 1 being ***to identify the major controlling factors of infiltration process and quantify their relationships with infiltration parameters by small plot trials*****.** This objective was proposed as it has been a challenging and time-consuming process to determine the input parameters for infiltration models due to the difficulties in the direct measurement of their values. This has greatly limited the application of these models for the prediction of infiltration and runoff. Therefore, a hypothesis was proposed that these parameters are affected by the soil, rainfall and vegetation characteristics and can be estimated from some of these dependent and readily measurable factors. To test this hypothesis, infiltration experiments were conducted on small plots using a field rainfall simulator at a UQ experimental farm located at Pinjarra Hills, Queensland, Eastern Australia (Chapter

3). Four well-established and widely applied infiltration models, including Philip, Green-Ampt, Horton and Holtan models, were investigated in this study and they were all found to be able to well describe the infiltration processes in continuous rainfall events under different site conditions. The effects of various factors on the input parameters of these infiltration models were also investigated, and the results showed that not only the soil properties, but also the vegetation and rainfall factors, have great impacts on these infiltration parameters. Then their relationships were quantified using the principle component analysis and linear regression analysis. Predictive regression equations for each infiltration parameter were further successfully developed on the basis of a full set of identified major controlling factors, as well as a simpler factor set including only five most readily obtainable factors (i.e., rainfall intensity, vegetation cover, plant height, initial soil moisture and saturated hydraulic conductivity).

The second objective was ***to evaluate the performance of the modified infiltration models for the simulation of complex rainfall conditions***. Some classical infiltration models have been modified or improved by previous studies to extend their applications from continuous rainfall events to more complex rainfall conditions. A systematic and comparative evaluation of their performance, however, has not been investigated. Therefore, based on the hypothesis that the performance of the infiltration models can be evaluated by the infiltration experiments conducted on small scale plots using the rainfall produced by the field rainfall simulator, three modified infiltration models were investigated in the experiments conducted at a UQ experimental farm located at Pinjarra Hills, Queensland, Eastern Australia (Chapter 4). The modified Holtan model (MHL) and modified Green-Ampt model (MGA) were both found to have satisfactory performance in describing the infiltration processes during a sequence of rainfall events with varied intensities, while the modified Horton model (MHR) tended to produce significant errors by overestimating the soil drainage rates and thus the recovery of infiltration capacity during the rainfall hiatuses. Hence improvement was further incorporated into MHR by introducing a constraint in form of field capacity and a reduction coefficient to its drainage formula. The improved MHR (IMHR) greatly increased the simulation accuracy and had comparative performance with MHL and MGA. This study also showed that the accuracy of these models were not affected by soil properties, rainfall intensities or topography conditions, but tended to decrease with increased vegetation cover.

On the basis of the former two achieved objectives, a third objective was proposed ***to develop a more effective and universal surface runoff model by incorporating the evaluated infiltration models and Cellular Automata theories***. This objective was proposed because of the limitations of existing runoff models in simulation accuracy, computational efficiency and scale flexibility, and the lack of

application of Cellular Automata (CA) in surface hydrology. A hypothesis was then proposed that the production and distribution of surface runoff can be simulated by linking the surface hydrologic properties (e.g., infiltration) with the CA method. The Runoff Model Based on Cellular Automata (RunCA) was thereby developed in this study (Chapter 5), which predicts the runoff production within each of the spatial cells by incorporating the previously evaluated infiltration models and simulates the runoff distribution among these cells based upon the cardinal-direction-priority principle, the improved minimization-of-difference algorithm and the calculated spatially varied flow velocities. The developed RunCA model was further verified and validated by a systematic procedure consisting of the analytical solution under simplified conditions, the laboratory experiments at small plot scale and the field measurements at large basin scale (Chapter 6). Promising model performance, in terms of simulation accuracy and computational efficiency, was achieved in all the tests with different spatial scales.

After the development and initial testing of RunCA, a fourth objective was proposed ***to simulate the surface hydrological processes in rehabilitated landforms using the developed runoff model***. This objective was proposed as the changed surface hydrology is a major threaten to the stability of the rehabilitated landforms, and the developed RunCA model was expected to improve the rehabilitation designs by providing a simulation tool to predict and assess the runoff performance. To achieve this objective, a case study was conducted at Ranger Uranium Mine, northern Australia, to simulate the surface runoff in two 30 m $\times$30 m plots on a trial rehabilitated mining landform using RunCA (Chapter 7). The detailed model calibration procedure was demonstrated in this study, and the results from both event-based and long-term simulations proved the capacity of RunCA in precisely describing the temporal and spatial variations in the runoff behaviours on this landform. RunCA was also used to access the runoff performance on the virtual landforms with different heights of rip lines to optimise the landform designs for the closure of this mine site. In Chapter 8 the application of RunCA in more aspects of mined land rehabilitation designs, including hillslope designs, tailings dam landform designs, revegetation strategies and cover constructions, was further discussed by scenario analysis performed on virtual objects. The modelling results agreed with some previously finding, matched observations and could be supported by reasonable explanations. All these results have demonstrated the efficacy of RunCA as a simulation tool in assessing the surface hydrological behaviours in the rehabilitated landforms.

On the basis of these addressed research objectives, the understanding and prediction of the surface hydrological processes in the rehabilitated landforms were greatly improved, which provided supportive information for the optimisation of rehabilitation designs and water management to

improve the long-term stability of these landforms. Therefore, the research gaps identified from the literature review were filled and the overall aim of this research was achieved.

9.2 Contributions of this research

Systematic evaluation of the classical and modified infiltration models

The performance of four classical infiltration models, including two physically based models (Philip and Green-Ampt models) and two empirical models (Holtan and Horton model), was systematically evaluated on 1 m ×1 m field plots with different site conditions using continuous rainfall produced by a rainfall simulator (Chapter 3). The results showed that the performance of the two empirical models was slightly better than that of the two physically based model, probably due to the fact that the physically based models were initially developed from bare soil, without taking into account the surface conditions (e.g., vegetation) which would also have large influences on infiltration. Nevertheless, the simulated infiltration curves by the four models all well agreed with the observed infiltration rates, demonstrating their good efficacy in simulating the infiltration processes in this study. These models were also tested on 2 m × 1 m laboratory runoff plots by simulating the infiltration processes under different slope gradients and rainfall intensities (Chapter 6). Again satisfactory and comparative performance was achieved for all the four models.

In addition to the classical models, three modified infiltration models, including the modified Holtan model (MHL), modified Green-Ampt model (MGA) and modified Horton model (MHR), were also evaluated on 1 m ×1 m field plots under more complex rainfall conditions (Chapter 4). Results showed that both MHL and MGA had satisfactory performance during a sequence of rainfall events. MHR, however, failed in accurately describing the infiltration processes due to its overestimation of soil drainage rate. MHR was then improved by applying a constraint that soil only drains water when soil moisture exceeds field capacity and introducing a reduction coefficient which equalled to 0.2 to the formula for calculating soil drainage rate. Improved MHR was found to significantly improve the simulation accuracy of MHR, and its performance was comparative to that of MHL and MGA.

The evaluation of these infiltration models in this research have proven their good performance under different conditions and thus are recommended to be incorporated in hydrologic models to improve the outcomes for both event-based and long-term simulations.

Improved understanding of the effects of various factors on soil infiltration behaviours

While numerous previous studies have been carried out to identify the effects of different factors on soil infiltration (Dunne et al., 1991; Fox et al., 1997; Li et al., 2011; Mayor et al., 2009; Meek et al., 1992), they were mainly focused on the lumped infiltration volume or the final steady infiltration rate, rather than the temporally changed infiltration behaviours which are important for the simulation of runoff. Therefore, in this research the effects of various controlling factors, including soil properties, vegetation features and rainfall characteristics, on different infiltration parameters were investigated by the infiltration experiments conducted on small field plots. Soil related factors were found to play the most important role as they had significant influences on all the investigated infiltration parameters, however, different soil factors were associated with different parameters. Vegetation factors, including vegetation cover, plant height and root content, also greatly influenced most of the infiltration parameters through their effects in intercepting and storing rainfall, protecting the soil surface against the impact of raindrops, reducing their kinetic energy, preventing surface sealing, improving soil structure and consequently enhancing infiltration. In addition, the rainfall intensity was found to have positive impacts on soptivity and initial infiltration rate due to its roles in determining the available water amount for initial absorption and infiltration. The increased rainfall intensity also led to an increased infiltration decay factor because of the rapidly decreased infiltration rate caused by the rainfall introduced surface sealing. As these infiltration parameters reflect the infiltration characteristics at different stages, the determination of the effects of various factors on these parameters contributed to a better understanding on how these factors influence the entire infiltration processes. These identified relationships also laid a foundation for the estimation of the input parameters of infiltration models from their controlling factors.

Development of predictive equations for unmeasurable infiltration parameters

The difficulties in determining input parameters, especially the unmeasurable parameters, have greatly limited the applicability of infiltration models for the simulation of infiltration and runoff behaviours. Effort was hence made in this research to estimate these parameters from more easily available or measurable controlling factors (Chapter 3). By conducting rainfall simulation experiments on small field plots with a large range of site conditions, the predictive regression equations were developed for the unmeasurable infiltration parameters from various soil, rainfall and vegetation factors. While these equations showed high efficacies, the determination of some factors was still time-consuming and costly. Therefore, a simplified set of predictive equations were further developed from five readily obtainable factors, including saturated hydraulic conductivity, initial soil moisture, rainfall intensity, vegetation cover and plant height. Despite of a reduced factor number, these equations also had satisfactory prediction accuracies. The incorporated five factors can be quickly and directly measured

in the field without taking any samples or conducting any laboratory analysis. They have also been proven able to be potentially derived from remote sensing and GIS techniques by various studies, which makes the determination of the spatially varied parameter values much easier. Consequently, these developed predictive equations have improved the outcomes in regard to the effort, time and cost in determining these parameters, thus facilitating the application of infiltration models in the distributed hydrologic modelling at large spatial scales.

Development of an effective and universal runoff model for different spatial and temporal scales

Although a large number of runoff models have been developed over past decades, most of these traditional models are constrained to a certain spatial and/or temporal scale as the numerical methods, empirical relationships and simplifying assumptions used in these models are only correct at this specific scale. Large errors may be produced if they are applied to a scale different from that they were developed from. More effective and universal runoff models are therefore required, and such a model (RunCA) was developed in this research based on the Cellular Automata (CA) method (Chapter 5). Since CA is a dynamic system evolving by updating the states of spatial cells at discrete time steps, it has the advantage of suiting different spatial and temporal scales by adjusting the size of cells and the length of time steps. The transition rules for runoff distribution in RunCA are based on the straightforward minimisation-of-differences algorithm instead of solving the complex mathematic equations, and thus are applicable to different spatial scales. The classical and modified infiltration models incorporated in this model also allow the simulations of different temporal scales. The university of RunCA was demonstrated by its successful application to the small plot scale (Chapter 6), field scale (Chapter 7 and 8) and catchment scale (Chapter 6) for the simulations of continuous rainfall events (Chapter 6, 7 and 8), intermittent rainfall events (Chapter 6 and 7) and long-term runoff behaviours (Chapter 7). Therefore, RunCA has been proven to be a universal runoff model that can be applied at different spatial and temporal scales, for not only the rehabilitated landforms, but also any environment where the infiltration-excess runoff is dominant.

Application of Cellular Automata theory to surface hydrology

Cellular Automata (CA) has been proven to be an effective method for the simulations of dynamic and complex phenomenon as it determines the evolution of the entire system from local to global according to simple transition rules. While CA has been successfully applied to a wide range of disciplines, it has been rarely applied to surface hydrologic modelling, which is dominated by the numerical techniques and elevation based methods. These methods, however, all have their own limitations in simulation accuracy, computational efficiency and scale flexibility. A novel runoff model, RunCA,

was therefore proposed in this research by incorporating the CA theory (Chapter 5). The developed model was then validated at different scales (Chapter 6) and successfully applied to a case study (Chapter 7) and scenario analysis (Chapter 8) for runoff simulation on the rehabilitated landforms. RunCA showed better performance than ANSWERS (Beasley et al., 1980), a well well-known distributed physically based hydrologic model using numerical techniques, in predicting the hydrographs for a catchment (Chapter 6). When simulating the cumulative runoff curves for a rehabilitated mining landform (Chapter 7), RunCA also produced more accurate results than CAESAR (Coulthard et al., 2000), a CA-based landform evolution model which determines the runoff generation according to simple and empirical relationships. These results demonstrated the high efficacy of CA for the simulation of surface hydrology. Compared to the numerical techniques, the simple transition rules in the CA system are expected to reduce the complexity in computation as there is no need to solve any complex equations. These transition rules are also considered to be more realistic than the elevation based methods as the water component has been taken into account. RunCA is a large step for the application of CA to runoff modelling as it considers the spatially varied flow velocities, introduces a more realistic cardinal-direction-priority principle and incorporates the important surface hydraulic properties (e.g., infiltration) when determining the runoff production.

Providing a simulation tool for the optimisation of rehabilitation designs

Proper rehabilitation designs are essential to control the surface runoff and ensure the long-term landform stability. However, an effective simulation tool is lacked for assessing the runoff performance of designed landforms as most existing runoff models were developed for the natural environment and thus are not applicable for the rehabilitated landforms due to the different geomorphic features, spatial scales and landform complexities. In this research, a Cellular Automata based runoff model (RunCA) was developed for the runoff simulation at these rehabilitated landforms (Chapter 5). RunCA was used to evaluate the proposed landforms designs for the mine closure of Ranger Uranium Mine, northern Australia (Chapter 7). Simulation results by RunCA showed that in most rainfall events the designed rip lines on this landform could help control the surface runoff to very low levels by capturing flow water and interrupting runoff paths, however, they failed during several large rainfall events, leading very significant runoff. Improvement was then made to the original landform designs by raising the rip lines, and an optimum rip line height was achieved through the comparison of the simulated runoff behaviours by RunCA. The application of RunCA to landform designs of both hillslopes and tailings dams, revegetation strategies and cover constructions were further explored in Chapter 8. Simulation results showed that surface runoff increased with slope gradient and more runoff was produced on convex and straight slopes than on concave and S-shape slopes. Both mounds and

rip lines constructed on the tailings dam surface could help reduce the water discharge. Vegetation planted in rows were more effective than those in columns or patches in controlling runoff. Increased cover thickness had the potential in reducing runoff rates, and the covers with an increasing thickness from top to bottom of the slope tended to be more efficient than those with a constant thickness. All these results have demonstrated the efficacy of RunCA as a simulation tool in assessing the hydrologic behaviours of different rehabilitation designs.

9.3 Limitations and recommendations for future research

Validation of developed predictive equations for the infiltration parameters

Predictive regression equations were developed in this research for some unmeasurable infiltration parameters on the basis of both a full set of controlling factors and a simpler set of readily obtainable factors (Chapter 3). These equations were developed from a number of calibration rainfall events applied on the small plots at a UQ experimental farm in Pinjarra Hills, Queensland, Australia. Although these developed equations have been proven very effective for predicting these infiltration parameters in the validation rainfall events, unfortunately there was no opportunity in this thesis to test whether they would have comparative performance in the other areas where the site conditions are different from those they were developed from. Hence, the versatility of these equations are required to be tested in future studies. In addition, the influences of the estimation errors from these predictive equations on the simulation results of the distributed hydrologic models remain unclear and thus need further efforts. Furthermore, five factors (i.e., saturated hydraulic conductivity, initial soil moisture, vegetation cover, plant height and rainfall intensity) were selected in the simplified regression equations based on the consideration that they can be quickly derived from the remote sensing and GIS techniques for the large scale studies. However, one problem is that the accuracies of determining these factors in these ways have not been tested in this research, and thus further evaluations need to be conducted.

Evaluating the performance of infiltration models for the simulations of surface runoff

Four classical infiltration models and three modified infiltration models were evaluated in this research by predicting the infiltration processes on small field plots under either continuous or intermittent rainfall (Chapter 3 and 4). The purpose of evaluating these infiltration models was to provide supportive information for their incorporation in the hydrologic models to simulate surface runoff. While these models all showed satisfactory and comparable performance, no direct preference among

them could be derived from current results. Furthermore, although these model were all incorporated in a CA-based runoff model (RunCA), their influences on the runoff simulation accuracies were not tested or compared in this thesis due to the lack of input parameter information. Therefore, future research is recommended to be carried out to evaluate their performance for the runoff simulations by performing RunCA based on different infiltration models at different spatial and temporal scales.

Systematic comparison of RunCA to other hydrologic models

The limitations of existing methods for runoff modelling were analysed in this thesis (Chapter 2 and 5). To address these limitations, a new method, Cellular Automata, was used to develop a novel runoff model (RunCA) in this research (Chapter 5). The developed RunCA model is believed to have the advantages in capturing the spatial and temporal variations in the runoff behaviours when compared to the lumped conceptual models. It is also expected to have higher computational efficiency than the numerical techniques due to the simplicity of the CA transition rules. As RunCA determines runoff distribution according to the water surface elevations instead of land surface elevations, it would be more realistic than those elevation based algorithms. RunCA also tends to generate more accurate results in runoff prediction than the landform evolution models as the fundamental surface hydraulic properties are considered in this model. As expected, RunCA indeed showed better performance than ANSWERS and CAESAR in the runoff simulations for a rehabilitated catchment (Chapter 6) and a field plot on a rehabilitated landform (Chapter 7), respectively. Nevertheless, since the major objectives of this research were the development of a new runoff model and its application to rehabilitated landforms, a systematic comparison of RunCA to other models was not included. The lack of appropriate data was also an important obstacle for this comparison as different models would require different input parameters with different spatial or temporal resolutions. To well demonstrate and prove the potential advantages of RunCA over some other hydrologic models, a detailed comparison of their performance, in terms of availability of inputs, simulation accuracy, computational efficiency and scale flexibility, is recommended for future studies.

Verification of modelling results for rehabilitation designs by field experiments

The developed RunCA model was applied in this research to assess the runoff performance of different rehabilitation designs, including surface ripping designs, hillslope designs, tailings dam designs, revegetation strategies and cover constructions (Chapter 8). Some conclusions from the simulation results, such as the positive relationship between runoff and slope gradients, different runoff responses to the slope shapes, the decreased runoff coefficient with increasing vegetation cover, and the low runoff production on covers constructed with high infiltrability materials, were all in line with some

previous findings. In addition, some new finding, such as the roles of mounds and rip lines in reducing runoff on tailings dams, the impacts of vegetation distribution on runoff behaviours on batter slopes, and the effects of cover thickness on runoff rates, were supported by reasonable explanations. These demonstrated the potential ability of RunCA as a simulation tool to optimise the rehabilitation designs. However, a major limitation was that all these results were derived from the conceptual studies conducted on virtual objects, due to the lack of available field data and the difficulties in conducting experimental studies. Whether these conclusions would be valid in real cases are therefore unclear, and further investigations (e.g., field experiments) are required to verify the modelling results.

Extension of RunCA to different runoff generation mechanisms

At current stage RunCA focuses only on the simulation of the infiltration-excess runoff (Hortonian runoff) processes, as it was primary developed for the rehabilitated landforms, where the infiltration ability is characteristically low and surface runoff is dominated by the infiltration-excess runoff in most cases. However, some previous studies have identified that as vegetation establishes and pedogenic processes begin, alterations in soil characteristics may increase the infiltration capacity in rehabilitated areas (Jorgensen and Gardner, 1987), and the dominant runoff path would likely change in response to increased infiltration from infiltration-excess runoff to saturation-excess runoff and subsurface runoff (Guebert and Gardner, 1992). In these rehabilitated areas and other natural areas where the runoff is mainly attributed by the runoff generation mechanisms other than the infiltration-excess runoff, RunCA would produce unexpected errors due to its inability in simulating these runoff behaviours. It is therefore a major constraint to the applicability and versatility of RunCA. This problem can be potentially solved by incorporating the other runoff generation paths in RunCA in future studies. To achieve this, it is required to develop some appropriate algorithms and transition rules for the simulations of saturation-excess runoff and subsurface runoff (Figure 9.1). As no relevant CA-based models for this purpose have been found in literature yet, this would be a great contribution to the current knowledge of integrated runoff modelling.

Incorporation of soil erosion component

The improved understanding and prediction of the surface hydrological processes by this research would contribute to the prevention of the harmful environmental consequences caused by surface runoff. However, most of these consequences, such as the landform instability, loss of top soil and nutrients, revegetation failure and sediment transport to water courses, are also directly associated with soil erosion, which further demands the prediction of the soil erosion process. In addition, while the accurate simulation of surface runoff by RunCA provides valuable supporting information for the

rehabilitation designs at the early stages, the surface hydrological behaviours on the designed landforms may change with time due to the evolution of these landforms caused by various factors. Soil erosion is such a major forcing factor that would greatly change the characteristics of these landforms. Therefore, to better simulate the surface hydrological behaviours over a long term, in future research it is worthwhile to further incorporate the soil erosion component in RunCA to capture the evolution of landforms. For this purpose, the according CA transition rules for sediment generation and movement require to be developed on the basis of relevant physical principles for these processes (Figure 9.1).

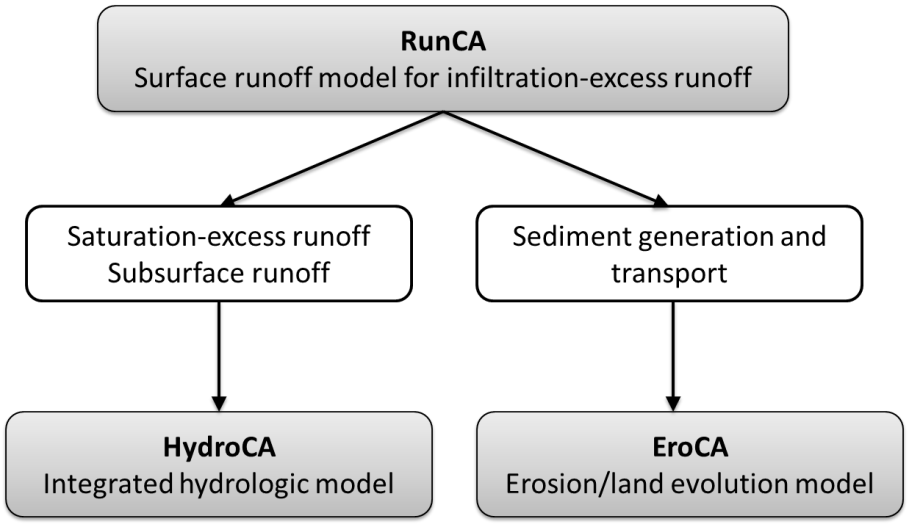

Figure 9.1 Future directions for the improvement of RunCA.

References

Aassine, S., El Jaï, M.C., 2002. Vegetation dynamics modelling: a method for coupling local and space dynamics. Ecological Modelling, 154(3): 237-249.

Abbott, M.B., Bathurst, J.C., Cunge, J.A., O'Connell, P.E., Rasmussen, J., 1986. An introduction to the European Hydrological System — Systeme Hydrologique Europeen, “SHE”, 2: Structure of a physically-based, distributed modelling system. Journal of Hydrology, 87(1–2): 61-77.

Abrahams, A.D., Parsons, A.J., 1991. Relation between infiltration and stone cover on a semiarid hillslope, southern Arizona. Journal of Hydrology, 122(1-4): 49-59.

Adams, J.E., 1966. Influence of mulches on runoff, erosion and soil moisture depletion. Soil Science Society of America Proceedings, 30: 101-114.

Ahuja, L.R., Nofziger, D.L., Swartzendruber, D., Ross, J.D., 1989. Relationship between green and ampt parameters based on scaling concepts and field-measured hydraulic data. Water Resources Research, 25(7): 1766-1770.

Al-Qinna, M.I., Abu-Awwad, A.M., 1998. Infiltration rate measurements in arid soils with surface crust. Irrigation Science, 18(2): 83-89.

Amin, S., 1982. Modeling of phosphorous transport in surface runoff from agriculture watersheds. PhD Thesis Thesis, Purdue University, West Lafayette, USA.

Anderson, M.G., Burt, T.P., 1978. Toward more detail field monitoring of variable source areas. Water Resources Research, 14: 1123-1131.

Anderson, M.G., Burt, T.P., 1990. Process studies in hillslope hydrology: an overview. In: Anderson, M.G., Burt, T.P. (Eds.), Process studies in hillslope hydrology. John Wiley and Sons, New York, pp. 1-8.

Anderson, M.G., Kneale, P.E., 1982. The influence of low-angled topography on hillslope soil-water convergence and stream discharge. Journal of Hydrology, 57: 65-80.

Andrés, P., Jorba, M., 2000. Mitigation Strategies in Some Motorway Embankments (Catalonia, Spain). Restoration Ecology, 8(3): 268-275.

Antoine, M., Javaux, M., Bielders, C., 2009. What indicators can capture runoff-relevant connectivity properties of the micro-topography at the plot scale? Advances in Water Resources, 32(8): 1297-1310.

Aron, G., 1992. Adaptation of Horton and SCS Infiltration Equations to Complex Storms. Journal of Irrigation and Drainage Engineering, 118(2): 275-284.

Aston, A.R., 1979. Rainfall interception by eight small trees. Journal of Hydrology, 42(3-4): 383-396.

Aubertin, G.M., 1971. Nature and extent of macropores in forest soils and their influence on subsurface water movement. USDA Forest Service Research Paper NE-192, North-eastern Forest Experiment Station, Upper Derby, PA.

Bauer, S.W., 1974. A modified Horton equation for infiltration during intermittent rainfall. Hydrological Sciences Bulletin, 19(2): 219-225.

Baumhardt, R.L., 1985. The effect of rainstorm characteristics on soil sealing and infiltration. Ph.D. Thesis, Mississippi State University, Mississippi, United States.

Beasley, D.B., Huggins, L.F., 1981. ANSWERS Users Manual. U.S. Environmental Protection Agency, Chicago, 53 pp.

Beasley, D.B., Huggins, L.H., Monke, E.J., 1980. ANSWERS: a model for watershed planning. Transactions of the American Society of Agricultural Engineers, 23: 938-944.

Berg, P., Moseley, C., Haerter, J.O., 2013. Strong increase in convective precipitation in response to higher temperatures. Nature Geosci, 6(3): 181-185.

Bergkamp, G., Cammeraat, L.H., Martinez-Fernandez, J., 1996. Water movement and vegetation patterns on shrubland and an abandoned field in two desertification-threatened areas in Spain. Earth Surface Processes and Landforms, 21(12): 1073-1090.

Beven, K., Germann, P., 1981. Water flow in soil macropores, 2, a combined flow model. J. Soil Sci. , 32: 15-29.

Beven, K., Germann, P., 1982. Macropores and water flow in soils. Water Resour. Res., 18: 1311-1325.

Bhuyan, S.J., Kalita, P.K., Janssen, K.A., Barnes, P.L., 2002. Soil loss predictions with three erosion simulation models. Environmental Modelling & Software, 17(2): 135-144.

Bingeman, A., Kouwen, N., Soulis, E., 2006. Validation of the Hydrological Processes in a Hydrological Model. Journal of Hydrologic Engineering, 11(5): 451-463.

Blackburn, W.H., 1975. Factors influencing infiltration and sediment production of semi-arid rangelands in Nevada. Water Resour. Res., 11(6): 929-937.

Blaney, H.F., Criddle, W.D., 1950. Determining Water Requirements in Irrigated Areas from Climatological and Irrigation Data. United States Department of Agriculture, Soil Conservation Service, pp. 96.

Bochet, E., Poesen, J., Rubio, J.L., 2006. Runoff and soil loss under individual plants of a semi-arid Mediterranean shrubland: influence of plant morphology and rainfall intensity. Earth Surface Processes and Landforms, 31(5): 536-549.

Bochet, E., Rubio, J.L., Poesen, J., 1999. Modified topsoil islands within patchy Mediterranean vegetation in SE Spain. CATENA, 38(1): 23-44.

Boix-Fayos, C., Calvo-Cases, A., Imeson, A.C., Soriano-Soto, M.D., Tiemes-sen, I.R., 1998. Spatial and short-term temporal variations in runoff, soil aggregation and other soil properties along a mediterranean climatological gradient. Catena, 33: 123-138.

Bollhöfer, A. et al., 2008. Airborne gamma survey of the historic Sleisbeck mine area in the Northern Territory, Australia, and its use for site rehabilitation planning. Journal of Environmental Radioactivity, 99(11): 1770-1774.

Bonta, J.V., 1991. Erosion and runoff control using bulldozer imprints on surface-mine spoil. Transactions of the ASAE, 34(1): 97.

Borah, K., D., Bera, M., 2004. Watershed-scale hydrologic and nonpoint-source pollution models: Review of applications. Transactions of the ASAE, 47(3): 789-803.

Bos, M.G., Replogle, J.A., Clemmens, A.J., 1984. Flow Measuring Flumes for Open Channel Systems. John Wiley and Sons, New York.

Bouraoui, F., Dillaha, T., 1996. ANSWERS-2000: Runoff and Sediment Transport Model. Journal of Environmental Engineering, 122(6): 493-502.

Bradford, J.M., Ferris, J.E., Remley, P.A., 1987. Interrill Soil Erosion Processes: I. Effect of Surface Sealing on Infiltration, Runoff, and Soil Splash Detachment. Soil Sci. Soc. Am. J., 51(6): 1566-1571.

Brakensiek, D.L., Onstad, C.A., 1977. Parameter estimation of the Green and Ampt Infiltration Equation. Water Resources Research, 13(6): 1009-1012.

Bryan, R.B., Poesen, J., 1989. Laboratory experiments on the influence of slope length on runoff, percolation and rill development. Earth Surface Processes and Landforms, 14(3): 211-231.

Burch, G.J., Bath, R.K., Moore, I.D., O'Loughlin, E.M., 1987. Comparative hydrological behaviour of forested and cleared catchments in southeastern Australia. Journal of Hydrology, 90(1-2): 19-42.

Calvo-Cases, A., Boix-Fayos, C., Imeson, A.C., 2003. Runoff generation, sediment movement and soil water behaviour on calcareous (limestone) slopes of some Mediterranean environments in southeast Spain. Geomorphology, 50(1-3): 269-291.

Cammeraat, E.L.H., 2004. Scale dependent thresholds in hydrological and erosion response of a semi-arid catchment in southeast Spain. Agriculture, Ecosystems & Environment, 104(2): 317-332.

Carlsson, E., Büchel, G., 2005. Screening of residual contamination at a former uranium heap leaching site, Thuringia, Germany. Chemie der Erde - Geochemistry, 65, Supplement 1(0): 75-95.

Cerdà, A., 1997. Seasonal changes of the infiltration rates in a Mediterranean scrubland on limestone. Journal of Hydrology, 198(1-4): 209-225.

Cerdà, A., 2001. Effects of rock fragment cover on soil infiltration, interrill runoff and erosion. European Journal of Soil Science, 52(1): 59-68.

Chahinian, N., Moussa, R., Andrieux, P., Voltz, M., 2005. Comparison of infiltration models to simulate flood events at the field scale. Journal of Hydrology, 306(1-4): 191-214.

Childs, E.C., Bybordi, M., 1969. The vertical movement of water in stratified porous material. 1. Infiltration. Water Resources Research, 5(2): 446-459.

Chorley, R.J., 1978. The hillslope hydrological cycle. In: Kirkey, M.J. (Ed.), Hillslope hydrology. John Wiley and Sons, New York.

Chow, V.T., 1964. Handbook of Applied Hydrology. McGraw-Hill, New York.

Chow, V.T., Maidment, D.R., Mays, L.W., 1988. Applied Hydrology. McGraw-Hill, New York.

Clarke, K.C., Brass, J.A., Riggan, P.J., 1994. A cellular automaton model of wild fire propagation and extinction. Photogrammetric Engineering and Remote Sensing, 11: 1355-1367.

Cook, H.L., 1946. The infiltration approach to the calculation of surface runoff. Eos Trans. AGU, 27: 726-747.

Corradini, C., Melone, F., Smith, R.E., 1994. Modeling infiltration during complex rainfall sequences. Water Resources Research, 30(10): 2777-2784.

Corradini, C., Melone, F., Smith, R.E., 1997. A unified model for infiltration and redistribution during complex rainfall patterns. Journal of Hydrology, 192(1–4): 104-124.

Costa-Cabral, M.C., Burges, S.J., 1994. Digital Elevation Model Networks (DEMON): A model of flow over hillslopes for computation of contributing and dispersal areas. Water Resour. Res., 30(6): 1681-1692.

Coulthard, T.J., Hancock, G.R., Lowry, J.B.C., 2012. Modelling soil erosion with a downscaled landscape evolution model. Earth Surface Processes and Landforms, 37(10): 1046-1055.

Coulthard, T.J., Kirkby, M.J., Macklin, M.G., 2000. Modelling geomorphic response to environmental change in an upland catchment. Hydrological Processes, 14(11-12): 2031-2045.

Coulthard, T.J. et al., 2013. Integrating the LISFLOOD-FP 2D hydrodynamic model with the CAESAR model: implications for modelling landscape evolution. Earth Surface Processes and Landforms, 38(15): 1897-1906.

D'Ambrosio, D., Di Gregorio, S., Gabriele, S., Gaudio, R., 2001. A Cellular Automata model for soil erosion by water. Physics and Chemistry of the Earth, Part B: Hydrology, Oceans and Atmosphere, 26(1): 33-39.

Darmer, G., Dietrich, N.L., 1992. Landscape and Surface Mining: Ecological guidelines for reclamation. Van Nostrand Reinhold, New York, United States of America.

Davidoff, B., Selim, H.M., 1986. Goodness of fit for eight water infiltration models. Soil Science Society of America journal 50: 759-764.

De Roo, A.P.J., Jetten, V.G., 1999. Calibrating and validating the LISEM model for two data sets from the Netherlands and South Africa. CATENA, 37(3–4): 477-493.

De Roo, A.P.J., Wesseling, C.G., Ritsema, C.J., 1996. LISEM: a single-event physically based hydrological and soil erosion model for drainage basins. I: Theory, input and output. Hydrological Processes, 10(8): 1107-1117.

Deadman, P., Brown, R.D., Gimblett, H.R., 1993. Modelling Rural Residential Settlement Patterns with Cellular Automata. Journal of Environmental Management, 37(2): 147-160.

Deb, S.K., Shukla, M.K., 2012. Variability of hydraulic conductivity due to multiple factors. American Journal of Environmental Sciences, 8(5): 489-502.

Decagon Devices, I., 2012. Mini Disk Infiltrometer - User's Manual, Version 10, Pullman, WA.

Descroix, L., Viramontes, D., Vauclin, M., Gonzalez Barrios, J.L., Esteves, M., 2001. Influence of soil surface features and vegetation on runoff and erosion in the Western Sierra Madre (Durango, Northwest Mexico). Catena, 43: 115-135.

Desmet, P.J.J., Govers, G., 1996. Comparison of routing algorithms for digital elevation models and their implications for predicting ephemeral gullies. Int. J. Geogr. Inf. Syst., 10(3): 311-331.

Deuchars, S.A., Townend, J., Aitkenhead, M.J., FitzPatrick, E.A., 1999. Changes in soil structure and hydraulic properties in regenerating rain forest. Soil Use and Management, 15(3): 183-187.

Division, S.S., 1999. Environmental requirements for the Ranger Uranium Mine. In: Department of Sustainability, E., Water, Populations and Communities (Ed.).

Donald, E.O., Michael, E.M., 1976. Stormwater Modeling Academic Press, New York.

Dos Reis Castro, N.M., Auzet, A.-V., Chevallier, P., Leprun, J.-C., 1999. Land use change effects on runoff and erosion from plot to catchment scale on the basaltic plateau of Southern Brazil. Hydrological Processes, 13(11): 1621-1628.

Dunin, F.X., 1976. Infiltration: Its Simulation for Field Conditions. In: Rodda, J.C. (Ed.), Facets of Hydrology. John Wiley & Sons, New York.

Dunne, T., 1978. Field studies of hillslope flow processes. In: Kirkby, M.J. (Ed.), Hillslope hydrology. John Wiley and Sons, New York, pp. 227-293.

Dunne, T., Black, R.D., 1970. An experimental investigation of runoff production in permeable soils. Water Resources Research, 6(2): 478-490.

Dunne, T., Dietrich, W.E., 1980. Experimental study of Horton overland flow on tropical hillslopes, II, Sheetflow hydraulics and hillslope hydrographs. Geomorphol, Suppl., 33: 40-80.

Dunne, T., Moore, T.R., Taylor, C.H., 1975. Recognition and prediction of runoff producing zones in humid regions. Hydrological Sciences Bulletin, 20: 305-327.

Dunne, T., Zhang, W., Aubry, B.F., 1991. Effects of rainfall, vegetation, and microtopography on infiltration and runoff. Water Resources Research, 27(9): 2271-2285.

Eerkes, G.R., 2003. The effect of bedrock topography on runoff-contributing areas in a forested basin: A slope-scale experiment on the Precambrian Shield in south central Ontario, Canada. M.Sc. Thesis, Trent University, Canada.

Ekwue, E.I., Bharat, C., Samaroo, K., 2009. Effect of soil type, peat and farmyard manure addition, slope and their interactions on wash erosion by overland flow of some Trinidadian soils. Biosystems Engineering, 102(2): 236-243.

Ekwue, E.I., Harrilal, A., 2010. Effect of soil type, peat, slope, compaction effort and their interactions on infiltration, runoff and raindrop erosion of some Trinidadian soils. Biosystems Engineering, 105(1): 112-118.

El Boushi, I.M., Davis, S.N., 1969. Water retention characteristics of coarse rock particles. Journal of Hydrology, 8: 431-441.

Endreny, T.A., Wood, E.F., 2003. Maximizing spatial congruence of observed and DEM-delineated overland flow networks. International Journal of Geographical Information Science, 17(7): 699-713.

EPA, Q., 2006. Ernest Henry Mining Pty Ltd, Environmental Authority No. MIM900341305. In: Agency, Q.E.P. (Ed.), Brisbane, Australia.

Erik, Økland, T., 2002. Estimating tree height and tree crown properties using airborne scanning laser in a boreal nature reserve. Remote Sensing of Environment, 79(1): 105-115.

Ermentrout, G., Edelstein-Keshet, L., 1993. Cellular automata approaches to biological modeling. Journal of Theoretical Biology, 160: 97-133.

Erskine, R.H., Green, T.R., Ramirez, J.A., MacDonald, L.H., 2006. Comparison of grid-based algorithms for computing upslope contributing area. Water Resour. Res., 42(9): W09416.

Esteves, M., Faucher, X., Galle, S., Vauclin, M., 2000. Overland flow and infiltration modelling for small plots during unsteady rain: numerical results versus observed values. Journal of Hydrology, 228(3-4): 265-282.

Estupina-Borrell, V., Dartus, D., Alquier, M., 2002. Forecast of flash floods in ungaged basins with satellite data. In: Hubert, D.S.P., Takeuchi, K., Koide, S. (Eds.), Proceedings of the Brasilia PUB Meeting. IAHS, University of Brasilia, Brasil.

Evans, K.G., 2000. Methods for assessing mine site rehabilitation design for erosion impact. Soil Research, 38(2): 231-248.

Evans, K.G., Riley, S.J., 1993. Regression equations for the determination of discharge through RBC flumes, Supervising Scientist for the Alligator Rivers Region, Canberra.

Fairfield, J., Leymarie, P., 1991. Drainage networks from grid digital elevation models. Water Resour. Res., 27(5): 709-717.

Fattah, H.A., Upadhyaya, S.K., 1996. Effect of soil crust and soil compaction on infiltration in a Yolo loam soil. Trans. ASAE, 39: 79-84.

Favis-Mortlock, D., 1998. A self-organizing dynamic systems approach to the simulation of rill initiation and development on hillslopes. Computers & Geosciences, 24(4): 353-372.

Feldman, A.D., 1995. HEC-1 flood routing package. In: Singh, V.J. (Ed.), Computer Models of Watershed Hydrology. Water Resources Publication, Highlands Ranch, Colorado, pp. 119-150.

Foley, J.L., Loch, R.J., Glanville, S.F., Connolly, R.D., 1991. Effects of tillage, stubble and rainfall energy on infiltration. Soil and Tillage Research, 20(1): 45-55.

Folino, G., Mendicino, G., Senatore, A., Spezzano, G., Straface, S., 2006. A model based on cellular automata for the parallel simulation of 3D unsaturated flow. Parallel Computing, 32(5-6): 357-376.

Fox, D.M., Bryan, R.B., Price, A.G., 1997. The influence of slope angle on final infiltration rate for interrill conditions. Geoderma, 80(1-2): 181-194.

Francis, C.F., Thornes, J.B., 1990. Runoff hydrographs from three Mediterranean vegetation cover types. In: Thornes, J.B. (Ed.), Vegetation and Erosion: Processes and Environments. John Wiley & Sons Ltd., Chichester, UK, pp. 363-384.

Freeman, T.G., 1991. Calculating catchment area with divergent flow based on a regular grid. Computers & Geosciences, 17(3): 413-422.

Freeze, R.A., 1980. A stochastic-conceptual analysis of rainfall-runoff processes on a hillslope. Water Resources Research, 16(2): 391-408.

Frere, M.H., Onstad, C.A., Holtan, H.N., 1975. ACTMO, an agricultural chemical transport model. United States Department of Agriculture.

Gardner, M., 1970. Mathematical games: on cellular automata, self-reproduction, the Garden of Eden, and the game 'life'. Scientific American, 224(2): 112-117.

Gatzweiler, R., Jahn, S., Neubert, G., Paul, M., 2001. Cover design for radioactive and AMD-producing mine waste in the Ronneburg area, Eastern Thuringia. Waste Management, 21(2): 175-184.

Gee, G.W., Bauder, J.W., 1986. Particle size analysis. In: Klute, A. (Ed.), Methods of Soil Analysis Volume 1, Physical and Mineralogical Methods. American Society of Soil Agronomy and Soil Science Society of America, Madison, pp. 357-376.

Ghorbani Dashtaki, S., Homaee, M., Mahdian, M., Kouchakzadeh, M., 2009. Site-Dependence Performance of Infiltration Models. Water Resources Management, 23(13): 2777-2790.

Gómez, J.A., Nearing, M.A., 2005. Runoff and sediment losses from rough and smooth soil surfaces in a laboratory experiment. CATENA, 59(3): 253-266.

Gordon, H.B., Whetton, P.H., Pittock, A.B., Fowler, A.M., Haylock, M.R., 1992. Simulated changes in daily rainfall intensity due to the enhanced greenhouse effect: implications for extreme rainfall events. Climate Dynamics, 8(2): 83-102.

Gosh, R.K., 1983. A note on the infiltration equation. Soil Science, 136: 333-338.

Green, W.H., Ampt, C.A., 1911. Studies on soil physics I. The flow of air and water through soils. Journal of Agricultural Science, 5: 1-24.

Greene, R., 1992. Soil physical properties of three geomorphic zones in a semiarid mulga woodland. Soil Research, 30(1): 55-69.

Gregorio, S.D., Serra, R., 1999. An empirical method for modelling and simulating some complex macroscopic phenomena by cellular automata. Future Generation Computer Systems, 16(2-3): 259-271.

Guebert, M.D., Gardner, T.W., 1992. Macropore flow effect on infiltration, throughflow and surface runoff on a reclaimed surface-mined watershed, Land Reclamation: Advances in Research and Technology, Proceedings of the 1992 International Symposium. American Society of Agricultural Engineering, pp. 91-100.

Guebert, M.D., Gardner, T.W., 2001. Macropore flow on a reclaimed surface mine: Infiltration and hillslope hydrology. Geomorphology, 39(3-4): 151-169.

Gunst, R.F., Mason, R.L., 1980. Regression Analysis and its Application: A Data-Oriented Approach. Taylor & Francis.

Gupta, N., 2003. Investigation of rainfall-runoff mechanism on field scale. Ph.D. Thesis, University of Guelph (Canada), Canada.

Gyasi-Agyei, Y., Willgoose, G.R., 1996. Evaluation of the use of contour banks as a post-mining rehabilitation control option using a digital terrain based rainfall runoff erosion mode. In: Holzman, H., Nachtnebel, H.P. (Eds.), Application of Geographic Information Systems in Hydrology and Water Resources Management, HydroGIS '96, Vienna, Austria, pp. 143-150.

Haan, C.T., Johnson, H.P., Brakensiek, D.L., 1982. Hydrologic modeling of small watersheds. American Society of Agricultural Engineers, Michigan.

Haggard, B.E., Moore, P.A., Brye, K.R., 2005. Effect of slope on runoff from a small variable slope box-plot. Journal of Environmental Hydrology, 13(25): 1-8.

Haggett, P., Chorley, R.J., Stoddart, D.R., 1965. Scale Standards in Geographical Research: A New Measure of Areal Magnitude. Nature, 205(4974): 844-847.

Haigh, M.J., 1992. Problems in the reclamation of coal-mine disturbed lands in Wales. International Journal of Surface Mining and Reclamation, 6(31-37).

Hamon, W.R., 1961. Estimating potential evapo-transpiration. Journal of the Hydraulics Division, 87: 107-120.

Hancock, G.R., 2004. The use of landscape evolution models in mining rehabilitation design. Environmental Geology, 46(5): 561-573.

Hancock, G.R., Loch, R.J., Willgoose, G.R., 2003. The design of post-mining landscapes using geomorphic principles. Earth Surface Processes and Landforms, 28(10): 1097-1110.

Harms, T.E., 1996. Runoff generation on reclaimed watersheds. M.Sc. Thesis, University of Alberta, Canada.

Hawkins, R.H., 1982. Interpretation of source-area variability in rainfall-runoff relationships. In: Singh, V.P. (Ed.), Rainfall-Runoff Relationships. Water Resources Publication, Fort Collins, Colo., pp. 303-324.

Hidalgo, J.C.G., Raventos, J., Echevarria, M.T., 1997. Comparison of sediment ratio curves for plants with different architectures. CATENA, 29(3-4): 333-340.

Hillel, D., Gardner, W.R., 1970. Transient infiltration into crust topped profiles. Soil Science, 109: 69-76.

Holtan, H.N., 1961. A concept of infiltration estimates in watershed engineering. U.S. Department of Agricultural Service, Washington, DC.

Horton, R.E., 1933. The role of infiltration in the hydrological cycle. Transactions of American Geophysics Union., 14: 446-460.

Horton, R.E., 1940. An approach towards a physical interpretation of infiltration capacity. Soil Science Society of America Proceedings, 5: 399-417.

Huang, Z., Ouyang, Z., Li, F., Zheng, H., Wang, X., 2010. Response of runoff and soil loss to reforestation and rainfall type in red soil region of southern China. Journal of Environmental Sciences, 22(11): 1765-1773.

Huat, B.K., Ali, F., Low, T.H., 2006. Water infiltration characteristics of unsaturated soil slope and its effect on suction and stability. Geotech Geol Eng, 24(5): 1293-1306.

Huggins, L.F., Monke, E.J., 1966. The mathematical simulation of the hydrology of small watersheds, Water Resources Research Center, Purdue University.

Huggins, L.F., Monke, E.J., 1968. A Mathematical Model for Simulating the Hydrologic Response of a Watershed. Water Resources Research, 4(3): 529-539.

Inc, S.I., 2008. SAS/STAT 9.2 User's Guide. SAS Institute Inc., Cary, NC.

Itami, R.M., 1988. Cellular automations as a framework for dynamic simulations in geographic information systems, GIS/LIS' 88 Proceedings, pp. 590-607.

Jackson, T.J., 1993. III. Measuring surface soil moisture using passive microwave remote sensing. Hydrological Processes, 7(2): 139-152.

Jain, M.K., Kothyari, U.C., Ranga Raju, K.G., 2004. A GIS based distributed rainfall–runoff model. Journal of Hydrology, 299(1–2): 107-135.

Jens Christian, R., 1997. Parameterisation, calibration and validation of distributed hydrological models. Journal of Hydrology, 198(1-4): 69-97.

Jenson, S.K., 1991. Applications of hydrologic information automatically extracted from digital elevation models. Hydrological Processes, 5(1): 31-44.

Jones, M.R., Fowler, H.J., Kilsby, C.G., Blenkinsop, S., 2013. An assessment of changes in seasonal and annual extreme rainfall in the UK between 1961 and 2009. International Journal of Climatology, 33(5): 1178-1194.

Jorgensen, D.W., Gardner, T.W., 1987. Infiltration capacity of disturbed soils: Temporal change and lithologic control. Water Resour. Bull, 23: 1161-1172.

Kannan, N., White, S.M., Worrall, F., Whelan, M.J., 2007. Sensitivity analysis and identification of the best evapotranspiration and runoff options for hydrological modelling in SWAT-2000. Journal of Hydrology, 332(3–4): 456-466.

Kapolka, N.M., Dollhopf, D.J., 2001. Effect of slope gradient and plant growth on soil loss on reconstructed steep slopes. International Journal of Surface Mining, Reclamation and Environment, 15: 86-99.

Kincaid, D.R., Gardner, J.L., Schreiber, H.A., 1964. Soil and vegetation parameters affecting infiltration under semiarid conditions. IASH, 65: 440-453.

Kirkby, M., Bracken, L., Reaney, S., 2002. The influence of land use, soils and topography on the delivery of hillslope runoff to channels in SE Spain. Earth Surface Processes and Landforms, 27(13): 1459-1473.

Kirtland, D. et al., 1994. An analysis of human-induced land transformations in the San Francisco Bay/Sacramento area. World Resource Review, 6(2): 206-217.

Klute, A., Dirksen, C., 1986. Hydraulic Conductivity and Diffusivity: Laboratory Methods. In: Klute, A. (Ed.), Methods of Soil Analysis: Part 1—Physical and Mineralogical Methods. SSSA Book Series. Soil Science Society of America, American Society of Agronomy, pp. 687-734.

Knisel, W.G., 1980. CREAMS. A field scale model for chemicals, runoff and erosion from agricultural management systems. United States Department of Agriculture Conservation Research Report 26.

Kouwen, N., 2012. WATFLOOD/WATROUTE Hydrological Model Routing and Flow Forecasting System, Department of Civil Engineering, University of Waterloo, Waterloo, Ontario, Canada.

Laflen, J.M., Lane, L.J., Foster, G.R., 1991. WEPP: a new generation of erosion prediction technology. Journal of Soil & Water Conservation, 46(1): 34-38.

Lavee, H., Poesen, J.W.A., 1991. Overland flow generation and continuity on stone-covered soil surfaces. Hydrological Processes, 5(4): 345-360.

Lavee, H., Yair, A., 1987. Spatial variability of overland flow in a small arid basin, Erosion, Transport and Deposition Processes. IAHS Publication, pp. 105-120.

Le Bissonnais, Y. et al., 1998. Crusting, runoff and sheet erosion on silty loamy soils at various scales and upscaling from m2 to small catchments. Soil and Tillage Research, 46(1-2): 69-80.

Le Bissonnais, Y., Singer, M.J., 1992. Crusting, runoff, and erosion response to soil water content and successive rainfall. Soil Sci. Soc. Am. J., 56: 1898-1903.

Lea, N.L., 1992. An aspect driven kinematic routing algorithm. In: Parsons, A.J., Abrahams, A.D. (Eds.), Overland Flow: Hydraulics and Erosion Mechanics. CRC Press, Boca Raton, Fla, pp. 393-407.

Lemieux, C.R., 1987. Infiltration characteristics and hydrologic modelling of disturbed land, Moshannon, Pennsylvania, The Pennsylvania State University, University Park, 150 pp.

Leonard, J., Andrieux, P., 1998. Infiltration characteristics of soils in Mediterranean vineyards in Southern France. CATENA, 32(3–4): 209-223.

Leoni, G.L.s.M., Almeida, M.d.S.S., Fernandes, H.M., 2004. Computational modelling of final covers for uranium mill tailings impoundments. Journal of Hazardous Materials, 110(1–3): 139-149.

Li, X.-Y. et al., 2011. Controls of infiltration-runoff processes in Mediterranean karst rangelands in SE Spain. CATENA, 86(2): 98-109.

Lin, H.S., McInnes, K.J., Wilding, L.P., Hallmark, C.T., 1999. Effects of Soil Morphology on Hydraulic Properties II. Hydraulic Pedotransfer Functions Soil Science Society of America Journal, 63(4): 955-961.

Linsley, R.K., Kohler, M.A., Paulhus, J.L.H., 1949. Applied Hydrology. McGraw-Hill, New York.

Littleboy, M., Sachan, R., Smith, G., Cogle, A., 1996. Soil management and production of alfisols in the semi-arid tropics. II. Deriving USDA curve numbers from rainfall simulator data. Soil Research, 34(1): 103-111.

Loch, R.J., 2000a. Effects of vegetation cover on runoff and erosion under simulated rain and overland flow on a rehabilitated site on the Meandu Mine, Tarong, Queensland. Australian Journal of Soil Research, 38(2): 299-312.

Loch, R.J., 2000b. Using rainfall simulation to guide planning and management of rehabilitated areas: Part I. Experimental methods and results from a study at the Northparkes Mine, Australia. Land Degradation & Development, 11(3): 221-240.

Loch, R.J., Connolly, R.D., Littleboy, M., 2000. Using rainfall simulation to guide planning and management of rehabilitated areas: Part II. Computer simulations using parameters from rainfall simulation. Land Degradation & Development, 11(3): 241-255.

Loch, R.J. et al., 2001. A multi-purpose rainfall simulator for field infiltration and erosion studies. Australian Journal of Soil Research, 39(3): 599-610.

Lottermoser, B.G., Ashley, P.M., 2006. Physical dispersion of radioactive mine waste at the rehabilitated Radium Hill uranium mine site,South Australia. Australian Journal of Earth Sciences, 53(3): 485-499.

Lowry, J., Saynor, M., Erskine, W., Coulthard, T., Hancock, G., 2014. A multi-year assessment of landform evolution model predictions for a trial rehabilitated landform, Life-of-Mine 2014. The Australasian Institute of Mining and Metallurgy, Brisbane, Australia, pp. 67-80.

Lowry J.B.C., Coulthard T.J., G.R., H., D.R., J., 2011. Assessing soil erosion on a rehabilitated landform using the CAESAR landscape evolution model. . In: Fourie A.B., M., T., A., B. (Eds.), Proceedings of the 6th International Conference on Mine Closure, 18-21 September 2011. Australian Centre for Geomechanics, Perth.

Ma, T., Zhou, C.-H., Cai, Q.-G., 2009. Modeling of hillsloperunoff and soil erosion at rainfall events using Cellular Automata approach. Pedosphere, 19(6): 711-718.

MacArthur, R., DeVries, J.J., 1993. Introduction and Application of Kinematic Wave Routing Techniques Using HEC-1, Hydrologic Engineering Centre.

Majer, J.D., 1989. Fauna studies and land reclamation technology - A review of the history and need for such studies. In: Majer, J.D. (Ed.), Animals in primary succession - The role of fauna in reclaimed lands. Press Syndicate of the University of Cambridge, Melbourne, Australia.

Manley, R.E., 1993. HYSIM Reference Manual, R. E. Manley Consultancy, Cambridge.

Marston, 1980. Rainfall simulation for the assessment of the effects of crop management on soil erosion, University of New England, Armidale, Australia.

Marston, R.B., 1952. Ground cover requirements for summer storm runoff control on aspen sites in Northern Utah. Journal of Forestry, 50: 303-307.

Martinez-Mena, Albaladejo, M.J., Castillo, V.M., 1998. Factors influencing surface runoff generation in a Mediterranean semi-arid environment: Chicamo Watershed, SE Spain. Hydrological Processes, 12: 741-754.

Martz, L.W., Garbrecht, J., 1992. Numerical definition of drainage network and subcatchment areas from digital elevation models. Computer Geoscience, 18(6): 747-761.

Mayor, A.G., Bautista, S., Bellot, J., 2009. Factors and interactions controlling infiltration, runoff, and soil loss at the microscale in a patchy Mediterranean semiarid landscape. Earth Surface Processes and Landforms, 34: 1702-1711.

Mbagwu, J.S.C., 1995. Testing the goodness of fit of infiltration models for highly permeable soils under different tropical soil management systems. Soil and Tillage Research, 34(3): 199-205.

McCuen, R.H., Rawls, W.J., Brakensiek, D.L., 1981. Statistical analysis of the Brooks-Corey and the Green-Ampt parameters across soil textures. Water Resources Research, 17(4): 1005-1013.

McIntyre, D.S., 1958. Permeability measurements of soil crusts formed by raindrop impact. Soil Sci., 85: 185-189.

McIvor, J., Williams, J., Gardener, C., 1995. Pasture management influences runoff and soil movement in the semi-arid tropics. Australian Journal of Experimental Agriculture, 35(1): 55-65.

McIntyre, D.S., 1958. Soil splash and the formation of surface crusts by raindrop impacts. Soil Sci., 85: 261-266.

Meek, B.D., Rechel, E.R., Carter, L.M., DeTar, W.R., Urie, A.L., 1992. Infiltration Rate of a Sandy Loam Soil: Effects of Traffic, Tillage, and Plant Roots. Soil Sci. Soc. Am. J., 56(3): 908-913.

Meteorology, B.o., 2014. Climate statistics for Australian locations – Jabiru Airport [online].

Meyer, L.D., Johnson, C.B., Foster, G.R., 1972. Stone and woodchip mulches for erosion control on construction sites. Journal of Soil and Water Conservation, 27: 264-269.

Miller, F.T., Guthrie, R.L., 1984. Classification and distribution of soils containing rock fragments in the United States. In: Nichols, J.D., Brown, P.L., Grand, W.J. (Eds.), Erosion Productivity of Soils Containing Rock Fragments. Soil Science Society of America, 13Madison, WI, pp. 1-6.

Min, S.-K., Zhang, X., Zwiers, F.W., Hegerl, G.C., 2011. Human contribution to more-intense precipitation extremes. Nature, 470(7334): 378-381.

Mishra, S.K., Tyagi, J.V., Singh, V.P., 2003. Comparison of infiltration models. Hydrological Processes, 17(13): 2629-2652.

Mohanty, B.P., 2013. Soil hydraulic property estimation using remote sensing: a review. Vadose Zone Journal, 12(4).

Mohanty, B.P., Kanwar, R.S., Everts, C.J., 1994. Comparison of Saturated Hydraulic Conductivity Measurement Methods for a Glacial-Till Soil. Soil Sci. Soc. Am. J., 58(3): 672-677.

Moldenhauer, W.C., Barrows, W.C., Swarzendruber, D., 1960. Influence of rainstorm characteristics on infiltration measurements. Trans. Int. Cong. Soil Sci, 7: 426-432.

Moliere, D.R., Evans, K.G., Willgoose, G.R., Saynor, M.J., 2002. Temporal trends in erosion and hydrology for a postmining landform at Ranger Mine, Northern Territory, Supervising Scientist, Darwin.

Monteith, J.L., 1965. Evaporation and environment. In: Fogy, G.T. (Ed.), Proceedings of the 19th Symposium, Society of Experimental Biology. Cambridge University Press, London, pp. 205-234.

Moore, I.D., Grayson, R.B., 1991. Terrain-based catchment partitioning and runoff prediction using vector elevation data. Water Resour. Res., 27(6): 1177-1191.

Morel-Seytoux, H.J., 1989. Unsaturated Flow in Hydrologic Modeling: Theory and Practice. Kluwer Academic Publishers, Dordrecht.

Morgan, R.P.C., Quinton, J.N., Smith, R.E., Govers, G., Poesen, J.W.A., 1998a. The European soil erosion model (EUROSEM): documentation and user guide. Silsoe College, Cranfield University.

Morgan, R.P.C. et al., 1998b. The European Soil Erosion Model (EUROSEM): A dynamic approach for predicting sediment transport from fields and small catchments. Earth Surface Processes and Landforms, 23: 527-544.

Mualem, Y., Assouline, S., Rohdenburg, H., 1990. Rainfall induced soil seal (A) A critical review of observations and models. CATENA, 17(2): 185-203.

Murray, A.B., Paola, C., 1994. A cellular model of braided rivers. Nature, 371(1): 54-57.

Musgrave, G.W., 1955. How much of the rain enters the soil?, USDA Water Yearbook of Agriculture. Government Printing Office, Washington, D.C., pp. 151-159.

Nachabe, M., Illangasekare, T., Morel-Seytoux, H., Ahuja, L., Ruan, H., 1997. Infiltration over heterogenous watershed: Influence of rain excess. Journal of Hydrologic Engineering, 2(3): 140-143.

Nash, J.E., Sutcliffe, J.V., 1970. River flow forecasting through conceptual models part I — A discussion of principles. Journal of Hydrology, 10(3): 282-290.

Nearing, M.A., Deer-Ascough, L., Laflen, J.M., 1990. Sensitivity analysis of the WEPP hillslope profile erosion model. Transactions of the ASAE, 33(3): 839-849.

Nicolau, J.M., 2003. Trends in relief design and construction in opencast mining reclamation. Land Degradation & Development, 14(2): 215-226.

Nicolau, J.M., Asensio, E., 2000. Rainfall erosion on opencast coal-mine lands: ecological perspective. In: Haigh, M.J., Balkema, A.A. (Eds.), Reclaimed Land: Erosion Control, Soils and Ecology, Rotterdam, pp. 51-73.

O'Callaghan, J.F., Mark, D.M., 1984. The extraction of drainage networks from digital elevation data. Computer Vision Graphics and Image Processing 28(3): 323-344.

O'Kane, M., Wels, C., 2003. Mine waste cover system design – linking predicted performance to groundwater and surface water impacts, 6th ICARD Conference, Cairns, Queensland, pp. 341-349.

Owens, M.K., Lyons, R.K., Alejandro, C.L., 2006. Rainfall partitioning within semiarid juniper communities: effects of event size and canopy cover. Hydrological Processes, 20(15): 3179-3189.

Parlange, J.Y., Haverkamp, R., 1989. Infiltration and Ponding Time. In: Morel-Seytoux, H.J. (Ed.), Unsaturated Flow in Hydrologic Modeling: Theory and Practice. Kluwer Academic Publishers, Boston, pp. 95-126.

Parsons, J.A., Fonstad, M.A., 2007. A cellular automata model of surface water flow. Hydrological Processes, 21(16): 2189-2195.

Patin, J. et al., 2012. Analysis of runoff production at the plot scale during a long-term survey of a small agricultural catchment in Lao PDR. Journal of Hydrology, 426–427(0): 79-92.

Perroux, K.M., White, I., 1988. Designs for Disc Permeameters. Soil Sci. Soc. Am. J., 52(5): 1205-1215.

Philip, J.R., 1957a. The Theory of Infiltration: 1. the Infiltration Equation and Its Solution. Soil Science, 83: 345-357.

Philip, J.R., 1957b. The theory of infiltration: 4. Sorptivity and algebraic infiltration equations. Soil Science 84: 257-264.

Philip, J.R., 1969. Theory of infiltration. In: Chow, V.T. (Ed.), Advances in Hydroscience. Academic Press, New York.

Pierson, F.B., Spaeth, K.E., Weltz, M.A., Carlson, D.H., 2002. Hydrologic response of diverse western rangelands. Journal of Range Management, 55: 558-570.

Poesen, J., Ingelmo-Sanchez, F., Mucher, H., 1990. The hydrological response of soil surfaces to rainfall as affected by cover and position of rock fragments in the top layer. Earth Surface Processes and Landforms, 15(7): 653-671.

Poesen, J.W.A., 1984. The influence of slope angle on infiltration rate and Hortonian overland flow. Geomorphology, 2(49): 117-131.

Protection, D.o.E.a.H., 2014. Rehabilitation requirements for mining resource activities, Queensland.

Puigdefábregas, J., 2005. The role of vegetation patterns in structuring runoff and sediment fluxes in drylands. Earth Surface Processes and Landforms, 30(2): 133-147.

Quinn, P., Beven, K., Chevallier, P., Planchon, O., 1991. The prediction of hillslope flow paths for distributed hydrological modelling using digital terrain models. Hydrological Processes, 5(1): 59-79.

Quinton, J.N., Edwards, G.M., Morgan, R.P.C., 1997. The influence of vegetation species and plant properties on runoff and soil erosion: results from a rainfall simulation study in south east Spain. Soil Use and Management, 13(3): 143-148.

Ranjith B, M., 1995. Effect of reforestation using Tectona grandis on infiltration and soil water retention. Forest Ecology and Management, 77(1-3): 119-125.

Ravazzani, G., Rametta, D., Mancini, M., 2011. Macroscopic cellular automata for groundwater modelling: A first approach. Environmental Modelling & Software, 26(5): 634-643.

Rawls, W., Yates, P., Asmussen, L., 1976. Calibration of selected infiltration equations for the Georgia Coastal Plain. In: Agriculture, U.S.D.o. (Ed.). Agricultural Research Service.

Razavian, D., 1990. Hydrologic responses of an agricultural watershed to various hydrologic and management conditions. JAWRA Journal of the American Water Resources Association, 26(5): 777-785.

Refsgaard, J.C., 1996. Terminology, modelling protocol and classification of hydrological model codes. In: Abbott, M.B., Refsgaard, J.C. (Eds.), Distributed Hydrological Modelling. Kluwer Academic, pp. 17-39.

Regüés, D., Gallart, F., 2004. Seasonal patterns of runoff and erosion responses to simulated rainfall in a badland area in Mediterranean mountain conditions (Vallcebre, southeastern Pyrenees). Earth Surface Processes and Landforms, 29(6): 755-767.

Renard, K.G., Foster, G.R., Weesies, G.A., McCool, D.K., Yoder, D.C., 1997. Predicting soil erosion by water: a guide to conservation planning with the Revised Universal Soil Loss Equation (RUSLE), Agriculture Handbook. U.S. Department of Agriculture, Washington, D. C.

Reynolds, W.D., Bowman, B.T., Brunke, R.R., Drury, C.F., Tan, C.S., 2000. Comparison of Tension Infiltrometer, Pressure Infiltrometer, and Soil Core Estimates of Saturated Hydraulic Conductivity. Soil Sci. Soc. Am. J., 64(2): 478-484.

Richards, L.A., 1931. Capillary conduction through porous mediums. Physics, 1: 313-318.

Rinaldi, P.R., Dalponte, D.D., Vénere, M.J., Clausse, A., 2007. Cellular automata algorithm for simulation of surface flows in large plains. Simulation Modelling Practice and Theory, 15(3): 315-327.

Ritter, J.B., 1990. Surface hydrology of drainage basins disturbed by surface mining and reclamation, central Pennsylvania, Pennsylvania State University, University Park, PA, 182 pp.

Ritter, J.B., 1992. Application of field infiltration data to hydrologic model parameterization: an example from drainage basins disturbed by surface mining. Journal of Hydrology, 134(1-4): 173-202.

Ritter, J.R., Gardner, T.W., 1993. Hydrologic evolution of drainage basins disturbed by surface mining, central Pennsylvania. Geol. Soc. Am. Bull, 105: 101-115.

Rojas, R., Julien, P., Johnson, B., 2003. Reference Manual for A 2-Dimensional Rainfall-Runoff and Sediment Model, Colorado State University.

Römkens, M.J.M., Baumhardt, R.L., Parlange, J.Y., 1985. Effect of rainfall characteristics on seal hydraulic conductance, Proceedings of the Syposium on the assessment of Soil Surface Sealing and Crusting, State University of Ghent, Belgium.

Römkens, M.J.M., Helming, K., Prasad, S.N., 2002. Soil erosion under different rainfall intensities, surface roughness, and soil water regimes. CATENA, 46(2-3): 103-123.

Rossman, L.A., 2010. STORM WATER MANAGEMENT MODEL USER'S MANNUAL Version 5.0, Water Supply and Water Resources Division, National Risk Management Research Laboratory, Cincinnati.

Sabey, B.R., Kitt, D.G., 1982. Runoff and erosion from drastically disturbed land in the southwestern. U.S. Proceeding, Reclamation of Mined Lands in the Southwest, U.S. Dept. Agric. Forest Ser., Soil Cons. Serv, Albuquerque, NM (1982): 91-97.

Sanchez, C.E., Wood, M.K., 1987. The relationship of soil surface roughness with hydrologic variables on natural and reclaimed range land in New Mexico. Journal of Hydrology, 94(3-4): 345-354.

Saynor, M.J., Houghton, R., 2011. Ranger trial landform: particle size of surface material samples in 2009 with additional observations in 2010, Supervising Scientist, Darwin, Australia.

Saynor, M.J. et al., 2012a. Assessing erosion and run-off performance of a trial rehabilitated mining landform, Life-of-Mine Conference 2012. The Australasian Institute of Mining and Metallurgy, Brisbane, Australia, pp. 123-132.

Saynor, M.J. et al., 2012b. Assessing erosion and run-off performance of a trial rehabilitated mining landform (presentation), Life-of-Mine Conference 2012, Brisbane, Australia.

Schmidt, J., Werner, M.v., Michael, A., 1999. Application of the EROSION 3D model to the CATSOP watershed, The Netherlands. CATENA, 37(3–4): 449-456.

Schroeder, S.A., 1987. Runoff from reclaimed grasslands compared to undisturbed grasslands, Proceedings of Fourth Billings Symposium on Mining and Reclaimation in the West, Billings Montana, pp. G-8-1: G-8-7.

Schultz, G.A., 1994. Meso-scale modelling of runoff and water balances using remote sensing and other GIS data. Hydrological Sciences Journal, 39(2): 121 - 142.

Schwärzel, K., Punzel, J., 2007. Hood Infiltrometer—A New Type of Tension Infiltrometer. Soil Sci. Soc. Am. J., 71(5): 1438-1447.

Service, U.S.C., 1972. National Engineering Handbook, Section4, Hydrology, Washington, D. C.

Shainberg, I., 1992. Chemical and mineralogical components of crusting. In: Sumner, M.E., Stewart, B.A. (Eds.), Soil Crusting: Chemical and Physical Processes, Boca Raton, Fla., pp. 33-53.

Shao, Q., Baumgartl, T., 2014. Estimating Input Parameters for Four Infiltration Models from Basic Soil, Vegetation, and Rainfall Properties. Soil Science Society of America Journal, In press.

Shao, Q., Baumgartl, T., Under review. Field Evaluation of Three Modified Infiltration Models for the Simulation of Rainfall Sequences European Journal of Soil Science.

Shao, Q., Weatherley, D., Huang, L., Baumgartl, T., Under review. RunCA: A Cellular Automata Model for Simulating Surface Runoff at Different Scales. Journal of Hydrology.

Shukla, M.K., Lal, R., Underwood, J., Ebinger, M., 2004. Physical and hydrological characteristics of reclaimed minesoils in southern Ohio. Soil Sci. Soc. Am. J., 68: 1352-1359.

Sichani, S.A., Engel, B.A., 1990. Prediction of runoff and sediment from agricultural watersheds by a mathematical model: II. Mathematical simulation. Iran Agricultural Research, 9: 1-16.

Silburn, D.M., Connolly, R.D., Loch, R.J., 1991. Assessment of alternative dump designs for the proposed Coronation Hill mine, Consultancy Series no. KAC91/20, Kakadu Conservation Zone Inquiry, Resource Assessment Commission. Australian Government Publishing Service, Canberra.

Silburn, D.M., Loch, R.J., Connolly, R.D., Smith, G.D., 1990. Erosional stability of waste rock dumps at theproposed Coronation Hill mine, Consultancy Series, Kakadu Conservation Zone Inquiry, ResourceAssessment Commission. Australian Government Publishing Service, Canberra.

Silvertown, J., Holtier, S., Johnson, J., Dale, P., 1992. Cellular automaton models of interspecific competition for space - The effect of pattern on process. Journal of Ecology, 80(3): 527-533.

Simanton, J.R., Renard, K.G., 1982. Seasonal change in infi ltration and erosion from USLE plots in Southeastern Arizona. Hydrology and Water Resources in Arizona and the Southwest, 12: 37-46.

Singh, P., Narda, N.K., Singh, A., 1992. Evaluation of Horton and Philip infiltration functions for determining optimum slope of graded check borders. Journal of Agricultural Engineering, 29: 1-9.

Singh, R., Tiwari, K.N., Mal, B.C., 2006. Hydrological studies for small watershed in India using the ANSWERS model. Journal of Hydrology, 318(1–4): 184-199.

Singh, V.P., 1996. Kinematic wave modeling in water resources: surface-water hydrology. John Wiley, New York, 1399 pp.

Skaggs, R.W., Khaleel, R., 1982. Chapter 4: Infiltration. In: Joseph, S. (Ed.), Hydrology of Small Watersheds. ASAE, Michigan.

Smith, H.L., Leopold, L.B., 1942. Infiltration studies in the Pecos River watershed, New Mexico. Soil Sci., 53: 195-204.

Smith, R.E., 1981. A kinematic model for surface Mine sediment yield. Transactions of the ASAE, 24: 1508-1514.

Smith, R.E., Corradini, C., Melone, F., 1993. Modeling infiltration for multistorm runoff events. Water Resources Research, 29(1): 133-144.

Stow, D.A. et al., 2004. Remote sensing of vegetation and land-cover change in Arctic Tundra Ecosystems. Remote Sensing of Environment, 89(3): 281-308.

Struthers, I., Hinz, C., Sivapalan, M., 2006. A multiple wetting front gravitational infiltration and redistribution model for water balance applications. Water Resources Research, 42(6): W06406.

Suppiah, R., Hennessy, K.J., 1998. Trends in total rainfall, heavy rain events and number of dry days in Australia, 1910–1990. International Journal of Climatology, 18(10): 1141-1164.

Swartzendruber, D., Youngs, E.G., 1974. A comparison of physically-based infiltration equations. Soil Science, 117: 165-167.

Swensson, M.T., 2003. Refinements on a GIS-Based, Spatially Distributed Rainfall-Runoff Model for a Small Watershed, University of Pittsburgh, 125 pp.

Tarboton, D.G., 1997. A new method for the determination of flow directions and upslope areas in grid digital elevation models. Water Resources Research, 33(2): 309-319.

Tarchitzky, J., Banin, A., Morin, J., Chen, Y., 1984. Nature, formation and effects of soil crusts formed by water drop impact. Geoderma, 33(2): 135-155.

Tekeste, M.Z., Tollner, E.W., Raper, R.L., Way, T.R., E., J.C., 2006. Non-linear finite element analysis of cone penetration in layered sandy loam soil: considering the precompression stress state. In: Zazueta, F., Kin, J., Ninomiva, S., Schiefer, G. (Eds.), Computers in Agriculture and Natural Resources, Fourth World Congress Conference. ASABE Publications, Orlando, Florida, USA.

Tian, G.M., Wang, F.F., Chen, Y.X., He, Y.F., 2003. Effect of different vegetation system on soil erosion and soil nutrients in red soil region of southeastern China. Pedosphere, 13(2): 121-128.

Tommaso, T., 1984. Cellular automata as an alternative to (rather than an approximation of) differential equations in modeling physics. Physica D: Nonlinear Phenomena, 10(1-2): 117-127.

Torri, D., Regüés, D., Pellegrini, S., Bazzoffi, P., 1999. Within-storm soil surface dynamics and erosive effects of rainstorms. CATENA, 38(2): 131-150.

Toy, T.J., Black, J.P., 2000. Topographic Reconstruction: The Theory and Practice. In: Barnhisel, R.I., Darmody, R.G., Daniels, W.L. (Eds.), Reclamation of Drastically Disturbed Lands. Agronomy Monograph. American Society of Agronomy, Crop Science Society of America, Soil Science Society of America, pp. 41-75.

Toy, T.J., Chuse, W.R., 2005. Topographic reconstruction: a geomorphic approach. Ecological Engineering, 24(1-2): 29-35.

Tucker, G.E., Slingerland, R.L., 1994. Erosional dynamics, flexural isostasy, and long-lived escarpments: A numerical modeling study. J. Geophys. Res., 99(B6): 12229-12243.

Tuppad, P., Douglas-Mankin, K.R., Lee, T., Srinivasan, R., Arnold, J.G., 2011. Soil and Water Assessment Tool (SWAT) hydrologic/water quality model: Extended capability and wider adoption. Transactions of the ASABE, 54(5): 1677-1684.

Turner, E., 2006. Comparison of Infiltration Equations and their Field Validation with Rainfall Simulation, University of Maryland.

U.S. Department of Agriculture, S.C.S., 1972. Hydrology, SCS National Engineering Handbook. Section 4. U.S. Gov. Print. Office, Washington, D.C.

Van De Genachte, G., Mallants, D., Ramos, J., Deckers, J.A., Feyen, J., 1996. Estimating Infiltration Parameters from Basic Soil Properties. Hydrological Processes, 10(5): 687-701.

Van den Putte, A. et al., 2013. Estimating the parameters of the Green–Ampt infiltration equation from rainfall simulation data: Why simpler is better. Journal of Hydrology, 476(0): 332-344.

Vereecken, H., 1988. Pedotransfer functions for the generation of hydraulic properties for Belgian soils. PhD Thesis Thesis, KU Leuven, 211 pp.

Von Hoyningen-Huene, J., 1981. Die Interzeption des Niederschlags in landwirtschaftlichen Pflanzenbeständen. Arbeitsbericht Deutscher Verband für Wasserwirtschaft und Kulturbau, DVWK, Braunschweig, 63 pp.

Von Neumann, J., 1966. Theory of Self Reproducing Automata. University of Illinois Press Champaign, IL, USA

Voorhees, M.E., 1986. Infiltration rate of bentonite mine spoil as affected by amendments of gypsum, sawdust and inorganic fertilizer. Reclamation & revegetation research, 5(4): 483-490.

Waddington, J.M., Roulet, N.T., Hill, A.R., 1993. Runoff mechanisms in a forested groundwater discharge wetland. Journal of Hydrology, 147: 37-60.

Wahle, J., Neubert, L., Esser, J., Schreckenberg, M., 2001. A cellular automaton traffic flow model for online simulation of traffic. Parallel Computing, 27(5): 719-735.

Walling, D.E., He, Q., Whelan, P.A., 2003. Using 137Cs measurements to validate the application of the AGNPS and ANSWERS erosion and sediment yield models in two small Devon catchments. Soil and Tillage Research, 69(1–2): 27-43.

Wang, S., Roache, P., Schmalz, R., Jia, Y., Smith, P., 2009. Verification and Validation of 3D Free-Surface Flow Models. American Society of Civil Engineers.

Wang, S., Wu, W., 2004. River sedimentation and morphology modeling - The state of the art and future development, Proceedings of the Ninth International Symposium on River Sedimentation, Yichang, China, pp. 71-94.

Warrington, D., Shainberg, I., Agassi, M., Morin, J., 1989. Slope and Phosphogypsum's Effects on Runoff and Erosion. Soil Sci. Soc. Am. J., 53(4): 1201-1205.

Whipkey, R.Z., 1965. Subsurface stromflow from forested slope. International Association. Hydrological Sciences Bulletin, 10(2): 74-85.

Whisler, F.D., Bouwer, H., 1970. Comparison of methods for calculating vertical drainage and infiltration for soils. Journal of Hydrology, 10(1): 1-19.

Wilcox, B.P., K., W.M., M., T.J., 1988. Factors influencing infiltrability of semiarid mountain slopes. Journal of Range Management, 41: 197-206.

Wilcox, B.P., Wilding, L.P., Woodruff, C.M., Jr., 2007. Soil and topographic controls on runoff generation from stepped landforms in the Edwards Plateau of Central Texas. Geophys. Res. Lett., 34(24): L24S24.

Willard, A., 2010. Hydrologic soil grouping determination for Appalachian minesoils. M.S. Thesis, West Virginia University, West Virginia, United States

Willgoose, G., Bras, R.L., Rodriguez-Iturbe, I., 1991. Results from a new model of river basin evolution. Earth Surface Processes and Landforms, 16(3): 237-254.

Wischmeier, W.H., Smith, D.D., 1978. Predicting rainfall erosion losses: A guide to conservation planning, Agriculture Handbook. U.S. Department of Agriculture, Washington, D. C.

Wolfram, S., 1984a. Computation theory of cellular automata. Communications in Mathematical Physics, 96(1): 15-57.

Wolfram, S., 1984b. Universality and complexity in cellular automata. Physica D: Nonlinear Phenomena, 10(1-2): 1-35.

Wösten, J.H.M., Pachepsky, Y.A., Rawls, W.J., 2001. Pedotransfer functions: bridging the gap between available basic soil data and missing soil hydraulic characteristics. Journal of Hydrology, 251(3–4): 123-150.

Young, R.A., Onstad, C.A., Bosch, D.D., Anderson, W.P., 1989. AGNPS: A nonpoint-source pollution model for evaluating agricultural watersheds. Journal of Soil and Water Conservation, 44(2): 168-173.

Zaghloul, N.A., 1983. Sensitivity analysis of the SWMM Runoff-Transport parameters and the effects of catchment discretisation. Advances in Water Resources, 6(4): 214-223.

Zhang, X.C., Nearing, M.A., Risse, L.M., 1995. Estimation of Green-Ampt conductivity parameters. II. Perennial crops. American Society of Agricultural Engineers, 38(4): 1079-1087.

Zhu, T.X., Cai, Q.G., Zeng, B.Q., 1997. Runoff generation on a semi-arid agricultural catchment: field and experimental studies. Journal of Hydrology, 196: 99-118.

Zuazo, V.c.H.D., Pleguezuelo, C.R.o.R., 2009. Soil-Erosion and Runoff Prevention by Plant Covers: A Review. In: Lichtfouse, E., Navarrete, M., Debaeke, P., Véronique, S., Alberola, C. (Eds.), Sustainable Agriculture. Springer Netherlands, pp. 785-811.